



Fakultät für Medizin

Forschungszentrum für krebskranke Kinder

Klinik und Poliklinik der Kinder- und Jugendmedizin

Viro-immunotherapy against Ewing sarcoma: synergistic antitumor effects of the oncolytic adenovirus XVir-N-31 with T cell receptor-transgenic T cells and cell cycle inhibition

Dr. med. Sebastian Johannes Schober

Vollständiger Abdruck der von der Fakultät für Medizin der Technischen Universität München zur Erlangung des akademischen Grades eines

Doctor of Philosophy (Ph.D.)

genehmigten Dissertation.

Vorsitzender: Prof. Dr. Marc Schmidt-Supprian

Betreuer: Prof. Dr. Stefan E.G. Burdach

Prüfer der Dissertation:

1. Prof. Dr. Per Sonne Holm
2. PD Dr. Uwe Thiel
3. Prof. Dr. Stefan Kochanek

Die Dissertation wurde am 05.11.2021 bei der Technischen Universität München eingereicht und durch die Fakultät für Medizin am 01.02.2022 angenommen.

For my wife Patcharee and my daughter Lea Pailin

Contents

1	INTRODUCTION	6
1.1	Ewing sarcoma (EwS).....	6
1.1.1	Epidemiology, localization, histology, and genetic alterations _____	6
1.1.2	Prognosis and standard of care _____	6
1.1.3	Relapse, salvage therapy and outcome _____	7
1.1.4	Immunological features of Ewing sarcoma _____	7
1.1.5	Experimental treatment options and early clinical trials _____	9
1.2	Generating specific T cell responses against EwS	10
1.2.1	Chimeric antigen receptor (CAR) T cell therapies _____	10
1.2.2	T cell receptor (TCR) T cell therapies _____	11
1.2.3	Antitumor vaccination _____	12
1.3	Cell cycle regulation and inhibition in EwS.....	13
1.3.1	CDK4/6 and the canonical mechanism of action/inhibition _____	13
1.3.2	CDK4/6 inhibition and non-canonical mechanism of immune activation _____	14
1.4	Oncolytic virotherapy	15
1.4.1	Spectrum of viruses and tumor-selective replication _____	15
1.4.2	Oncolytic adenoviruses and clinical application _____	15
1.4.3	The YB-1-dependent oncolytic adenovirus XVir-N-31 _____	16
1.5	Immunological features of oncolytic virotherapy.....	17
1.5.1	Immunogenic cell death _____	17
1.5.2	Interplay of adenovirus with innate and adaptive immunity _____	18
1.5.3	Abscopal effect _____	18
1.5.4	Combination with immune checkpoint blockade _____	18
1.6	Combinations of cellular-, target-, and virotherapy.....	19
1.6.1	Adoptive T cell therapy and small molecule inhibitors _____	19
1.6.2	Adoptive T cell therapy and oncolytic virotherapy _____	19
1.6.3	Small molecule inhibitors and virotherapy _____	20
2	RESEARCH OBJECTIVE and SPECIFIC AIMS of the study	21
2.1	Research objective	21
2.2	Specific aims of the study.....	21
3	MATERIALS and METHODS.....	22
3.1	Materials	22
3.1.1	List of manufacturers _____	22
3.1.2	List of chemicals and reagents _____	23
3.1.3	List of consumables _____	25
3.1.4	Equipment _____	25
3.1.5	Software _____	27
3.1.6	Kits _____	27
3.1.7	Buffers, media, and solutions _____	27
3.1.7.1	Buffers and gels for western blot analysis _____	27
3.1.7.2	Buffers and solutions for cell cycle analysis _____	28
3.1.7.3	Media _____	28
3.1.7.4	Solutions _____	28
3.1.8	Cell lines _____	29
3.1.9	Antibodies _____	29
3.1.9.1	Antibodies for Flow Cytometry _____	29
3.1.9.2	Antibodies for Western blotting (WB), hexon titer test (HTT), immunofluorescence (IF), and flow cytometry (non-conjugated) _____	31

3.1.10	Primer sequences for semi-quantitative PCR experiments	31
3.1.11	Small molecule inhibitors	32
3.1.12	Retroviral TCR constructs	32
3.2	Methods	32
3.2.1	Ethical considerations	32
3.2.2	Cell biology techniques	32
3.2.2.1	Cell culture	32
3.2.2.2	Isolation of peripheral blood mononuclear cells (PBMCs)	33
3.2.2.3	Generation of monocyte-derived dendritic cells (moDCs)	33
3.2.2.4	Generation of tumor-conditioned medium	33
3.2.2.5	Generation of TCR transgenic T cells	33
3.2.2.6	Generation of adenovirus constructs	34
3.2.2.7	Infection of cell lines with adenoviruses	34
3.2.2.8	Determination of adenovirus particles	34
3.2.2.9	Flow Cytometry	34
3.2.2.10	Phagocytosis assay	35
3.2.2.11	T cell proliferation assay	36
3.2.2.12	xCELLigence Assay	36
3.2.2.13	Histopathology	36
3.2.2.14	Immunofluorescence (IF) staining	36
3.2.3	Molecular biology techniques	37
3.2.3.1	DNA and RNA isolation	37
3.2.3.2	Reverse transcription	37
3.2.3.3	Semi-quantitative Real Time PCR (sqPCR)	37
3.2.3.4	Determination of viral genomic copies	37
3.2.3.5	Knock-down experiments	38
3.2.3.6	Microarray analysis	38
3.2.3.7	Western blot analysis	38
3.2.3.8	Multiplex Chemo-/Cytokine Assay	38
3.2.4	Animal experiments	39
3.2.5	Computational analyses	40
3.2.5.1	Statistical analysis	40
3.2.5.2	Bioinformatic analysis	40
4	RESULTS	41
4.1	Innate and adaptive antitumor immunity against EwS	41
4.1.1	Transcriptome-based analysis reveals CXCL10 expression as a possible determinate for T cell infiltration, antigen presenting capacity and antitumor phenotype of myeloid subsets	41
4.1.2	EwS-redirected TCR transgenic CD4 ⁺ T cells exhibit antitumor activity <i>in vitro</i> and mediate local control of xenografted A673 cell line	43
4.2	EwS cell lines are lysed by XVir-N-31 and support viral replication	46
4.3	Combination therapy of EwS-redirected CD8⁺ T cells and XVir-N-31	49
4.3.1	CHM1 T cells and XVir-N-31 synergistically lyse EwS tumor cells <i>in vitro</i>	49
4.3.2	Combination of CHM1 ³¹⁹ /HLA-A*02:01-restricted TCR-transgenic CD8 ⁺ T cells and XVir-N-31 increases therapy response and survival	51
4.3.3	XVir-N-31 increases phagocytic and antigen-presenting capacities resulting in superior antigen-specific CD8 ⁺ T cell proliferation	53
4.4	Combination therapy of XVir-N-31 and cell cycle blockade (combo Tx)	55
4.4.1	Combo Tx increase oncolysis and viral replication <i>in vitro</i> and increases therapy response and survival <i>in vivo</i>	56
4.4.2	Knock-down of RB increases adenoviral <i>fiber DNA</i>	58
4.4.3	Combo Tx induces proinflammatory chemo- and cytokine release	59
4.4.4	Combo Tx increases viral replication and exerts immunological antitumor effects <i>in vivo</i>	61
4.4.5	Combo Tx increases survival <i>in vivo</i>	64
4.4.6	Combo Tx induces T cell infiltration	66
4.4.7	Combo Tx induces an abscopal effect	67
4.4.8	Combo Tx induces CXCL10 in the tumor microenvironment of injected tumors	69
4.4.9	Combo Tx induces mouse monocyte infiltration in injected tumors	70

4.4.10	Combo Tx induces maturation of THP-1 and monocytic immature dendritic cells <i>in vitro</i>	72
4.4.11	Combo Tx increase antigen-specific T cell proliferation and activation <i>in vitro</i>	74
4.4.12	Combo Tx of XVir-N-31, CDK4/6i and therapeutic T cells further increase synergistic tumor cell killing <i>in vitro</i>	76
5	DISCUSSION	79
5.1	Limitations of this study	80
5.1.1	Combination of XVir-N-31 and CHM1 T cells	80
5.1.2	Combination of CDK4/6i and XVir-N-31	81
5.1.3	Oncolytic virotherapy and antitumor adaptive immune responses	84
5.1.4	Limitations of human oncolytic adenoviruses in animal models	85
5.1.5	Oncolytic capacity versus induction of ICD – determinants of response	86
5.2	Conclusion	86
5.3	Impact and outlook	87
6	SUMMARY	88
7	REFERENCES	89
8	APPENDIX	108
8.1	Supplemental Figures	108
8.2	List of figures	121
8.3	List of tables	122
8.4	List of abbreviations	123
8.5	Declaration of shared data in two dissertations	127
8.6	Acknowledgement	128
8.7	Publications related to this PhD work	129

1 Introduction

1.1 Ewing sarcoma (EwS)

1.1.1 Epidemiology, localization, histology, and genetic alterations

Ewing sarcoma (EwS) is a highly malignant and metastatic tumor of the bone and soft tissue which was first described exactly 100 years ago by James Ewing². Within pediatric sarcoma entities, it is the second most common cancer with ~1.5 cases per million in patients with European descent^{3, 4}. It mostly affects children, adolescents and young adults (AYA) with a median age at diagnosis of 15 years and a slight predominance in males (ratio male: female = 3: 2)^{3, 5}. Most frequent primary sites of bone disease include lower extremity, pelvis, chest wall, upper extremity and spine; extraosseous primary disease commonly presents at trunk, extremity, head and neck, and peritoneum⁶.

Histologically, EwS is a member of the heterogenous entities of small round cell sarcomas with diffuse cell surface expression of the glycoprotein CD99, which is present in ~95% of cases⁷. A genetically unifying feature of the disease is a recurrent balanced chromosomal translocation, in most cases t(11;22)(q24;q12)⁸. This results in an oncogenic fusion gene comprised of the FET family gene *EWS RNA Binding Protein 1* (EWSR1) and the DNA-binding ETS transcription factor *Friend Leukemia Virus Integration 1* (FLI1)⁹. In those 15-20% of EwS, which are negative for the EWSR1-FLI1 oncogene, other ETS translocation partners for *EWSR1* such as *ERG*¹⁰, *ETV1*¹¹, *ETV4*¹², and *FEV*¹³ can be identified¹⁴. The resulting fusion gene products form aberrant transcription factors influencing a plethora of genes involved in cell cycle progression, signal transduction, migration, telomerase activity, chromatin remodeling and many others¹⁵⁻¹⁷.

Other recurrent somatic mutations in EwS are scarce¹⁸, with alterations in *Cohesion Subunit SA2* (STAG2), *Tumor Suppressor P53* (TP53) and deletion of *CDK4 Inhibitor P16-INK4* (CDKN2A) being detected at diagnosis in 15-27%, 5-7% and 10-20% of cases, respectively¹⁹⁻²¹. Of note, all these mutations are associated with poorer prognosis^{21, 22}.

1.1.2 Prognosis and standard of care

Metastatic disease at diagnosis (~25% of cases^{23, 24}) dramatically decreases 5-year overall survival rates from ~70-80%, for localized state, to <30% for metastatic state, whereas for isolated metastasis to the lungs an overall survival of ~50% is expected^{25, 26}. Patients with ≥ 2 bone metastases, relapse ≤ 2 years after diagnosis, and/or bone marrow involvement carry worse prognosis with survival rates <15%²⁷⁻²⁹.

Current standard of care for patients with newly diagnosed EwS in Germany, treated according to the Ewing 2008 protocol, is comprised of neoadjuvant multidrug chemotherapy (induction), local disease control by surgery and/or radiotherapy and consolidation chemotherapy. Induction chemotherapy consists of vincristine, ifosfamide, doxorubicin and etoposide (VIDE) at 21-day intervals for a total of 6 cycles for all patients. Consolidation therapy implies the use of vincristine, actinomycin D, ifosfamide, cyclophosphamide or busulfan and melphalan with autologous stem cell rescue, depending on risk stratification and response to induction therapy³⁰.

1.1.3 Relapse, salvage therapy and outcome

Therapy after recurrence remains challenging and currently there is no standard of care for these patients. Unfortunately, ~30-40% of patients with localized disease and ~60-80% with metastases experience a relapse with a median time of recurrence at 1.4 years and 1.0 years after diagnosis, respectively³¹. Factors associated with poor outcome are: early relapse (≤ 2 years after diagnosis), systemic relapse, older age and high LDH (*lactate dehydrogenase*) levels^{26, 31}.

In this context, the role and *Y-box binding protein 1* (YB-1), *hypoxia-inducible factor 1 α* (HIF1 α) and formation of stress granules, regarding metastatic capacity and disease progression were extensively studied by Evdokimova, Sorensen and colleagues³²⁻³⁵. Here, high YB-1 expression was associated with poor outcome in high-risk sarcoma patients and YB-1 was identified as a driver of sarcoma metastasis by increasing EwS cell motility and invasiveness through enhancing HIF1 α levels and angiogenesis³².

Also in other cancer entities, multifunctional YB-1 was shown to promote tumor growth by multiple mechanisms, such as enhancing aerobic glycolysis (Warburg effect)³⁶ or inducing multidrug resistance³⁷ and DNA repair mechanisms³⁸.

Concerning clinical management of relapsed EwS, most therapeutic insights are drawn from retrospective studies and there is no general consent on treatment recommendation. Current strategies include high-dose chemotherapy with autologous stem cell rescue³⁹ and other multiagent regimens with combinations of irinotecan plus temozolomide, cyclophosphamide plus topotecan, gemcitabine plus docetaxel or single agent high-dose ifosfamide⁴⁰⁻⁴⁴. One international randomized controlled phase II/III trial comparing those 4 chemotherapy regimens for the treatment of recurrent or primary refractory EwS is still ongoing (EudraCT number: 2014-000259-99).

Despite those intensive treatments, post-relapse survival could not be increased in the past 2 decades stagnating at <10% for early relapsed patients and 22-24% for localized relapses (5-year overall survival) with a median time to death of 6 months, when a second complete remission could not be achieved^{25, 45}.

It remains to be elucidated if sole application of conventional chemotherapies in general, is appropriate for treating the sensitive group of early relapsed patients in the future, given the severe side effects and compromised quality of life induced by these highly toxic agents. Therefore, the field of pediatric cancer research broadened its' focus not only on the intrinsic tumor features of EwS but also on immunological characteristics and the tumor microenvironment.

1.1.4 Immunological features of Ewing sarcoma

Tumor microenvironment (TME)

As most pediatric solid malignances, EwS is an immunologically *cold*, non-T cell-inflamed tumor with low or even absent T cell infiltration^{46, 47}. One possibility for this observation might be the relatively low somatic mutational burden¹⁸ and hence neoantigen load which is often consider a prerequisite for mounting an antitumor T cell response after immune checkpoint

blockade (ICB)^{48, 49}. This also serves as a reasonable explanation for the low response rate of EwS to immune checkpoint blockade in a phase I/II trial with nivolumab (3 out of 10 patients with initial stable disease, but only 1 patient with stable disease for 5 months)^{50, 51}. In the study of Davis et al., only one EwS patient showed ~1% PD-L1⁺ tumor cells (*Programmed cell death-ligand 1*)⁵⁰. This is in line with other published reports, showing mostly absent or low PD-L1 expression on tumor cells, although PD-L1 expression can be induced by interferon gamma (IFN γ) *in vitro*^{46, 52-54}.

As mentioned before, tumor infiltrating T cells are scarce in EwS. Reports describe the presence of CD8⁺ T cell infiltration in 15-38% of cases^{53, 54}. Berghuis et al.⁵⁵ and Stahl et al.⁴⁷ could associate higher T cell infiltration with a survival benefit via immunohistochemistry and transcriptome-based analyses, respectively. Furthermore, T cell infiltration was increased with higher intratumoral levels of CXCL9/10 and CCL5 (*C-X-C Motif Chemokine Ligand 9/10* and *C-C Motif Chemokine Ligand 5*). Respective infiltrating T cells also stained positive for cognate receptors *C-C Motif Chemokine Receptor 5* (CCR5, ~70%) and *C-X-C Motif Chemokine Receptor 3* (CXCR3, ~80%)⁵⁵.

As T cells recognize tumor antigens in the context of a peptide/MHC complex (major histocompatibility antigen), human leukocyte antigen (HLA) class I and II expression on tumors play a pivotal role for mediating adaptive antitumor immunity. Another study from Berghuis et al. found that HLA class II expression could not be detected in EwS, due to functional impairment of the endogenous class II transactivator (CIITA)⁵⁶. HLA class I expression was completely absent in 28% and partially absent in 51% of patient samples (n=61), and significant lower levels in metastatic lesions were observed. Comparable to PD-L1 induction, IFN γ could upregulate HLA class I *in vitro*⁵⁶, also previously shown by members of our group⁵⁷.

Besides classical HLA class I expression, constituting a prerequisite for antigen recognition by T cells, there are also non-classical HLA I molecules in existence (HLA-G⁵⁸, -E⁵⁹, -F⁶⁰), which are mainly attributed immunosuppressive characteristics⁶¹. Compared to classical HLAs, they exhibit little genetic diversity and do not play a major role in antigen presentation to T cell receptors (TCR)⁶¹. Non-classical HLA class I molecules were mostly studied in the context of immune tolerance at the fetal-maternal interface. Here, they are expressed together with HLA-C in trophoblasts and suppress maternal immunity against the semi-allogenic fetus⁶². HLA-G was also observed to be expressed in viral infection, autoimmune disease, and organ transplantation⁶³⁻⁶⁶. It was shown that HLA-G and -E can restrict effector functions of T cells, natural killer (NK) cells and myeloid cells through specific interaction with respective inhibitory receptors on immune cells⁶⁷⁻⁶⁹. Induction of HLA-G was associated with IFN- β and - γ , heat shock and hypoxia response elements and long interspersed elements (LINEs), amongst others^{70, 71}.

HLA-G is also physiologically expressed in mesenchymal stem cells (MSCs) being associated with this cell type's strong immunosuppressive features^{72, 73}. With a possible origin of EwS from MSCs sharing functional characteristics with this cell type^{74, 75}, Rössig et al. evaluated non-classical HLA class I expression in patient biopsies and xenograft models. Indeed, they observed substantial HLA-G and -E expression in biopsy samples (HLA-G: 66%, n=59; HLA-E: 85%, n=26) and their expression could be induced by inflammatory response to G_{D2}-specific chimeric antigen receptor (CAR) T cells in xenograft mouse models^{71, 76}. In these analyses, both HLA-G and -E were expressed on tumor cells, infiltrating immune cells or both, whereas

T cell suppression of ganglioside G_{D2}-specific CAR T cells was mediated only by HLA-G expressing myeloid cells⁷¹.

Myeloid cells, and within this compartment especially tumor-associated macrophages (TAMs), are the predominant immune cell population infiltrating EwS^{47, 71, 77, 78}. Two studies confirmed a survival disadvantage with higher numbers of infiltrating (protumorigenic M2) macrophages^{47, 77}. In line with these observations are *in vivo* experiments of macrophage-depletion resulting in delayed tumor outgrowth^{77, 79}.

Systemic characteristics of EwS

Other cells from the myeloid compartment with known immunosuppressive properties are immature or pathologically activated monocytic and granulocytic cells, so called myeloid-derived suppressor cells (MDSCs)^{80, 81}. They are scarce in healthy individuals but accumulate in the TME, in blood and lymphoid tissue when tumors progress^{82, 83}.

In EwS, Mackall and colleagues identified a novel MDSC subset in EwS patients' blood derived from fibrocytes. Those cells were shown to suppress T cell proliferation, primarily via indoleamine oxidase (IDO), and their expansion positively correlated with CD4⁺GATA3⁺ T cells levels (GATA Binding Protein 3 = transcription factor upregulated in Th2 helper cells)⁸⁴.

Furthermore, CD4⁺ and CD8⁺ T cells isolated from the peripheral blood or bone marrow (BM) of patients with EwS, showed T cell exhaustion (i.e., *Programmed cell death protein 1*, PD-1-positivity) compared to healthy individuals. Those T cells were only reactive towards a minority of EwS tumor antigens and only after unspecific restimulation, indicating a general lack of adaptive antitumor immunity in EwS^{85, 86}.

Cancer-host crosstalk can be mediated by various mechanisms with release of tumor-derived extracellular vesicles (EVs) being one of them⁸⁷. In our group, Dr. med. Hendrik Gaßmann could show that EwS EVs influence monocyte-derived dendritic cell (DC) maturation leading to pathological activation accompanied by inhibition of T cell proliferation⁸⁸.

Lissat et al. observed elevated plasma levels of interleukin-6 (IL6) in a subgroup of EwS patients with poor prognosis. When analyzing the IL6 signaling pathway and the source of IL-6 they found, that EwS cell were rescued from apoptosis upon serum starvation and increased their migratory capacity through IL6-IL6r/IL6ST interaction triggering *Signal Transducer And Activator Of Transcription 3* (STAT3). Interestingly, the authors identified cancer stromal cells of being the source of IL6⁸⁹. This links IL-6 as chronic inflammatory stimulus, a hallmarks of cancer⁹⁰, to uncontrolled tumor growth, angiogenesis, invasion and metastasis of EwS⁹¹.

1.1.5 Experimental treatment options and early clinical trials

Between 2005 and 2018 ~150 clinical trials (mainly phase I/II) were conducted worldwide for the treatment of recurrent EwS. Most of the trials were conducted in the United States of America (USA) as opposed to 20% in Europe, with ~30% of them in international collaborations. Mainly single-agent therapies (62%) were administered rather than combinations (38%). 23% of them tested chemotherapy and a rise of targeted as well as immunotherapies was observed. Tested immunotherapies mostly included the IGF1-IGFR1 pathway (*Insulin-Like Growth Factor 1 / Receptor 1*), followed by ICB and tumor vaccination. Other molecular targets studied in early clinical trials include *Vascular Endothelial Growth Factor Receptor* (VEGF-R), *Death Receptor 5* (TRAIL-R2), *Endosialin* (CD248, platelet-derived growth factor pathway), *B7-H3* (CD276) or G_{D2}. 88% of trials were designed as single-

arm interventions. In 79% of conducted trials response rate RR (complete or partial response) was defined as the primary endpoint rather than progression free or overall survival (PFS, OS). Results retrieved from a systematic review showed low RR of 10% with stable disease in 25% of 827 patients being the best response. Only 18% of published trials concluded a positive effect^{92, 93}.

Allogenic hematopoietic stem cell transplantation (allo-HSCT) was also applied for high-risk EwS patients to induce a graft-versus-tumor effect (GvT), inspired by positive result from the treatment of leukemia^{94, 95} and motivated by promising case report studies⁹⁶. In a retrospective analysis, our group compared patients, who were transplanted with HLA-matched grafts versus HLA-mismatched (haploidentical) grafts, where a supposed GvT effect should have been distinct in the HLA-mismatch-transplanted group due higher non-self recognition. Opposed to our hypothesis, there was no survival difference between HLA-matched (n=27) versus -mismatched groups (n=39) and a GvT effect, if present, was clinically not relevant in this analysis⁹⁷. In a smaller group of patients, we demonstrated that allo-HSCT combined with donor lymphocyte infusions (DLI) was associated with disease control and increased survival⁹⁸. In summary, a supposed GvT effect induced by sole allo-HSCT is rare and most likely not relevant for most of the patients. Also, patients who received allo-HSCT due to their high-risk profile did not survive longer than patients receiving conventional therapy, assessed by matched-pair analysis (*manuscript in preparation*).

As allo-HSCT and DLI are unspecific immunotherapies, great effort has been undertaken to specifically target EwS with the help of the adaptive immune system.

1.2 Generating specific T cell responses against EwS

In general, patients can benefit from specific T cell responses either through active or passive immunization. Vaccines induce a specific immune response after antigen uptake, processing, and presentation by antigen-presenting cells (APCs) and consecutive priming of naïve T cells for vaccinated antigens (active immunization). The idea of passive immunization is, to directly administer effector molecules or cells, which specifically recognize the antigen or target cell without priming. When cells are altered *ex vivo* (e.g. isolated from tumor samples, expanded or genetically engineered) and reinfused back into the patient, this process is referred as adoptive (T) cell transfer (ACT).

1.2.1 Chimeric antigen receptor (CAR) T cell therapies

CARs usually consist of (1) an antigen-binding domain (single-chain variable fragment, scFv) derived from a monoclonal antibody, (2) a transmembrane CD3 ζ domain(1st generation)^{99, 100} and of (3) one or several co-stimulatory signaling domains, such as CD28 or 41BB (2nd generation)¹⁰¹. Nowadays, there are even more advanced genetic constructs (3rd and 4th generation CARs), combining both co-stimulatory domains, and introducing genes coding for cytokines (e.g. IL12, IL15 or IL18)^{102, 103}, chemokine receptors (e.g. CXCR1/2 for IL8)¹⁰⁴, extracellular matrix (ECM)-degrading enzymes (e.g. heparinase)¹⁰⁵ amongst others.

CAR T cell therapies are on the rise, with several CAR T cell products currently having *Food and Drug Administration*-(FDA) and *European Medicine Agency*-(EMA)¹⁰⁶ approval for the treatment of leukemia and other B cell malignancies¹⁰⁷.

Thus far, the great success of CAR T cells against above-mentioned malignancies has not been observed in the treatment of solid tumors. This might be due to the hostile TME, where T cells face adverse stroma composition, hypoxia, immunosuppressive tumor metabolites etc.¹⁰⁸

Regarding CAR T cell therapies for EwS, G_{D2} ¹⁰⁹, *Human Epithelia Growth Factor Receptor 2* (HER2) and B7-H3¹¹⁰ have been established as most promising target antigens and, after successful preclinical evaluation, are now being studied in currently ongoing or yet to be started clinical trials (NCT03356782, NCT04433221, NCT04897321, NCT03618381, NCT04483778, NCT03635632).

One successful application of HER2 CAR T cells in a patient with alveolar rhabdomyosarcoma and metastatic disease to the bone marrow has been published, describing induction of complete remission even after initial relapse, which was again treated with several CAR T cell infusion in combination with ICB (NCT00902044)¹¹¹. Of note, this impressive response included the application of 9 cycles of 1×10^8 HER2 CAR T cells/m²/cycle, with preparative lymphodepletion by cyclophosphamide and fludarabine before the first 3 infusions. Nevertheless, the patient relapsed after 6 months with bone marrow disease and received another 8 cycles with the same dose of therapeutic cells and lymphodepletion regimen with additional ICB (pembrolizumab) every 3 weeks. The 2nd relapse therapy lasted 62 weeks, and pembrolizumab was given for a total of 52 weeks (~7 cycles, calculated as not specified in the manuscript). At time of this report, the patient was still in remission, 20 months after cessation of T cell infusion¹¹¹.

This illustrates well, that intense as well as combination immunotherapies are necessary to achieve treatment success, comparable to multimodal chemotherapy.

Despite emerging success in the field of CAR T cell therapy, CARs inherit 2 major disadvantages compared to TCR T cell therapy: (1) Given its artificial nature, CAR T cells are restricted to recognition of surface antigens, whereas TCRs can recognize intracellular and surface proteins, after proteasomal degradation and loading onto MHCs.

(2) CARs are dependent on a certain surface antigen density for proper activation^{112, 113}, whereas TCR are much more sensitive for their cognate peptide/MHC complex (~10-100-fold more sensitive)¹¹⁴ and there is evidence that one single peptide/MHC complex can mount a T cell response¹¹⁵.

1.2.2 T cell receptor (TCR) T cell therapies

In the context of sarcoma, specific TCR-based immunotherapies were initially studied against synovial sarcoma targeting the cancer/testis antigen *New York Esophageal Squamous Cell Carcinoma 1* (NY-ESO-1), which is re-expressed in several tumors and only expressed in germ cells of testis and placenta physiologically¹¹⁶. The first adoptive transfer of these therapeutic T cells resulted in objective responses in 4 out of 6 patients with metastatic synovial sarcoma¹¹⁷. Further studies confirmed good tolerability and convincing response rates in this entity, with only 3 out of 42 patients showing disease progression, including 1 patient with a complete response¹¹⁸.

As somatic mutation load in EwS is rather low¹⁸, hence mutated peptide antigens (neoantigens) are less likely to occur. Thus far, peptides derived from EWSR1-FLI1 fusion oncogene were

weak binders for HLA-A2 and were unable to elicit strong T cell responses. Only a modified peptide (with 3 amino acid substitutions compared to the original nonamer) from the breakpoint raised antitumor T cell responses *in vitro* and *in vivo*¹¹⁹. Furthermore, an immunogenic MHC-II peptide was identified to stimulate T helper cells by our group previously but was not further pursued for clinical translation due to the absence of MHC-II expression on EwS and uncertain relevance of this peptide regarding natural procession¹²⁰.

Therefore, productive research thus far mostly focused on the identification of peptide candidates derived from cancer/testis and overexpressed antigens associated with malignant phenotypes. In this regard Staeger et al. identified 37 relevant gene transcripts including *Chondromodulin-1* (CHM1), *Six transmembrane epithelia antigen of the prostate 1* (STEAP1) or *Lipase I* (LIPI), which could serve as suitable target antigens for a TCR, and functional relevance for some antigens was studied afterwards, e.g. for invasiveness of metastasis^{121, 122}. Later, Gallegos et al. showed that EWSR1-FLI1 activates the cancer/testis antigen *Fetal And Adult Testis-Expressed Transcript Protein 1* (FATE1), and this activation was linked to promoting EwS survival¹²³. *X Antigen Family Member 1A* (XAGE-1)¹²⁴ and others were also found to be expressed in EwS¹²⁵.

Previously, our group could identify several reactive TCRs, derived from the allo-TCR repertoire, and functionally evaluated candidate TCRs against peptides from CHM1, STEAP1, *Pregnancy-Associated Plasma Protein A*, *Pappalysin 1* (PAPPA) and others¹²⁶⁻¹²⁹. Thereby, a CHM1³¹⁹⁻³¹²⁸/HLA-A*02:01-restricted TCR exhibited most promising characteristics. In the clinical setting, therapeutic CHM1-specific CD8⁺ T cells in combination with ICB in one patient induced partial regression of bone metastases associated with T cell homing to involved lesions¹³⁰.

Apart from first promising results confirming the rationale of this therapy, TCR T cell approach failed to mediate convincing disease control in EwS, being in line with the limited success of ICB or CAR T cells in this disease. Again, suggesting the need for combination treatments.

1.2.3 Antitumor vaccination

Antitumor vaccination constitutes another possible approach for mounting cancer specific T cell responses, with the prerequisite of intact pathways of antigen uptake, processing, presentation necessary for priming naïve T cells or stimulating pre-existing antitumor immunity. Until now, promising preclinical peptide vaccines, using antigens from the EWSR1-FLI1 fusion protein loaded onto DCs^{120, 131}, did not translate into tumor control in an early clinical trial when used as monotherapy¹³², hinting again low immunogenicity of fusion oncogene-derived peptides. When used as consolidation therapy after/ in combination with high-dose chemotherapy and autologous HSCT, tumor lysate- or peptide-loaded DC vaccination showed evidence of therapeutic activity, inducing specific T cell responses in treated patients associated with better prognosis^{133, 134}.

Most promising vaccination approaches for EwS patients were obtained through a vaccine called Virgil (or FANG). Here, the patient's tumor cells were transfected with a GM-CSF transgene (*Granulocyte-Macrophage Colony-Stimulating Factor*) and the bifunctional shRNA^{furin} (short hairpin) leading to: (1) tumor antigen release, (2) recruitment, stimulation and enhanced migration of DC, and (3) blocking of furin-induced activation of immunosuppressive *Transforming Growth Factor Beta 1/2* (TGFβ1 and -2)¹³⁵. Monthly intradermal injections

resulted in a 1-year survival of 73% (n=16) versus 23% (n=14) in a contemporaneous control group successfully inducing tumor-specific T cell responses^{136, 137}. This led to the initiation of a phase IIb trial in combination with temozolomide and irinotecan, results are pending (NCT02511132).

1.3 Cell cycle regulation and inhibition in EwS

Cyclin-Dependent Kinases (CDK) are important molecules regulating the cell cycle state of a cell. To ensure controlled cell cycle progression, they act together with a complex signaling network, consisting of different cyclin molecules and cell-intrinsic inhibitors of cyclin kinases. Many studies on cell cycle control have been conducted in the last decades attributing the CDK4/6-RB/E2F pathway (RB, *Retinoblastoma*; E2F, *E2F Transcription Factors*) a major role in regulating transcription¹³⁸⁻¹⁴¹.

As the somatic translocation EWSR1-FLI1 is the main driver of EwS mediating oncogenic potential by inducing a specific transcriptome signature, epigenetic deregulation was further studied. Riggi et al. found that EWSR1-FLI1 induces chromatin opening and thereby creating *de novo* enhancers which interact with promotor regions; at the same time, conserved enhancers are silenced¹⁷. To identify the most relevant promotors/enhancers (i.e. super-enhancers) and their target molecules, Kennedy et al. assessed epigenetic contributions to this malignancy in two EwS cell lines by chromatin immunoprecipitation and high-throughput sequencing (ChIP-seq). Most interestingly, one super-enhancer regulates cyclin D1 and promotes its expression, thereby rendering EwS selectively dependent on cyclin D1/CDK4¹⁴².

1.3.1 CDK4/6 and the canonical mechanism of action/inhibition

After mitotic stimuli, cells in G0/1 cell cycle state induce cyclin D1, which then forms an activating complex with CDK4/6 unleashing its kinase activity. The major target of phosphorylation is the tumor suppressor RB. The pocket protein RB, when active and hypophosphorylated, binds E2Fs within the pocket domain and thereby exerts its suppressive function by preventing G1-S transition. In turn, when phosphorylated by the cyclin D/CDK4/6 and consecutively by the CDK2/cyclin E complex, leading to hyperphosphorylated and inactive (pRB), the pocket function is abrogated and E2Fs are being released, resulting in S-phase induction¹⁴³⁻¹⁴⁶.

A deregulation of this pathway is frequently observed in human cancer, leading to the development of several specific inhibitors targeting CDK4/6. CDK4/6 inhibitors (CDK4/6i) induce a G1 cell cycle arrest by inhibiting the phosphorylation of RB^{139, 140, 147}. Furthermore, a reduction of total RB and E2F1 is often observed^{140, 148, 149}.

Three different CK4/6 inhibitors have FDA approval for the therapy of metastatic breast cancer in combination with hormonal therapy¹⁵⁰: abemaciclib (LY2835219, LY, Eli Lilly), palbociclib (PD-0332991, PD, Pfizer) and ribociclib (LEE011, LEE, Roche).

Regarding EwS, LY and LEE have been studied in preclinical models as monotherapy¹⁴² and in combination with chemotherapy¹⁵¹ or IGFR1 inhibition¹⁵², providing rationale for further testing. Early clinical trials for recurrent/refractory solid tumors (including EwS) established the maximum tolerated dose (MTD) and the general safety of all inhibitors as monotherapy with

acceptable toxicities, such as leuko- and neutropenia, anemia, thrombocytopenia, and diarrhea^{153, 154}.

Most of the 3 substances did not show signs of objective response (secondary endpoint) when administered as monotherapy¹⁵⁴, except for LEE, which induced stable disease in 9 out of 32 patients (7 patients with neuroblastoma)¹⁵⁵.

Currently, mostly combination with chemotherapy, especially with agents used for salvage treatment (1.1.3), undergo clinical investigation (NCT04238819, NCT02644460, NCT03709680).

Possible mechanisms explaining low response rates include acquired resistance, due to stronger cyclin E induction or E2F overexpression, which were shown to abrogate G1 arrest after CDK4/6 inhibition^{156, 157}.

1.3.2 CDK4/6 inhibition and non-canonical mechanism of immune activation

Interestingly, recent evidence suggests that the canonical pathway of cell cycle inhibition might not be the major mechanism of action in a living organism. Those novel and indirect effects result in the activation of immune surveillance¹⁵⁸.

First hints for a immunomodulating role of the CDK4/6-RB/E2F pathway were already discovered before the development of CDK4/6 inhibitors¹⁵⁹, when IFN γ stimulation induced MHC class II genes in a RB-dependent way^{160, 161}.

In the context of CDK4/6 inhibitor therapy, Goel and colleagues were the first ones to describe effects of enhancing antitumor immunity by abemaciclib (LY). They could demonstrate increased antigen presenting capacities, and downregulation of the E2F target *DNA Methyltransferase 1* (DNMT1). Resulting hypomethylation occurred at loci coding for endogenous retroviral elements (ERVs). Re-expression of ERVs was associated with Type III interferon secretion and induction of double-stranded (ds)RNA pattern recognition receptors, resembling an antiviral response in RB wild-type tumors.

Addressing aspects of adaptive T cell immunity, Goel et al. found an increase of T cell infiltrating CD3⁺ T cells, whereas immunosuppressive T-regulatory helper cells (Tregs) were reduced, due to relatively selective suppression (mediated through reduced levels of DNMT1 and *Cyclin-Dependent Kinase Inhibitor 1*, p21)¹⁶². Additional research identified the *T cell Transcription Factor NFAT4* (NFAT4), which regulates IL2 secretion, as a target of CDK6 kinase, as stated by the authors. Through CDK4/6 inhibition, inactivating phosphorylation of NFAT4 is prevented and T cell cytokines are induced, especially being the case for tumor antigen-experienced T cells¹⁶³ and memory CD4⁺ T cells¹⁶⁴. Moreover, innate MDSCs and pro-tumorigenic M2 macrophage population were shown to be reduced, although possible mechanisms are currently unclear¹⁶⁵.

Comparable effects in EwS cell lines concerning antigen presentation and ERV reactivation were assumed due to STAT1 activation, without addressing features of innate or adaptive immunity¹⁵¹.

More importantly, when combining CDK4/6 inhibition with ICB (i.e. PD-L1 blocking pembrolizumab), all above-mentioned preclinical reports observed a strong increase of therapeutic efficacy^{162, 163, 165-167}, marking the beginning of clinical investigation of this highly attractive combination therapy in several tumor entities (NCT03997448, NCT04220892, NCT03938337).

Another interesting aspect of CDK4/6 blockade was described by Uzhachenko and colleagues. They associated tumor-secreted chemokines *Chemokine Ligand 5* (CCL5), CXCL9, and CXCL10 upon CDK4/6 inhibition with (1) mTOR-mediated metabolic stress induction and (2) T cell infiltration. Despite G1-arrested cell tumor cycle state, metabolic activity, especially mitochondrial, was maintained at high levels, leading to tumor cell hypertrophy, oxidative stress, cytokine secretion and inflammation with consecutive increase of tumor-infiltrating lymphocytes (TILs)¹⁶⁸.

1.4 Oncolytic virotherapy

An oncolytic virus (OV) selectively infects and kills cancer cells without damaging normal tissues¹⁶⁹.

The potential of viruses to lyse tumor cells dates back to the mid-1800s, when virus infection coincidence with tumor regression, mostly in hematological malignancies and only short lasting^{170, 171}.

One of the first studies of anticancer effects of wildtype adenovirus (Ad) was performed in the 1960s for cervical cancer. Here side-effects were reported as mild, flu-like symptoms, but chemotherapeutic agents, which were established at that time, fared better in terms to response and survival benefit^{172, 173}.

It took until the 1990s until genomic editing of viruses produced reliable stains utilized for (cancer) gene therapy, after initial proposition of genomic attenuation by Southam in 1960¹⁷⁴.

1.4.1 Spectrum of viruses and tumor-selective replication

Cell tropisms for a given virus determines which tissue will be infected preferentially¹⁷⁵. In this regard, there are several viruses with a natural preference for tumors cell (e.g. parvovirus, reovirus, Newcastle disease virus, mumps virus and Moloney leukemia virus), whereas other viruses have to be engineered to render them specific for cancer cells (e.g. adenovirus, measles¹⁷⁶, vesicular stomatitis virus (VSV), vaccinia and herpes simplex virus (HSV))¹⁷⁵.

Most engineered viruses include adeno-, paramyxo-, and herpes viruses. Common strategies aiming to acquire tumor-selective replication include: (1) deletions of viral functions dispensable in cancer cells, (2) introducing tumor-specific or tissue-specific promoters to control essential viral genes (Ad)¹⁷⁷, (3) usage of non-pathogenic vaccination virus stains (such as the Edmonston B measles vaccine strain)¹⁷⁸, or (4) deletion of factors important for virulence (neurovirulence gene depletion in HSV-1, used in *Talimogene laherparepvec*, short T-VEC^{179, 180, 181}).

1.4.2 Oncolytic adenoviruses and clinical application

As mentioned above, tumor-selective replication of oncolytic adenoviruses (OAd) can be generated either through the induction of deletions (especially the E1 region of the virome, the first and therefore most important gene transcribed) or by rendering the expression of essential viral genes under cancer/tissue-specific cell promoters.

Deletions in the conserved region (CR) 2 in the E1A region, responsible for RB protein binding, are used in 2 oncolytic viruses, known as Ad-Delta24¹⁸² and dl922-947¹⁸³. In proliferating tumor cells with inactive RB due to deletion or constitutive phosphorylation, the RB binding domain in CR2 of E1A is dispensable, as free E2F is already present to drive replication¹⁸⁴.

Some of these constructs with additional deletions and especially the introduction of an RGD-motif (Arginine, Glycine, and Aspartate), facilitating integrin-mediated binding to host cells¹⁸⁵, were already evaluated in early clinical trials. They proved to be safe, and the maximal tolerated dose was not reached with already some striking clinical responses being observed, such as in recurrent glioblastoma (~20% of participants were still alive after 3 years)¹⁸⁶.

Another prominent representative of OAd with clinical approval in China since 2005, is called ONYX-015 containing a deletion of E1B-55K (nucleotides 2019-3509). Naturally E1B-55K forms a complex with E4orf6 and the tumor suppressor p53 inducing degradation of p53, which would otherwise induce DNA repair (e.g. of linear Ad DNA) or induce early apoptosis thus preventing viral propagation. Hence, when functional loss of p53 is present in a host cell, E1B-55K is dispensable as proposed by the developers, leading to clinical investigation of this OAd for treatment of p53-defective head and neck tumors^{184, 187}. A later study revealed that ONYX-015 replication was actually independent of p53 but rather related to the presence of YB-1¹⁸⁸ and as E1B-55K is an important multifunctional protein involved in mRNA transport, OAd with E1B-55K-depletions were not further developed in the Western world.

Regarding the introduction of cancer- or tissue specific promoters to drive viral gene expression, examples include the utilization of a prostate-specific antigen promoter to activate E1A¹⁸⁹, tissue-specific tyrosinase for the treatment of melanoma¹⁹⁰, or the elegant usage of the human telomerase reverse transcriptase promoter^{191, 192}, as telomerase activation being a general hallmark of cancer⁹⁰.

Also, for the treatment of pediatric malignancies, mostly Ad-Delta24-derivates or other constructs with deletions in regard to RB protein interaction, are in preclinical evaluation or assessed in early in clinical trials¹⁹³⁻¹⁹⁶.

1.4.3 The YB-1-dependent oncolytic adenovirus XVir-N-31

The established OAd used in the present study to evaluate combination therapies with tumor-redirected T cells and CDK4/6i is called XVir-N-31. The human species C Ad type 5 served for genetic modifications.

Tumor selective replication of XVir-N-31 (Ad dl520) was implemented by Prof. Dr. rer. nat. Per Sonne Holm and colleagues through a deletion in the CR3 domain of E1A affecting the splice variant of E1A-13S.

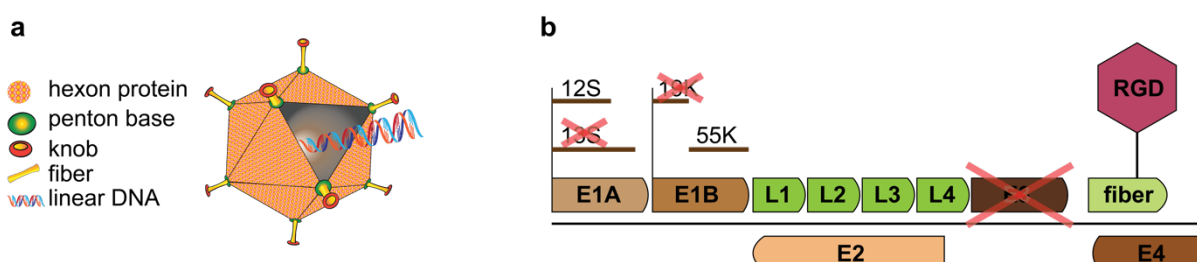


Illustration 1: Adenovirus – important structures and modifications of XVir-N-31. (a) Major components of a human species C adenovirus type 5 are: capsid protein *hexon*, *penton base*, *fiber* and *knob* as well as the *linear DNA* with a length of ~ 35kpb. (b) XVir-N-31 contains following deletions: E1A13S, E1B19K, E3 und was modified to express an RGD motif in the fiber protein (Adapted from Per Sonne Holm and colleagues).

CR3 is essential to transactivate several early viral promoters, such as E2 early. E1A-13S transactivates E4orf6, which then, together with E1B-55K, actively translocate YB-1 into the nucleus where the E2 late promotor is being activated. Due to the depletion of E1A-13S, viral gene expression is uniquely dependent of the E2 late promotor.

In tumor cells, viral gene expression especially concerning transactivation, can be compensated by nuclear expression of YB-1. As mention in **1.1.3**, YB-1 was shown to drive pediatric sarcoma malignancy³², being associated with survival disadvantages, when present in the nucleus¹⁹⁷, rendering this OAd highly attractive for the treatment of pediatric sarcoma entities at a disease state, when standard-of-care therapies failed.

Furthermore, XVir-N-31 contains a deletion of the antiapoptotic E1B-19K¹⁹⁸, the E3 region¹⁹⁹ increasing antigen-presenting capacities²⁰⁰ and an RGD-insertion in the fiber knob enhancing adenoviral tropism^{201, 202}.

1.5 Immunological features of oncolytic virotherapy

Naturally, Ad infection causes an immune response, due to host cell sensing of Ad DNA associated with type I interferon induction²⁰³, host cell lysis and consecutive priming of specific cellular and humoral antiviral responses²⁰⁴. The induction of inflammation through an OAd causes a multitude of changes at the site of injection as well as systemically, which can be exploited for cancer therapy. But Ads also developed several strategies to evade intracellular and systemic antiviral defense mechanisms, mostly associated with the E3 region²⁰⁵, which have to be taken into account.

1.5.1 Immunogenic cell death

A specific feature of OV-mediated tumor lysis is called immunogenic cell death (ICD)²⁰⁶. This specific way of cell death is associated with an activation of the immune system, involving changes at the cell surface as well as the release of humoral factors²⁰⁷. These timely coordinated processes affect several receptors on antigen-presenting cells, which in the context of tumor cell death, induces and maintains tumor-/viral-specific T cell responses²⁰⁸.

Specific factors attributed to ICD are pathogen- or danger-associated patterns (DAMP, PAMP). They are mainly characterized by the surface expression of calreticulin (CALR)²⁰⁹ and active release of immunostimulatory molecules, such as adenosine triphosphate (ATP)²¹⁰ and high-mobility group box 1 (HMGB1)^{206, 211, 212}.

In this context, OAd are often characterized according to their potentials to induce ICD^{193, 213} by assessing CALR surface expression, ATP or HMGB1 release.

1.5.2 Interplay of adenovirus with innate and adaptive immunity

Innate and adaptive immunity has been widely studied due to the use of adenoviral vectors for gene-delivery. Concerning Ad, innate immune sensing was mainly attributed to both Toll-like Receptor (TLR)-dependent and -independent pathways, including the Ad DNA recognition by TLR9²¹⁴ (and TLR2²¹⁵) and the cytosolic cyclic GMP-AMP synthase (cGAS), which are critical to mediate downstream type-I interferon signaling^{203, 216}.

In this regard, it is known that myeloid cells immediately react to Ad infection²¹⁷. Usually, inflammatory stimuli such as Ad infection, initially cause a response of tissue-resident macrophages and the recruitment of neutrophils to the site of infection. As a second line of defense, monocytes are being mobilized from the bone marrow becoming the dominant immune cell population at this point, which then differentiate into macrophages or dendritic cells and connect with the adaptive immune system after ~72h²¹⁸.

Adaptive immune responses were shown to be triggered most commonly by the capsid protein *hexon* (e.g. H910-924), directed against immunogenic peptides presented on various HLA haplotypes, such as HLA-A2 or HLA-DP4²¹⁹⁻²²¹.

1.5.3 Abscopal effect

The abscopal effect describes the phenomenon of tumor regression in localizations which were not directly treated, initially observed in irradiation²²². The underlying potential mechanisms also include the stimulation of immunogenic genes and activation of interferon signaling promoting DC migration, maturation and consecutively T cell priming and activation²²³. Mostly associated with systemic T cell responses after priming and activation, distant tumor lesions (e.g. non-irradiated) can then be recognized and lysed by T cells.

Results from early clinical trials described an abscopal effect also in the context of OV, especially in combination with ICB or other co-stimulatory molecules introduced as transgene with the OV²²⁴⁻²²⁷.

A recently published study also demonstrated the induction of an abscopal effect via tumor-derived EVs. Here, infectious viral units were packaged and released from injected tumor lesions via EVs, capable of infecting distant tumors²²⁸.

1.5.4 Combination with immune checkpoint blockade

As OVs are immunogenic oncolytic agents, combination strategies with ICB are highly promising. Indeed, the addition of T-VEC to pembrolizumab for the treatment of malignant metastatic melanoma could double response rates compared to pembrolizumab-monotherapy and was able to induce a complete response rate of 33%. These responses were observed independent of baseline CD8⁺ T cell infiltration, resulting in an even further increase of T cell infiltration in responding patients²²⁶.

Also, for the treatment of glioblastoma/ -sarcoma, an Ad-Delat24 (called DNX-2401) is currently assessed together with pembrolizumab (NCT02798406) with final results being

pending. A press release from 2020 reported of a median overall survival of 12.5 months, with 4 patients being alive beyond 23 months including 2 durable complete responses²²⁹.

Currently, most OVs (Ad, HSV, vaccinia virus, VSV, Reo- and Maraba virus) are being studied in early clinical trials together with ICB²³⁰.

1.6 Combinations of cellular-, target-, and virotherapy

Similar to the development of multiagent chemotherapies, future directions in the field of cancer immunotherapy also point towards combination approaches. They are mainly designed to increase and maintain therapeutic T cell responses. With growing knowledge of mechanism of target-antigen presentation/ - variation, and -loss as well as better understanding of immunosuppressive cellular and humoral factors, therapies become even more elaborate.

1.6.1 Adoptive T cell therapy and small molecule inhibitors

Adoptively transferred T cells (CAR-or TCR-transgenic) are combined with ICB²³¹ due to obvious reasons of T cell exhaustion and PD-L1 expression of tumor cells in several clinical trials, with ICB being often assessed for relapse therapy after T cell transfer²³².

Other interesting combinations especially developed for EwS included the usage of small molecule inhibitors (smi) such as an inhibitor of EZH2 (Enhancer of Zeste Homolog 2) to induce the surface expression of G_{D2} which is associated with superior target recognition and killing by G_{D2}-specific CAR-T cells²³³.

Interestingly, G_{D2}-specific CAR-T cells also showed synergistic effects with HGF-neutralizing antibody (AMG102) *in vitro* and in an *in vivo* EwS model, but underlying mechanisms are yet to be clarified²³⁴.

Also, the CDK4/6 inhibitor palbociclib was studied in the context of ACT due to its non-canonical effects of enhancing antigen presentation and T cell functionality.

Uzhachenko et al.¹⁶⁸ used an OT-1-OVA mouse model of ACT, where implanted mouse tumors express ovalbumin (OVA) and tumor-specific CD8⁺ T can be harvested from OT-1 mice which contain transgenic TCR inserts specific for the recognition of OVA-peptide²⁵⁷⁻²⁶⁴ on tumor cells²³⁵, recapitulating ACT in a syngeneic setting. The authors showed that palbociclib pretreatment for 2 weeks increased OT-1 T cell recruitment into the tumors associated with better outcomes and efficacy of exogenous transferred tumor-redirected T cells¹⁶⁸.

1.6.2 Adoptive T cell therapy and oncolytic virotherapy

Unfortunately, ACT for solid tumors, mostly utilizing CAR-T cells, did not translate into convincing clinical responses thus far, as observed for CD19-CAR-T cells against lymphoblastic malignancies²³⁶. Several reasons contribute to the limited success of ACT in solid tumors: (1) target antigen expression is variable and can be lost, especially when dispensable for tumors, (2) long and complex T cell trafficking routes (from the bloodstream into the dense TME, matching chemo-/cytokine receptors are needed), (3) immunosuppressive

local (TME) and systemic factors (limiting T-cell expansion, infiltration, and cytotoxicity), as well as (4) T cell exhaustion after exposure to the cognate antigen²³⁷.

In order to overcome those obstacles, OV has the potential to address and abrogate many of these limitations. As OVs are known to induce IFNs, cytotoxic CAR-T cell functionality and clonal expansion, which was shown to be increased by type I IFNs, can be enhanced through combination with OV, thereby providing a potent *signal 3* in addition to inherent *signal 1* (antigen recognition) and *signal 2* (co-stimulation, e.g. via CD28)²³⁸⁻²⁴⁰. Concerning the hostile TME, ICD by OV (as described in **1.5.3**) has the potential to reverse immunosuppression by depleting MDSCs or regulatory T cells, by increasing antigen (cross-) presentation, epitope spreading, breaking the tumor-induced peripheral tolerance, and inducing cytotoxic T cell infiltration^{241, 242}.

To further ameliorate synergistic effects of CAR-T cells and OV, various approaches through genetically editing either OV or CAR-T cells are applied. Comparable to the 'armored CAR T cells', cytokine-armed OVs were designed to produce various pro-inflammatory cytokines associated with increased T cell activity^{243, 244}. First combination strategies are currently evaluated in phase I trials (NCT03740256, NCT01953900).

1.6.3 Small molecule inhibitors and virotherapy

The rationale to combine small molecule inhibitors with OV either aims to increase viral replication, or to abrogate immunosuppressive characteristics, compared to the concept of cytokine-armed OVs.

In this context, blockade of immunosuppressive TGF- β -signaling was shown to increase therapeutic efficacy of an oncolytic HSV (oHSV) in a (patient-derived) glioblastoma model²⁴⁵. Similar, VEGF blockade was demonstrated to modulate tumor-infiltrating myeloid cells and thereby enabling stronger effects of oHSV²⁴⁶.

Regarding, viral replication or adenoviral vector-mediated gene delivery, Lv et al. could show that JQ1, an inhibitor of the bromodomain and extra-terminal (BET) family proteins, increased adenoviral efficacy due to superior association of BRD4 with CDK9²⁴⁷. Other classes of inhibitors, which were studied in regard to increased gene-delivery or replication, target histone acetylation (HDACi), such as vorinostat or FK288. Whereas, CAR expression and gene-delivery were increased by respective inhibitors, viral replication was rather antagonized²⁴⁸, reflecting the high complexity of the adenoviral life cycle when interfering with histone acetylation.

One study also described positive effects of the CDK4/6i palbociclib resulting in increased oncolytic activity of Ad5/3-delta24, which was only observed in estrogen receptor-positive but not in -negative cell lines. Here, the role of RB/E2F1 protein complex was not further studied²⁴⁹.

2 Research objective and specific aims of the study

2.1 Research objective

The main objective of this study was to introduce and preclinically assess combination therapies including the oncolytic adenovirus XVir-N-31 for the treatment of EwS.

2.2 Specific aims of the study

As EwS is considered a non-immunogenic tumor, due to low somatic mutational burden, scarce T cell infiltration, accompanied by little-to-no response to ICB, the oncolytic adenovirus XVir-N-31 (in combination with tumor-redirectioned T cells and CDK4/6i) was tested towards its suitability for EwS therapy and the induction of synergistic effects concerning antitumoral immunological changes.

Specific hypotheses were defined as follows:

1. EwS-redirectioned TCR transgenic CD4⁺ T cells synergize with CD8⁺ counterparts regarding antitumor activity and control *in vivo*
2. EwS cell lines are susceptible to oncolytic adenovirus XVir-N-31 leading to *de novo* formation of infectious viral particles and inducing tumor cell lysis
3. EwS-redirectioned (i.e. TCR transgenic T cells) synergize with XVir-N-31 concerning tumor cell lysis
4. XVir-N-31 induces markers of immunogenic cell death in infected tumor cells
5. XVir-N-31 in combination with CDK4/6i increases oncolytic capacity in EwS
6. XVir-N-31 in combination with CDK4/6i augments immunogenicity of EwS and induces tumor-infiltrating T cells resulting in tumor regression

3 Materials and Methods

3.1 Materials

3.1.1 List of manufacturers

Table 1: List of manufacturers

Manufacturer	Location
Abcam	Cambridge, UK
ACEA	San Diego, California, USA
Agilent Technologies	Santa Clara, California, USA
Analytik Jena	Jena, Germany
AppliChem	Darmstadt, Germany
Applied Biosystems	Darmstadt, Germany
ATCC	Rockyville, Maryland, USA
B. Braun Biotech	Melsungen, Germany
BD Biosciences Europe	Heidelberg, Germany
Berthold detection systems	Pforzheim, Germany
Biochrom	Berlin, Germany
BioLegend	San Diego, California, USA
Bio-Rad Laboratories	Richmond, California, USA
Bio-Techne	Minneapolis, Minnesota, USA
Brand	Wertheim, Germany
Branson	Connecticut, USA
Carestream Health	Rochester, New York, USA
Cayman Chemical Company	Ann Arbor, Michigan, USA
Cell Signaling Technology	Frankfurt a. M., Germany
Clarivate Analytics	Philadelphia, Pennsylvania, USA
Childhood Cancer Repository (CCR)	Texas Tech University, USA
Corning	Corning, New York, USA
CP-Pharma	Burgdorf, Germany
Dako	Hamburg, Germany
DRK-Blutspendedienst	Ulm, Germany
DSMZ	Braunschweig, Germany
Elma	Singen, Germany
Eppendorf	Hamburg, Germany
Exbio	Prague, Czech Republic
Falcon	Oxnard, California, USA
Feather	Osaka, Japan
Gamon Technology Corp.	Guangzhou, China
Cayman Chemical Company	Ann Arbor, Michigan, USA
Gamma-Service Medical	Leipzig, Germany
GE Healthcare	Little Chalfont, UK
Genzyme	Neu-Isenburg, Germany
GLW	Würzburg, Germany
Greiner Bio-One	Frickenhausen, Germany
Heidolph Instruments	Schwabach, Germany
Heraeus	Hanau, Germany
Hoffmann Group	Munich, Germany
ibidi	Gräfelfing, Germany
IKA-Werke	Staufen, Germany
Implen	München, Germany
Instech Laboratories	Plymouth Meeting, Pennsylvania, USA
Kern & Sohn	Balingen, Germany
Kodak	Rochester, New York, USA
Leica	Wetzlar, Germany
Life Technologies	Carlsbad, California, USA
Lonza	Basel, Switzerland
MedChem Express	Monmouth Junction, New Jersey, USA
Merck Millipore	Darmstadt, Germany

Metabion	Planegg, Germany
Mettler Toledo	Greifensee, Switzerland
Microsoft	Albuquerque, New Mexico, USA
Miltenyi Biotec	Bergisch Gladbach, Germany
Mirus	Madison, Wisconsin, USA
Nalgene	Rochester, New York, USA
Nobamed	Wetter, Germany
Paul Marienfeld	Lauda-Königshofen, Germany
PerkinElmer	Akron, Ohio, USA
Promega	Madison, Wisconsin, USA
Qiagen	Chatsworth, California, USA
R&D Systems	Minneapolis, Minnesota, USA
Roche	Penzberg, Germany
Roth	Karlsruhe, Germany
Sanofi	Bridgewater, New Jersey, USA
Santa Cruz Biotechnology (Biotech)	Heidelberg, Germany
Sarstedt	Nümbrecht, Germany
Sartorius	Göttingen, Germany
Scientific Industries	Bohemia, New York, USA
Selleck Chemicals	Houston, Texas, USA
Siemens	Munich, Germany
Sigma Aldrich	St. Louis, Missouri, USA
Starlab	Hamburg, Germany
Systemc	Wettenberg, Germany
TaKaRa Bio Europe	Paris, France
Tanon Science & Technology	Shanghai, China
Taylor-Wharton (Auguste Cryogenics Germany)	Husum, Germany
Tecan	Männedorf, Switzerland
Thermo Fisher Scientific	Waltham, Massachusetts, USA
TKA	Niederelbert, Germany
TPP	Trasadingen, Switzerland
UniEquip	Planegg, Germany
VWR	Radnor, Pennsylvania, USA
Wessamat	Kaiserslautern, Germany
Zeiss	Jena, Germany

3.1.2 List of chemicals and reagents

Table 2: List of chemicals and reagents

Chemical/reagent	Manufacturer
Acetic acid $\geq 99,7\%$	Sigma-Aldrich
ACK Lysis Buffer (Red blood cell lysis)	Thermo Fisher Scientific
Acrylamide/Bis-acrylamide solution 30%	Sigma-Aldrich
AIM-V Medium	Thermo Fisher Scientific
Albumin standard	Thermo Fisher Scientific
Amersham ECL Western Blotting Reagent Pack	GE Healthcare
Ammonium persulfate (APS)	Sigma-Aldrich
Anti-CD3/CD28 Dynabeads	Thermo Fisher Scientific
Anti-PE Microbeads	Miltenyi Biotec
autoMACS Rinse Solution	Miltenyi Biotec
β_2 -microglobulin	Sigma-Aldrich
Bovine serum albumin (BSA) $\geq 96\%$	Sigma-Aldrich
Bromophenol blue	Merck Millipore
CHM1 ³¹⁹ -peptide (VIMPCSWWV)	Thermo Fisher Scientific
Collagenase (Type IV) from <i>Clostridium histolyticum</i>	Sigma-Aldrich
cOmplete, EDTA-free Protease Inhibitor Cocktail	Roche
DAPI (4',6-diamidino-2-phenylindole)	Sigma-Aldrich
DAPI staining solution	Miltenyi Biotec
DEPC-treated water	Thermo Fisher Scientific
Dimethylsulfoxide (DMSO)	AppliChem
Dithiothreitol (DTT)	VWR

DNase I, RNase-free	Thermo Fisher Scientific
dNTP	Roche
D-luciferin	PerkinElmer
Dulbecco's Modified Eagle's Medium (DMEM)	Thermo Fisher Scientific
Dulbecco's Phosphate Buffered Saline 10x (PBS)	Thermo Fisher Scientific
D(+)-Glucose	Merck Millipore
Ethanol (EtOH) \geq 99,8%	Roth
FACS Clean	BD Biosciences
FACS Flow	BD Biosciences
FACS Rinse	BD Biosciences
Fetal bovine serum (fetal calf serum, FCS)	Biochrom
Ficoll-Paque	GE Healthcare
GoTaq qPCR master mix	Promega
Glycerine \geq 99%	Sigma-Aldrich
Glycine \geq 99%	Sigma-Aldrich
HBSS (Hank's buffered salt solution)	Thermo Fisher Scientific
HEPES	Sigma-Aldrich
Human AB serum	Sigma-Aldrich
Human IgG	Genzyme
Hydrochloric acid (HCl) 32%	Merck Millipore
Isofluran	CP-Pharma
Isopropanol	Merck Millipore
Influenza-peptide (GILGFVFTL)	Thermo Fisher Scientific
L-Glutamine 200mM	Thermo Fisher Scientific
Lipofectamine RNAiMAX Transfection Reagent	Thermo Fisher Scientific
Liquid DAB+ Substrate Chromogen System	Dako
MACSQuant Calibration Beads	Miltenyi Biotec
MACSQuant/MACSiMa Storage Solution	Miltenyi Biotec
MACSQuant Running Buffer	Miltenyi Biotec
MACSQuant Washing Solution	Miltenyi Biotec
Methanol (MeOH) \geq 99,8%	Merck Millipore
Methylcellulose, viscosity: 400 cP	Merck Millipore
Minimum Essential Medium Non-Essential Amino Acids (100x, NEAAs)	Thermo Fisher Scientific
Nonidet P40 Substitute (NP40)	Sigma-Aldrich
Opti-MEM, Reduced Serum Medium (1x)	Thermo Fisher Scientific
PageRule Prestained Protein Ladder	Thermo Fisher Scientific
Formaldehyde solution about 37%	Merck Millipore
Penicillin-streptomycin 10.000U/ml	Thermo Fisher Scientific
Proleukin (recombinant human, rh IL-2)	Novartis
Propidium iodide \leq 95%	Sigma-Aldrich
Prostaglandin E ₂ (PGE ₂)	Cayman Chemical Company
Protamine sulfate	Sigma-Aldrich
Retronectin	TaKaRa
rh GM-CSF	Sanofi
rh IFN γ	R&D Systems
rh IL-1 β	R&D Systems
rh IL-4	R&D Systems
rh IL-6	R&D Systems
Rh IL-7	
rh IL-15	R&D Systems
RNase A, DNase and protease-free(10mg/mL)	Thermo Fisher Scientific
Roswell Park Memorial Institute Medium (RPMI-1640)	Thermo Fisher Scientific
Skim milk powder	Sigma-Aldrich
Sodium azide (NaN ₃)	Sigma-Aldrich
Sodium chloride (NaCl)	Sigma-Aldrich
Sodium hydroxide (NaOH)	Merck Millipore
Sodium dodecyl sulfate (SDS) \geq 98,5%	Sigma-Aldrich
Sodium metavanadate (NaVO ₃)	Sigma-Aldrich
Sodium (Na-)pyruvate (100mM)	Thermo Fisher Scientific
Sodium phosphate dibasic (NaH ₂ PO ₄)	Merck Millipore

Sodium phosphate monobasic (Na ₂ HPO ₄)	Merck Millipore
Sulforhodamine B sodium salt (SRB)	Sigma-Aldrich
Tetramethylethylenediamine (TMED)	Sigma-Aldrich
TransIT-293	Mirus
Trichloroacetic acid (TCA) ≥ 99,7%	Sigma-Aldrich
Tris(hydroxymethyl)aminomethane (TRIS)	Merck Millipore
Trypsin EDTA	Thermo Fisher Scientific
Trypan blue stain (0.4%)	Thermo Fisher Scientific
Tween-20	Sigma-Aldrich
X-VIVO 15 medium	Lonza

3.1.3 List of consumables

Table 3: List of consumables

Material	Manufacturer
Tissue Culture Dish (100 x 20 mm)	Falcon
Tissue Culture Plate, 6 and 24 well	Falcon
Tissue Culture Plate, 96 well (U, round bottom)	TPP
Cell culture flasks (25, 75, and 175 cm ²)	Greiner Bio-One
Cell scraper (16 cm)	Sarstedt
Cell strainers (EASY stainer) 40 and 70 μm	Greiner Bio-One
Columns (MACS, LS, MS)	Miltenyi Biotec
CryoPure Tube 1.6 mL	Sarstedt
Cuvettes	Roth
E-plate 96 (for xCELLigence assay)	ACEA
Fast Optical Reaction Plate (MicroAmp, 96 well)	Applied Biosystems
Filters, 0.2 and 0.45 μm	Sartorius
FTP-20-38 Plastic Feeding Tubes, 20gs x 38mm	Instech Laboratories
Gloves (latex), size S-L	Nobamed
Hybond-P PVDF membrane	GE Healthcare
Hypodermic needle (23G and 27G)	B. Braun Biotech
Hypodermic syringe (for intratumoral injection) Micro-Fine 0.5 mL 30G	BD Biosciences
Optical Adhesive Film (MicroAmp)	Applied Biosystems
Pipettes (2, 5, 10, and 25 mL)	Greiner Bio-One
Pipette tips (10, 20, 100, 200, 1000 γL) with and without filter	Starlab
Scalpel (disposable) No. 10	Feather
Safe-lock micro tubes (0.2, 1.5, 2 mL), DNA-/ DNase-/ RNase-/PCR inhibitor-free	Sarstedt
Safe-lock microcentrifuge tubes (1.5, 2 mL)	Eppendorf
Syringes (Original Perfusor 50 mL; Omnifix-1, 10, 20 mL)	B. Braun Biotech
Tubes for cell culture (CELLSTAR); 15, 50 mL	Greiner Bio-One
Tubes for flow cytometry (5 mL)	Sarstedt
Whatman gel blot paper	GE Healthcare
μ-slides (6 channels)	Ibidi

3.1.4 Equipment

Table 4: Equipment

Instrument	Specification	Manufacturer
Analytical balances	770-14, EW3000-2M	Kern & Sohn
Autoclaves	V95, 2540 EL	Systec
RNA analysis	Bioanalyzer 2100	Agilent Technologies
Biological Safety Cabinets	HERAsafe KS 18, Class II	Thermo Fisher Scientific
Caliper (digital)	ABS Horex	Hoffmann Group
Cell count chamber	Neubauer	Paul Marienfeld
Centrifuges	Microcentrifuge 5415 R	Eppendorf
	Multifuge 3SR (Heraeus)	Thermo Fisher Scientific

CO ₂ Incubators	HERA cell 150	Thermo Fisher Scientific
Cryotank	K series CryoStorage System 24K	Worthington Industries
Electrophoresis Cell	VE-180 Mini Vertical Gel	Tanon Science & Technology
Electrophoresis Blotting System (semi-dry)	Biometra Fastblot B43	Analytik Jena
Freezing containers	Mr. Frosty, Nalgene	Sigma-Aldrich
Flow Cytometers	FACSCalibur	BD Biosciences
	MACSQuant Analyzer 10	Miltenyi Biotec
FACS sorter	FACS Aria	BD Biosciences
Freezer (-80°C)	HERA freeze	Thermo Fisher Scientific
Fridge + Freezer (-20°C)	Siemens coolVario	Siemens
Heating block	ThermoMixer comfort 5355	Eppendorf
Ice machine	Flake Line	Wessamat
Irradiation machine	BioBeam 8000	Gamma-Service Medical
Bioluminescence Monitoring	IVIS Lumina LT-Series III instrument	PerkinElmer
Light Pad	LED Light Pad GB4	Gamon Technology Corp.
Sonifier	Digital Sonifier 250	Branson
Magnetic separators	BD Cell Separation Magnet	BD Biosciences
	MidiMACS	Miltenyi Biotec
	QuadroMACS	Miltenyi Biotec
Magnetic stirrer	IKAMAG REO	IKA-Werke
Micropipettes (adjustable)	10, 20, 100, 200, 1000 µL	Eppendorf
	Multichannel 100 µL	Eppendorf
Microscopes	Axiovert 100	Zeiss
	Camera AxioCam Mrm	Zeiss
	Fluorescent Light HBO 50	Zeiss
	Leica DM IL LED	Leica
Multiplex Immunoassay Reader	Bio-Plex 200 System (Luminex 200)	Bio-Rad Laboratories
Nanophotometer	NanoPhotomete Pearl	Implen
PCR cycler	iCycler	Bio-Rad Laboratories
pH meter	FiveEasy	Mettler Toledo
Photometer	Infinite M Nano	Tecan
Pipette controllers	accu-jet pro	Brand
	Stripettor Ultra	Corning
Power supply	Biometra Standard Power Pack P25	Analytik Jena
Real-Time PCR System	StepOnePlus	Applied Biosystems
Shakers	Duomax 2030	Heidolph Instruments
	Orbital Shaker UniTwist 3D	UniEquip
	IKA Rocker 3D digital	IKA-Werke
Vortexers	Genie 2 G560-E	Scientific Industries
	Microplate Genie	Scientific Industries
	MS2 Minishaker	IKA-Werke
	Relax Top	Heidolph Instruments
Western blot documentation	Gel Logic 1500 Imaging System	Kodak
Proliferation system	xCELLigence RTCA	Roche/ACEA

3.1.5 Software

Table 5: Software

Software	Version	Company	Application
Adobe Illustrator	24.2.1	Adobe	Data presentation, cartoons
Adobe Photoshop	21.2.1	Adobe	Image editing
AxioVision	4.7.1	Zeiss	Immunofluorescence
Bio-Plax Manager	6.2	Bio-Rad Laboratories	Multiplex Analysis
Capture Molecular Imaging	5.0.7.24	Carestream Health	Western blot
CellQuest Pro	6.1	BD Biosciences	Flow Cytometry
EndNote	X9.3.3	Clarivate Analytics	References
Excel for Mac	16.54	Microsoft	Data analysis
FlowJo	10.8.0	BD Biosciences	Flow Cytometry
i-control for Infinite 200 Pro	2.0	Tecan	Cell survival assay
MACSQuantify	2.13.1	Miltenyi Biotec	Flow Cytometry
Prism for macOS	9.1.2	GraphPad Software	Data presentation, statistical analyses
R studio	1.3.1093	Public-benefit Corp	Heatmaps, Synergyfinder
R for Mac OS X Cocoa GUI	4.1.0	The R Foundation	Heatmaps, Synergyfinder
StepOne	2.3	Thermo Fisher Scientific	sqPCR
Word for Mac	16.54	Microsoft	Writing

3.1.6 Kits

Table 6: Kits

Name	Manufacturer
Anti-Human CD14 Magnetic Particles	BD Biosciences
CD8 ⁺ T cell Isolation Kit	Miltenyi Biotec
DNeasy Blood & Tissue Kit (50)	Qiagen
Dynabeads CD4 Positive Isolation Kit	Thermo Fisher Scientific
Dynabeads CD8 Positive Isolation Kit	Thermo Fisher Scientific
FoxP3 Staining Buffer Set	Miltenyi Biotec
High-Capacity cDNA Reverse Transcription Kit	Applied Biosystems
Human Cytokine Screening 48-Plax Panel	Bio-Rad Laboratories
Human ProcartaPlex Mix&Match 7-plex	Thermo Fisher Scientific
Inside Stain Kit	Miltenyi Biotec
MACSQuant Comp Bead Kit anti-REA	Miltenyi Biotec
Pierce BCA Protein Assay Kit	Thermo Fisher Scientific
RNA Nano Chips	Agilent Technologies
RNeasy Mini Kit (50)	Qiagen
MycoAlert Mycoplasma Detection Kit	Lonza

3.1.7 Buffers, media, and solutions

3.1.7.1 Buffers and gels for western blot analysis

Table 7: Buffers and gels for western blot analysis

Buffer/gel	Ingredients
Antibody dilution buffer	5% BSA in TBS-T, 0.02% NaN ₃
Protein loading buffer	0.25M TRIS-HCl (pH 6.8), 40% glycerine, 8% SDS, 0.04% bromophenol blue
Protein lysis buffer	10mM TRIS-HCl (pH 7.2), 1% SDS, 1mM NaVO ₃ , 1 tablets protease inhibitor
Running buffer (1x), immunoblot	25nM TRIS, 192mM glycine, 0.1% SDS
Separating gel (10%), 10mL	4.0 mL ddH ₂ O

	3.3 mL Acrylamide/Bis-acrylamide 30%	2.5 mL 1.5M TRIS (pH 8.8)
	0.1 mL 10% SDS (in ddH ₂ O)	
	0.1 mL 10% APS (in ddH ₂ O)	
	0.004 mL TMED	
Stacking gel, 4mL	2.7 mL ddH ₂ O	
	0.67 mL Acrylamide/Bis-acrylamide 30%	
	0.5 mL 1M TRIS (pH 6.8)	
	0.04 mL 10% SDS (in ddH ₂ O)	
	0.04 mL 10% APS (in ddH ₂ O)	
	0.004 mL TMED	
Transfer buffer (1x)	48mM TRIS, 39mM glycine, 10% MeOH	
TBS (10x)	0.5M TRIS-HCl (pH 7.6), 1.5M NaCl	
TBS-T	0.1% Tween-20 in TBS (1x)	

3.1.7.2 Buffers and solutions for cell cycle analysis

Table 8: Buffers and solutions for cell cycle analysis

Name	Ingredients
Sample buffer	0.1% glucose in PBS (1x), 0.22 μ m filtration
PI staining solution	Propidium iodide (PI) 50 μ g/mL and 100 U/mL RNase A in sample buffer

3.1.7.3 Media

Table 9: Media

Name	Ingredients
Cryo medium	90% FCS, 10%DMSO, (for T cells, hAB serum was used)
DC medium	X-VIVO 15, 1% hAB serum
Standard medium (tumor)	RPMI-1640 medium 500 mL, FCS 10%, 2mM L-glutamine, penicillin 100 U/mL, streptomycin 100 μ g/mL
T cell medium	AIM-V medium 500 mL, 5% hAB serum, penicillin 100 U/mL, streptomycin 100 μ g/mL
LCL medium	RPMI-1640 medium 500 mL, FCS 10%, Na-pyruvate 1mM, NEAAs 1mM, penicillin 100 U/mL, streptomycin 100 μ g/mL
NSO medium	DMEM medium 500 mL, FCS 10%, Na-pyruvate 1mM, NEAAs 1mM, penicillin 100 U/mL, streptomycin 100 μ g/mL
HEK293	DMEM, FCS 10%, penicillin 100 U/mL, streptomycin 100 μ g/mL

3.1.7.4 Solutions

Table 10: Universal and specific buffers/solutions

Name	Ingredients	Application
4% formaldehyde (buffered)	4% formaldehyde solution, 55nM Na ₂ HPO ₄ , 12mM NaH ₂ PO ₄ , 2 H ₂ O	Immunofluorescence, histopathology
Blocking solution HTT	1% BSA in PBS (1x)	Hexon titer test
Blocking solution IF	3% BSA in PBS (1x)	Immunofluorescence
Blocking solution WB	5% skim milk powder in TBS (1x)	Western blot
Tumor digestion buffer <i>in vivo</i>	RPMI-1640, collagenase IV 200 U/mL, DNase I 100 μ g/mL	Enzymatic dissection
Flow cytometry staining buffer	2% FCS in PBS (1%)	Flow cytometry
Permeabilization solution IF	0.4% NP40 in PBS (1x)	Immunofluorescence
SRB staining solution (0.05%)	0.05% SRB (w/v) in 1% acetic acid	Cell survival assay

3.1.8 Cell lines

Cell line A673 was purchased from ATCC. A4573 was a kind gift of Prof. Poul Sorensen (University of British Columbia, Vancouver, Canada) and Dr Valentina Evdokimova (Ontario Institute for Cancer Research, Toronto, Canada), originally purchased from ATCC. TC32 was also kindly provided by Prof. Poul Sorensen, which was initially obtained from the Childhood Cancer Repository (CCR, Alex's Lemonade Stand Foundation, Children's Oncology Group, COG). SB-KMS-KS1 was established in our laboratory. HEK293 cells were kindly provided by Prof. Per Sonne Holm, originally purchased from ATCC. IL-15-producing NSO cells were a kind gift of Prof. Stanley Riddell (University of Washington School of Medicine, Seattle, USA). RD114 packaging cells were a kind gift from Prof. Manuel Caruso (Centre de recherche de Québec, Université Laval). Healthy donor buffy coats for extraction of peripheral blood monocytes were purchased from DRK-Blutspendedienst after informed consent and approval of local government regulatory authorities. All other cell lines were purchased from the German Collection of Microorganism and Cell Culture (DSMZ).

Table 11: Cell lines used for experiments

Cell line	Location	Age, sex	pre-treatment	Relevant mutations/ Pathway functionality	Source
A4573	unknown	17, f	unknown	unknown	ATCC
A673	unknown	15, f	unknown	p53: non-function ²⁵⁰ RB/E2F: functional ¹⁵¹	ATCC
MHH-ES1	Peritoneal metastasis	12, m	unknown	unknown	DSMZ
SK-N-MC	retroorbital metastasis	12, f	post-chemo (VCDA)	p53: non-function ²⁵⁰ RB/E2F: non-functional ¹⁵¹ RB1 (missense: p.R698S) ¹⁵¹	DSMZ
SB-KMS-KS1	Extra-osseous metastasis	17, f	unknown	unknown	TUM
TC32	ileum, soft tissue	17, f	at diagnosis	p53: functional ²⁵⁰ RB/E2F: functional ¹⁵² RB1 (splice site: p.P776R) ²⁰	CCR

Table 12: Cell lines used for experimental support

Cell line	Used for	Source
Healthy PBMCs	Feeder cells, generation of monocyte-derived DCs and TCR-transgenic T cells	DRK-Blutspendedienst
HEK293	Adenovirus production, hexon titer test	Per Sonne Holm
LCL	Feeder cells, T cell expansion	DSMZ
NSO_{IL-15}	in vivo experiments, IL-15 secretion	Stanley Riddell
(293Vec-) RD114	Packaging cell line, retrovirus production	Manuel Caruso
THP-1	DC maturation, T cell proliferation assay	DSMZ

3.1.9 Antibodies

3.1.9.1 Antibodies for Flow Cytometry

Table 13: Antibodies for flow cytometry – anti-human

Specificity	Fluorochrome	Clone	Concentration	Company
CAR	FITC	E1-1	1 μ g/10 ⁶ cells	Santa Cruz Biotech
CD3	PE-Vio770	REA613	1:100	Miltenyi Biotech
CD4	FITC	SK3	1:100	BD Biosciences
CD4	APC-Vio770	REA623	1:100	Miltenyi Biotech

CD8	APC	RPA-T8	1:100	BD Biosciences
CD8	FITC	REA734	1:100	Miltenyi Biotech
CD25	APC	REA579	1:100	Miltenyi Biotech
CD11c	APC	B-ly6	1:50	BD Biosciences
CD40	VioBright FITC	REA733	1:100	Miltenyi Biotech
CD45	VioGreen	REA747	1:100	Miltenyi Biotech
CD45	APC	REA747	1:100	Miltenyi Biotech
CD47	FITC	REA220	1:100	Miltenyi Biotech
CD54 (ICAM-1)	PE	REA266	1:100	Miltenyi Biotech
CD80	PE	REA661	1:100	Miltenyi Biotech
CD83	APC-Vio770	REA714	1:100	Miltenyi Biotech
CD86	VioBlue	REA968	1:100	Miltenyi Biotech
CHM1-multimer	PE	-	1:100	Busch Lab
HLA-ABC	APC	REA230	1:100	Miltenyi Biotech
HLA-ABC	PerCP-Vio700	REA230	1:100	Miltenyi Biotech
HLA-A2	FITC	BB7.2	1:100	BD Biosciences
HLA-DR	APC	REA804	1:100	Miltenyi Biotech
HLA-DR	PE-Vio770	REA805	1:100	Miltenyi Biotech
CD183 (CXCR3)	PE	REA232	1:100	Miltenyi Biotech
CD273 (PD-L2)	APC-Vio770	REA985	1:100	Miltenyi Biotech
CD274 (PD-L1)	APC	REA1197	1:100	Miltenyi Biotech
CD274 (PD-L1)	VioBright B515	REA1197	1:100	Miltenyi Biotech
CD279 (PD-1)	APC	PD1.3.1.3	1:100	Miltenyi Biotech
Ctrl Mouse IgG _{1,κ}	APC	X40	1:100	BD Biosciences
Ctrl Mouse IgG _{1,κ}	FITC	X40	1:100	BD Biosciences
Ctrl Mouse IgG _{1,κ}	PE	X40	1:100	BD Biosciences
Ctrl Mouse IgG _{2a,κ}	FITC	G155-178	1:100	BD Biosciences
REA Ctrl	APC	REA293	1:100	Miltenyi Biotech
REA Ctrl	FITC	REA293	1:100	Miltenyi Biotech
REA Ctrl	VioBright B515	REA293	1:100	Miltenyi Biotech
STEAP1-multimer	PE	-	1:100	Busch Lab

Table 14: Antibodies for flow cytometry/purification – anti-mouse

Specificity	Fluorochrome	Clone	Concentration	Company
CD11b	VioBright FITC	REA592	1:100	Miltenyi Biotech
CD45	PE-Vio770	REA737	1:100	Miltenyi Biotech
CD279 (PD-1)	APC	REA802	1:100	Miltenyi Biotech
F4/80	PE	REA126	1:100	Miltenyi Biotech
Ly6C	VioGreen	REA796	1:100	Miltenyi Biotech
Ly6G	PerCP-Vio700	REA526	1:100	Miltenyi Biotech
MHC Class II (I-Ab)	APC-Vio770	REA528	1:100	Miltenyi Biotech
TCR β chain	PE	H57-597	1:100	BioLegend

Table 15: Antibodies for flow cytometry – intracellular staining (human and mouse)

Specificity	Fluorochrome	Clone	Concentration	Company
FoxP3	PE	3G3	1:13	Miltenyi Biotech
GATA3	APC	REA174	1:13	Miltenyi Biotech
ROR γ (t)	APC	REA278	1:13	Miltenyi Biotech
T-bet	PE	REA102	1:13	Miltenyi Biotech

Table 16: Further dyes and solutions used for flow cytometry

Application	Dye/Name	REF	Concentration	Company
Cell proliferation	eFluor450	65-0842-85	According to protocol	Thermo Fisher Scientific
Dead cell exclusion	DAPI staining solution	130-111-570	1:100	Miltenyi Biotech
Dead cell exclusion	Propidium iodide (PI= solution	130-093-233	1:100	Miltenyi Biotech
Dead cell exclusion	Viability 405/520 Fixable Dye	130-109-814	According to protocol	Miltenyi Biotech

3.1.9.2 Antibodies for Western blotting (WB), hexon titer test (HTT), immunofluorescence (IF), and flow cytometry (non-conjugated)

Table 17: Antibodies for WB, HTT, IF and flow cytometry (non-conjugated)

Specificity	REF	Concentration	Method	Company
Adenovirus-2/5 E1A	Sc-25	1:500	WB	Santa Cruz Biotech
Adenovirus (hexon)	AB1056	1:1000	HTT, WB	Merck Millipore
AlexaFluor488 goat anti-mouse IgG (H+L)	A11029	1:250	IF, FlowCy	Thermo Fisher Scientific
AlexaFluor594 goat anti-rabbit IgG (H+L)	A11012	1:250	IF	Thermo Fisher Scientific
Anti-mouse IgG κ -HRP	Sc-516102	1:1000	WB	Santa Cruz Biotech
Calreticulin	MAB38981	0.25 μ g/10 ⁶ cells	FlowCy	R&D Systems
CXCL10	Sc-101500	1:100	WB	Santa Cruz Biotech
E2F1	3742S	1:500	WB	Cell Signaling Technology
E2F1	Sc-251	1:250	IF	Santa Cruz Biotech
GAPDH	2118S	1:2000	WB	Cell Signaling Technology
HLA A+B	EPR1394Y		1:2000	Abcam
HLA G	EXB-1B-499-C025	1:500	WB	Exbio
MIF	Sc-271631	1:250	WB	Santa Cruz Biotech
MmTC	MAB141700			
Mouse anti-rabbit IgG-HRP	Sc-2357	1:1000	WB	Santa Cruz Biotech
Mouse IgG _{2a} Isotype Control	MAB0031	1:250	FlowCy	R&D Systems
p21	12D1	1:1000	WB	Cell Signaling Technology
p-RB	D59B7	1:1000	WB	Cell Signaling Technology
Rabbit anti-goat IgG-HRP	P0449	1:1000	HTT	Dako
RB	554136	1:500	WB	BD Biosciences
YB-1	EP2708Y	1:2000	WB, IF	Abcam

3.1.10 Primer sequences for semi-quantitative PCR experiments

All primers were ordered from Metabion. Mouse specific primer sequences for CXCL10, IL1B, TGFB1, MMP9 were used from Castro et.²⁵¹, ARG1 primers were designed by Caroline Schöning and HLA-A by Busheng Xue using Premier Primers software, NOS2 sequences are from Misson et al.²⁵². Sequences for fiber and β actin were kindly provided by Prof. Per Sonne Holm. Mouse GAPDH primers are from Leiro et al.²⁵³ Human CXCL10, HLA-B, and GAPDH primers are from PrimerBank (<https://pga.mgh.harvard.edu/primerbank/>).

Table 18: Primer Sequences

Name	Specificity	Forward 5'-3'	Reverse 5'-3'
ARG1	mouse	AAC ACG GCA GTG GCT TTA AC	GGT TTT CAT GTG GCG CAT TC
CXCL10	human	GTG GCA TTC AAG GAG TAC CT	TGA TGG CCT TCG ATT CTG GA
CXCL10	mouse	AAG TGC TGC CGT CAT TTT CT	TCT TTT TCA TCG TGG CAA TG
Fiber DNA	human Ad	AAGCTAGCCCTGC AAACATCA	CCCAAGCTACCAGTGGCAGTA
GAPDH	human	CTC TGC TCC TCC TGT TCG AC	ACG ACC AAA TCC GTT GAC TC
GAPDH	mouse	ACC GCA TCT TCT TGT GCA GT	GCC AAA GTT GTC ATG GAT GA
HLA-A	human	TCA CCC TGA GAT GGG AGC	ATG TGG AGG AGG AAG AGC T
HLA-B	human	CAG TTC GTG AGG TTC GAC AG	CAG CCG TAC ATG CTC TGG A
IL1B	mouse	ACG GAT TCC ATG GTG AAG TC	GAG TGT GGA TCC AAG CAA T
MMP9	mouse	CAC CAC CAC AAC TGA ACC AC	CTC AGA AGA GCC CGC AGT AG
NOS2	mouse	CAG CTG GGC TGT ACA AAC CT	CAT TGG AAG TGA AGC GTT TC
TGFB1	mouse	TGC GCT TGC AGA GAT TAA AA	GCT GAA TCG AAA GCC CTG TA
β actin	human	TAA GTA GGT GCA CAG TAG GTC TGA	AAA GTG CAA AGA ACA CGG CTA AG

3.1.11 Small molecule inhibitors

Following inhibitors were used for *in vitro* experiments: abemaciclib (LY, LY2835219), nutlin-3a, palbociclib (PD, PD0332991), ribociclib (LEE, LEE011) and 10 μ M stocks were generated according to supplier's instruction using DMSO. All inhibitors were ordered from Selleck Chemicals. Ribociclib (succinate) for *in vivo* studies was purchased from MedChem Express and resuspended in 0.5% methylcellulose for oral gavage, according to manufacturer's recommendation. Chemical compounds were stored at -20°C.

3.1.12 Retroviral TCR constructs

Identification of TCR V α and V β -chains of TCRs specific for STEAP1¹³⁰ and CHM1³¹⁹ in the context of HLA-A*02:01 as well as synthesis of retroviral TCR constructs with TCR modifications (codon optimization, murinization) was described by colleagues of this laboratory before^{126, 127, 129}.

3.2 Methods

3.2.1 Ethical considerations

This study was conducted in accordance with the Declaration of Helsinki and approved by the German regional regulatory government authorities. Isolation of PBMCs from healthy donors and generation of TCR transgenic T cells was approved under permission number 50-8791-139.754.2122. Animal experiments were approved under permission numbers: 55.2-2532.Vet_02-15-102, 55.2-2532.Vet_02-17-225, 55.2-2532.Vet_02-20-165.

3.2.2 Cell biology techniques

3.2.2.1 Cell culture

The culture media used for specific cell types are described in [Table 9](#). All cell lines were kept in a humidified incubator (37°C, 5% CO₂). Cells were passaged when reaching confluency of 80-90% (for adherent cells). Non-adherent cells were kept at concentration of $\sim 2 \times 10^6$ /mL. Heat-inactivated FCS or huAB serum was used as cell culture supplement.

Specific T cell medium (Table 9) was utilized for culturing (TCR transgenic) T cells. Culture medium for CD4⁺ T cells was replenished with 50 U/mL IL-2 and 5 ng/mL IL-7, or 100 U/mL IL-2 and 2 ng/mL IL-15 for CD8⁺ T cells.

Cell lines were routinely tested for mycoplasma contamination (MycoAlert Mycoplasma Detection Kit) according to manufacturer's protocol.

3.2.2.2 Isolation of peripheral blood mononuclear cells (PBMCs)

Health donor buffy coats were purchased from DRK-Blutspendedienst and peripheral mononuclear cells (PBMCs) were isolated by centrifugation with a density gradient using Ficoll-Paque according to manufacturer's instruction and as previously described²⁵⁴. In case of red blood cell contamination, after harvesting of the PBMC fraction, consecutive erythrocyte lysis was performed using ACK Lysis Buffer.

3.2.2.3 Generation of monocyte-derived dendritic cells (moDCs)

As previously described¹²⁶, CD14⁺ monocytes were purified from fresh PBMC using the Anti-Human CD14 Magnetic Particles kit and the BD Cell Separation Magnet according to supplier's instructions. Then, CD14⁺ cells were cultured in DC medium (Table 9) supplemented with 1000 U/mL IL-4 and 800 U/mL GM-CSF to induce DC differentiation. After 3 days, cytokines were renewed before immature DCs (imDCs) were used for experiments on day 5. DC maturation (as control) was induced for another 2 days by a maturation cocktail (MC) containing: 10 ng/mL IL-1 β , 1000 U/mL IL-6, 10 ng/mL TNF, and 1 μ g/mL PGE₂. For the generation of THP-1-derived imDC, IL-4 and GM-CSF in identical concentrations was used.

3.2.2.4 Generation of tumor-conditioned medium

1.5x10⁵ tumor cells were seeding in 6-well plates. 24 hours(h) afterwards, cells were treated with inhibitor or infected with virus. In case, the combination of CDK4/6i and XVir-N-31 was assessed, virus infection was performed 24h after addition of the inhibitor/mock. 48h post infection (hpi), supernatant was collected, centrifuged (Multifuge 3SR, 2200 rounds per minute (rpm), 5 min) and stored at -80°C until further usage.

3.2.2.5 Generation of TCR transgenic T cells

For generation of STEAP¹³⁰/HLA-A*02:01-specific TCR-transgenic CD4⁺ and CD8⁺ T cells, T cell subset were positively isolated from fresh HLA-A*02-negative donor PBMC with respective Dynabead Positive Isolation Kits and the BD Cell Separation Magnet in accordance with manufacturer's protocols. Here, T cells were activated with anti-CD3/CD28 Dynabeads (pre-washed 25 γ L/10⁶ cells in 24-well plates), as previously described²⁵⁴. For the generation of CHM1³¹⁹/HLA-A*02:01-specific TCR-transgenic T cells, the CD8⁺ subset was negatively isolated with the 'untouched' CD8⁺ T cell Isolation Kit using recommended MidiMACS and QuadroMACS magnets as well as LS columns from Miltenyi Biotech according to supplier's instructions. Here, T cell activation was performed with 50 ng/mL OKT3.

Introduction of respective TCR transgenes were performed with a retroviral infection system as previously published^{127, 129}. In short, 3x10⁵ RD114 packaging cells (plated in 6-well plates the day before) were transfected with TCR encoding retroviral plasmids (1 μ g plasmid together with 9 μ L TransIT/well). 2 and 3 days afterwards, retrovirus-containing supernatant was collected and used for T cell transduction. Transduction was performed by centrifugation (2200 rpm, 90 min, 32°C) of ~10⁶ T cells (activated 2 days before) in Retronectin-coated 24-well plates (5 μ g Retronectin/well, non-tissue) supplemented with cytokines, 1% HEPES, and 4 μ g/mL protamine sulfate.

Transduction efficacy was evaluated by flow cytometry using STEAP1- or CHM1-specific multimers, compared to irrelevant multimers (kindly provided by the laboratory of Prof. Dr. Dirk Busch, Busch Lab), as previously published^{126, 127, 255}. To obtain purities of $\geq 95\%$, TCR-transgenic T cells were further enriched by Anti-PE Microbeads with the MidiMACS magnet and respective columns according to manufacturer's protocol, after specific multimer-staining (PE). After enrichment, transgenic T cells were expanded with 5×10^6 irradiated LCL (100 Gray, Gy) and 2.5×10^7 irradiated PBMCs (30 Gy, pooled from 5 different donors) in 25 mL T cell medium. Cytokines were supplemented every 2-3 days. Irradiation of cells was performed with BioBeam8000.

3.2.2.6 Generation of adenovirus constructs

XVir-N-31 was designed by Prof. Per Sonne Holm and produced by Klaus Mantwill. They kindly provided the virus for all *in vitro* and *in vivo* studies. Their laboratory also kindly supplied adenovirus wildtype, which was originally obtained from Prof. David Curiel (Washington University, St. Louis, Missouri). The E1-deleted adenovirus vector expressing GFP under the control of a CMV promoter and additional RGD, was also provided by Prof. Per Sonne Holm and Klaus Mantwill. All adenovirus constructs were produced in HEK293 cells and purified by CsCl-gradient centrifugations (2 consecutive times) followed by chromatography-based size-exclusion using disposable PD-10 desalting columns (GE Healthcare).

3.2.2.7 Infection of cell lines with adenoviruses

For infection, cells were plated in 10cm, 6- or 24-well plates. In case, inhibitors treatment was used in combination, desired concentrations of inhibitors were added 24h before virus infection and afterwards (only nutlin-3a was discontinued after infection). Desired multiplicities of infection (MOI, i.e. IFU/mL, previously established by a hexon titer test) were added in 2 mL, 500 μ L, or 150 μ L serum-free medium for 1h (with gentle pivoting every 15 min). Afterwards, standard medium was replenished. Cells or supernatant were further processed at specific time points as indicated in respective experiments or figure legends.

3.2.2.8 Determination of adenovirus particles

Quantification of adenoviral viral infectious units (IFU) was done with a hexon titer test (HTT). Formation of infectious particles was assessed by immunohistochemistry staining of virus-infected HEK293 cells (in a serial dilution) which were seeded in 24-well plates and infected at the same time. At ~ 44 hpi, cells were fixed with ice-cold methanol and stained with a primary goat-anti-hexon antibody and a horseradish peroxidase (HRP)-conjugated secondary rabbit-anti-goat antibody (Table 17) and developed with the Liquid DAB (3,3'-diaminobenzidine in chromogen) + Substrate Chromogen System. Positively stained cells were counted (10 random fields across the well) and viral titer was determined as IFU/mL with following formula: (average number of stained cells/field*fields/well)/(volume of diluted virus per well (mL)* dilution factor). Methodological comparison of hexon titer tests was ensured.

De novo production of XVir-N-31 in EwS cell lines was assessed at indicated time points. Here, supernatant and cells were collected after the use of a cell scraper, viral particles were released from intact cells by multiple thaw-freeze cycles, followed by centrifugation (1600rcf, 10 min). Afterwards, supernatant was serially diluted and used to infect HEK293 in duplicates.

3.2.2.9 Flow Cytometry

Cell cycle analysis

Cell cycle state of EwS cell lines was assessed by flow cytometry using PI. Here, 2×10^5 cells were plated in 6-well plates and treated with different concentrations of inhibitors the day

afterwards. After another 24h, cells were washed with sample buffer ([Table 8](#)), then fixed with 70% ice-cold EtOH (drop-wise addition and continuous vortexing) and stored for at least 18h at -20°C. After thawing, cells were centrifuged and resuspended in 1mL staining buffer ([Table 8](#)) and incubated for 30 min, at room temperature before acquisition in a FACSCalibur flow cytometer.

Analysis of cell surface markers

Cells in single cell suspension were stained in 96-well plates in PBS with primary fluochrome-coupled antibodies. When using REA antibodies from Miltenyi Biotech ([Table 13](#)) a minimum incubation period of 15 min (at 4°C), otherwise antibody staining of 30 min was ensured. Staining concentration for respective antibodies are also given in [Table 13](#), usually in regard to total staining volume. A maximum of 2×10^6 cells per well were stained with REA antibodies (xenografts), usually cell numbers from *in vitro* experiments ranged from $5-20 \times 10^4$ cell per staining. For multicolor staining panels (all in *in vivo* experiments and all *in vitro* DC maturation and T cell activation experiments) auto-compensation with specific REA-compensation beads according to Miltenyi's recommendation was performed. Dead cell exclusion was ensured by either DAPI, PI (added right before acquisition) or the fixable Viobility 405/520 dye (staining together with surface markers, according to manufacturer's protocol).

When indicated, isotype staining with respective fluorophore was performed, or fluorescence-minus one (FMO) controls were used. Anti-CALR staining was done with an uncouple primary mouse antibody (controlled with monoclonal IgG_{2a} isotype), which was incubated at room temperature for 30 min, followed by a washing step and consecutive staining with a secondary AlexaFluor488 goat-anti-mouse IgG antibody for another 30 min at 4°C. All cells were washed with PBS after staining before acquisition.

Analysis of intracellular transcription factors

For intracellular analysis of transcription factors, first surface staining (together with fixable Viobility dye) was performed, as described above. Afterwards, cells were permeabilized and fixed for 30 min (4°C) and stained for T cell subset-specific transcription factors afterwards ([Table 15](#)). Here, specific kits from Miltenyi containing fixation/permeabilization buffer and specific solution were used according to supplier's recommendation ([Table 6](#)).

Cells for analysis of surface markers, transcription factors and T cell proliferation were acquired with MACSQuant Analyzer 10.

Data analysis and gating strategy

All fcs raw data was processed using FlowJo. Following gating strategy was applied in all analyses: doublet discrimination in FSC-H vs FSC-A → identification of cells in SSC-A vs FSC-A → dead cell exclusion using DAPI (V1 vs V2) PI (B3 vs B2) or Viobility dye (V2 vs V1 or B1). When several populations were present, specific cells were identified as follows: human T cells by double-positivity for CD45/CD3 (or CD3/CD4 or CD3/CD8), human tumor cells by mouse and humane double-negativity for CD45, mouse myeloid cells by CD45/CD11b double-positivity, neutrophils by Ly6G positivity in myeloid population, monocytes by Ly6C high-positivity in Ly6G-negative myeloid population, and macrophages by F4/80 positivity in Ly6C/Ly6G double-negative myeloid cells. If specific marker expression in aforementioned subsets was analyzed, isotype controls or FMO controls were used.

3.2.2.10 Phagocytosis assay

GFP-expressing A673 cells, were retrovirally transduced with a GFP-expressing vector by Josefine von Oven. The pMP71_GFP-vector was a kind gift of Prof. Dr. med. Angela

Krackhardt (Medizinische Klinik III, Klinikum rechts der Isar, TUM). After flow cytometric validation of transduction efficacy, GFP-expressing tumor cells were sorted at the Department of Microbiology (Klinikum rechts der Isar, TUM) with FACS Aria

Phagocytosis of GFP-transduced A673 cells was analyzed via flow cytometry in 96-well plates after a 4-h-coculture-period of THP-1-derived and monocyte-derived imDCs. A673 cells were infected 48hpi prior coculture at indicated MOI. Tumor cells were considered as phagocytosed when staining double-positive for GFP and a monocyte/lymphocyte-lineage specific marker, such as CD11c-APC or CD45-APC. Each experiment was performed in biological replicates, as further specified in figure legend.

3.2.2.11 T cell proliferation assay

After culturing THP-1 in CM for 72h and maturation state via flow cytometry was assessed, THP-1 cells were pulsed with 10 $\mu\text{g}/\text{mL}$ peptide and 20 $\mu\text{g}/\text{mL}$ β_2 -microglobulin for 4h at 37°C and washed afterwards before CHM1³¹⁹/HLA-A*02:01-specific TCR-transgenic CD8⁺ T cells were added at a 2:1 ratio in T cell medium containing 30 U/mL IL-2. CHM1³¹⁹-peptide (VIMPCSWWV) and influenza-peptide (GILGFVFTL, as control, when indicated) were used for pulsation. Before start of coculture, T cells were labeled with 10 μM eFluor450 dye according to manufacturer's recommendation and washed 3 times before adding to peptide-pulsed THP-1 cells. T cell proliferation/activation was assessed 96h after start of coculture via flow cytometry after dead cell exclusion with DAPI or Viability dye.

3.2.2.12 xCELLigence Assay

Virus- and/or T cell-mediated cytotoxicity was also studied by the xCELLigence assay installed in an incubator, which allows continuous detection of adherent cell growth by impedance-based measurement. Cytotoxicity of T cells and OAd can be detected by detachment of adherent tumor cells after addition of effector cells or virus infection in a time-dependent manner. Here, $1\text{-}2 \times 10^4$ tumor cells were plated in specific E plates (96 wells) in triplicates or quadruplicates and therapeutic cells or virus was added at indicated timepoints at different effector-to-target ratios and different MOI. Virus infection was performed at a cell index of $\sim 0.5 - 1$ and T cells were added at a cell index of $\sim 1 - 2$.

3.2.2.13 Histopathology

For analyzing metastatic tumor spread in the *in vivo* model of experimental metastasis, liver and lungs from mice were fixed with 4% buffered formaldehyde (Table 10). Paraffin-embedding and staining for hematoxylin/eosin (HE) was done by Prof. Dr. med. Thomas Grünwald at the Institute of Pathology of the Ludwig Maximilian University (LMU) of Munich. Then, the percentage of tumor involvement of each organ from a representative slide per animal was assessed and calculated in organ overview at 4x magnification.

3.2.2.14 Immunofluorescence (IF) staining

$2\text{-}4 \times 10^4$ EwS cells were plated in ibidi μ -slide and fixed 24-36h afterwards using 4% buffered formaldehyde (30 min), followed by permeabilization (10 min) and blocking for 1h at room temperature (Table 10). Primary antibodies were diluted in 0.5% nonfat milk in TBS-T (Table 17) and incubated in a humidified, dark chamber over night at 4°C. Secondary fluorochrome-coupled antibodies (Table 10) were added also in 0.5% milk in TBS-T at room temperature for 30 min. After a consecutive staining step with DAPI (1:5000 in MeOH) for 10 min in the dark, followed by washing of cells, they were acquired and photographed with a Axiovert 100 microscope using fluorescent light with 100x magnification.

3.2.3 Molecular biology techniques

3.2.3.1 DNA and RNA isolation

Genomic DNA, for the assessment of viral genomic copies, was isolated using the DNeasy Blood & Tissue Kit and RNA, for reverse transcription and microarray analysis, was isolated using RNeasy Mini Kit according to manufacturer's protocols. Afterwards, concentrations of DNA and RNA were determined by NanoPhotometer measurement before further processing.

3.2.3.2 Reverse transcription

To analyze gene expression, RNA was transcribed into complementary DNA (cDNA) using the High-Capacity cDNA Reverse Transcription Kit with a total volume of 20 μL containing 2 μL dNTP mix (100 mM), 1 μL MultiScribe Reverse Transcriptase (50 U/ μL), 2 μL random primers (10x), 2 μL buffer (10x), and 1 μg RNA in 14.2 μL ddH₂O. The reverse transcription program in the iCycler consisted of 3 steps: (1) Initiation at 25°C for 10 min, (2) Elongation at 37°C for 120 min, and (3) Inactivation at 85°C for 5 min.

3.2.3.3 Semi-quantitative Real Time PCR (sqPCR)

SqPCR was used to determine viral genomic copies (*fiber DNA*) and to assess gene expression after reverse transcription (RT). For detection adenoviral genomic copies and gene expression of human genes from xenograft experiments 50ng genomic or cDNA per reaction were used. For the detection of mouse immune cell genes 375ng of cDNA was used for sqRT-PCR due to the relative low numbers of tumor-infiltrating mouse cells. Total reaction volume adjusted in 96-well MicroAmp Fast Optical Reaction Plates was 15 μL , comprised of 7.5 μL GoTaq qPCR master mix, 0.75 μL of forward and reverse primers each, 1 μL of DEPC-H₂O and 5 μL of genomic or cDNA in DEPC-H₂O. Plates were sealed, centrifuged, and analyzed. Reaction and recording of fluorescence (with respective *cycle threshold* ct values, indicating the cycle number when excess of fluorescence intensity was significantly higher than background), were done in a StepOnePlus Real-Time PCR System, according to manufacturer's recommendation, using settings described in [Table 19](#). A melting curve analysis was performed to confirm specific PCR products.

Table 19: sqPCR protocol

Step	Process	Temperature	duration
1	Initiation	94°C	90 sec
2	Denaturation	94°C	15 sec
3	Annealing	60°C	15 sec
4	Polymerase activity (go to step 2, 40x)	72°C	15 sec

Relative quantification of synthesized products was performed using the Pfaffl method²⁵⁶:

Relative normalized gene expression = $2^{-\Delta\Delta\text{ct}}$, whereas $\Delta\text{ct} = \text{ct}(\text{gene of interest}) - \text{ct}(\text{house-keeping gene})$ and $\Delta\Delta\text{ct} = \Delta\text{ct}(\text{treated condition}) - \text{ct}(\text{control condition})$

3.2.3.4 Determination of viral genomic copies

Viral genomic DNA *in vitro*, indicative for viral replication, was studied using sqPCR with specific *fiber DNA* primers, applying the $\Delta\Delta\text{ct}$ method (3.2.3.3), normalized to β actin ([Table 18](#)), and compared to viral DNA 4hpi (i.e. entry levels). To assess viral genomic DNA from explanted tumors (*in vivo* experiments), *fiber DNA* was normalized to β actin, applying Δct analysis.

3.2.3.5 Knock-down experiments

siRNA-mediated knock-down experiments were performed using small inhibitory RNA, namely siE2F1 (Sigma-Aldrich: SASI_Hs01_00162220), siRB (Qiagen: SI0007091), and scramble siRNA (Qiagen: 1022076) to transfect cells in 6-well plates or 10cm dishes using Lipofectamine RNAiMAX Transfection Reagent together with Opti-MEM according to manufacturer's instructions with final concentrations of siRNAs of 25pmol. Knock-down for specific targets was confirmed by immunoblotting ([3.2.3.7](#)) after overnight transfection and afterwards adenovirus infection was performed as described in [3.2.1.7](#).

3.2.3.6 Microarray analysis

Microarrays were generated at our facility as previously described^{121, 257} (see www.affymetrix.com for the detailed protocol). Microarray chips were generated by Caroline Schöning, Dr. rer. nat. Kristina von Heyking and Jennifer Eck. Affymetrix Human Gene 1.0 ST microarrays were used for sample hybridization. CEL files were read using *brainarray cdf*. Before data analysis robust chip average (RMA) normalization and background correction was performed. An R script for data analyses was kindly provided by Carolin Prexler, a PhD bioinformatic student in our laboratory. Pathway analysis was performed with the online open-access analysis tool Reactome (reactome.org).

3.2.3.7 Western blot analysis

Cells were lysed on ice using a protein lysis buffer ([Table 7](#)). For *in vitro* experiments $\sim 2 \times 10^6$ cells and for explanted xenografts $3\text{-}5 \times 10^6$ cells (single cell suspension after mechanical and enzymatic dissociation) were used. Lysates were homogenized by sonification and sheared (27G needle) thoroughly before centrifugation at 30,000rcf (4°C) for 30 min. Protein concentration in respective supernatant was measured using the Pierce BCA Protein Assay Kit according to supplier's recommendation. After equalization of protein concentration in protein loading buffer (supplemented with 100 μL 1M DTT to 500 μL buffer) and boiling (5 min, 100°C), samples were either stored at -80°C or used directly for immunoblotting. Therefore, samples (with protein concentration of 20-40 μg per lane) were loaded into pockets of SDS gels ([Table 7](#)) and separated at 75-90 Volt in running buffer. Afterwards, proteins were transferred onto PVDF membranes, which were activated before in MeOH for ~ 2 min, with transfer buffer soaked Whatman papers connecting up with the electrodes of the semi-dry blotting system. Membranes were blocked with 5% nonfat dry milk in TBS-T. Protein band were detected with specific antibodies ([Table 17](#)) and the Amersham ECL Western Blotting Reagent Pack and visualized with the Gel Logic 1500 luminometer.

3.2.3.8 Multiplex Chemo-/Cytokine Assay

For *in vitro* screening assays, the Human Cytokine Screening 48-Plax Panel was used. To analyze chemo-/cytokines present in the TME, the Human ProcartaPlex Mix&Match 7-plex (containing IL-29, IL-8, CXCL10, LAP, MIF, SCGF beta, TNF alpha) was utilized. Both panels were used according to supplier's recommendations and samples we acquired with a Bio-Plex 200 System (Luminex 200). Supernatant from *in vitro* experiments was prepared as described in [3.2.1.5](#) at different MOI and time point, specified in figure legend. To assess chemo-/cytokine levels in the TME, tumors were mechanically dissected with a scalpel (no. 10) in PBS. Afterwards, cell suspension was centrifuged, and supernatant was stored (as described in [3.2.1.5](#)) at -80°C until measurement.

3.2.4 Animal experiments

In vivo setups

Different animal experiments were performed for this study, all approved by local authorities (also see [3.2.1 Ethical Considerations](#)). Rag2^{-/-}γc^{-/-} mice (BALB/c background) were bred in our animal facility at Klinikum rechts der Isar (TranslaTUM) under pathogen-free conditions. Rag2^{-/-}γc^{-/-} mice were initially obtained from the Central Institute of Experimental Animals (Kawasaki, Japan). Experiments were performed in 12-30-week-old mice, both male and female. Experiments in female nude mice (NMRI-Foxn1nu/nu), purchased from Charles River Laboratories, were performed at an age of 10-20 weeks. For assessment of subcutaneous tumor growth (tumor volume), tumor cells were injected into the right and/or left flank as single cell suspension in PBS. Specific numbers of injected tumor cells are given in respective figure legends. When tumors reach a certain volume (also further specified in the result section), measured by caliper (volume = 0.5 x length x width²), animals were randomly assigned to indicated treatment groups and therapy was initiated. CDK4/6i was administered by oral gavage using specific, flexible plastic feeding tubes (Instech Laboratories). Tumor-HLA-matched healthy donor non-specific PBMCs (matched for HLA-A2) were prepared as described in [3.2.2.2](#) for humanization, when indicated. For further introduction of peptide/HLA-A*02:01-specific TCRs, HLA-A2-negative PBMCs were used and generated as described in [3.2.2.5](#). IL-15-producing NSO cells were irradiated with 80 Gy prior to application. Both T cells and NSO cells were injected intraperitoneally (i.p.). Transferred cell numbers and intervals are given at each section.

STEAP1¹³⁰/HLA-A*02:01-TCR transgenic T cells were tested in 2 different setting, after a culturing and expansion period of ~ 6 weeks. For s.c. tumor growth, mice were irradiated with 3.5 Gy once the tumor was palpable (~ 3 days after tumor inoculation with 2x10⁶ A673 cells) and randomly divided into treatment/control groups: (1) 1x10⁷ non-specific PBMCs, (2) 5x10⁶ transgenic CD4⁺ T cells together with 5x10⁶ CD4-depleted non-specific PBMCs, (3) 5x10⁶ transgenic CD8⁺ T cells together with 5x10⁶ CD8-depleted non-specific PBMCs, and (4) 2.5x10⁶ transgenic CD4⁺ T cells together with 2.5x10⁶ transgenic CD8⁺ T cells and 5x10⁶ non-specific PBMCs. Mice also received 10⁷ IL-15-producing NSO cells biweekly until the end of experiment at day 17. For experimental metastasis, assessing the effect of therapeutic STEAP1-specific T cells on metastatic organotropism, mice were irradiated (3.5 Gy) one day prior to tail vein-injection of both 2.5x10⁶ A673 cells and T cells (groups 1-4, as described above), combined with biweekly i.p.-injections of 1x10⁷ irradiated NSO cells. 30 days after tumor/T cell injection mice were sacrificed, organs were explanted (spleen, lung, and liver), and fixed in 4% buffered formaldehyde ([Table 10](#)).

Bioluminescence monitoring of implanted tumor cells

Tumor control of firefly luciferase-expressing A673-Luc (after s.c.-implantation) with STEAP1-specific T cells was assessed as described above. A673-Luc was transfected in our lab before. Total photon flux (maximum; at 3-10 min after luciferin administration, i.p. 150 mg luciferin/kg body weight) was measured at indicated time points at the Institute of Molecular Immunology and Experimental Oncology (TUM), after introduction by PD Dr. rer. nat. Wohlleber to the IVIS Lumina LT-Series III instrument (exposure time of 10s). For acquisition, mice were shortly anesthetized with 2% isofluran.

Harvesting and processing of tumors and organs

Mice were sacrificed at the end of experiment by isofluran narcosis and cervical dislocation. Experiments were stopped when s.c. tumor reached a tumor volume of ≥ 1 cm³, deterioration

in well-being, such weight loss, increased frequency of breathing, decreased movement, changes in flight reactions, and others, as defined in respective approvals from local government regulatory authorities. Depending on desired read out, explanted tumors/spleens were cut into half (one part fixed in 4% buffered formaldehyde) or mechanically dissected with a scalped (No.10) as a whole in 4mL PBS. Next, 0.5mL of the tumor cell suspension was stored at -20°C for DNA isolation and sq-PCR analyses. Then, supernatant was stored at -80°C after centrifugation (2200 rpm, 5 min, for multiplex chemo-/cytokine analyses) followed by the addition of 1mL tumor digestion buffer ([Table 10](#)) for enzymatic dissociation and incubation of samples at 37°C for 30 min. Afterwards, samples were filtered (70 μ m) and washed in standard medium before distribution for further RNA and protein isolation, flow cytometry and cryopreservation. Spleens for flow cytometry analysis were treated comparably. All steps were performed on ice, if not indicated otherwise.

3.2.5 Computational analyses

3.2.5.1 Statistical analysis

Statistical analysis was performed using Prism 9. For values with normal distribution, student's t-tests and ordinary one-way or two-way analysis of variance (ANOVA) in combination with Tukey's multiple comparison methods were conducted, as indicated in figure legends. For arbitrarily distributed values, Kruskal-Wallis and Mann-Whitney U test were applied, simple linear and non-linear regression modelling was used to identify correlations, further specified in respective figure legends. Survival differences were analyzed using the Mantel-Cox log-rank test. Levels of significance are given as asterisks. Analyses were performed with Prism 9.

3.2.5.2 Bioinformatic analysis

Bioinformatic analyses were supported by Carolin Prexler (PhD student in bioinformatics) who kindly provided an R-based analysis algorithm for microarray data. For publicly available data, raw expression datasets were download from the GEO database. Then RMA normalization and background correction was computed and annotation using brainarray cdf (ENTREZG) was performed. The CIBERSORT online-tool (cibersort.standord.edu) was used to analyze relative immune cell populations in publicly available data applying standard setting (LM22-ref-sample, 100 permutations). Relative values were exported in excel and grouped towards CXCL10 expression levels as specified in the figure legends and analyzed with Prism 9. SynergyFinder Plus installation in R and performance of analysis was performed according to recommendation (<https://synergyfinder.org>)²⁵⁸.

4 Results

4.1 Innate and adaptive antitumor immunity against EwS

4.1.1 Transcriptome-based analysis reveals CXCL10 expression as a possible determinant for T cell infiltration, antigen presenting capacity and antitumor phenotype of myeloid subsets

As previously published, CXCL9 and CXCL10 expression within the TME was associated with T cell infiltration⁵⁵. Given the ambivalent role of the CXCL9/10-CXCR3-axis concerning antitumor immunity²⁵⁹ and tumor escape (e.g. due to autocrine signaling from tumors²⁶⁰), further insights were sought to be identified by transcriptome analysis from publicly available data.

Utilizing relative gene expression values in combination with CIBERORT²⁶¹ relative immune cell profiles from 117 EwS biopsies, the role of CXCL10 was further analyzed. Biopsies were grouped into: *CXCL10 low* with relative expression <100, *CXCL10 induced* with relative expression >100 and *CXCL10 high* with relative expression values >1000.

Indeed, CD8⁺ T cell transcripts were gradually increased in patient biopsies with higher CXCL10 expression levels (*CXCL10 induced* or *high*) ([Figure 1a](#)), which is in agreement with previously published literature. In addition, transcripts associated with resting CD4⁺ memory T cells were decreased with higher CXCL10 levels. Regarding tumor-associated macrophages (TAMs), an increase of gene sets associated with antitumoral M1 macrophages was detected in *CXCL10 induced* and *CXCL10 high* biopsies with a concurrent decrease of immunosuppressive M2 macrophages in *CXCL10 high* patients ([Figure 1b](#)).

Due to the observed induction of CXCL10, further possible associations with immunogenicity and antigen (cross-) presentation were analyzed. Therefore, respective transcripts were correlated with CXCL10 expression levels. Here, 2 patient data sets were combined (GSE34620 and GSE142162), and a total of 196 transcriptomes were evaluated.

Of note, a selection of genes known to have co-stimulatory properties (CD80, CD83, and CD86) and all MHC class I haplotypes showed weak to moderate positive correlation with CXCL10 expression levels ([Figure 1c-h](#)).

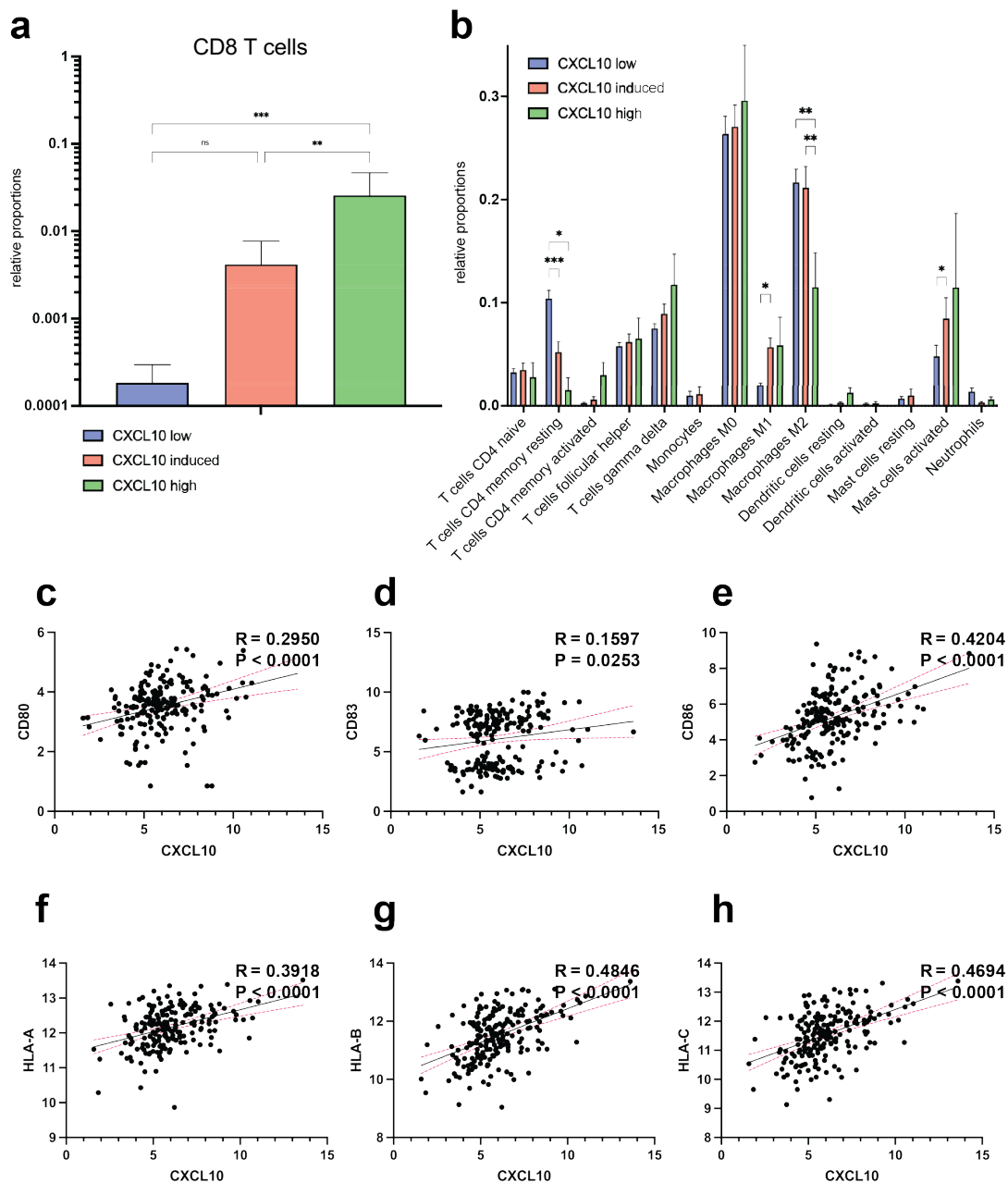


Figure 1: Transcriptome-based analysis reveals positive correlation of CXCL10 expression with increased CD8⁺ T cell and M1 macrophage transcripts and genes involved in antigen presentation. (A) Relative proportion of CD8⁺ T cells in bulk tumor transcripts, extracted from CIBERSORT after grouping respective patient biopsy samples into CXCL10 low-induced-high. Here, statistics were generated with the multiple comparison tool from Prism 9 (Version 9.1.2) in combination with ordinary one-way ANOVA. (b) Additional relative immune cell populations from CIBERSORT analyses were grouped in regard to CXCL10 expression (low-induced-high). The same software was used to analyze statistical differences but the multiple comparison tool in combination with 2-way ANOVA was utilized. (c-h) Correlation analyses were performed using Prism 9 linear regression modelling after extraction from the R2 platform¹ (pre-analyzed with *correlate 2 genes*, log2 gene expression) and combination of data sets Delattre GSE34620 (n=117) and Surdez GSE142162 (n=79). Pearson r (R) and p-values were generated in Prism 9. Significance levels are indicated as asterisks: * p < 0.05, ** p < 0.005, ns = not significant or not show in (b); Error bars indicate the SEM.

4.1.2 EwS-redirected TCR transgenic CD4⁺ T cells exhibit antitumor activity *in vitro* and mediate local control of xenografted A673 cell line²⁵⁴

Our group previously established a set of EwS-redirecting TCRs with potent antitumor efficacy *in vitro* and *in vivo*¹²⁶⁻¹²⁹. Those TCRs were cloned and identified from CD8⁺ T cells in an HLA-A*02:01-mismatch approach against overexpressed tumor-associated antigens. Thus far, only antitumor activities of CD8⁺ T cells equipped with respective TCRs were assessed. Interestingly, we also observed CD4⁺ T cell infiltration in metastatic lesions in a model of experimental metastasis after i.v.-injection of EwS-redirected CD8⁺ T cells together with CD4⁺ T cells of unknown specificity derived from the same healthy donor²⁶².

This observation led to the hypothesis that CD4⁺ T cells contribute to tumor control in this model of experimental metastasis when co-injecting A673 EwS tumor cells and therapeutic EwS-redirected T cells. Hence, to study the contributing role of tumor-redirected CD4⁺ T cells, healthy donor cells were genetically modified to express an EwS antigen-specific TCR recognizing the nonameric peptide STEAP1¹³⁰ (*six transmembrane epithelial antigen of prostate 1*) in the context of HLA-A*02:01.

Indeed, those therapeutic TCR transgenic (tg)CD4⁺ T cells exhibited antitumor activity *in vitro* (Figure 2a-d) and furthermore contributed to local tumor control (Figure 2f+g). But when applied with tgCD8⁺ T cells neither synergistic nor additive effects were observed (Figure 2e-g). In our model of experimental metastasis after concurrent tail vein injection of both A673 cells together with tgCD4⁺ T cells, or tgCD8⁺ T cells, or both cell types together, metastatic outgrowth in liver and lungs was only inhibited when administering tgCD8⁺ T cells without tgCD4⁺ T cells (Figure 2h-i).

Assessing cytokine profiles from *in vitro* cocultures, conditioned medium (CM) from tgCD4⁺ T cells contained increased amounts of CXCL10 but lacked specific effector cytokines, such as IFN γ or *tumor necrosis factor* (TNF). In comparison to CM from tgCD4⁺ T cells, induction of IFN γ and TNF was observed in CM containing tgCD8⁺ T cells (Extended Data Figure 1a-c).

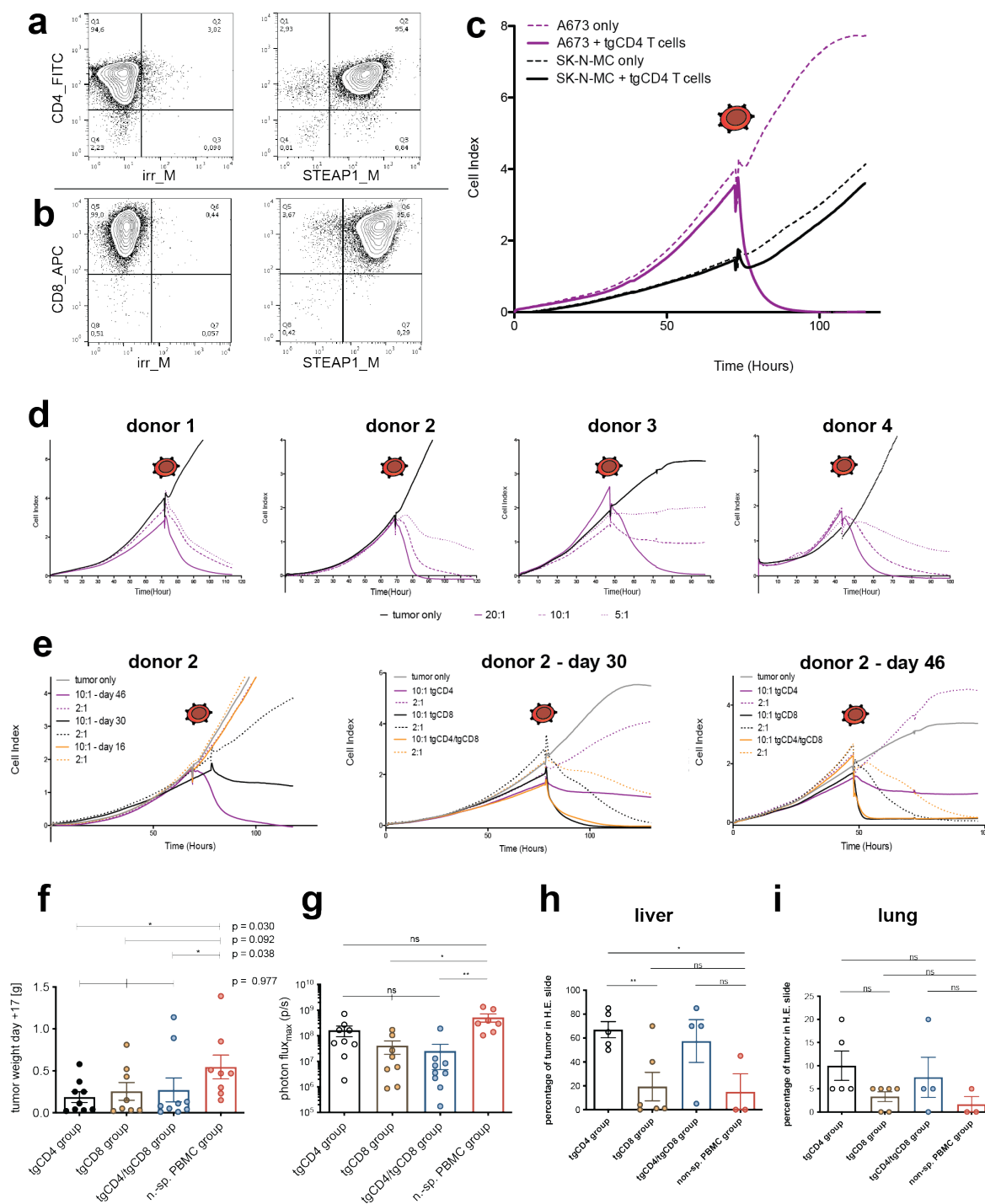


Figure 2: EwS-redirected TCR transgenic CD4⁺ T cells exhibit antitumor activity *in vitro* and mediate local control of s.c.-xenografted A673 cell line. (a) Validation of high purity of STEAP1¹³⁰/HLA-A*02:01-specific TCR-transgenic CD4⁺ (tgCD4) and (b) tgCD8⁺ T cell, stained with CD4-FITC or CD8-APC and irrelevant multimer-PE (irr_M) or relevant multimer (STEAP1_M), before experimental use. (c) xCELLigence assays of contact-dependent A673 (HLA-A*02:01-positive) or SK-N-MC (HLA-A*02:01-negative) tumor growth was measured and tgCD4 T cells (red cell) were added at an effector-to-target ratio (E:T) of 20:1 (at 46 days of T cell culture). Specific T cell recognition of target cells resulted in growth inhibition (detachment) of A673 tumor cells (purple line) but not of HLA-A*02:01-negative SK-N-MC cells (black lines). (d) Donor-specific variation of antitumor activity of tgCD4⁺ T cells in xCELLigence assay at different E:T ratios, at 6 weeks of T cell culture (4 donors, red cell indicates the time of T cell addition). (e) Increase of antitumor activity of tgCD4 T cells with the time of T cell culture (assessed at day 16, left figure) day 30 or day 46, respectively. Furthermore, antitumor activity of tgCD8, and tgCD4/tgCD8 (1:1) T cells was measured at E:T of 10:1 and 2:1, indicating the superiority

of tgCD8 T cells at all time points, irrespective of E:T ratio and co-administration with tgCD4 T cells. (f) Antitumor activity of tgCD4, tgCD8, tgCD4/tgCD8 (1:1), and non-specific (n.-sp.) PBMC was analyzed at the end of experiment (i.e. day 17 after application) measured by tumor weight and (g) bioluminescence, each dot corresponds to one animal. (h + i) Control of metastatic organotropism was also analyzed for aforementioned treatment groups at 30 days after i.v.-injection of both tumor and therapeutic T cells in liver and lung. Each dot corresponds to the percentage of tumor spread in respective organ of one individual animal. Significance levels are indicated as asterisks: * $p < 0.05$, ** $p < 0.005$, ns = not significant; Man-Whitney U test was applied in case of skewed distribution, otherwise unpaired, two-tailed student's t-test was performed. Error bars indicate the SEM.

Results from this section can be summarized as follows:

1. Higher levels of CXCL10 are associated with CD8⁺ T cell infiltration (relative immune cell populations, RNA-based).
2. Higher levels of CXCL10 are associated with increased antitumor M1 macrophages and decreased M2 macrophages (both based on RNA-based relative immune cell characterization).
3. Higher levels of CXCL10 are associated with increased immunogenicity and antigen-presenting capacities (RNA-based)
4. Increased protein levels (secretion) of CXCL10 are associated with tumor control *in vitro*.
5. Tumor-redirection CD8⁺ T cells are more potent to control metastatic spread than tumor-redirection CD4⁺ T cells in a model of experimental metastasis.

As CXCL10, also known as IP-10 (*Interferon gamma-induced protein 10*), is a downstream target of IFN γ , other therapies known to induce IFN signaling axes might be beneficial in controlling EwS and might synergize with cellular therapeutics.

Hence, the YB-1-dependent oncolytic adenovirus XVir-N-31, designed by Prof. Per Sonne Holm, was assessed for preclinically targeting EwS in the upcoming section

4.2 EwS cell lines are lysed by XVir-N-31 and support viral replication

Initially, EwS cell lines used in this project were screened for the expression of the natural receptor (CAR, CXADR) for AdV species C, type 5 which is a prerequisite for efficient entry into the cell. With the online-tool *Cell Line Selector* from the DepMap Portal (Broad Institute: depmap.org) expression values also for other possible receptors for AdV cell entry through RGD interactions such as ITGAV, ITGB3, and ITGB5 were extracted from the *Cancer Cell Line Encyclopedia (CCLE)-expression data set 'Expression 21Q3 Public'* to generate a heatmap (Figure 3a).

In addition, CAR surface expression on a selection of EwS cell lines was examined by flow cytometry (Figure 3b). Here, CAR expression was observed to be the lowest on A673, which is in accordance with transcriptomic data and furthermore reflected by the higher need of MOI for A673 to induce tumor lysis in comparison to SK-N-MC or TC32 *in vitro* (Figure 4b).

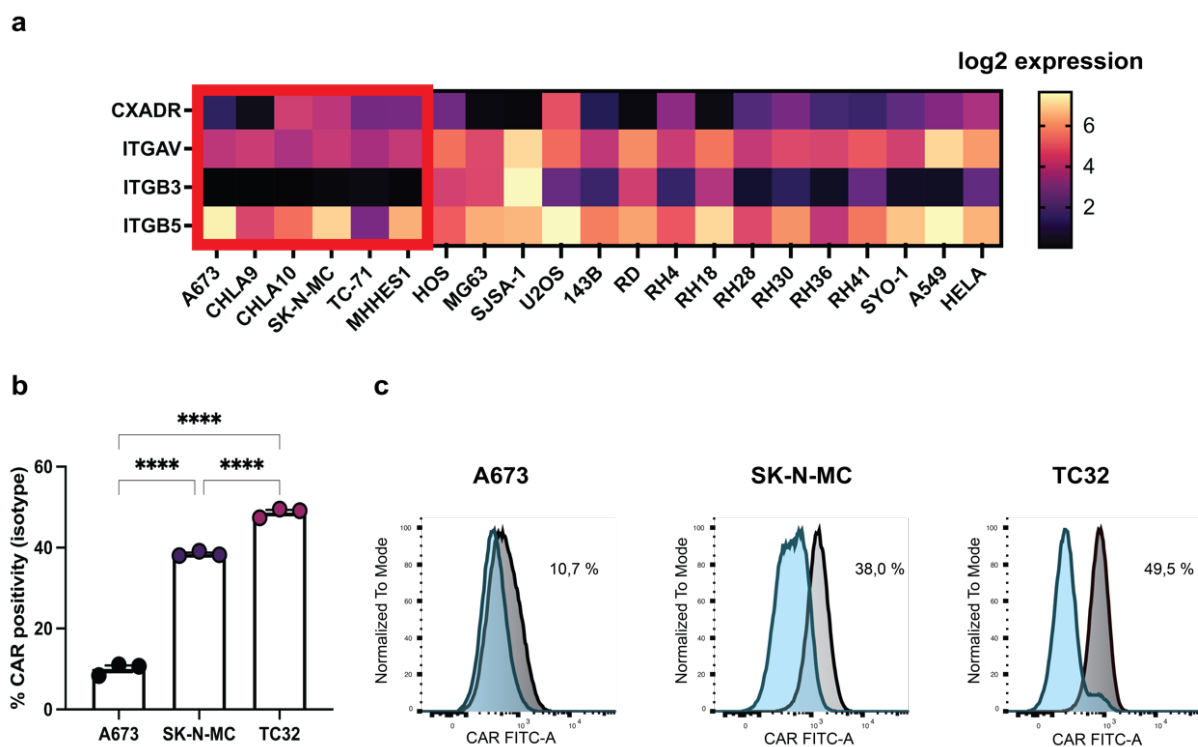


Figure 3: Analysis of receptor expression for oncolytic adenovirus XVir-N-31 (AdDelo3RGD). (a) Gene expression values (log₂ expression) of relevant receptors with known potential of interaction with Ad-RGD (CXADR, ITGAV, ITGB3, ITGB5) were extracted with the tool *Cell Line Selector* from the DepMap Portal (*Broad Institute: depmap.org*) and visualized with the heatmap-function of Prism 9. (b+c) Flow cytometric analysis of cognate Ad5 receptor (CAR) surface expression with CAR-FITC, compared to isotype-FITC on 3 EwS cell lines A673, SK-N-MC, and TC32 after dead-cell-exclusion via DAPI staining. Measurement was performed from 3 replicates per cell line. Significance levels are indicated as asterisks: ****p < 0.0001, ns = not significant; generated with Tukey's multiple comparison in combination with ordinary one-way ANOVA in Prism 9 (Version 9.1.2). Error bars indicate the SEM.

Further transcriptome analysis of patient biopsies concerning receptor expression relevant for AdV cell entry was extracted from the *R2 database*¹. Here, relative CXADR expression in all 4 available EwS data sets (*Francesconi, Surdez, Savola, Delattre*) was lower than in other tumors (e.g. glioblastoma, medulloblastoma, or rhabdoid tumors) but higher than in healthy tissues *blood* and *muscle*, which were included as controls. Expression of ITGAV, ITGB3, and ITGB5 was comparable to other tumor entities (Extended Data Figure 2).

Also, a variety of established EwS cell lines were infected with an E1A-deleted (replication-deficient) adenovirus carrying transgene-expression of GFP and RGD to test the susceptibility of respective cell lines towards adenovirus infection.

Compared to the cell line HEK293, which is also utilized for AdV production due to high infectivity and strong support AdV replication (used as reference), EwS cell lines can be infected with an RGD-expressing AdV but to a lesser degree than HEK293 cells (Figure 4a). To test the potential of XVir-N-31 to mediate oncolysis, EwS cell lines were infected with increasing MOI allowing to draw 'dose-response curves' (Figure 4c). Here, all tested cell lines were lysed with MOI100 after 4-5 days after infection. Also, the cell line A673 presented as the least sensitive cell line tested (Figure 4b). Of note, all analyzed cell lines supported viral replication resulting in *de novo* production of infectious units (IFU), assessed by hexon titer test with EwS cell line lysates 48hpi and 72hpi.

As productive replication of XVir-N-31 is dependent on the presence of YB-1 within the nucleus, immunofluorescence staining was performed to examine the distribution of YB-1 (cytoplasmic versus nuclear). In general, high amounts of YB-1 can be detected in EwS cell lines, although the majority of YB-1 is located within the cytoplasm (Extended Data Figure 3).

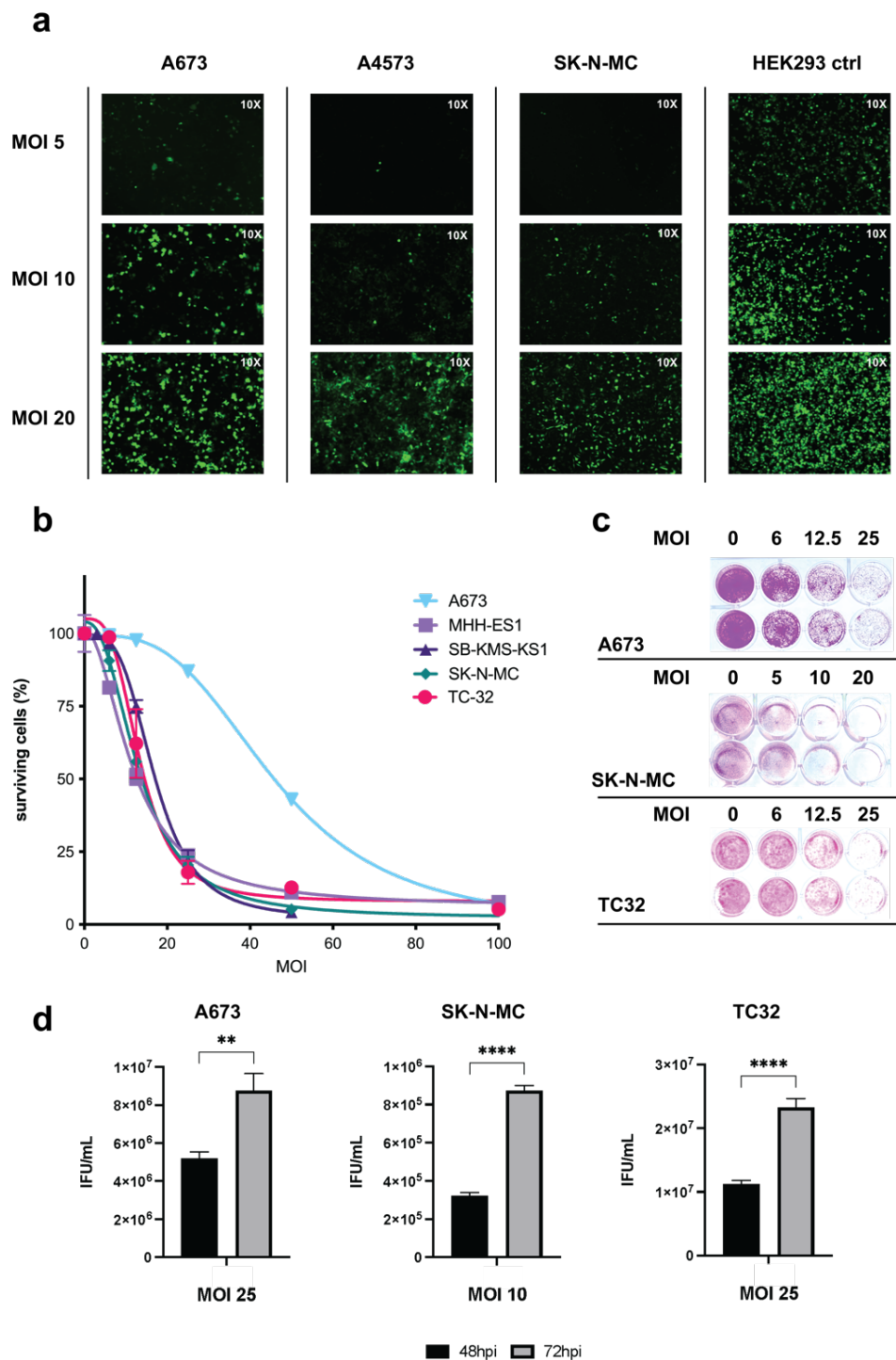


Figure 4: Established EwS cell lines are susceptible to adenovirus-RGD infection inducing XVir-N-31-mediated oncolysis and *de novo* formation of infectious viral particles. (a) 1×10^5 cells were plated on 24-well plates and infected with GFP-expressing adenovirus-RGD with different multiplicities of infection (MOI) the day after. Immunofluorescence photos were taken 48 hours post-infection (hpi) using 10X magnification. HEK293 cells served as positive control. (b+c) A selection of EwS cell lines were infected with increasing MOI of XVir-N-31. 4-6 days after infection, cell viability was analyzed via SRB staining and photometric measurement of extinction. (d) *De novo* viral particle formation was analyzed by hexon titer test of EwS cell line lysates 48hpi and 72hpi, previously infected with indicated MOI. Significance levels are indicated as asterisks: * $p < 0.05$, ** $p < 0.01$, *** $p < 0.005$, **** $p < 0.0001$, ns = not significant; unpaired, two-tailed student's t-test was performed. Error bars indicate the SEM.

Results from the section 4.2 can be summarized as follows:

1. Coxsackie and adenovirus receptor (CAR) is expressed in and on EwS cell lines with varying RNA and surface levels.
2. EwS cell lines are susceptible to adenovirus infection.
3. High CAR expression is associated with lower MOI needed for complete tumor cell lysis *in vitro*.
4. All tested EwS cell lines can be lysed by XVir-N-31.
5. XVir-N-31 replicates in EwS cell lines leading to *de novo* formation of infectious units.

4.3 Combination therapy of EwS-redirection CD8⁺ T cells and XVir-N-31

After the establishment of productive infection of EwS cell lines resulting in tumor cell lysis, combination therapy of XVir-N-31 was initiated utilizing EwS-redirection CD8⁺ T cells. Those T cells were genetically modified to express a TCR recognizing the CHM1-derived nonameric peptide CHM1³¹⁹ expressed on HLA-A*02:01 (CHM1 T cells). Respective TCR was previously characterized *in vitro* and *in vivo* by our group, confirming EwS antitumor activity against HLA-A*02:01⁺ Ewing tumors/ cell lines^{126, 129, 130}.

4.3.1 CHM1 T cells and XVir-N-31 synergistically lyse EwS tumor cells *in vitro*

Contact-dependent tumor cell growth over time and consecutive detachment of tumor cells (i.e. tumor cell killing) was analyzed by the xCELLigence assay. In [Figure 5a-c](#), T cell killing activity of non-specific (n.-sp.) CD8⁺ T cells at an E:T ratio of 1:1 in combination with XVir-N-31 at MOI10 and MOI100 was examined. Tumor cells were infected 24h before addition of T cells. In this setting, T cell-mediated killing was only increased 24h after addition of non-specific T cells with MOI100. This indicates that peptide-MHC/TCR-independent mechanisms of tumor cell recognition and lysis, such as a non-classical formation of immunological synapses (e.g. via CD11a and CD54, also known as *Lymphocyte Function Associated Antigen*-, LFA-1 and the counter-receptor *Intercellular Adhesion Molecule 1*, ICAM-1)^{263, 264}, might be in play when tumor cells are infected at high MOI.

When assessing T cell killing activity of tumor-redirection CD8⁺ T cells (CHM1 CD8 T cells) together with XVir-N-31 (XVir), an increase of tumor cell killing was observed already at 12h after T cell addition which also showed a dose-dependent increase with higher MOI ([Figure 5d-f](#)). To better distinguish and elaborate synergistic effects of XVir-N31 and CHM1 T cells, cell survival/viability of A673 and TC32 tumor cells were analyzed at 48hpi and 24h after addition of T cells utilizing SRB staining and the R tool *SynergyFinder*^{265, 266}. Synergistic effects (red) occurred most likely at MOI50-100 and E:T ratios of 1:1 – 0.25:1, whereas lower MOI most likely induced additive effects in this experimental setting ([Figure 5g+h](#)).

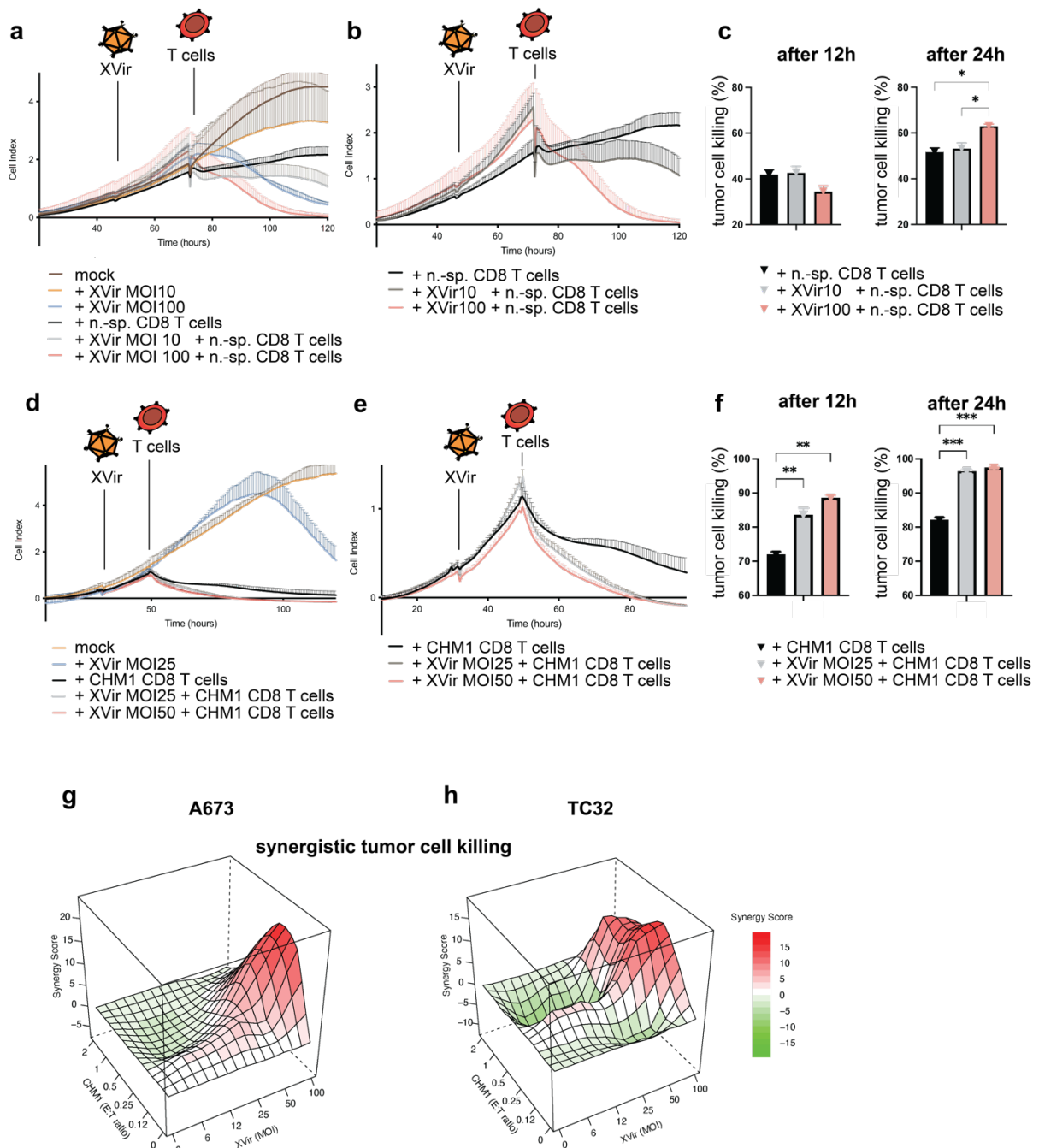


Figure 5: CHM1³¹⁹/HLA-A*02:01-restricted TCR-transgenic CD8⁺ T cells and XVir-N-31 synergistically lyse tumor cells *in vitro*. (a) Contact-dependent A673 tumor growth was analyzed with the xCELLigence assay to determine effects of XVir at indicated MOI and n.-sp CD8 T cells (E:T = 1:1) and combinations of both, with respective controls. Infection with XVir and addition of T cells is indicated. (b) For better comprehensibility, data complexity of (a) was reduced to T cell-containing conditions only. (c) T cell-mediated tumor cell killing was analyzed 12h and 24h after addition of T cells by subtracting respective cell index values of e.g. *mock* from *n.-sp. T cells*. (d-f) CHM1³¹⁹/HLA-A*02:01-restricted TCR-transgenic CD8⁺ T cell (*CHM1 CD8 T cells*) activity against A673 tumors was analyzed with indicated MOI, as described for n.-sp. CD8 T cells (a-c). (g+h) The likelihood of synergistic interactions of XVir and CHM1 CD8 T cells concerning tumor cell killing was evaluated via cell viability assays 24h after addition of T cells (i.e. 48hpi) and the *SynergyFinder* tool in R (experiments were performed in biological replicates and repeated, n=2). Synergy Score explanation: interactions larger than 10 are considered as likely *synergistic*; interactions from -10 to 10 are most likely *additive* and interactions less than -10 are likely to be *antagonistic*. Significance levels are indicated as asterisks: * p < 0.05, ** p < 0.01, p*** < 0.005, ****p < 0.0001, ns = not significant; multiple comparison by ANOVA was performed in (c) and (f). Error bars indicate the SEM.

4.3.2 Combination of CHM1³¹⁹/HLA-A*02:01-restricted TCR-transgenic CD8⁺ T cells and XVir-N-31 increases therapy response and survival

After the establishment of synergistic cooperation of *XVir-N-31* and *CHM1 T cells in vitro*, translational relevance was further studied in a tumor xenograft mouse model (*Rag2^{-/-}γc^{-/-}*) with subcutaneously (s.c.)-implanted A673 cells and consecutive intratumoral (i.t.)-injection of *XVir-N-31* as well as administration of human *CHM1 T cells* intraperitoneally (i.p.) ([Figure 1a](#)).

Tumor control was significantly enhanced in animals receiving *XVir + CHM1 T cells*, compared to *mock* and monotherapies, when analyzing therapy (Tx) response 8-10 days after initiation of Tx ([Figure 6b+c](#)). The observed delay in tumor growth also resulted in a significant increase in median survival of animals receiving the combination Tx compared to all other experimental conditions ([Figure 6d](#)). When analyzing human tumor-infiltrating T cells (TILs) in xenografted tumors at the end of experiment, human T cell infiltration could only be induced when combined with *XVir-N-31* within this experimental setting ([Figure 6e](#)). Induction of TILs in animals receiving *XVir + CHM1 T cells*, was also accompanied by higher numbers of human T cells in spleens, indicative of superior T cell engraftment compared to *CHM1 T cell* monotherapy ([Extended Data Figure 4c](#)).

Apart from above-mentioned differences in TILs and human T cell engraftment, no differences were observed for: MHC-I (antigen presentation), CD47 ('don't-eat-me signal'), ICAM-1 (lymphocyte adhesion), CD83 (co-stimulatory molecule for T cells), PD-1, PD-L1, and PD-L2 (immune checkpoint molecules) which were assessed by flow cytometry using specific antibodies and analyzing the geometric mean of the fluorescence intensity ([Extended Data Figure 4a](#)). Also, gene induction of HLA-A, -B and CXCL did not alter significantly in-between groups ([Extended Data Figure 4b](#)).

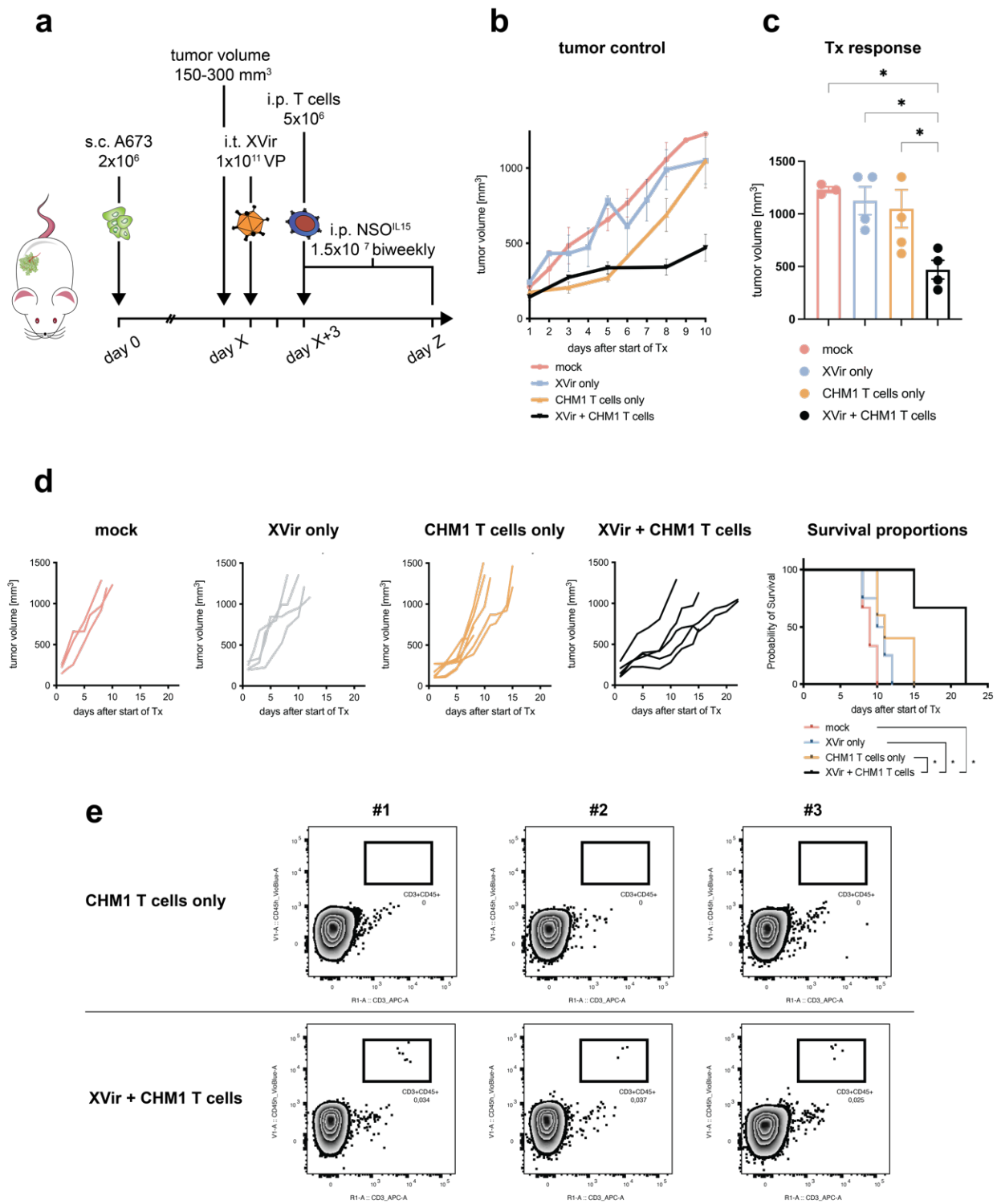


Figure 6: Combination of CHM1³¹⁹/HLA-A*02:01-restricted TCR-transgenic CD8⁺ T cells (CHM1 T cells) and XVir-N-31 increase therapy response and survival. (a) Experimental setup: 2x10⁶ A673 tumor cells were injected s.c. in the flank of Rag2^{-/-}γc^{-/-} mice at day 0. When tumors reached a volume of 150-300 mm³ (day X), animals were randomized to treatment groups: *mock*, *Xvir only*, *CHM1 T cells only*, and *XVir + CHM1 T cells*. Then, 1x10¹¹ viral particles (VP) of XVir-N-31 or PBS were injected i.t. at day X+1. 2 days later (day X+3), 5x10⁶ purified CHM1 T cells (validated by flow cytometry before administration, data not shown) were administered i.p. combined with 1.5x10⁷ IL-15-producing NSO cells i.p. (previously irradiated with 3.5 Gray). NSO application was repeated biweekly until the end of experiment (defined by tumor volume ≥ 1000 mm³). (b+d) Tumor control in respective treatment groups is shown as mean tumor growth until 10 days after start of therapy (Tx) in (b) and for each animal per group until the end of experiment in (d); *mock* n=3, *Xvir only* n=4, *CHM1 T cells only* n=5, and *XVir + CHM1 T cells* n=5. (c) Tx response was evaluated on day 7-10 after start of Tx. Statistical analyses

were performed in Prism 9 using the multiple comparison tool in combination with ordinary one-way ANOVA. (d) Kaplan-Meier survival curves were generated with Prism 9 from animals which reached a tumor volume $\geq 1000 \text{ mm}^3$ using the Mantel-Cox log-rank test. (e) Percentage of tumor-infiltrating T cells (TILs, i.e. *CHM1 T cells*) in explanted tumors (in relation to all gated cells, after live-dead-cell exclusion with Viability Dye) was evaluated at the end of experiment from 3 representative animals per group (*CHM1 T cells only* and *XVir + CHM1 T cells*) via flow cytometry using anti-humanCD45-VioBlue and anti-humanCD3-APC antibodies. Significance levels are indicated as asterisks: * $p < 0.05$, ** $p < 0.01$, p*** < 0.005 , ****p < 0.0001 , ns = not significant. Error bars indicate the SEM.

4.3.3 XVir-N-31 increases phagocytic and antigen-presenting capacities resulting in superior antigen-specific CD8⁺ T cell proliferation

As oncolytic virotherapy is known to be a potent inducer of immunogenic cell death (ICD) resulting in increased activity of innate and adaptive immune responses, relevant surface marker expressions associated with pro- and anti-phagocytic activity, as well as dendritic cell (DC) maturation were evaluated and complemented by functional assays for phagocytosis and T cell activation.

As Calreticulin (CALR) was shown to be the dominant pro-phagocytic signal which can be counterbalanced by CD47²⁶⁷, EwS cell lines A673 and SK-N-MC were infected with AdV wildtype and XVir-N-31, and respective surface marker expression was analyzed 48hpi. The *eat-me* signal CALR was significantly increased with high MOI of XVir-N-31 (MOI50 or MOI100) in both cell lines, comparable to the known inducer of ICD doxorubicin (*doxo*), which served as positive control (Figure 7a+b, left panels). Whereas the *don't-eat-me* signal CD47 was decreased in all experimental conditions in A673, an increase in SK-N-MC at lower MOI was detected, indicating variable tumor host cell responses due to adenoviral infection in this experimental setting (Figure 7a+b, right panels).

Next, phagocytic activity of immature DCs (imDC) was assessed after a 4h-coculture-period with XVir-N-31-infected A673-GFP⁺ tumor cells, according to literature²⁶⁸. Here, a significant increase of phagocytosis was observed for imDCs, derived from THP-1 cells and preselected monocytic CD14⁺-PBMCs, when cocultured with XVir-N-31-infected tumor cells (Figure 7c+d).

Also, soluble factors secreted from tumor cells into the supernatant after viral infection (termed condition medium, *CM*), were capable to upregulate markers associated with T cells co-stimulation (*CD40*, *CD86*) or abrogate the downregulation of *MHC-I* and *-II*, which was observed in *CM* from *mock*-treated tumor cells (Figure 7e).

To further test, if respective DCs or DC-like cells after exposure to *CM* are more potent in stimulating antigen-specific T cell functionality, T cell proliferation of *CHM1 T cells* was studied. For these experiments, pre-conditioned THP-1-derived DCs, which express HLA-A*02:01, were pulsed with the CHM1³¹⁹-peptide before fluorescence-labeled (eFluor450) CHM1³¹⁹/HLA-A*02:01-restricted TCR-transgenic CD8⁺ T cells were added. Of note, the highest percentage of T cell proliferation (96h after start of coculture) was measured in coculture conditions together with DCs previously exposed to *CM* from XVir-N-31-infected A673 tumor cells (*CM XVir MOI25 + peptide*). In the same condition, *CHM1 T cells* showed increase CXCR3 surface expression, which is associated with CD8⁺ T cell effector function and migratory capacity of respective cells into peripheral tissues²⁶⁹ (Figure 7f-h).

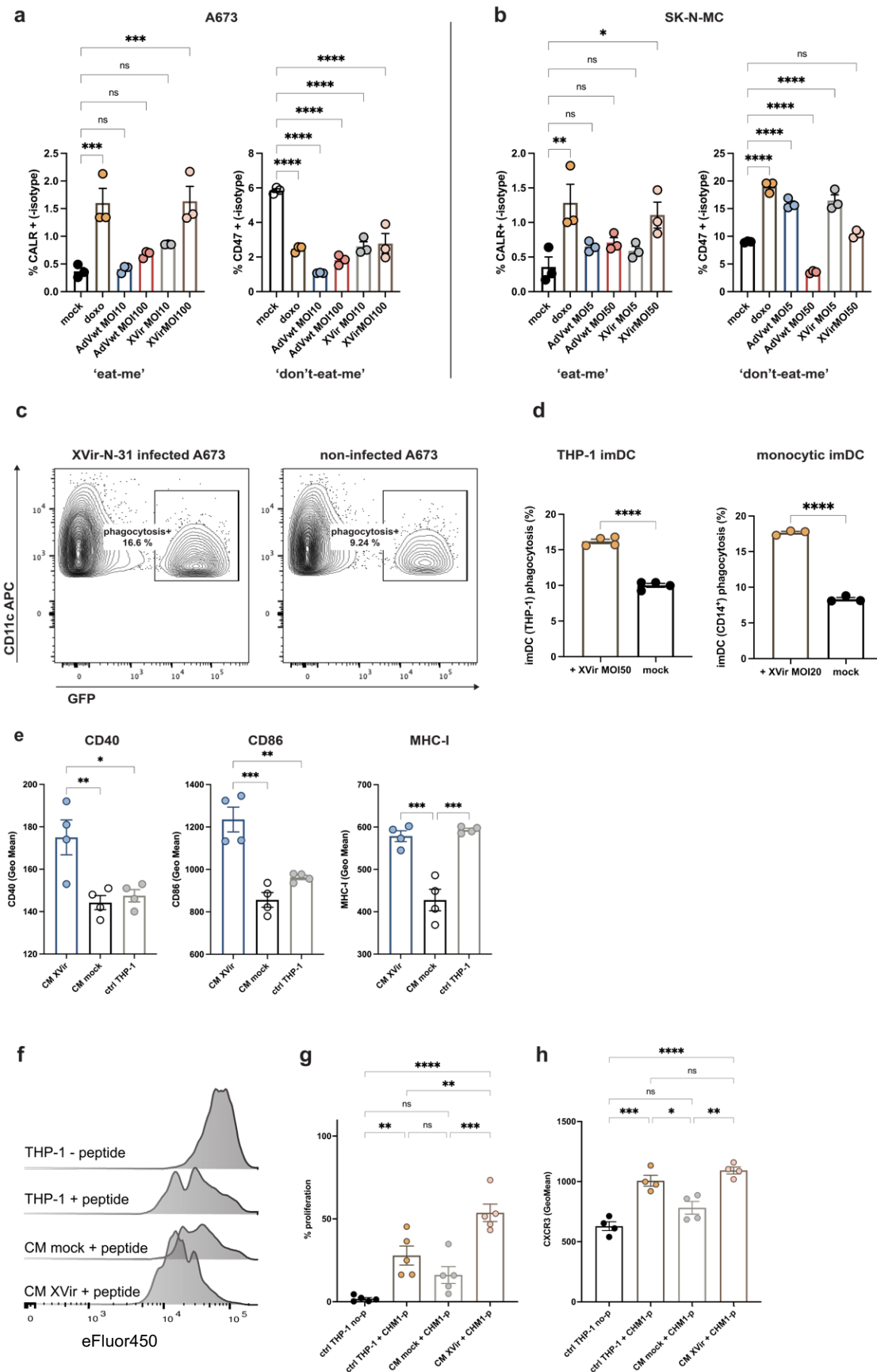


Figure 7: XVir-N-31 increases phagocytic and antigen-presenting capacities resulting in superior antigen-specific CD8⁺ T cell proliferation. (a) Calreticulin (CALR) and CD47 surface expression was evaluated via flow cytometry with adenovirus wildtype (AdVwt) and XVir-N-31 (XVir) at 48hpi in A673 and (b) SK-N-MC at indicated MOI, after exclusion of dead cells via DAPI staining. Doxorubicin (doxo 1 μ M) served as positive control. CALR was first stained with a primary mouse antibody (and a respective

isotype control) and afterwards a fluorescence-labeled (AlexaFLuor488) anti-mouse antibody was used. For CD47 staining, an anti-CD47-FITC (and FITC isotype) antibody was applied. (c) Phagocytosis of GFP-transduced A673 cells was analyzed via flow cytometry after a 4-h-coculture-period of THP-1-derived immature DCs (imDCs) and (d) monocyte-derived imDCs. A673 cells were infected 48hpi prior coculture at indicated MOI. Tumor cells were considered as phagocytosed when staining double-positive for GFP and a monocyte/lymphocyte-lineage specific marker, such as CD11c-APC or CD45-APC, as shown in (c). Each experiment was performed in biological replicates, as indicated by the number of dots and repeated (n=2). (e) The geometric mean (GeoMean) of fluorescence intensity on THP-1 cells after a 72h-coculture-period in condition medium (CM) from XVir-infected A673 cells (MOI50, collected 48hpi), *mock* infected A673 or non-conditioned THP1 (*THP-1 ctrl*) was studied utilizing flow cytometric antibodies against CD40-VioBright-FITC, CD86-VioBlue, HLA-ABC (HLA-I)-PerCP-Vio700. (f+g) T cell proliferation and (h) CXCR3-surface expression was analyzed after 96h of coculture with conditioned THP-1 (from e). Therefore, THP-1 cells were pulsed with CHM1³¹⁹ peptide (*+peptide*) for 4h before fluorescence-labeled CHM1³¹⁹/HLA-A*02:01-restricted TCR-transgenic CD8⁺ T cells were added. Non-conditioned THP-1 cells served as controls (ctrl THP-1, + and – CHM1-peptide, y-axis: % of max). The percentage of proliferated cells was compared to ctrl THP-1 without CHM1³¹⁹-peptide (no-p). Statistical analyses were performed in Prism 9 using the multiple comparison tool in combination with ordinary one-way ANOVA or unpaired, two-tailed student's t-test. Significance levels are indicated as asterisks: * p < 0.05, ** p < 0.01, *** p < 0.005, ****p < 0.0001, ns = not significant. Error bars indicate the SEM.

Results from section 4.3 can be summarized as follows:

1. The oncolytic adenovirus XVir-N-31 synergizes with CHM1³¹⁹/HLA-A*02:01-restricted TCR-transgenic CD8⁺ T cells *in vitro* and *in vivo*.
2. XVir-N-31-intratumoral injection induces tumor-antigen specific T cell infiltration in s.c.-implanted EwS (at low levels) after a single injection of XVir-N-31 and a single application of therapeutic T cells.
3. XVir-N-31 induces CALR, a marker of ICD, increases phagocytic and antigen-presenting capacities of APCs resulting in superior antigen-specific T cell activation.

4.4 Combination therapy of XVir-N-31 and cell cycle blockade (combo Tx)

Due early clinical data of OV monotherapy only showing convincing disease controls in a minority of tumor entities and the inferior replicative capacity of OVs compared to respective wildtypes (because of genomic deletion responsible for tumor-selectivity), novel combination strategies are sought to be identified to increase viral replication and thereby extending the therapeutic effect.

The groups of Prof. Dr. rer. nat. Per Sonne Holm and PD Dr. rer. nat. Roman Nawroth previously showed that CDK4/6 inhibition (CDK4/6i) with palbociclib, abemaciclib, and ribociclib significantly increased adenoviral replication resulting in enhance cell lysis in bladder cancer cell lines, hence also synergize with the oncolytic adenovirus XVir-N-31^{270, 271}.

This interplay was not expected, as the adenoviral life cycle, according to widely accepted understanding in the scientific community, is dependent on the induction of S-phase²⁷², whereas CDK4/6i induces a cell cycle arrest²⁷³.

As mentioned in the introduction, another group also observed increased oncolytic activity of an OAd (Ad5/3-delta24) when combined with the CDK4/6i palbociclib in estrogen receptor-positive but not in -negative cell lines. Differences in response to OAd together with CDK4/6i were possibly attributed to different states STAT1 activation but the role of RB/E2F1 protein complex in mediating Ad replication was not further studied²⁴⁹.

4.4.1 Combo Tx increase oncolysis and viral replication *in vitro* and increases therapy response and survival *in vivo*

When analyzing virus-mediated cytotoxicity in EwS cell lines *in vitro*, CDK4/6i significantly decreased cell survival in those cell lines responding to cell cycle blockade with (1) an increase in G1 cell cycle state and (2) a simultaneous downregulation of RB/E2F1 protein levels ([Figure 8a](#) and [Extended Data Figure 5](#)).

The cell line SK-N-MC, with a known homozygous mutation in the RB pocket domain (RB1-R698M/S) and hence compromised RB function²⁷⁴, considered resistant to CDK4/6i¹⁵¹, did not show enhanced oncolysis nor increased particle formation upon inhibitor Tx. In contrast, CDK4/6i-sensitive A673²⁷¹ and TC32 responded with a significant increase in particle formation and tumor cell lysis ([Figure 8a+](#) and [Extended Data Figure 5](#)). When utilizing xCELLigence-*live* tumor growth measurement, CDK4/6i only slowed down tumor growth. The addition of XVir-N-31 induced tumor cell detachment (i.e. lysis), which occurred earlier when applied together with CDK4/6i ([Extended Data Figure 5e](#)).

To validate whether aforementioned findings also translate into a therapeutic benefit in an *in vivo* model, s.c. tumor growth of xenografted A673 EwS cells with respective combination and mono-Tx were evaluated in immunocompromised nude mice (NMRI-Foxn1nu/nu). Animal experiments were performed together with Dr. med. Vet. Ulrike Schillinger.

After a second i.t.-injection of XVir-N-31 a remarkable decrease in tumor volume was observed for combination (*combo*) Tx of XVir-N-31 and CDK4/6i ribociclib (*LEE011*, *LEE*) ([Figure 8c+d](#)). Assessing Tx response in-between groups at day 12-21, when biggest differences were observed, *combo* Tx significantly increase the therapeutic benefit, which was also became evident when taking longitudinal growth curve comparison to tumor volume into account ([Figure 8d+f](#); analyses were done using the open-access web tool *TumGrowth*²⁷⁵).

Histopathological analyses from representative animals at 2 days after 2nd injection confirmed higher tumor cell necrosis and degeneration ([Figure 8e](#)) accompanied by a significant increase in viral *fiber DNA*, indicative of higher replication (assessed by PhD student Florian Klein). As a result, animals treated with *combo* Tx as well as XVir-N-31 mono Tx exhibited a significant increase in median survival compared to *mock* (*combo* ^{***}, XVir-N-31 *only* ^{*})²⁷¹.

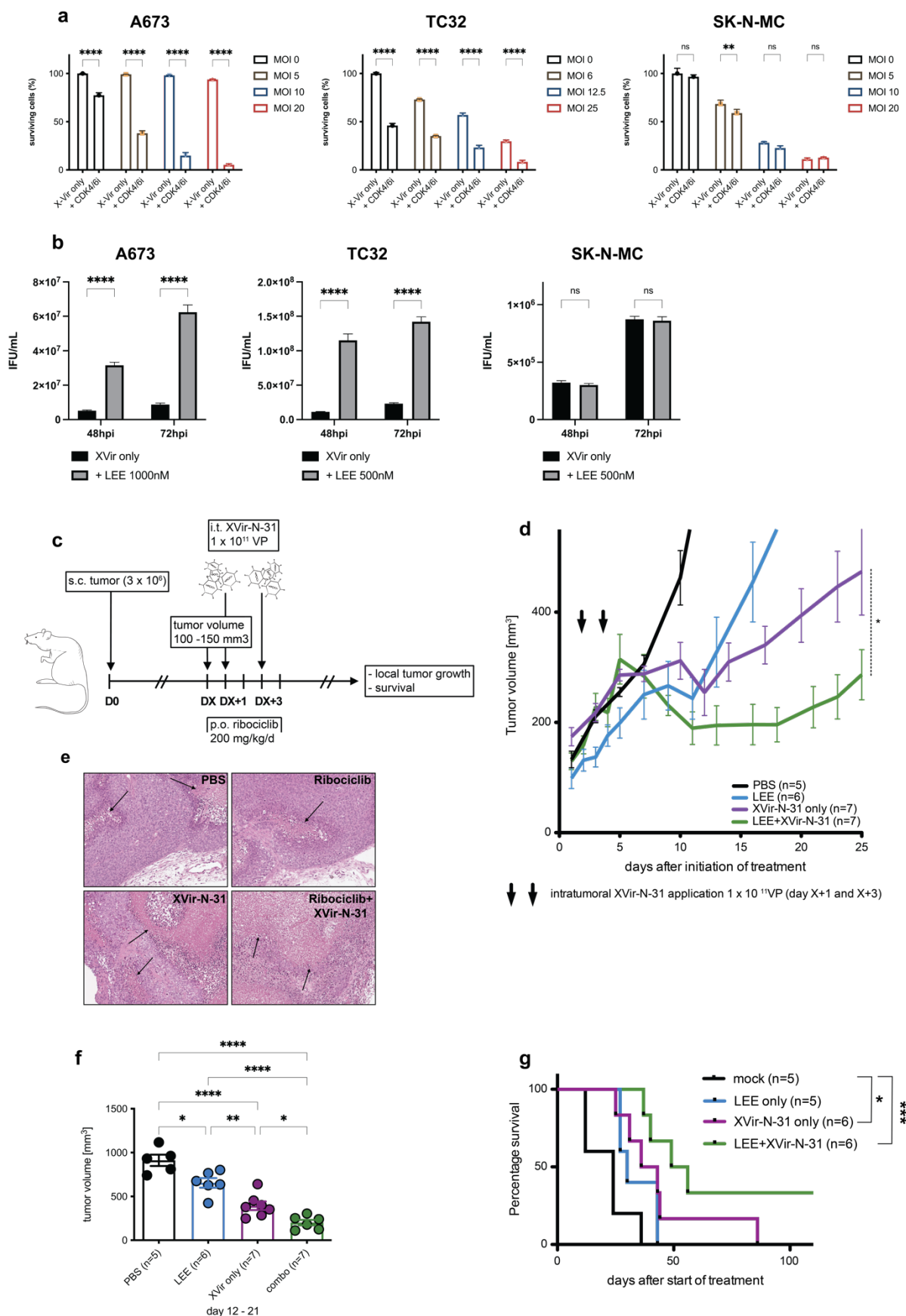


Figure 8: Combination of XVir-N-31 and CDK4/6 inhibition increase oncolysis and viral replication *in vitro* and increases therapy response and survival *in vivo*. (a) EwS cell lines A673, TC32, and SK-N-MC were pre-treated with ribociclib (LEE; A673 with $1\mu\text{M}$, TC32 with $0.5\mu\text{M}$) or palbociclib (SK-N-MC with $0.5\mu\text{M}$) for 24h and afterwards infected with XVir-N-31 (XVir). Inhibitor

treatment was continued until cell survival/viability was assessed at 4dpi. Relative cell survival (compared to mock Tx = MOI0) was depicted in column bars. **(b)** *De novo* particle formation was measured using the hexon titer test, at 2 time points (48 and 72hpi) for each cell line +/- CDK4/6i at indicated concentrations. Statistics in (a)+(b) were generated by unpaired, two-tailed student's t-test. **(c)** Experimental setup: 3×10^6 A673 tumor cells were injected s.c. in the flank of NMRI-Fox1nu/nu mice at day 0. When tumors reached a volume of 100-150 mm³ (day X, DX), animals were randomized to treatment groups (*mock/PBS*, *XVir-N-31 only*, *LEE only*, and *LEE + XVir-N-31*) and 200mg/kg/d of *LEE* or *mock* was applied by oral gavage for 5 consecutive days. At DX+1 and DX+3, 1×10^{11} viral particles (VP) of XVir-N-31 or PBS were injected into tumors. Tumor volumes were measured by caliper every 2-3 days until the end of experiment (defined by tumor volume ≥ 1000 mm³). **(d)** Control of s.c.-implanted tumors in respective treatment groups is shown as mean tumor growth until day 25 after start of treatment (arrows indicate the application of XVir-N-31). Here, longitudinal linear comparison of growth curves was analyzed by the open-access web tool *TumGrowth*²⁷⁵ and therapy (Tx) response, measured my maximum tumor volume at day 12-21 of each animal, was plotted with Prism 9 **(f)**, as well as Kaplan-Meier survival curves **(g)**, which were analyzed statistically with Mantel-Cox log-rank test in Prism 9. **(e)** Explanted tumors were stained with hematoxylin and eosin. Arrows point to necrotic and degenerated areas. Significance levels are indicated as asterisks: * $p < 0.05$, ** $p < 0.01$, *** $p < 0.005$, **** $p < 0.0001$, ns = not significant or not shown. Error bars indicate the SEM.

4.4.2 Knock-down of RB increases adenoviral fiber DNA

Further experimental insights supporting the possible role of RB as an *adenoviral repressor*, next to its known role as a *tumor suppressor*, were generated with RB and E2F1 knock-down (KD) experiments using siRNA (*small inhibitory RNA*) against respective targets.

After confirmation of KD on protein level, viral *fiber DNA* increased especially in the siRB-experimental settings (Figure 9). Further mechanistic insights regarding the role of RB protein and adenoviral replication were studied by the groups of Per Sonne Holm and Roman Nawroth²⁷¹.

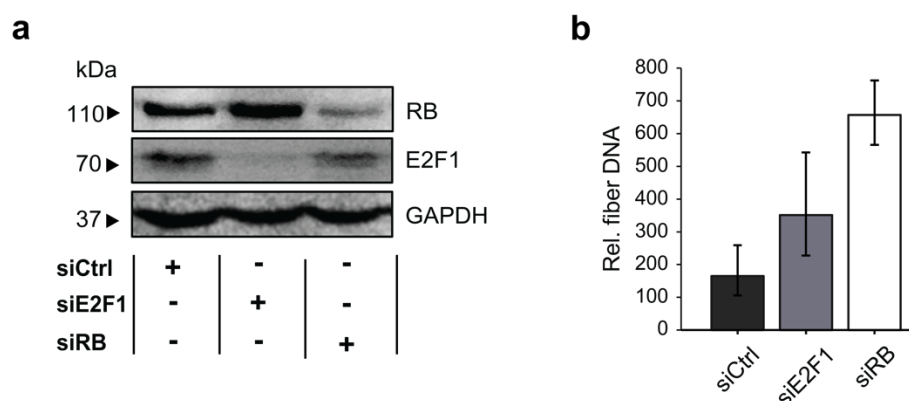


Figure 9: siRNA-mediated knock-down of RB protein increases viral fiber DNA in CDK4/6i-resistant cell line SK-N-MC. **(a)** Immunoblots confirming knock-down on protein level, generated from cell lysates after overnight siRNA transfection. **(b)** Relative fiber DNA was studied after respective siRNA transfection at 48hpi with MOI20 (one representative experiment). Both experiments (a+b) were repeated (n=2) and rel. fiber DNA was measured in triplicates. Error bars indicate the SEM.

4.4.3 Combo Tx induces proinflammatory chemo- and cytokine release

Given the beneficial effects of CDK4/6i on adenoviral replication and virus-mediated oncolysis both *in vitro* and *in vivo*, the immunological effects of the *combo* Tx were addressed. As CDK4/6 inhibitors also were described to mediate antitumor immunological effects associated with an increase in especially adaptive antitumor immunity, immunological effects of the *combo* Tx were even more pressing.

To get a first idea of relevant immunological changes directly induced in EwS cells infected with *XVir-N-31*, or treated with *LEE* and *combo* Tx, multiplex cytokine screenings were performed.

A673 and SK-N-MC cells were infected with *MOI100* and supernatant was subjected to a 48-multiplex cytokine/chemokine screening at: 2-10-18-24-72*hpi*. Interestingly, no striking changes could be observed. There was a tendency in several analyzed cytokines for decreased cytokine/chemokine levels at 72*hpi* compared to *mock*, being the case for: e.g. IL-8, *Monocyte Chemoattractant Protein-1* (MCP-1, also known as CCL2), *Macrophage Migration Inhibitory Factor* (MIF), *Platelet-derived Growth Factor-beta* (PDGF-b), *Stem Cell Growth Factor-beta* (SCGF-b) in A673 ([Extended Data Figure 6a](#)).

Then, the cell line A673 was screened for cytokines and chemokines with *combo* Tx and the highest levels were found for *CXCL10*, *IL-8*, *VEGF*, and *TNF*. Most notably, CDK4/6i alone and in combination with *XVir-N-31* increased *CXCL10* levels, whereas *VEGF* was decreased ([Figure 10](#)). A heatmap of the complete 48-multiplex cytokine/chemokine is provided in [Extended Data Figure 6b](#).

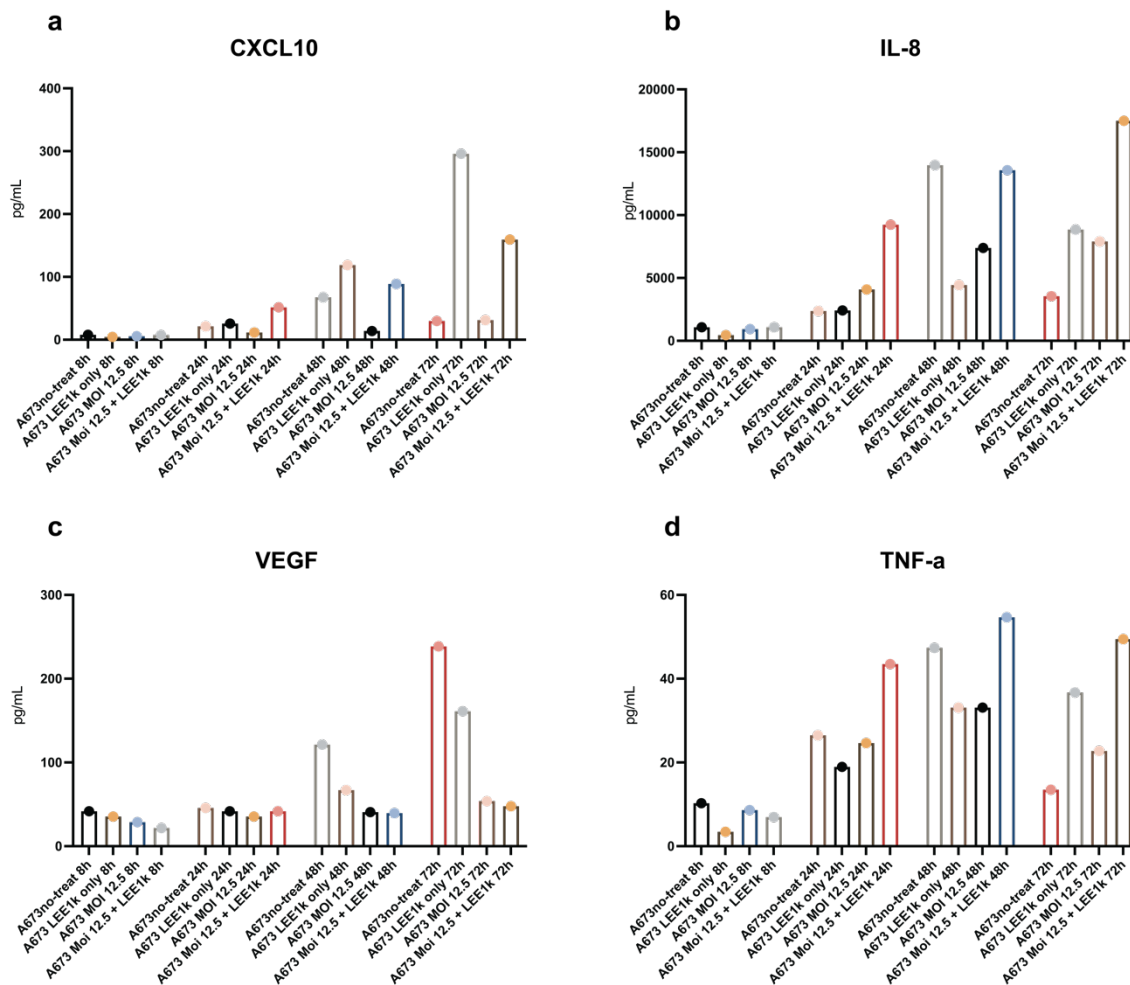


Figure 10: Combo Tx increases CXCL10 release in XVir-N-31-infected A673 condition medium. Chemo-/Cytokine screening of secreted/release factors from treated A673 tumor cells at different time points (8-24-48-72hpi). Treatments consisted of ribociclib (1000nM, *A673 LEE1k only*), XVir-N-31 with MOI12.5 (*A673 MOI12.5*) and combination of both (*A673 MOI12.5 + LEE1k*). Concentration of (a) CXCL10, (b) IL-8, (c) VEGF, and (d) TNF in cell culture supernatant is shown in column bars, no replicates, single measurement per time point and condition.

To verify the induction of CXCL10 on protein level immunoblotting was performed *in vitro* (Figure 11). CDK4/6i induced CXCL10 48hpi in *combo*- and *LEE*-treated A673 tumor cells (i.e. 72 after addition of LEE, as CDK4/6i was added 24h before infection). Of note, CXCL10-induction in *combo* Tx was comparable to *LEE*-treatment. Hence, neither adenovirus E1A and hexon levels or E2F1-stabilization, nor p21-induction did affect CXCL10. CXCL10-induction rather was associated with the strong reduction of RB and p-RB, both visible at 48hpi in *combo* and *LEE* settings. Another interesting observation was the reduction of MIF, especially in XVir-N-31-containing treatments.

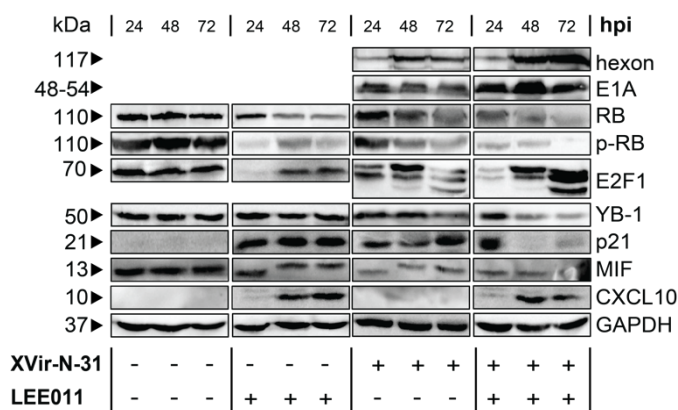


Figure 11: CDK4/6-inhibition with LEE011 induces CXCL10 protein levels in LEE and Combo Tx *in vitro*. Viral protein expression (hexon, E1A) as well as cell cycle regulators RB, phosphorylated RB (p-RB), E2F1, p21 was analyzed by western blotting in A673 cells at indicated timepoints with XVir-N-31 at MOI50 and 1 μ M LEE011. Furthermore, YB-1 protein level and chemokine levels of MIF and CXCL10 were visualized. One representative blot is shown of 2 independent experiments.

4.4.4 Combo Tx increases viral replication and exerts immunological antitumor effects *in vivo*

To gain further insights in possible immunological changes relevant for EwS immunogenicity, initial *in vivo* xenograft experiments were performed using s.c. implanted A673 and TC32 cell lines in Rag2^{-/-} γ c^{-/-} mice (Figure 12a).

As previously shown for A673 xenografts in NMRI-Foxn1nu/nu mice, significant increase of viral *fiber DNA* could be confirmed for the *combo* group 3 days after i.t.-injection, indicative of enhanced viral replication (Figure 12b). Immunoblotting of tumor lysates from explanted tumors 3dpi further verified an increase in adenoviral *hexon* protein for animals receiving *combo* Tx as compared to *XVir* mono-Tx. This observation was accompanied by downregulation of RB protein levels and upregulation of them MHC-I molecules HLA-A+B, which was also detectable in tumors from *LEE*-treated animals (Figure 12c).

Additional flow cytometric assessment of explanted tumors showed upregulation of surface MHC-I and PD-L1. Interestingly, the *don't-eat-me* molecule CD47 was significantly decreased in *combo* Tx only in A673 xenografts, whereas no significant change could be stated in TC32 (Figure 12d).

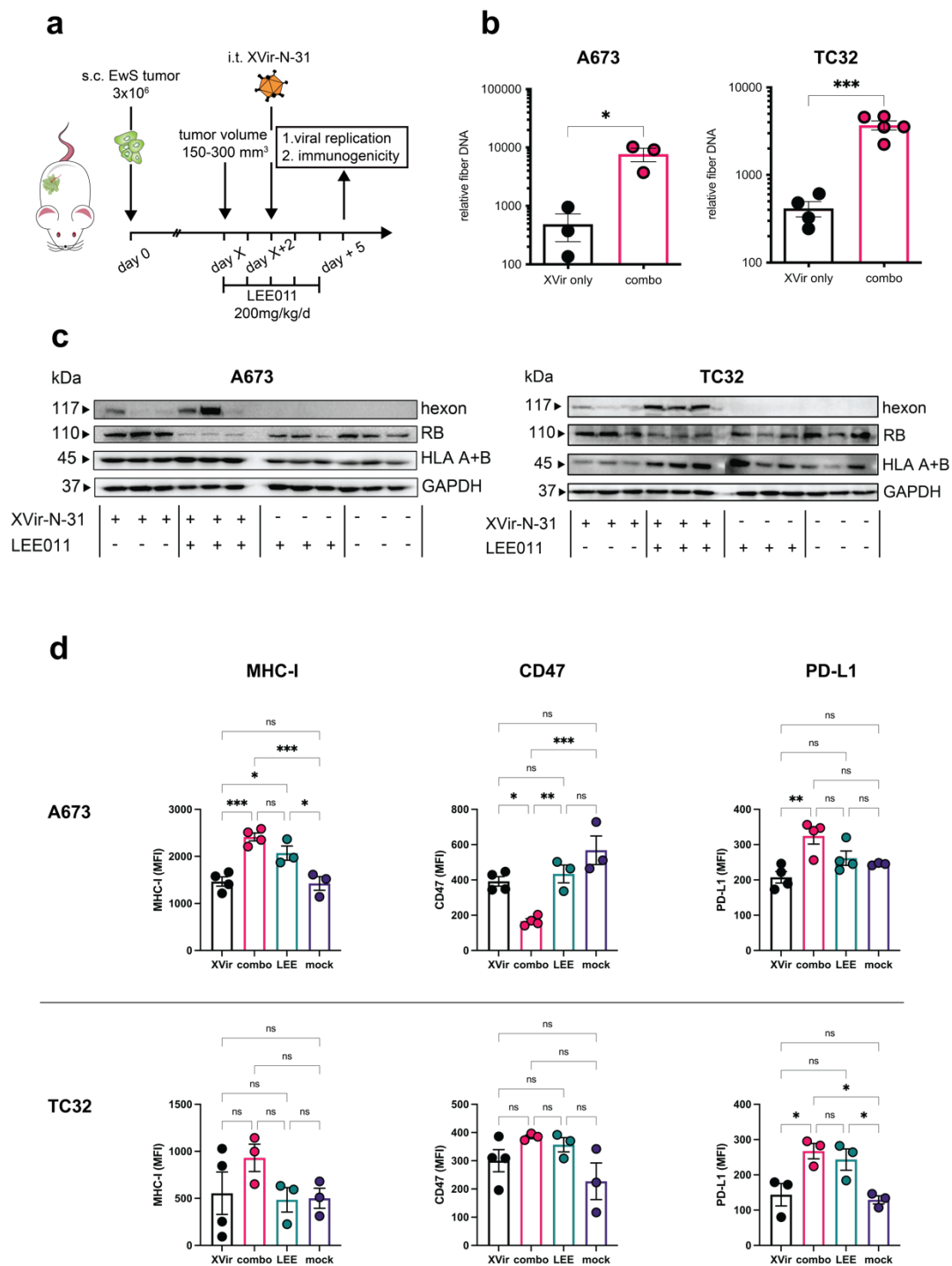


Figure 12: Combination of XVir-N-31 and CDK4/6 inhibitor LEE011 increases viral replication and immunogenicity of xenografted EwS tumors *in vivo*. (a) Experimental setup: 3×10^6 A673 or TC32 tumor cells were injected s.c. in the flank of $Rag2^{-/-}\gamma c^{-/-}$ mice at day 0. When tumors reached a volume of 150–300 mm^3 (day X), animals were randomized to treatment groups: *mock*, *Xvir (only)*, *LEE(011)*, and *combo* and inhibitor Tx via oral gavage was started with 200mg/kg/d for 5 consecutive days. On day X+2, 1×10^{11} viral particles (VP) of XVir-N-31 or PBS were injected i.t. (TC32 tumors were injected with 5×10^{10} VP). At day X+5 (3dpi) mice were sacrificed for further analyses. Single cell suspensions were generated from whole tumors. (b) Relative *fiber DNA*, indicative of viral replication, was measured by sqPCR. Each dot represents one injected tumor. Unpaired, two-tailed student's t-test was used for statistical comparison. (c) Immunoblots of explanted tumors were performed, showing protein expression of adenovirus-specific hexon, RB and HLA-A+B. GAPDH was used as loading control. Each lane represents one explanted tumor. (d) Flow cytometry assessment of MHC-I, the *don't-eat-me* CD47 molecule and the immune-checkpoint ligand PD-L1 was done after dead-cell exclusion (by Viability Dye) and median fluorescence intensity was depicted in column bars (anti-human HLA-ABC-PerCPVio700,

CD47-FITC and PD-L1-APC antibodies were used). Each dot represents one explanted tumor. Statistical analyses were performed in Prism 9 using Tukey's multiple comparison in combination with ordinary one-way ANOVA. Significance levels are indicated as asterisks: * $p < 0.05$, ** $p < 0.01$, $p^{***} < 0.005$, $p^{****} < 0.0001$, ns = not significant. Error bars indicate the SEM.

Table 20 and Extended Data Figure 7 show exemplary genes associated with pathway activation of possible relevance (one representative animal per group). Transcriptomes were generated with the Affymetrix Human Gene 1.0 ST array.

On one hand, *XVir* and *LEE* Tx complemented each other (e.g. regarding the induction of inflammation) but on the other hand, the combination of both (*combo*) had the capacity to upregulate additional new gene expression patterns. By analyzing different signaling cascades utilizing the online tool *reactome*, it seemed that (1) *LEE* Tx was decisive for the increase in antigen-processing and -presentation. (2) Monotherapy of *XVir* compared to *mock* showed the strongest induction of cascades associated with phagosome formation via the endoplasmatic reticulum and *combo* Tx lead to a superior induction of α - and β -interferon signaling.

Pathway name	Entities				Reactions	
	found	ratio	p-value	FDR*	found	ratio
Antigen Presentation: Folding, assembly and peptide loading of class I MHC	59 / 102	0.007	1.11e-16	4.88e-15	14 / 16	0.001
ER-Phagosome pathway	60 / 165	0.011	1.11e-16	4.88e-15	8 / 10	7.56e-04
Endosomal/Vacuolar pathway	57 / 82	0.006	1.11e-16	4.88e-15	3 / 4	3.02e-04
Class I MHC mediated antigen processing & presentation	64 / 465	0.032	1.11e-16	4.88e-15	29 / 48	0.004
Interferon gamma signaling	69 / 255	0.017	1.11e-16	4.88e-15	9 / 16	0.001
Antigen processing-Cross presentation	60 / 187	0.013	1.11e-16	4.88e-15	11 / 23	0.002
Interferon alpha/beta signaling	86 / 191	0.013	1.11e-16	4.88e-15	9 / 22	0.002
Interferon Signaling	90 / 401	0.027	1.11e-16	4.88e-15	26 / 69	0.005
Immune System	117 / 2,713	0.184	1.11e-16	4.88e-15	314 / 1,593	0.12
Adaptive Immune System	68 / 1,003	0.068	1.11e-16	4.88e-15	50 / 264	0.02
Cytokine Signaling in Immune system	100 / 1,108	0.075	1.11e-16	4.88e-15	130 / 687	0.052

Table 20: Analysis of significantly overexpressed pathway-associated genes in *combo* Tx compared to *mock*. ≥ 2 -fold overexpressed genes ($n = 183$) were analyzed with the online software *reactome* (<https://reactome.org>). One respective animal per group (TC32 xenografts, 3dpi).

Given observed phenomena, being in line with an increase of EwS immunogenicity, further *in vivo* experiments with the additional application of human PBMCs were performed. With this model of *transient humanization* possible interaction in-between xenografted EwS tumors and transplanted human PBMCs were assessed together with Dr. med. candidate Caroline Schöning. Moreover, mouse immune cell populations were characterized with the goal to assess phenotypic changes associated with antitumor innate activity and antigen-presenting capacities.

4.4.5 Combo Tx increases survival *in vivo*

An optimized therapeutic setup with 2 x i.t.-injection of XVir-N-31 was chosen to evaluate tumor growth control and survival. Subsequent i.t.-applications of OV_s (mostly 3 injections) are commonly used in animal experiments, especially when evaluating s.c. tumor growth^{193, 276, 277} and multiple injections also are currently evaluated in early clinical trials, in case tumors are relatively easy to access (e.g NCT03206073, NCT03954067, or NCT04673942).

In both xenograft experiments (A673 and TC32) *combo* Tx resulted in a significant survival benefit as compared to monotherapies and *mock* Tx. Of note, TC32 xenografts responded less than A673, reflected by shorted survival rates and inferior growth inhibition of s.c.-implanted tumors (Figure 13 b-d).

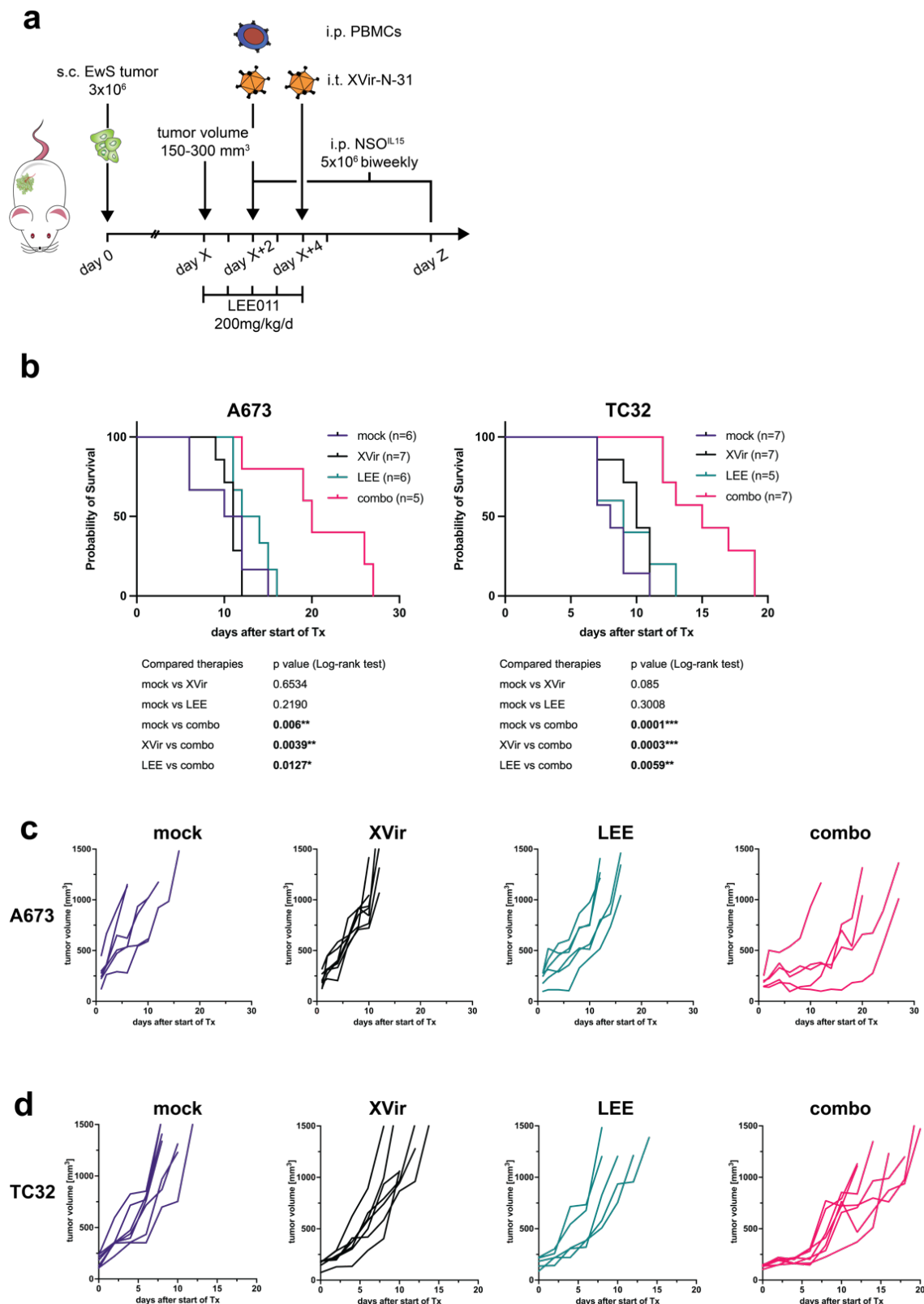


Figure 13: Combination of XVir-N-31 and CDK4/6 inhibitor LEE011 increases survival and local tumor control. (a) Experimental setup: 3×10^6 A673 or TC32 tumor cells were injected s.c. in the flank of $Rag2^{-/-}\gamma c^{-/-}$ mice at day 0. When tumors reached a volume of 150-300 mm^3 (day X), animals were randomized to treatment groups: *mock*, *XVir*, *LEE*, and *combo* and inhibitor Tx via oral gavage was started with 200mg/kg/d for 5 consecutive days. On day X+2, and day X+4 1×10^{11} viral particles (VP) of XVir-N-31 or PBS were injected into the tumors. Furthermore, all mice received i.p.-injections of 1×10^7 HLA-A2-positive PBMCs and 5×10^6 IL-15-producing NSO cells (previously irradiated with 80 Gray). NSO application was repeated biweekly until the end of experiment (defined by tumor volume $\geq 1000 \text{ mm}^3$). (b) Kaplan-Meier survival curves were generated, and statistical differences were evaluated by Mantel-

Cox log-rank test in Prism 9. Number (*n*) of animals per group is indicated. Tumor control in respective treatment groups is shown for each animal per group until the end of experiment for (c) A673 and (d) TC32 xenografts.

4.4.6 Combo Tx induces T cell infiltration

At the end of the experiment (tumor volume $\geq 1 \text{ cm}^3$) human T cell distribution was analyzed by flow cytometry and confirmed by immunofluorescence (last, not shown). Animals from the *combo* Tx group exhibited significantly more TILs in xenografted A673 tumors. A similar, albeit non-significant, tendency was confirmed in TC32 xenografts (Figure 14a). Due to lower numbers of infiltrating T cells in *mock* and *XVir* groups, here further T cell characterization did not produce robust results.

T cell phenotyping in *LEE* and *combo* Tx animals however revealed a dominance of CD4⁺ T cell infiltration (Extended Data Figure 8a+b). Interestingly, the cognate CXCL10-receptor CXCR3 stained also positive on most of infiltrating T cells in *combo* Tx, whereas CXCR3 was only observed on a minority of T cells in *LEE* Tx. Of note, the majority of infiltrating T cells in all aforementioned groups expressed PD-1, indicating a features of T cell exhaustion (Extended Data Figure 8c+d).

Furthermore, representative intracellular stainings of T cell transcription factors were performed in tumors with the highest numbers of TILs (Extended Data Figure 8). Here, infiltration of T regulatory helper cells (T_{reg}), type II helper cells (T_{H2}), and T_{H17} cells could be excluded, whereas the transcription factor *T-bet* showed upregulation in the majority of CD4⁺ T cells indicative for a T_{H1} differentiation.

Also, human T cells engraftment in spleens from A673 xenografts was compared in-between groups at the end of experiment demonstrating superior engraftment in *combo*- and *LEE*-treated animals. Especially CD4⁺ T cell engraftment was significantly enhanced and a tendency towards increased CD8⁺ T cell engraftment was observed for *combo* Tx (Figure 14c+d). Further phenotyping via transcription factors revealed that most engrafted CD4⁺ T cells in *combo* and *LEE* groups expressed T-bet, demonstrating a specific engraftment of T_{H1} cells (Figure 14e). Especially in comparison to *XVir* monotherapy, the induction of T_{reg} cells was significantly decreased (Extended Data Figure 9e, left).

Also, CXCR3 expression on engrafted T cells was the highest in *combo* Tx, further indicating a possible role of this signaling axis regarding engraftment and tumor infiltration (Extended Data Figure 9e, right).

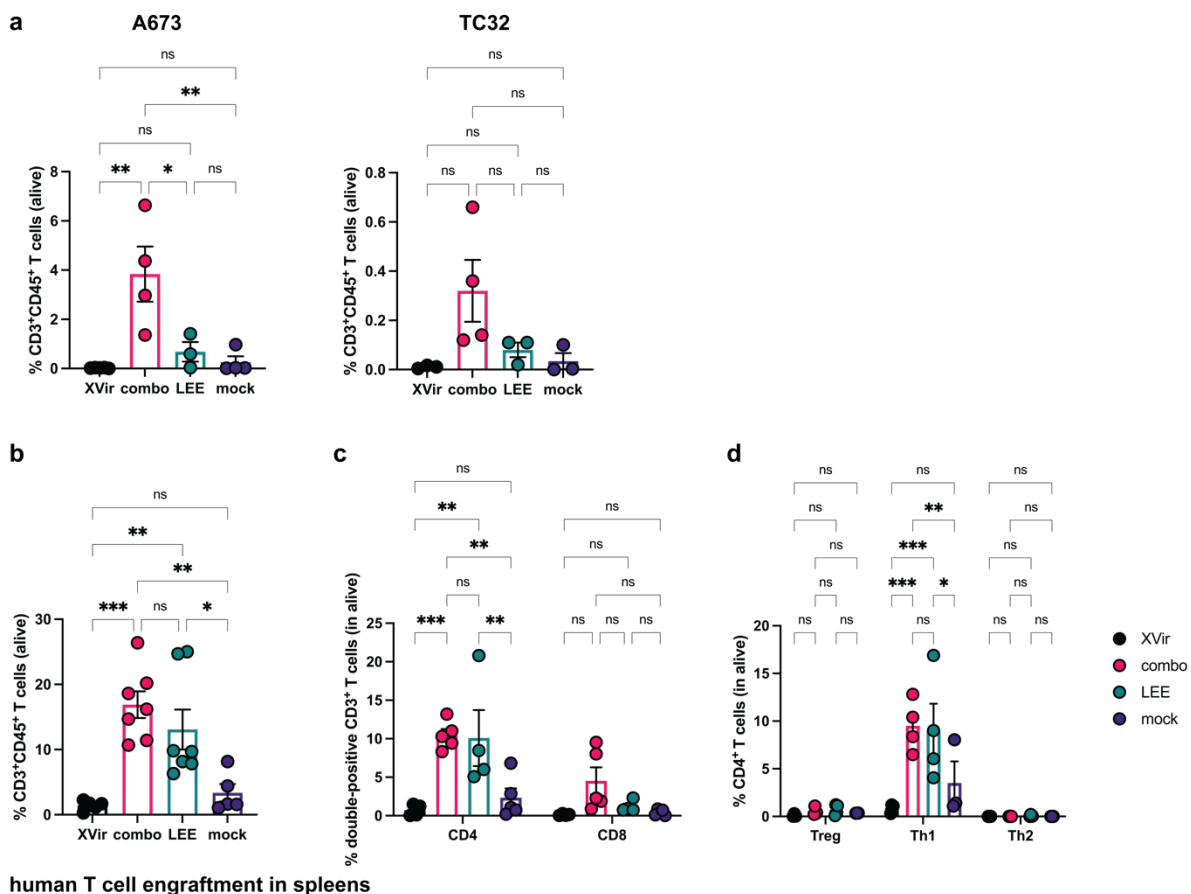


Figure 14: Combination of XVir-N-31 and CDK4/6 inhibitor LEE011 induces T cell infiltration and increases T cell engraftment. (a) Tumor-infiltration by human T cells was analyzed by flow cytometry from 3-4 representative animals at the end of experiment. Percentage of anti-human CD45-VioGreen and CD3-PE-Vio770 double positive cell in all gated cells alive (after live-dead-exclusion via DAPI) was plotted as column bars per treatment group and statistical comparisons were done by Tukey's multiple comparison within ordinary one-way ANOVA. Each dot represents one animal. (b) Analyses of human T cell engraftment in spleens were performed like described in (a). (c) Subset analyses of T cell engraftment in spleens was studied by co-staining against CD4-APC-Vio770 and CD8-FITC, and further characterization of CD4 subsets was done by intracellular staining of (d) transcription factors T-bet-PE (Th1 cells), GATA3-APC (Th2), and Foxp3-PE combined with CD25-APC (Treg). Here, a fixable live-dead-dye (Viability 405/520) was utilized before membrane permeabilization. Statistical assessment was performed by Tukey's multiple comparison within ordinary one-way (in a+b) and two-way ANOVA (in c+d). Significance levels are indicated as asterisks: * $p < 0.05$, ** $p < 0.01$, *** $p < 0.005$, **** $p < 0.0001$, ns = not significant. Error bars indicate the SEM.

4.4.7 Combo Tx induces an abscopal effect

To analyze the potential of XVir and *combo* Tx to induce an abscopal effect, a group of mice were s.c.-implanted with EwS cell lines at both flanks. Measurement of tumor volume, over a period of 7-10 days after start of Tx, showed a reduced growth of non-injected tumor lesions only in animals receiving *combo* Tx, indicative of an abscopal effect.

Further analysis by flow cytometry did not show a significant difference in treatment groups concerning T cell infiltration. In general, numbers of tumor-infiltrating T cells were low, compared to T cell infiltration at the end of the experiment, although there was a tendency towards more TILs especially in non-injected tumors of animals treated with *combo* and *LEE*.

When assessing non-injected A673 xenografts for viral DNA by sqPCR, genomic *fiber DNA* was detected in amounts indicative of replication, which was not the case in TC32 xenografts (data not shown).

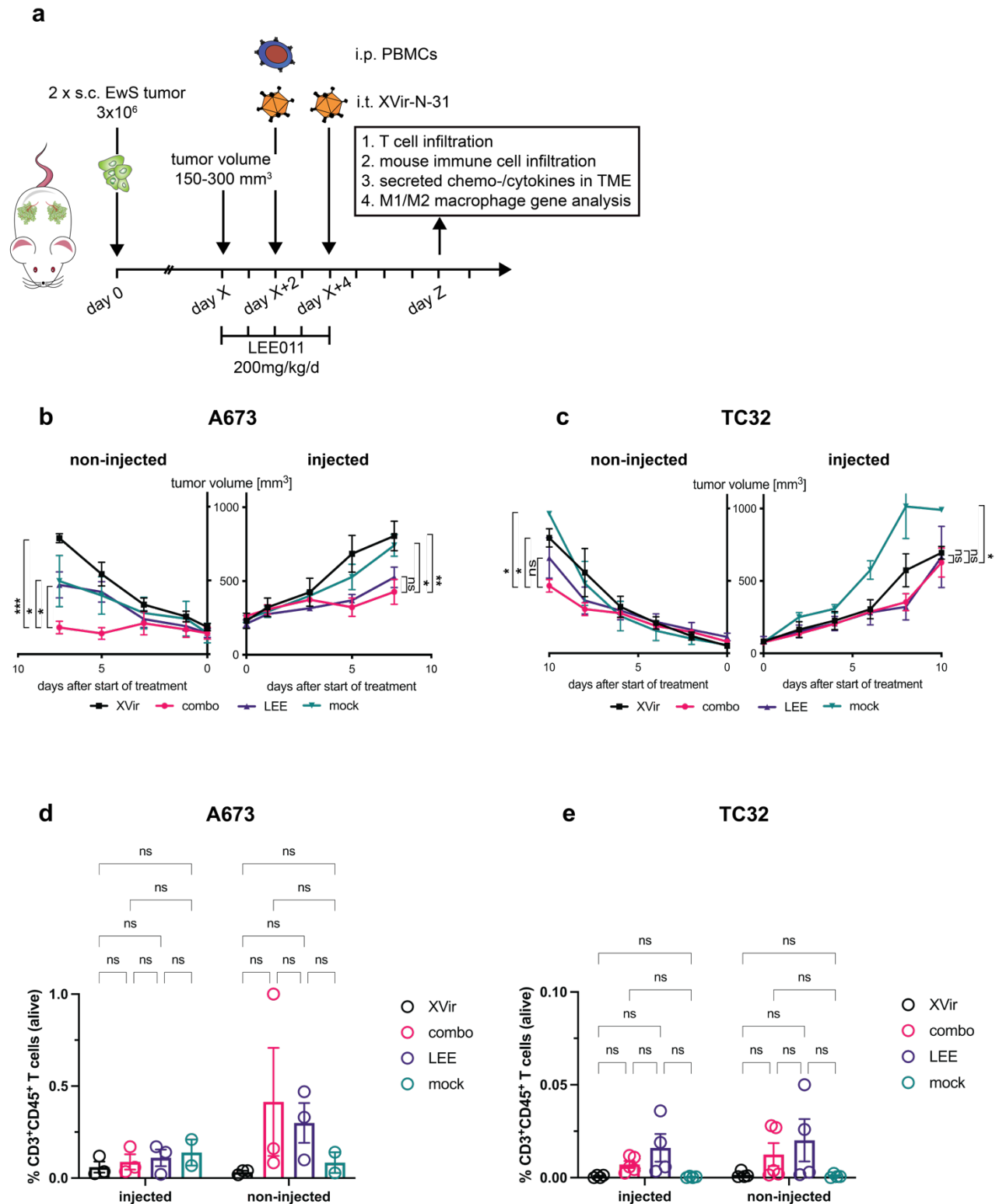


Figure 15: Combination of XVir-N-31 and CDK4/6 inhibitor LEE011 induces an abscopal effect. (a) Experimental setup corresponds to the previous experiment (described in Figure 13, with the exception that tumor cells were injected in both flanks of mice and that animals were sacrificed 4 days after 2nd XVir-injection. (b+c) Mean A673 and TC32 tumor volumes per Tx group is shown 7-10 days after start of Tx for *non-injected* (left graphs) and *XVir-injected* (right graphs) s.c.-implanted tumors. Statistical analysis was done with the open-access online tool *TumorGrowth*²⁷⁵ using pairwise

comparisons of longitudinal tumor growth (holm post-test adjustment was done in b). Human T cell infiltration (equally studied as described in [Figure 14](#)) was analyzed by flow cytometry, statistical comparison was done with two-way ANOVA Tukey's multiple comparison test.

Furthermore, human T cell engraftment was analyzed in spleens of respective groups. T cell engraftment at this time point was low and a tendency of superior engraftment was observed with *LEE* Tx ([Extended Data Figure 10](#)).

4.4.8 Combo Tx induces CXCL10 in the tumor microenvironment of injected tumors

As T cell infiltration with CXCR3⁺ T cells was observed at the end of *in vivo* experiments ([Figure 14](#)) and *in vitro* chemo-/cytokine screenings revealed a possible role of CXCL10 (ligand for CXCR10) for the induction of immunogenicity and T cell infiltration, a selection of chemo-/cytokines was analyzed from xenografted tumors to get a deeper understanding of changes in the TME. Furthermore, CXCL10 gene induction was assessed from xenografted tumors ([Figure 12](#)) which were harvested 3 days after XVir-N-31-injection.

Interestingly, CXCL10 was induced on gene expression levels in both of xenografted EwS cell lines (3dpi) in animals which received *combo* Tx ([Figure 15a+b](#)). This phenomenon was confirmed in the second set of xenograft experiments where animals received 2 i.t. injection of XVir-N-31 (4 days after 2nd injection) by evaluating CXCL10 protein levels in harvested tumors after mechanical dissection in PBS. Of further importance was the observation that CXCL10 in non-injected tumors was not altered in-between Tx groups. ([Figure 15c+d](#)).

Furthermore, *combo* Tx also significantly increased IL-8 in A673 xenografts and a tendency of IL-8 increase was also observed in TC32 with XVir and *combo* Tx. In contrast, TNF was increased by *LEE* Tx ([Extended Data Figure 11](#)).

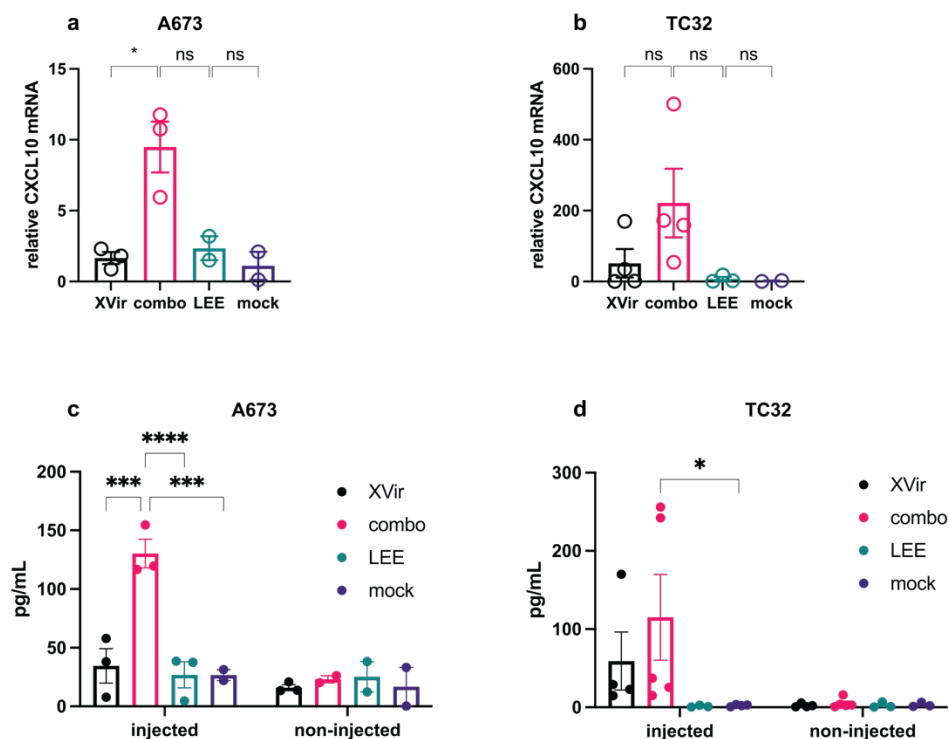


Figure 16: Combination of XVir-N-31 and CDK4/6 inhibitor LEE011 induces CXCL10 in the tumor microenvironment. (a) Relative gene expression of CXCL10 was analyzed in explanted A673 (3dpi, [Figure 12](#)) and (b) TC32 tumors. Each dot represents one tumor. Unpaired, two-tailed student's t-test

was used performed for statistical analysis. (c) CXCL10 concentration in the tumor microenvironment of explanted xenografts was evaluated after mechanical dissection of tumors in 4mL PBS for (c) A673 and (d) TC32. Statistical analysis was performed by Tukey's multiple comparison combined with two-way ANOVA. Significance levels are indicated as asterisks: * $p < 0.05$, ** $p < 0.01$, p*** < 0.005 , **** $p < 0.0001$, ns = not significant, or not shown. Error bars indicate the SEM.

4.4.9 Combo Tx induces mouse monocyte infiltration in injected tumors

Studying the response to human AdV in *in vivo* mouse experiments is challenging, as mouse cells are not permissive for human AdV replication. Therefore, most data concerning immunological changes are derived from syngeneic mouse models where a human oncolytic adenovirus was applied^{193, 194}. In this context, inflammatory responses after virus application are studied without productive replication in the tumor.

Analyses from these experiments allow the assessment of innate immune populations (monocytes, neutrophils, macrophages) towards virus-induced inflammatory stimuli^{203, 217} which can be altered by the *combo* Tx, in terms of intratumoral replication and cell death induction.

In vivo experiments from both xenografted cell lines confirmed the infiltration of monocytes in all *combo*-treated animals at both 3 days after 1st injection and 4 days after 2nd injection (only shown for timepoint: 4 days after 2nd injection) (Figure 15b+c). This is in line with known dynamics of innate immune response (of neutrophils and monocytes), with monocytes becoming the dominant population around 24 hours after the inflammatory stimulus^{218, 278, 279}.

Due to an absolute and relative increase of tumor-infiltrating monocytes (only relative are shown in Figure 15b+c), relative numbers of neutrophils and TAMs decreased but only in virus-infected tumor lesions, with most distinct changes being observed for *combo* Tx. In this context, viral *fiber DNA* (indicative of replication) showed a strong positive correlation with mouse immune cell infiltration and more specifically with mouse monocytes (Figure 15d).

Further characterization with regard to MHC-II and co-stimulatory CD86 expression on tumor-infiltrating mouse immune cells and mouse gene expression allowing further differentiation of monocytes/macrophages with antitumoral (M1) and protumoral (M2) properties was studied by Caroline Schöning (MD thesis, in preparation). Here, especially *combo* Tx and to a lesser extent also *XVir* monotherapy significantly increased the M1/M2 macrophage ratio further indicating antitumoral activity of cells of the innate compartment.

Figure 15 e illustrated exemplary upregulated mouse immune cell genes associated with M1 and M2 TAMs²⁵¹ (in explanted A673 tumors), with CXCL10 and IL1B portraying the strongest upregulation through *combo* Tx.

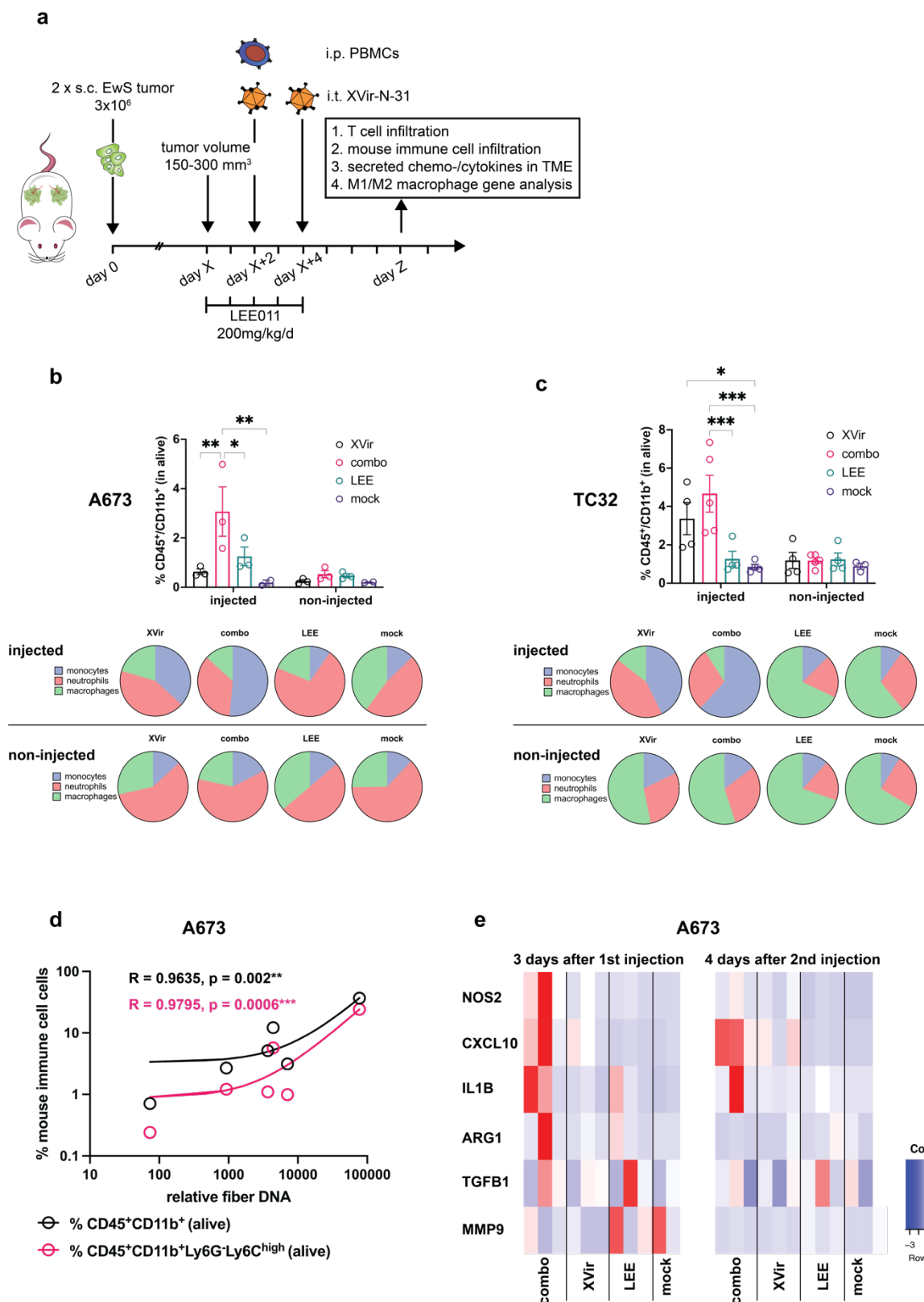


Figure 17: Combination of XVir-N-31 and CDK4/6 inhibitor LEE011 induces mouse monocyte infiltration in injected tumors. (a) Experimental setup corresponds to the previous experiment (described in Figure 15) and animals were sacrificed 4 days after 2nd XVir-injection for further analyses. Relative numbers of tumor-infiltrating mouse innate myeloid immune cells were assessed via flow cytometry (compared to all cells alive, after dead-cell exclusion with DAPI staining), utilizing anti-mouse antibodies against CD45-PE-Vio770, CD11b-VioBright-FITC. Statistical analysis was performed by applying Tukey's multiple comparison analysis and two-way ANOVA. Further characterization of innate

myeloid cells was achieved by addition use of anti-Ly-6G-PerCP-Vio700 (for neutrophils), anti-Ly6C-VioGreen (Ly6C^{high} for monocytes) as well as F4/80-PE (for macrophages). Respective percentages of neutrophils, monocytes and macrophages of all myeloid cell are shown as pie charts. (d) Positive correlation of viral *relative fiber DNA* with infiltrating myeloid cells (CD45⁺CD11b⁺) and especially monocytes (CD45⁺CD11b⁺Ly6G⁺Ly6C^{high}) in relation to all cells alive using non-linear regression analysis in Prism 9. Pearson r (R) and p-values are indicated. (e) Gene expression analysis of macrophage M1 (NOS2, CXCL10, IL1B)- and M2 (ARG1, TGFB1, MMP9)-associated transcripts using mouse-specific primer pairs²⁵¹ from explanted A673 tumors 3days after 1st and 4 days after 2nd XVir-injection (from experiments described in [Figure 12 and 15-17](#); 3 animals per group were analyzed). Heatmaps were generated using the script *heatmap2* in R²⁶⁶ (red = high expression, blue = low expression). Significance levels are indicated as asterisks: * p < 0.05, ** p < 0.01, p*** < 0.005, ****p < 0.0001, ns = not significant. Error bars indicate the SEM.

4.4.10 Combo Tx induces maturation of THP-1 and monocytic immature dendritic cells *in vitro*

After observing these remarkable changes in mouse innate immune cell populations *in vivo* by the *combo* Tx and due to the limitations of the *in vivo* model used in this work, which does not allow studying interconnections of innate and adaptive immunity, *in vitro* models of antigen presentation by monocyte (mo)- and THP-1-derived DCs were applied^{280, 281}.

The maturation of mo-derived imDCs after exposure to CM (*supernatant*), tumor cells (after exchange of CM, *cells only*) and both (*full*) was significantly increased after 48h of coculture by *combo* Tx, assessed by double-positivity of T cell-co-stimulatory markers CD80 and CD86 ([Figure 16b+c](#)). Of note, the best induction of maturation was observed for tumor *cells only*, possibly indicating immunosuppressive properties of soluble factors in the supernatant/CM ([Figure 16b](#)), which is in line with recent finding from Gassmann et al.⁸⁸ identifying EVs secreted into CM to be relevant for pathological activation of moDCs. Here, also *LEE* was identified as the major contributor for upregulation of maturation markers, which could be further enhanced by the addition of XVir-M-31 in all conditions ([Figure 16b](#)).

As THP-1 cells are often used as a model for antigen presentation^{282, 283}, functionally resembling monocytes²⁸¹, and coculturing of THP-1 in CM of tumor cells was already described in the literature to possibly affect THP-1 phenotype and function²⁸⁴, THP-1 cells were used in a second model to confirm aforementioned observations.

To a very similar extend compared to moDCs, THP-1 cells changed maturation marker after 72h-coculture in respective CM, with *combo* Tx being the strongest inductor of THP-1 maturation ([Figure 16d+e](#)).

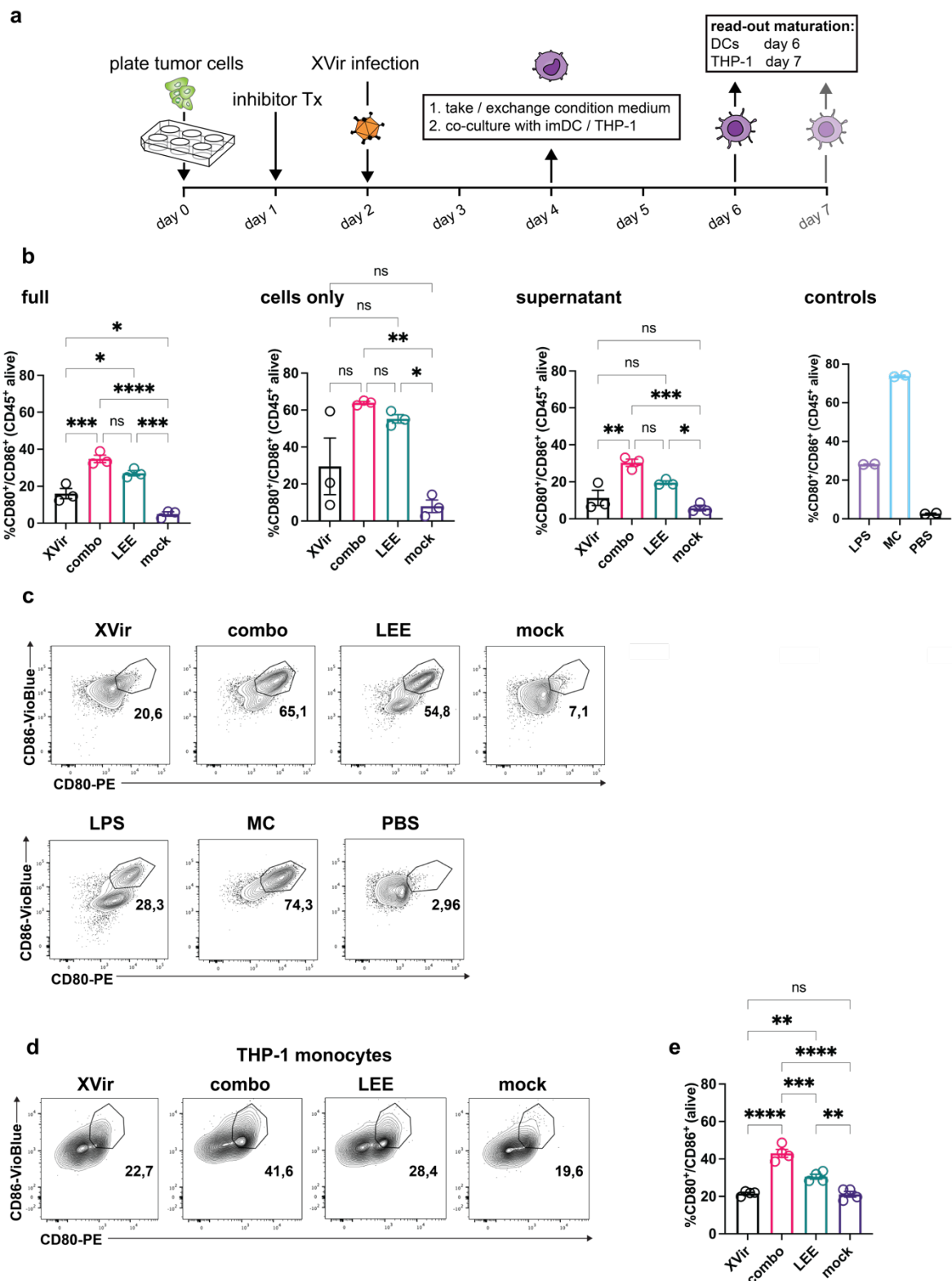


Figure 18: Combination of XVir-N-31 and CDK4/6 inhibitor LEE011 induces maturation of THP-1 and monocytic immature dendritic cells *in vitro*. (a) Experimental setup: A673 tumor cells were plated in 6-well-plates. The day after, LEE 1 μ M was added and 24h later tumor cells were infected with XVir-N-31 at MOI25. At day 4 (i.e. 48hpi) supernatant was collected/exchanged and monocytic imDCs (differentiated with 100 ng/mL IL-4 and 800 U/mL GM-CSF for 5 days before start of coculture) or THP-1 cells were added to the condition medium (CM, after centrifugation) or to the tumor cells at ratio of 1:1. Maturation of monocytic imDCs was assessed after 48h of coculture and THP-1 cell maturation after 72h²⁸⁴ by flow cytometry measurement of CD86-VioBlue and CD80-PE double-positivity after dead-cell-exclusion by DAPI staining. In case coculture was done together with tumor cells, receptor surface expression was assessed on CD45-VioGreen-positive (i.e. immune) cells. (b+c) Maturation (indicated

as CD80/CD86-double-positivity, given in percentage of parental) of moDCs was assessed after coculture in CM (*supernatant*), tumor cells (after exchange of CM, *cells only*) and both (*full*). Statistical analysis was performed with Tukey's multiple comparison combined with ordinary one-way ANOV in Prism 9. 10 ng/mL lipopolysaccharide (LPS), PBS and maturation cocktail (consisting of 1000 U/mL IL-6, 10 ng/mL IL-1b, 10 ng/mL TNF, and 1mg/mL prostaglandin E2) served as controls. **(d+e)** Induction of maturation markers, as described above, was also verified in THP-1 cells after 72h of culture in CM. Significance levels are indicated as asterisks: * $p < 0.05$, ** $p < 0.01$, p*** < 0.005 , ****p < 0.0001 , ns = not significant. Error bars indicate the SEM.

4.4.11 Combo Tx increase antigen-specific T cell proliferation and activation *in vitro*

As Uzhachenko et al.¹⁶⁸ already described positive effects of CDK4/6i on adoptive T cell transfer (ACT) using an OT-1-OVA mouse model, the next step in this study was to assess effects of the triple combination: tumor-redirection T cells (CHM1 T cells), LEE and XVir.

Hence, due to the (1) availability of CHM1 T cells in our lab, (2) observed differences in maturation markers for THP-1 cells when cultured in CM, and (3) the HLA-match in HLA-A*02:01 of TCR-specificity and THP-1 cells, T cell proliferation and activation was assessed, taking relevant literature into account when designing the experimental setup ([Figure 17a](#))^{88, 283}.

After assessment of markers associated with antigen presentation and T cell co-stimulation on THP-1 cells (after 72h coculture in CM, [Figure 17b-g](#)), THP-1 cells were pulsed with CHM1³¹⁹ peptide, before fluorescence-labeled (eFluor450) CHM1³¹⁹/HLA-A*02:01-restricted TCR-transgenic CD8⁺ T cells were added at a ratio of 2:1. After THP-1 priming in CM, *combo Tx (XVir+LEE)* most significantly increased all assessed surface markers (CD80, CD83, CD86m HC-I, HLA-DR, and CD40; [Figure 17b-g](#)). When evaluating T cell proliferation and activation (via CD25) after another 96h of coculture, *combo Tx (XVir+LEE)* significantly increased T cell activity after antigen-specific stimulation ([Figure 17h-j](#)).

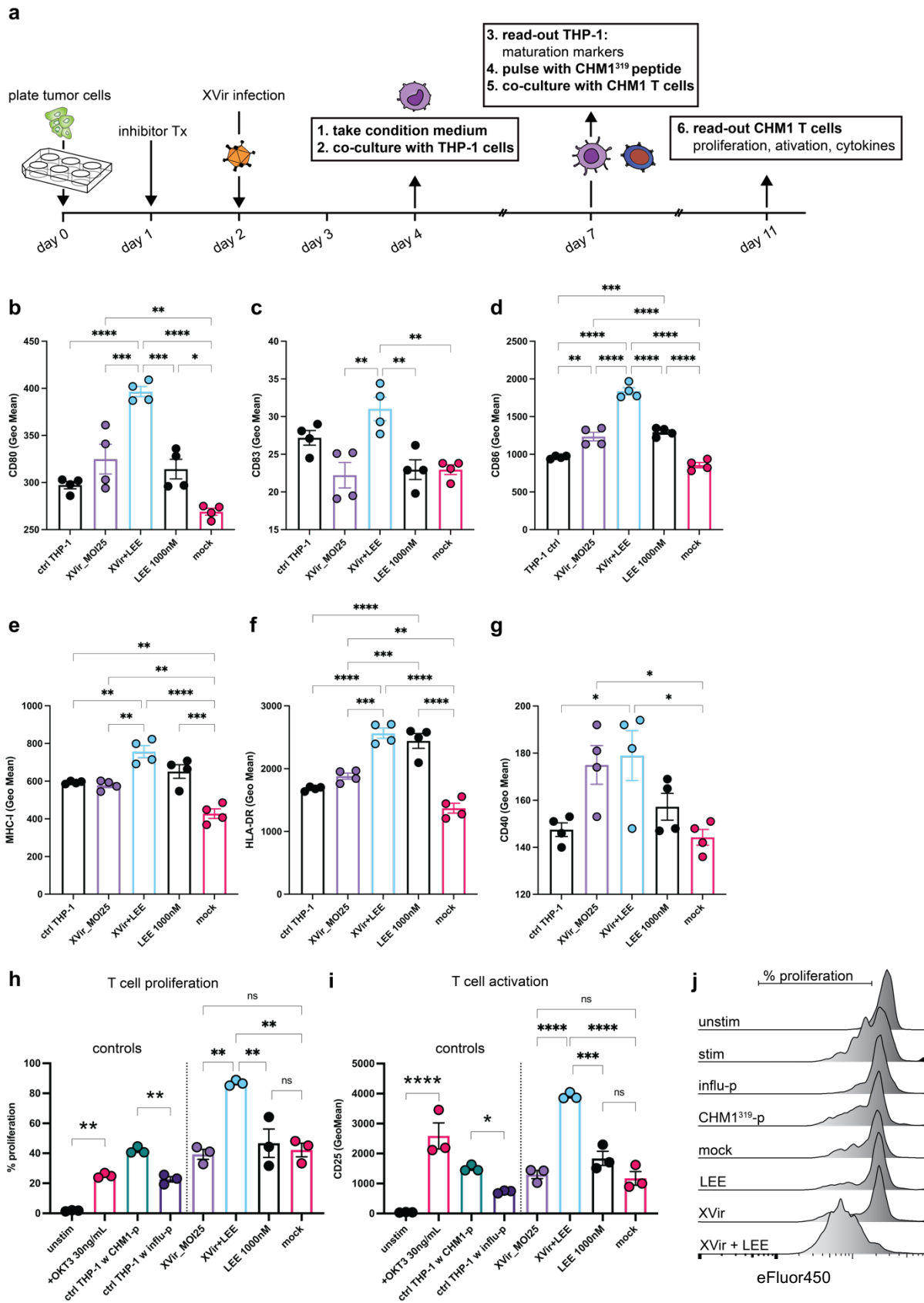


Figure 19: Combination of XVir-N-31 and CDK4/6 inhibitor LEE011 increase antigen-specific T cell proliferation and activation. (a) Equal experimental setting as in Figure 18 with the addition of fluorescence-labeled (eFluor450) CHM1³¹⁹/HLA-A*02:01-specific TCR-transgenic CD8⁺ T cells, which were cocultured with CHM1³¹⁹-peptide pulsed THP-1 cells at day 7, to evaluate antigen-specific T cell activation (at day 11, i.e. 96h after start of coculture). Two independent experiments were performed. (b-g) Surface expression of markers for T cell costimulation (CD80-PE, CD83-APC-Vio770, and CD86-

VioBlue) and antigen presentation (HLA-ABC-PerCP-Vio700 and HLA-DR-APC) were studied at day 7. Respective GeoMeans are shown as column bars and statistical analysis was performed by Tukey's multiple comparison combined with ordinary one-way ANOVA. (h+j) Percentage of proliferated T cells (gated on CD3-PerCP-Vio700) was compared to unstimulated control (y-axis: % of max). (i) GeoMean of CD25-APC, indicative of T cell activation (in CD3 gate) was plotted as column bars with Prism 9. Statistical analysis for control was done with unpaired, two-tailed student's t-test and experimental condition with Tukey's multiple comparison combined with ordinary one-way ANOVA. Significance levels are indicated as asterisks: * $p < 0.05$, ** $p < 0.01$, p*** < 0.005 , ****p < 0.0001 , ns = not significant. Error bars indicate the SEM.

4.4.12 Combo Tx of XVir-N-31, CDK4/6i and therapeutic T cells further increase synergistic tumor cell killing *in vitro*

After demonstrating that antigen-specific T cell activity is enhanced after coculture with APCs, direct tumor killing activity of CDK4/6i with *LEE*, *XVir* and *CHM1 CD8 T cells (CHM1)* was examined focusing on synergistic effects, again utilizing cell survival assays (SRB staining) after 48hpi and 24h after addition of T cells combined with analyses with the R tool *SynergyFinder* evaluating possible changes in synergistic effects^{265, 266}. Compared to previous experimental conditions (*Figure 5: CHM1 T cells and XVir-N-31 show synergistically lyse EwS tumor cells in vitro*), tumor cells were primed for 24h with *LEE* before *XVir*-infection.

As described in 4.3.1, synergistic effects in cell lysis were observed at *MOI*50-100 and at an E:T ratio of 1:1 – 0.25:1. When adding *LEE*, half-maximal inhibitory concentration (IC50) was lower for *XVir + LEE*, as expected but did not lead to a remarkable change in IC50 E:T ratio for *CHM1 T cells + LEE* (*Figure 18a-b*). When comparing *XVir + CHM1 T cells* with *XVir + CHM1 T cells + LEE*, strong synergism also occurs at lower *MOI* (6-50) and lower E:T ratios (0.5:1 - 0.125:1), meaning that the addition of CDK4/6i led to an extension of synergistic cell killing towards lower amounts for each therapeutic agent (*Figure 18c+d*).

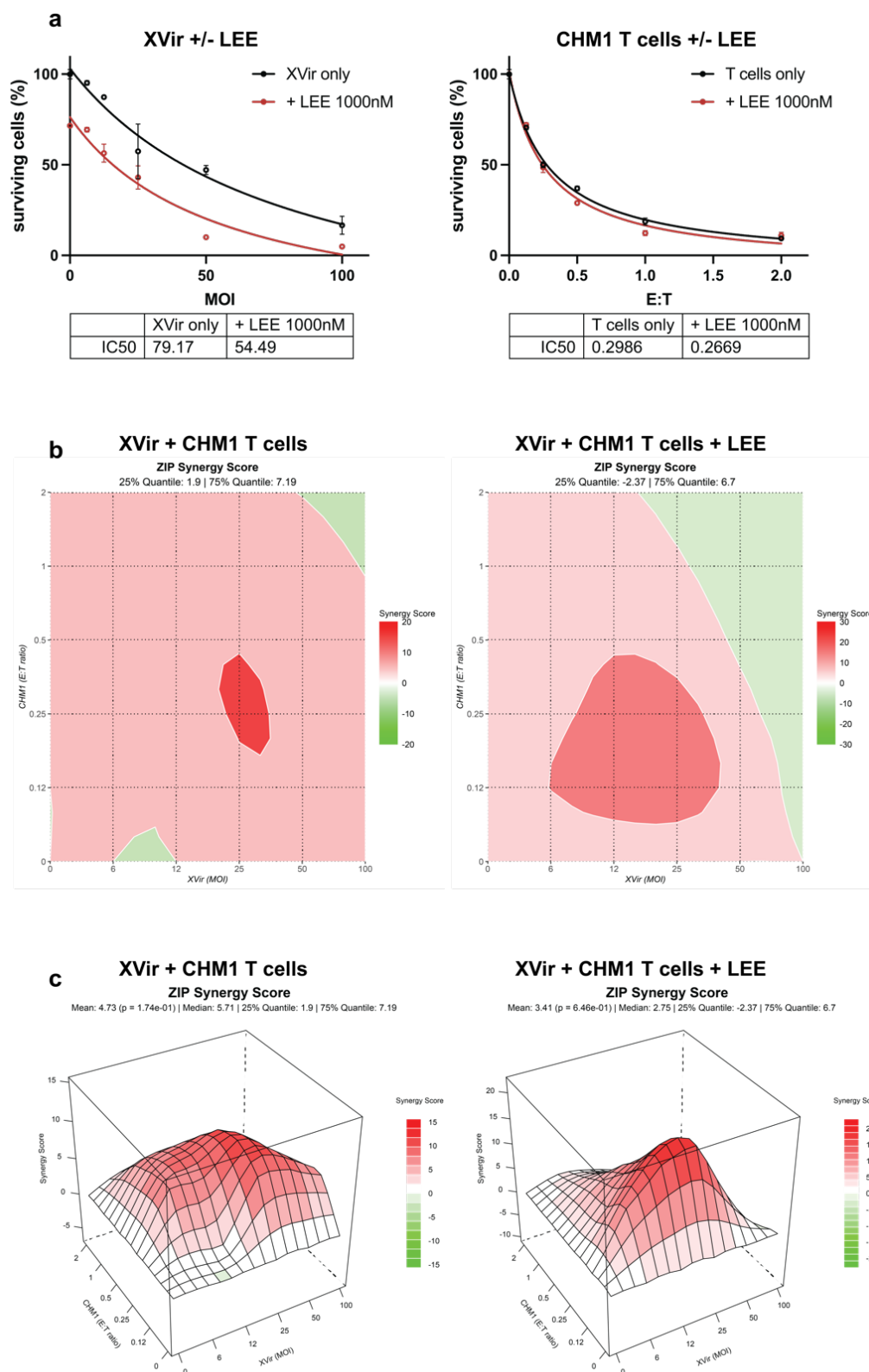


Figure 20: Combination of XVir-N-31, LEE011, and CHM1 CD8⁺ T cells further increases synergistic killing of tumor cells *in vitro*. The likelihood of synergistic interactions of XVir and LEE together with CHM1 CD8 T cells concerning tumor cell killing was evaluated via cell viability assays 24h after addition of T cells (i.e. 48hpi) and the *SynergyFinder* tool in R (experiments were performed in biological replicates and repeated, n=2). (a) Cell survival/viability assay: dose-response of XVir only and in combination with LEE at indicated concentration (IC50-values were exported from Prism 9 using the *inhibitor vs response* equation for dose-response – inhibition), with corresponding dose-response of CHM1 (CD8) T cells and LEE (right figure). (b) 2D-ZIP Synergy Score generated with R for experimental conditions: XVir + CHM1 T cells and XVir + CHM1 T cells + LEE, also depicted as 3D ZIP score in (c).

Synergy Score explanation: interactions larger than 10 are considered as likely *synergistic*; interactions from -10 to 10 are most likely *additive* and interactions less than -10 are likely to be *antagonistic*.

Results from section 4.4 can be summarized as follows:

1. The oncolytic adenovirus XVir-N-31 in combination with CDK4/6i increases oncolysis and viral replication in CDK4/6i-sensitive tumors *in vitro* and *in vivo* and thereby increases therapy response to XVir-N-31 resulting in a survival benefit in a xenograft sarcoma nude mouse model for animals receiving *combo Tx*²⁷¹.
2. *Combo Tx* induced A673 cell line derived CXCL10 levels accompanied by downregulation of RB/E2F1 proteins.
3. Increase of viral *fiber DNA*, indicative of replication, was confirmed in a second mouse model (Rag2^{-/-}γc^{-/-}) of two s.c.-implanted cell lines (A673, TC32) by the addition of CDK4/6i ribociclib.
4. HLA class I upregulation was confirmed on both total protein level and surface expression in explanted A673 and TC32 tumors (3dpi) in animals receiving *combo Tx*.
5. *Combo Tx* increases survival of transiently humanized mice with s.c.-implanted A673 and TC32 tumor cells, associated with enhanced T cell engraftment of T_{H1} cells and higher numbers of infiltrating T cells.
6. *Combo Tx* induces an abscopal effect assessed by tumor growth- inhibition of non-injected lesions.
7. *Combo Tx* is associated with the induction of CXCL10 in injected tumor lesions.
8. *Combo Tx* further induces mouse monocyte infiltration into injected tumors, positively correlating with viral *fiber DNA*.
9. *In vitro* conditioning of monocyte-derived DCs and THP-1 cells with supernatant from *combo*-treated tumor cells induces maturation and enhances antigen-specific T cell activity.
10. *In vitro* tumor cell killing of XVir-N-31 + CHM1 T cells can be further improved by CDK4/6i.

5 Discussion

This study preclinically assessed the suitability of the oncolytic adenovirus XVir-N-31 in combination with EwS-redirected T cells and CDK4/6i for the treatment of EwS.

For the first time, immunological properties of the oncolytic adenovirus XVir-N-31 in combination settings with EwS-redirected TCR transgenic T cells and CDK4/6i were characterized applying both functional *in vitro* and *in vivo* experiments.

First, it could be demonstrated that EwS cells are susceptible to XVir-N-31 infection resulting in tumor cell lysis and propagation of viral progeny. XVir-N-31-infected cell lines exhibited CALR surface expression (a markers of ICD, 'eat-me') accompanied by increased phagocytosis by imDCs.

Furthermore, synergistic effects of XVir-N-31 with both EwS-redirected TCR-transgenic T cells and CDK4/6i were demonstrated *in vitro* concerning tumor cell killing. These synergistic effects also translated into significant survival benefits *in vivo* of respective animals receiving either combination of XVir-N-31 with a) CHM1 T cells or b) CDK4/6i in (humanized) tumor xenograft mouse models, in both cases associated with superior T cell engraftment and induction of TILs. Further characterization of engrafted human T cells in the A673 model revealed a specific stimulation of CD4⁺ T cells expressing the T_{H1}-specific transcription factor T-bet. Increase of viral fiber DNA by CDK4/6i, indicative of superior replication, was demonstrated in 2 xenograft models.

Possible mechanistic insight for observed synergism coinciding with superior tumor control were gathered especially with CDK4/6i, revealing enhanced maturation of myeloid/monocytic DCs attributed to XVir-N-31-tumor cell lysis. The addition of CDK4/6i proved to be further beneficial for maturation of respective APCs resulting in superior antigen-specific T cell activation. The combination of XVir-N-31 and CDK4/6i also induced tumor features associated with increase immunogenicity, such as MHC-I upregulation and induction of CXCL10 in both xenograft models.

First hints towards the induction of an abscopal effect could be observed for the combination of XVir-N-31 and LEE *in vivo*, although underlying mechanisms were not further pursued.

Herein presented results and dynamic changes of immune cell populations induced by the *combo* Tx can be described as a novel ***multifactorial prime-boost-pull immunotherapeutic strategy***:

Prime: Tumor cells are primed (1) for enhances viral replication and (2) for an immune attack.

Boost: (1) Viral replication as well as (2) cell death induction is boosted leading to the enhanced activity of (3) pre-existing T cell responses (anti-tumor or anti-Ad, last not tested).

Pull: The inflammatory stimulus by this boosting-combination regiment attracts (1) innate cells which in turn show enhanced phagocytotic as well as antigen-presenting and co-stimulatory capacities which supposedly stimulate adaptive immunity and (2) induce TILs.

5.1 Limitations of this study

5.1.1 Combination of XVir-N-31 and CHM1 T cells

Current study assessed combination approaches of XVir-N-31 and CHM1 T cells *in vitro* and *in vivo*. Although *in vitro* effects of synergistic tumor cell killing occurred with high likelihood, only one experimental setup concerning timing of infection and addition of T cells was studied in more detail. This included the initial infection after 24-48h (depending on the presence of CDK4/6i) after tumor cell seeding and the addition of T cells 24h thereafter. Other reports studying different OV also evaluated different time points of infection and ACT. But literature research revealed that usually a relatively short interval in-between OV application and ACT was described to be most beneficial^{285, 286}.

Nevertheless, to further analyze mechanisms of synergistic tumor cell killing, different points in time would be needed as the replication cycle of XVir-N-31 takes ~48h, and changes of tumor surface molecules, such as MHC-I, were detected at 48hpi and not yet done at different time points (Figure 21).

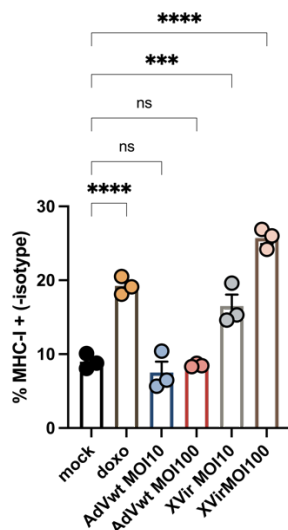


Figure 21: Evaluation of MHC-I surface expression after virus infection 48hpi. Surface expression was measured via flow cytometry with adenovirus wildtype (AdVwt) and XVir-N-31 (XVir) at 48hpi in A673 indicated MOI, after exclusion of dead cells via DAPI staining. Doxorubicin (doxo 1 μ M) served as positive control. HLA-ABC-APC and respective isotype was used.

Additionally, the evaluation of T cell effector cytokines, e.g. from cocultures with XVir-N-31-infected tumors cells, are needed to gain further mechanistic insights.

Also, characterization of T cell memory and/or effector populations as well as the profiling of respective chemokine-/cytokine-receptors and ligands could be helpful to better understand the interplay of both therapeutic agents, especially in an *in vivo* setting. In this regard, Watanabe et al.²⁸⁶ could demonstrate, that the combination of a cytokine-armed OAd (TNF+IL-2) together with anti-mesothelin-CAR-T cells inhibited metastatic spread, and CAR-T cell as well as non-CAR-T cells were attracted into the TME, which was enriched with CXCL10, CCL2, and CCL5. In the same study, luciferase-expressing CAR-T cells were applied, showing superior infiltration of respective T cells into xenografted tumors, providing important insights into time-dependent interactions with tumor cells²⁸⁶. Similar techniques to monitor T cell dynamics and distribution could be applied in the future.

Analyses of explanted tumors from animals receiving XVir-N-31 and CHM1 T cells did not show significant differences in comparison to respective monotherapies regarding tumor features of antigen presentation (MHC-I), expression of PD-1/PD-L1/2 or induction of CXCL10 (Extended Data Figure 4). This might be attributed to the fact that therapeutic agents were only

applied once, as compared to repetitive applications in most other reports^{79, 277, 287}. Nevertheless, superior tumor growth control was observed for the combination therapy in this setting, accompanied by induction of T cell infiltration (albeit in low numbers) and superior *in vivo* persistence.

5.1.2 Combination of CDK4/6i and XVir-N-31

Unfortunately, the full immunostimulatory potential of CDK4/6i could not be exploited during this study because the absence of functional B, T, and NK cells^{288, 289} in herein applied *in vivo* models was the limiting factor. At this point it is worth to mention, that attempts to generate reliable transgenic/syngeneic EwS mouse models failed thus far²⁹⁰. Therefore, to study immunological changes towards EwS *in vivo*, humanized mice carrying human xenografted tumors²⁹¹, such as implemented in this study, can be considered as the best attempt to gain cancer-immunological insights for this disease. Another drawback of this model is that humanization wasn't established in newborn mice. In case of an early establishment, possible human adaptive immune responses could have been characterized in more detail^{288, 292}. This aspect will be considered in the planning of future *in vivo* evaluations.

In terms of changes in possible antigens (e.g., viral and neoantigens for T cells), further methods like RNA sequencing or immunopeptidomics (further elaborate in the next chapter) were currently not implied. This would allow for more in-depth characterization of inflammatory pathways in addition to the mere measurement of a selection of cytokines in the TME of explanted tumors.

Concerning the content of herein presented experiments, human T cells could have been characterized in more detail, concerning chemo-/cytokine receptor expression and markers of immune exhaustion. In present work, only a possible contribution of the PD-1/PD-L1 axis was analyzed to some extent, due to the common combination of OV with ICB targeting respective axis (a more in-depth analysis of PD-L1 expression was done by Caroline Schöning, *Dr. med.* MD thesis). Nevertheless, analyses in this study revealed the preferential engraftment of human T cells exhibiting a T_{H1}-phenotype by *combo* Tx, most likely mediated by *LEE* (compare [Figure 14c+d](#)), whereas the induction of T_{reg} cells was also inhibited in both *combo* and *LEE*-treated animals (compare [Extended Data Figure 9](#)). This observation is in line with previously published reports demonstrating a decrease of T_{reg} populations and an increase of T_{H1} through CDK4/6i^{162, 166}.

At this point it has to be clarified that PBMCs used for humanization were only matched for HLA-A*02. Increasing the HLA-match might allow to broaden adaptive T cell responses and to reinvigorate preexisting (e.g. anti-Ad) donor T cell responses. Due to limited availability of matched PBMC at the time of experimental conduct, the aspect of HLA-match could not be fully considered but will be incorporated at best for future *in vivo* experiments.

The high increase in murine myeloid cells in injected tumors with *combo* Tx, also compared to *XVir only*, may also indicate a strong increase of the inflammatory stimulus (XVir-N-31) by the combination. These CD45⁺CD11b⁺Ly6G⁻Ly6C^{high} monocytes were not further characterized as they were observed for the first time in this *in vivo* setup. It is likely that these monocytes are of inflammatory nature (exhibiting addition CCR2). When focusing on functional consequences of inflammatory Ly6C^{high} monocytes, published reports attribute these subsets important roles in antigen presentation and profound host defense in the context of parasites²⁹³ or mediating antiviral immunity or auto-inflammation in cerebral diseases. Furthermore, they were shown to

differentiate into M1 macrophages or dendritic cells²⁹⁴. Taken together, they are responsible for mediating anti-pathogen immunity and do not promote tumor cell growth and T cell suppression as described for CD11b⁺Ly6G⁺Ly6C^{high} myeloid cells in the context of oncolytic reovirus²⁹⁵. Actually, the Ly6G⁺ neutrophilic population is (relative) reduced in this study, and MHC-II as well as co-stimulatory CD86 expression via FACs analysis of infiltrating myeloid cells was observed to be induced with *combo* Tx (shown in the MD thesis of Caroline Schöning). Together with the evaluation of M1/M2 macrophages-associated genes (increase, especially with *combo* Tx), the induction of an antitumor immunostimulatory effect is very likely, but functional analysis of isolated myeloid populations would be needed to determine possible T cell stimulating capacities.

Analysis of inflammatory pathway-induction by *combo* Tx was restricted to a selection of supposedly important chemo-/cytokines. RNA sequencing would allow for a deeper understanding of respective changes. On the other hand, it was demonstrated that CXCL10, also known as *Interferon-inducible Protein-10*, was upregulated by *combo* Tx. This resulted in increased concentrations in the TME of explanted tumors (compare [Figure 16](#)) accompanied by higher human T cell engraftment rates. Furthermore, engrafted T cells as well as TILs also exhibited the highest surface expression for the cognate receptor CXCR3 compared to other groups, highlighting the relevance of this axis concerning T cell infiltration, as described earlier by Berguis et al.⁵⁵. Analysis of publicly available RNA datasets from EwS patients, additionally connected higher CXCL10 levels with higher HLA and T cell co-stimulatory molecules, and an increase of M1 macrophage-associated genes whilst reducing M2 transcripts (compare [Figure 1](#)).

Concerning the observations of decreased tumor growth of non-injected tumors in *combo*-treated animals indicative of an abscopal effect, it has to be discussed which mechanisms might have contributed to the phenomenon. Relative numbers of TILs at that time point (4 days after 2nd injection) were low (compared to analyses from the end of experiments) and a dominant role of T cells in mediating observed abscopal effect is questionable. Also differences in relative numbers and subpopulations of murine myeloid cells in non-injected tumors did not differ, nor did transcripts associated with M1 or M2 macrophages change significantly. Solely a slight tendency towards higher MHC-II expression in non-injected TC32 tumors was detected for *combo* and *LEE* Tx.

As Ct-values for viral fiber DNA in 2 out of 3 *combo* animals, measured in non-injected A673 tumors, appeared at relatively early PCR synthesis cycles, a possible transfer of infectious viral particles to non-injected tumor lesions might serve as an explanation. In this regard, Kakiuchi et al. recently described a mechanism of OAd transfer via tumor-derived extracellular vesicles. Here, they could demonstrate that the OAd is wrapped into the membrane of a vesicle, which was secreted from tumor cells after being infected. Irrespective of the mouse model used (both immunocompromised as well as non-compromised) an abscopal effect could be induced and furthermore a preferential homing of those OAd-containing EVs into distant tumor lesions was observed²²⁸.

Complete tumor regression in all aforementioned *in vivo* models was not observed, but a temporal control of tumor growth could be demonstrated.

A reasonable explanation for the lack of long-lasting tumor control might be associated with the frequency of viral injection, the number of viral particles, and/or the limited time of inhibitor treatment (5 consecutive days only). Most other reports in the field, apply OVs more often²⁷⁷ or treat with an inhibitor until the end of experiment¹⁶². The main goal of this study was to

introduce and preclinically assess combination therapies with XVir-N-31 and identify immunological alterations associated with therapeutic benefits. CDK4/6i was applied to prime tumor cells before adenoviral replication and thereby boosting viral replication and immunological responses. In this context, this study successfully demonstrated both aspect of this prime-boost-pull strategy, with T cell infiltration as well as mouse monocytes being pulled into the tumor. Nevertheless, possible determinants for the induction of complete tumor regression, such as number of applications (virus and/or therapeutic T cells) and duration of inhibitor therapy should be evaluated in future studies.

Similarly important, compared to identifying determinants for tumor regression, would be to characterize mechanisms of tumor escape after OV or combination therapies.

In this regard, A673 xenografts were analyzed at the end of experiment, focusing on classical and non-classical HLA expression to better understand why observed TILs did not mediate longer tumor controls.

Immunoblotting of representative tumors revealed a strong upregulation of HLA-G (Figure 22), which is associated with T cell anergy²⁹⁶. As already mention in the introduction, G_{D2}-CAR-T cell therapy against EwS was already shown to induce both non-classical HLA-G and -E, tightly associated with IFN γ ⁷¹. T cell infiltration in EwS patient samples was also associated with local expression of immune-inhibitory HLA-G⁷⁶. The upregulation of HLA-G in this work might also indicate the induction of immunological pressure, which was mediated by CDK4/6i and further enhanced by the combination with XVir-N-31, but successfully abrogated by inhibitory HLA-G resulting in tumor regrowth.

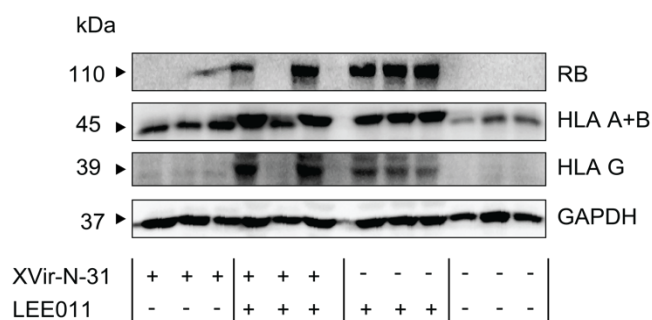


Figure 22: Evaluation of classical HLA A+B and non-classical HLA G expression in explanted A673 tumors at the end of experiment. Protein levels of indicated proteins were analyzed by western blot. GAPDH served as loading control. Each lane represents one explanted tumor.

Other mechanisms of resistance in tumor cells (next to PD-L1 expression), can also involve the activation of autocrine oncogenic CXCL10-CXCR3 signaling²⁶⁰, which might also be in play here and will be further discussed in the MD thesis of Caroline Schöning. In this regard, CXCL9/10-CXCR3 transcriptome levels were significantly upregulated in a neuroblastoma patient who relapsed after OAd (Celyvir) after initial disease stabilization²⁹⁷. Therefore, the ambiguous role of CXCL10 signaling still needs to be better understood. First mechanistic insights were described by Müller-Hermelink et al. for a dual role of CD4⁺ T cells. Depending on the absence or presence of either IFN γ (or TNF receptor 1), carcinogenesis was enhanced or controlled, mediated in part by CXCL9/10 in the TME²⁵⁹.

5.1.3 Oncolytic virotherapy and antitumor adaptive immune responses

A common phenomenon mediating relapse and refractory disease course after ACT is the loss of target antigen (by MHC loss/downregulation²⁹⁸ or actual antigen loss²⁹⁹), especially in the heterogeneous landscape of antigens and a highly immunosuppressive TME of solid tumors³⁰⁰. Addressing this hurdle, Walsh and colleagues could demonstrate that an OV not only increased *in vivo* persistence of adoptively transferred tumor-redirectioned T cells, but also protected from antigen loss variants due to increased activity of endogenous T cells. Those T cell responses were not attributed to epitope spreading but rather to the reinvigoration of pre-existing antitumor T cell responses by the combination of OV and ACT³⁰¹.

The aspect of epitope spreading is another feature coinciding with immunogenic cell death and release of tumor or viral antigens leading to the priming of novel T cell responses. It is important to overcome antigen escape variants by inducing sustained adaptive immunity against a broad spectrum of antigens³⁰². The occurrence of epitope spreading can be evaluated using model systems with known tumor and viral antigens or by identifying neoantigens and testing them toward their immunogenicity. Functioning axes of innate and adaptive immunity are a prerequisite. In this regard, Woller et al. was one of the first ones to demonstrate that an OAd in combination with ICB broadened the spectrum of neoantigen-specific T cell responses³⁰³, which was confirmed by other groups for different OVs^{304, 305}.

Another approach analyzing the antigenic landscape of virus-infected tumors is called immunopeptidomics. This mass spectrometry-based technique allows for the detection of the immunoprecipitated HLA-ligands which can be tested for their immunogenicity or utilized to generate antigen-specific vaccines or T cells in downstream approaches^{306, 307}. Using this technique in the context of OV, Rajaraman et al. could identify novel immunogenic epitopes from both viral and tumor-associated antigens³⁰⁸.

As the main aim of this study was to introduce YB-1-based oncolytic virotherapy and respective combinations for EwS treatment, and to test these approaches for *in vitro* and *in vivo* activity as well as basic changes of immunogenicity, more in-depth analyses concerning adaptive immune responses were not performed. Certainly, a deeper understanding of those immune activities is aspired for herein presented content and is planned to be evaluated in the future. Therefore, above-mentioned observations are of high relevance.

Due to the immunocompromised mouse model in this study lacking a connection in-between innate and adaptive immunity, *in vitro* experiments were performed focusing on EwS antigen-specific activation of T cells. Increased T cell activity could be demonstrated due to the presence of the OAd, indicating that as well as preexisting, novel antigen-specific or exogenous T cell responses can be augmented by XVir-N-31, and especially in combination with CDK4/6i. With current models available, epitope spreading is hard to assess for EwS *in vivo*, and not of high physiological relevance when assessed *in vitro*.

5.1.4 Limitations of human oncolytic adenovirus in animal models

Assessing the full spectrum of immunostimulatory effects of human adenoviruses in animal models always comes with certain limitations.

Usually, mouse cells are not permissive for human adenovirus infection, as the formation of new infectious particle is not supported in murine systems, with few exceptions (murine K-ras adenocarcinoma cell line ADS-12)³⁰⁹. Nevertheless, replication properties are not as productive as compared to levels observed in human cells³¹⁰. Therefore, accepted toxicology studies, as a prerequisite for clinical translation, are performed in Syrian hamsters, which are termed semi-permissive organisms for human adenoviruses³¹¹. Indeed, studies of OAd and induced immunological antitumor activities were already successfully recapitulated in such cancer models³¹².

Other groups utilize syngeneic mouse tumor models with little to no replication of the human OAd¹⁹³. Nevertheless, immunological antitumor activities were studied in this context thus far, also demonstrating the activation and successful rejection of murine tumors by T cells. Those studies were complemented by xenograft models using human tumor cell lines or patient-derived xenografts^{193, 194}.

Another interesting approach is the construction of murine oncolytic adenoviruses e.g. by utilizing the mouse adenovirus type 1³¹³. Several viral mouse constructs were generated in homology to Ad-Delta24 with deletions that compromise pRB-binding, rendering tumor-selective replication to cells exhibiting free E2F1 (such as tumors or cycling cells)³¹⁴. Indeed, those models showed promising results in terms of tumor control allowing the study of both arms of the immune system^{315, 316}.

Despite those efforts, the comparability of results to the human setting, still can only be evaluated in early clinical trials. In this regard, the OAd DNX2401 (Ad-Delta24-RGD) was preclinically evaluated for the treatment of glioblastoma in athymic nude mice (also used in this study). Results from a consecutive phase I trial in recurrent glioblastoma were very promising with 20% survival after 3 years and tumor reductions >95% in 3/25 patients¹⁸⁶. In this case, preclinical evaluation in an immunocompromised mouse model translated into real benefits for patients, although preclinical evaluation merely assessed *in vivo* replication of the OAd³¹⁷.

As adenoviruses are also often used as vectors for gene delivery, extensive studies were performed focusing on both innate and adaptive immune responses against Ad²¹⁷. Here, many aspects of host-interactions of human Ad were initially discovered in mice with comparable functionality in human systems and *vice versa*²¹⁷. Alemany et al. discovered that Ad type 5 was cleared in blood of mice in less than 2 minutes suggesting highly effective mechanisms for Ad clearance³¹⁸, which was confirmed later on³¹⁹. Therefore, delivery of OAd is only promising with i.t. injection, unless further strategies are implemented to shield the Ad from clearance, such as the loading into MSCs³¹⁶, antibody-retargeting³²⁰, or protein shielding of virions (e.g. PEGylation³²¹ or other coats³²²), allowing systemic delivery.

Taken together, humanized tumor xenograft models are useful tools to study (1) adenovirus replication, especially when combined with agents increasing the replication, as replication properties of human OAd can only be reliably reflected in human tumors. (2) Humanization might allow to assess immunostimulatory effects of OAd and combination approaches (as

shown in this work) but does not recapitulate the full spectrum of innate and adaptive crosstalk. (3) Those limitation should be addressed in *in vitro* assays, evaluating priming and especially T cell stimulatory capacities. (4) Generation of murine OAd applied in suitable tumor models (if available for a certain malignancy) might fill the remaining gap, allowing an in-depth understanding of both antitumor/-viral innate and adaptive responses, given that human and murine OAd comparability studies are performed concerning replication and induction of ICD.

5.1.5 Oncolytic capacity versus induction of ICD – determinants of response

The oncolytic virotherapy community generally agrees that the induction of ICD is a prerequisite for therapy response. Whether high *in vitro* replication also translates into beneficial tumor control *in vitro* remains questionable. In this regard, Workenhe et al. investigated differences in antitumor activity by comparing two similar oHSV (oHSV-1 and-2, both with ICP0 deletions) *in vitro* and *in vivo*³²³. The authors observed that (1) oHSV-1 with higher replicative capacity *in vitro* showed similar titers *in vivo* comparable to the supposedly 'weaker' oHSV-2 variant observed in *in vitro* comparison. (2) Little could be derived from *in vitro* cytotoxicity concerning *in vivo* immunogenicity. (3) Prolonged viral persistence was not a prerequisite for therapy response. And (4) most importantly, the "initial stages of immunogenic replication"³²³ appeared to be decisive for the induction of antitumor immunity, which was correlated with both innate and adaptive immune cell infiltration into tumors, the induction of *heat shock protein* (HSP)-70 and significantly higher serum levels of HMGB1 at 24h after first i.t.-injection.

This observation supports the notion, that a strong initial viral burst, which must be immunogenic, might be a predictor of therapy response and the development of long-lasting antitumor immunity. This in turn might favor an i.t.-injection over systemic delivery due to the higher local loads of an OV, although tumor-infiltration of immune cells was also shown to be increase with e.g. OAd-loaded MSCs (murine version of Celyvir)³¹⁵.

Understanding the biology of viral replication, and herein especially the determinants for ICD, then seems to be key for developing novel OV variants or combination approaches. In this regard, the proposed combination of XVir-N-31 and CDK4/6i addressed these considerations, as it increases viral replication whilst inducing immunogenicity.

Lastly, it was recently observed by the group of Prof. Dr. Per Sonne Holm and by MD students in our lab, that BETi dramatically increases the lytic capacity of XVir-N-31 by enhancing replicative capacity. If this superior replication also exhibits features of ICD which translates into increased therapy response *in vivo* is yet to be determined.

Also the role of tumor-redirected T cells, as an additional tool for the proposed prime-boos-pull-strategy should be addressed in future studies.

5.2 Conclusion

This study provides reasonable rationale on a preclinical level as to why combinations of the YB-1-based OAd XVir-N-31 with TCR transgenic T cells as well as CDK4/6i should be further pursued for the treatment of EwS, especially in combination with ICB. Taken together, this is the first report showing that each combination strategy led to survival benefits and superior

tumor control *in vivo*. Beneficial immunological changes resulting in antitumor immunity were studied in more detail for the combination of CDK4/6i and XVir-N-31, revealing promising alterations of tumor cells as well as immune cells indicating a general increase in immunogenicity by this prime-boost-pull strategy.

This is also for the first time, that immunological properties of the oncolytic adenovirus XVir-N-31 in combination settings with EwS-redirectioned TCR transgenic T cells and CDK4/6i were characterized applying both functional *in vitro* and *in vivo* experiments. Furthermore, CDK4/6i not only increases OAd genomic copy numbers, indicating increased viral replication *in vivo* but herein proposed *combo Tx* also induces systemic and local alterations with the capacity to abrogate tumor-induced immunosuppression of both the innate and the adaptive axis of the immune system.

5.3 Impact and outlook

Major hurdles need to be addressed in EwS when facing this tumor entity with cancer immunotherapy. Tackling the T cell hostile TME of EwS characterized by immunosuppressive cellular and soluble factors being one of them. Furthermore, MHC-I expression needs to be upregulated (e.g. by induction of IFNs) allowing endogenous T cell recognition or additional ACT to be successful. At the same time, immune-inhibitory non-classical HLAs have to be considered. As EwS is a systemic disease exhibiting factors of systemic immunosuppression (chronic inflammation), novel treatment strategies should address this phenomenon as well. Another aspect which needs proper consideration is the low mutational burden, hence very limited antigenic landscape for T cell recognition. The broadening of antitumor T cell responses can be considered as a prerequisite for successful downstream immunotherapies (e.g. ICB). When taking these considerations into account, a novel (combination) therapy might then allow for proper antigen presentation by APCs resulting in the induction of long-lasting antitumor T cell responses.

As demonstrated in this work, the combination of XVir-N-13 and CDK4/6i might have the potential to address these obstacles and EwS-redirectioned T cells could further enhance therapeutic effects (thus far only analyzed *in vitro*). The unique immunological strength of XVir-N-31 and CDK4/6i combination therapy can be explained by multifactorial synergisms utilizing 2 therapeutic tools with independent antitumor immunological properties. Due to the further increase of adenoviral replication and consecutive immunogenic cell lysis through CDK4/6i, the induced responses seem to be potentiated in both the innate as well as the adaptive axis of the immune system.

Due to the initiation of this PhD project and fruitful cooperation in-between the Department of Pediatrics and Experimental Urology (Klinikum rechts der Isar) the preparation and conduct of a phase I trial was funded by the BMBF entitled:

Single center, open-label, phase I, dose finding and safety study on the oncolytic adenovirus XVir-N-31 in combination with the CDK4/6 inhibitor ribociclib and the immune-checkpoint inhibitor pembrolizumab in patients with treatment-refractory sarcoma (XVIR-RIB-PEM) EN2019-060

6 Summary

Ewing sarcoma (EwS) is a highly metastatic pediatric tumor. Cure rates for localized disease increased over the last decades with intensified chemotherapy regimens addressing the systemic component of the disease. Nevertheless, metastatic, and relapsed disease states are still associated with very poor survival, emphasizing the need for novel and innovative strategies. Like most pediatric malignancies, EwS is considered a non-T cell-inflamed tumor due to its low mutational burden and immunosuppressive cellular and soluble factors. Hence, response to immune checkpoint blockade (ICB) is an exception.

For the first time, the YB-1-driven oncolytic adenovirus XVir-N-31 is studied in combination with (1) EwS-redirectioned T cell receptor (TCR)-transgenic T cells and (2) the CDK4/6 inhibitor ribociclib focusing on immunogenicity of EwS, innate immune cell changes and T cell activity. By using different *in vitro* and *in vivo* models it was shown that combination approaches increased immunogenicity of tumors, enhanced phagocytic and antigen-presenting capacities and thereby increased T cell activity. This was accompanied by prolonged survival, improved tumor control and induction of tumor-infiltrating T cells.

These preclinical data demonstrate that both combination strategies are highly promising for the treatment of EwS, especially when combined with ICB, warranting further evaluation in a clinical setting.

7 References

1. R2: Genomics Analysis and Visualization Platform (<http://r2.amc.nl>). In.
2. Ewing J. Classics in oncology. Diffuse endothelioma of bone. James Ewing. Proceedings of the New York Pathological Society, 1921. *CA Cancer J Clin* 1972; **22**(2): 95-98. e-pub ahead of print 1972/03/01; doi: 10.3322/canjclin.22.2.95
3. Jawad MU, Cheung MC, Min ES, Schneiderbauer MM, Koniaris LG, Scully SP. Ewing sarcoma demonstrates racial disparities in incidence-related and sex-related differences in outcome: an analysis of 1631 cases from the SEER database, 1973-2005. *Cancer* 2009; **115**(15): 3526-3536. e-pub ahead of print 2009/06/24; doi: 10.1002/cncr.24388
4. Riggi N, Suva ML, Stamenkovic I. Ewing's Sarcoma. *N Engl J Med* 2021; **384**(2): 154-164. e-pub ahead of print 2021/01/27; doi: 10.1056/NEJMra2028910
5. Paulussen M, Craft AW, Lewis I, Hackshaw A, Douglas C, Dunst J *et al*. Results of the EICESS-92 Study: two randomized trials of Ewing's sarcoma treatment--cyclophosphamide compared with ifosfamide in standard-risk patients and assessment of benefit of etoposide added to standard treatment in high-risk patients. *J Clin Oncol* 2008; **26**(27): 4385-4393. e-pub ahead of print 2008/09/20; doi: 10.1200/JCO.2008.16.5720
6. PDQ® Pediatric Treatment Editorial Board. In: *PDQ Ewing Sarcoma Treatment*. Bethesda, MD: National Cancer Institute, updated 02/03/2021. Available at: <https://www.cancer.gov/types/bone/hp/ewing-treatment-pdq>. Accessed 06/20/2021.
7. Ambros IM, Ambros PF, Strehl S, Kovar H, Gadner H, Salzer-Kuntschik M. MIC2 is a specific marker for Ewing's sarcoma and peripheral primitive neuroectodermal tumors. Evidence for a common histogenesis of Ewing's sarcoma and peripheral primitive neuroectodermal tumors from MIC2 expression and specific chromosome aberration. *Cancer* 1991; **67**(7): 1886-1893. e-pub ahead of print 1991/04/01; doi: 10.1002/1097-0142(19910401)67:7<1886::aid-cncr2820670712>3.0.co;2-u
8. Aurias A, Rimbaut C, Buffe D, Zucker JM, Mazabraud A. Translocation involving chromosome 22 in Ewing's sarcoma. A cytogenetic study of four fresh tumors. *Cancer Genet Cytogenet* 1984; **12**(1): 21-25. e-pub ahead of print 1984/05/01; doi: 10.1016/0165-4608(84)90003-7
9. Delattre O, Zucman J, Plougastel B, Desmaze C, Melot T, Peter M *et al*. Gene fusion with an ETS DNA-binding domain caused by chromosome translocation in human tumours. *Nature* 1992; **359**(6391): 162-165. e-pub ahead of print 1992/09/10; doi: 10.1038/359162a0
10. Ginsberg JP, de Alava E, Ladanyi M, Wexler LH, Kovar H, Paulussen M *et al*. EWS-FLI1 and EWS-ERG gene fusions are associated with similar clinical phenotypes in Ewing's sarcoma. *J Clin Oncol* 1999; **17**(6): 1809-1814. e-pub ahead of print 1999/11/24; doi: 10.1200/JCO.1999.17.6.1809
11. Jeon IS, Davis JN, Braun BS, Sublett JE, Roussel MF, Denny CT *et al*. A variant Ewing's sarcoma translocation (7;22) fuses the EWS gene to the ETS gene ETV1. *Oncogene* 1995; **10**(6): 1229-1234. e-pub ahead of print 1995/03/16;
12. Urano F, Umezawa A, Yabe H, Hong W, Yoshida K, Fujinaga K *et al*. Molecular analysis of Ewing's sarcoma: another fusion gene, EWS-E1AF, available for diagnosis. *Jpn J Cancer Res* 1998; **89**(7): 703-711. e-pub ahead of print 1998/09/17; doi: 10.1111/j.1349-7006.1998.tb03274.x
13. Peter M, Couturier J, Pacquement H, Michon J, Thomas G, Magdelenat H *et al*. A new member of the ETS family fused to EWS in Ewing tumors. *Oncogene* 1997; **14**(10): 1159-1164. e-pub ahead of print 1997/03/13; doi: 10.1038/sj.onc.1200933
14. Agelopoulos K, Richter GH, Schmidt E, Dirksen U, von Heyking K, Moser B *et al*. Deep Sequencing in Conjunction with Expression and Functional Analyses Reveals Activation of FGFR1 in Ewing Sarcoma. *Clin Cancer Res* 2015; **21**(21): 4935-4946. e-pub ahead of print 2015/07/17; doi: 10.1158/1078-0432.CCR-14-2744
15. Ohno T, Rao VN, Reddy ES. EWS/FlI-1 chimeric protein is a transcriptional activator. *Cancer Res* 1993; **53**(24): 5859-5863. e-pub ahead of print 1993/12/15;
16. Lessnick SL, Braun BS, Denny CT, May WA. Multiple domains mediate transformation by the Ewing's sarcoma EWS/FLI-1 fusion gene. *Oncogene* 1995; **10**(3): 423-431. e-pub ahead of print 1995/02/02;

17. Riggi N, Knoechel B, Gillespie SM, Rheinbay E, Boulay G, Suva ML *et al.* EWS-FLI1 utilizes divergent chromatin remodeling mechanisms to directly activate or repress enhancer elements in Ewing sarcoma. *Cancer Cell* 2014; **26**(5): 668-681. e-pub ahead of print 2014/12/03; doi: 10.1016/j.ccell.2014.10.004
18. Grobner SN, Worst BC, Weischenfeldt J, Buchhalter I, Kleinheinz K, Rudneva VA *et al.* The landscape of genomic alterations across childhood cancers. *Nature* 2018; **555**(7696): 321-327. e-pub ahead of print 2018/03/01; doi: 10.1038/nature25480
19. Brohl AS, Solomon DA, Chang W, Wang J, Song Y, Sindiri S *et al.* The genomic landscape of the Ewing Sarcoma family of tumors reveals recurrent STAG2 mutation. *PLoS Genet* 2014; **10**(7): e1004475. e-pub ahead of print 2014/07/11; doi: 10.1371/journal.pgen.1004475
20. Crompton BD, Stewart C, Taylor-Weiner A, Alexe G, Kurek KC, Calicchio ML *et al.* The genomic landscape of pediatric Ewing sarcoma. *Cancer Discov* 2014; **4**(11): 1326-1341. e-pub ahead of print 2014/09/05; doi: 10.1158/2159-8290.CD-13-1037
21. Tirode F, Surdez D, Ma X, Parker M, Le Deley MC, Bahrami A *et al.* Genomic landscape of Ewing sarcoma defines an aggressive subtype with co-association of STAG2 and TP53 mutations. *Cancer Discov* 2014; **4**(11): 1342-1353. e-pub ahead of print 2014/09/17; doi: 10.1158/2159-8290.CD-14-0622
22. Huang HY, Illei PB, Zhao Z, Mazumdar M, Huvos AG, Healey JH *et al.* Ewing sarcomas with p53 mutation or p16/p14ARF homozygous deletion: a highly lethal subset associated with poor chemoresponse. *J Clin Oncol* 2005; **23**(3): 548-558. e-pub ahead of print 2005/01/22; doi: 10.1200/JCO.2005.02.081
23. Esiashvili N, Goodman M, Marcus RB, Jr. Changes in incidence and survival of Ewing sarcoma patients over the past 3 decades: Surveillance Epidemiology and End Results data. *J Pediatr Hematol Oncol* 2008; **30**(6): 425-430. e-pub ahead of print 2008/06/06; doi: 10.1097/MPH.0b013e31816e22f3
24. Cotterill SJ, Ahrens S, Paulussen M, Jurgens HF, Voute PA, Gadner H *et al.* Prognostic factors in Ewing's tumor of bone: analysis of 975 patients from the European Intergroup Cooperative Ewing's Sarcoma Study Group. *J Clin Oncol* 2000; **18**(17): 3108-3114. e-pub ahead of print 2000/08/30; doi: 10.1200/JCO.2000.18.17.3108
25. Gaspar N, Hawkins DS, Dirksen U, Lewis IJ, Ferrari S, Le Deley MC *et al.* Ewing Sarcoma: Current Management and Future Approaches Through Collaboration. *J Clin Oncol* 2015; **33**(27): 3036-3046. e-pub ahead of print 2015/08/26; doi: 10.1200/JCO.2014.59.5256
26. Stahl M, Ranft A, Paulussen M, Bolling T, Vieth V, Bielack S *et al.* Risk of recurrence and survival after relapse in patients with Ewing sarcoma. *Pediatr Blood Cancer* 2011; **57**(4): 549-553. e-pub ahead of print 2011/03/29; doi: 10.1002/psc.23040
27. Thiel U, Wawer A, Wolf P, Badoglio M, Santucci A, Klingebiel T *et al.* No improvement of survival with reduced- versus high-intensity conditioning for allogeneic stem cell transplants in Ewing tumor patients. *Ann Oncol* 2011; **22**(7): 1614-1621. e-pub ahead of print 2011/01/20; doi: 10.1093/annonc/mdq703
28. Burdach S, Jurgens H, Peters C, Nurnberger W, Mauz-Korholz C, Korholz D *et al.* Myeloablative radiochemotherapy and hematopoietic stem-cell rescue in poor-prognosis Ewing's sarcoma. *J Clin Oncol* 1993; **11**(8): 1482-1488. e-pub ahead of print 1993/08/01; doi: 10.1200/JCO.1993.11.8.1482
29. Whelan J, Le Deley MC, Dirksen U, Le Teuff G, Brennan B, Gaspar N *et al.* High-Dose Chemotherapy and Blood Autologous Stem-Cell Rescue Compared With Standard Chemotherapy in Localized High-Risk Ewing Sarcoma: Results of Euro-E.W.I.N.G.99 and Ewing-2008. *J Clin Oncol* 2018; JCO2018782516. e-pub ahead of print 2018/09/07; doi: 10.1200/JCO.2018.78.2516
30. Grunewald TGP, Cidre-Aranaz F, Surdez D, Tomazou EM, de Alava E, Kovar H *et al.* Ewing sarcoma. *Nat Rev Dis Primers* 2018; **4**(1): 5. e-pub ahead of print 2018/07/07; doi: 10.1038/s41572-018-0003-x
31. Leavey PJ, Collier AB. Ewing sarcoma: prognostic criteria, outcomes and future treatment. *Expert Rev Anticancer Ther* 2008; **8**(4): 617-624. e-pub ahead of print 2008/04/12; doi: 10.1586/14737140.8.4.617
32. El-Naggar AM, Veinotte CJ, Cheng H, Grunewald TG, Negri GL, Somasekharan SP *et al.* Translational Activation of HIF1alpha by YB-1 Promotes Sarcoma Metastasis. *Cancer Cell* 2015; **27**(5): 682-697. e-pub ahead of print 2015/05/13; doi: 10.1016/j.ccell.2015.04.003
33. Evdokimova V, Ruzanov P, Anglesio MS, Sorokin AV, Ovchinnikov LP, Buckley J *et al.* Akt-mediated YB-1 phosphorylation activates translation of silent mRNA species. *Mol Cell Biol* 2006; **26**(1): 277-292. e-pub ahead of print 2005/12/16; doi: 10.1128/MCB.26.1.277-292.2006

34. Evdokimova V, Tognon C, Ng T, Ruzanov P, Melnyk N, Fink D *et al.* Translational activation of snail1 and other developmentally regulated transcription factors by YB-1 promotes an epithelial-mesenchymal transition. *Cancer Cell* 2009; **15**(5): 402-415. e-pub ahead of print 2009/05/05; doi: 10.1016/j.ccr.2009.03.017
35. Somasekharan SP, El-Naggar A, Leprivier G, Cheng H, Hajee S, Grunewald TG *et al.* YB-1 regulates stress granule formation and tumor progression by translationally activating G3BP1. *J Cell Biol* 2015; **208**(7): 913-929. e-pub ahead of print 2015/03/25; doi: 10.1083/jcb.201411047
36. Xu L, Li H, Wu L, Huang S. YBX1 promotes tumor growth by elevating glycolysis in human bladder cancer. *Oncotarget* 2017; **8**(39): 65946-65956. e-pub ahead of print 2017/10/17; doi: 10.18632/oncotarget.19583
37. Chattopadhyay R, Das S, Maiti AK, Boldogh I, Xie J, Hazra TK *et al.* Regulatory role of human AP-endonuclease (APE1/Ref-1) in YB-1-mediated activation of the multidrug resistance gene MDR1. *Mol Cell Biol* 2008; **28**(23): 7066-7080. e-pub ahead of print 2008/09/24; doi: 10.1128/MCB.00244-08
38. Dutta A, Yang C, Sengupta S, Mitra S, Hegde ML. New paradigms in the repair of oxidative damage in human genome: mechanisms ensuring repair of mutagenic base lesions during replication and involvement of accessory proteins. *Cell Mol Life Sci* 2015; **72**(9): 1679-1698. e-pub ahead of print 2015/01/13; doi: 10.1007/s00018-014-1820-z
39. Rasper M, Jabar S, Ranft A, Jurgens H, Amler S, Dirksen U. The value of high-dose chemotherapy in patients with first relapsed Ewing sarcoma. *Pediatr Blood Cancer* 2014; **61**(8): 1382-1386. e-pub ahead of print 2014/04/15; doi: 10.1002/pbc.25042
40. Raciborska A, Biliska K, Drabko K, Chaber R, Pogorzala M, Wyrobek E *et al.* Vincristine, irinotecan, and temozolomide in patients with relapsed and refractory Ewing sarcoma. *Pediatr Blood Cancer* 2013; **60**(10): 1621-1625. e-pub ahead of print 2013/06/19; doi: 10.1002/pbc.24621
41. Hunold A, Weddeling N, Paulussen M, Ranft A, Liebscher C, Jurgens H. Topotecan and cyclophosphamide in patients with refractory or relapsed Ewing tumors. *Pediatr Blood Cancer* 2006; **47**(6): 795-800. e-pub ahead of print 2006/01/18; doi: 10.1002/pbc.20719
42. Casey DA, Wexler LH, Merchant MS, Chou AJ, Merola PR, Price AP *et al.* Irinotecan and temozolomide for Ewing sarcoma: the Memorial Sloan-Kettering experience. *Pediatr Blood Cancer* 2009; **53**(6): 1029-1034. e-pub ahead of print 2009/07/29; doi: 10.1002/pbc.22206
43. Fox E, Patel S, Wathen JK, Schuetze S, Chawla S, Harmon D *et al.* Phase II study of sequential gemcitabine followed by docetaxel for recurrent Ewing sarcoma, osteosarcoma, or unresectable or locally recurrent chondrosarcoma: results of Sarcoma Alliance for Research Through Collaboration Study 003. *Oncologist* 2012; **17**(3): 321. e-pub ahead of print 2012/03/01; doi: 10.1634/theoncologist.2010-0265
44. Ferrari S, del Prever AB, Palmerini E, Staals E, Berta M, Balladelli A *et al.* Response to high-dose ifosfamide in patients with advanced/recurrent Ewing sarcoma. *Pediatr Blood Cancer* 2009; **52**(5): 581-584. e-pub ahead of print 2009/01/15; doi: 10.1002/pbc.21917
45. Ferrari S, Luksch R, Hall KS, Fagioli F, Prete A, Tamburini A *et al.* Post-relapse survival in patients with Ewing sarcoma. *Pediatr Blood Cancer* 2015; **62**(6): 994-999. e-pub ahead of print 2015/01/15; doi: 10.1002/pbc.25388
46. Majzner RG, Simon JS, Grosso JF, Martinez D, Pawel BR, Santi M *et al.* Assessment of programmed death-ligand 1 expression and tumor-associated immune cells in pediatric cancer tissues. *Cancer* 2017; **123**(19): 3807-3815. e-pub ahead of print 2017/06/14; doi: 10.1002/cncr.30724
47. Stahl D, Gentles AJ, Thiele R, Gutgemann I. Prognostic profiling of the immune cell microenvironment in Ewing s Sarcoma Family of Tumors. *Oncoimmunology* 2019; **8**(12): e1674113. e-pub ahead of print 2019/11/20; doi: 10.1080/2162402X.2019.1674113
48. Snyder A, Makarov V, Merghoub T, Yuan J, Zaretsky JM, Desrichard A *et al.* Genetic basis for clinical response to CTLA-4 blockade in melanoma. *N Engl J Med* 2014; **371**(23): 2189-2199. e-pub ahead of print 2014/11/20; doi: 10.1056/NEJMoa1406498
49. Le DT, Uram JN, Wang H, Bartlett BR, Kemberling H, Eyring AD *et al.* PD-1 Blockade in Tumors with Mismatch-Repair Deficiency. *N Engl J Med* 2015; **372**(26): 2509-2520. e-pub ahead of print 2015/06/02; doi: 10.1056/NEJMoa1500596
50. Davis KL, Fox E, Merchant MS, Reid JM, Kudgus RA, Liu X *et al.* Nivolumab in children and young adults with relapsed or refractory solid tumours or lymphoma (ADVL1412): a multicentre, open-label, single-arm,

- phase 1-2 trial. *Lancet Oncol* 2020; **21**(4): 541-550. e-pub ahead of print 2020/03/21; doi: 10.1016/S1470-2045(20)30023-1
51. D'Angelo SP, Mahoney MR, Van Tine BA, Atkins J, Milhem MM, Jahagirdar BN *et al.* Nivolumab with or without ipilimumab treatment for metastatic sarcoma (Alliance A091401): two open-label, non-comparative, randomised, phase 2 trials. *Lancet Oncol* 2018; **19**(3): 416-426. e-pub ahead of print 2018/01/27; doi: 10.1016/S1470-2045(18)30006-8
 52. Spurny C, Kailayangiri S, Jamitzky S, Altvater B, Wardelmann E, Dirksen U *et al.* Programmed cell death ligand 1 (PD-L1) expression is not a predominant feature in Ewing sarcomas. *Pediatr Blood Cancer* 2018; **65**(1). e-pub ahead of print 2017/09/05; doi: 10.1002/pbc.26719
 53. van Erp AEM, Versleijen-Jonkers YMH, Hillebrandt-Roeffen MHS, van Houdt L, Gorris MAJ, van Dam LS *et al.* Expression and clinical association of programmed cell death-1, programmed death-ligand-1 and CD8(+) lymphocytes in primary sarcomas is subtype dependent. *Oncotarget* 2017; **8**(41): 71371-71384. e-pub ahead of print 2017/10/21; doi: 10.18632/oncotarget.19071
 54. Machado I, Lopez-Guerrero JA, Scotlandi K, Picci P, Llombart-Bosch A. Immunohistochemical analysis and prognostic significance of PD-L1, PD-1, and CD8+ tumor-infiltrating lymphocytes in Ewing's sarcoma family of tumors (ESFT). *Virchows Arch* 2018; **472**(5): 815-824. e-pub ahead of print 2018/02/16; doi: 10.1007/s00428-018-2316-2
 55. Berghuis D, Santos SJ, Baelde HJ, Taminiau AH, Egeler RM, Schilham MW *et al.* Pro-inflammatory chemokine-chemokine receptor interactions within the Ewing sarcoma microenvironment determine CD8(+) T-lymphocyte infiltration and affect tumour progression. *J Pathol* 2011; **223**(3): 347-357. e-pub ahead of print 2010/12/21; doi: 10.1002/path.2819
 56. Berghuis D, de Hooge AS, Santos SJ, Horst D, Wiertz EJ, van Eggermond MC *et al.* Reduced human leukocyte antigen expression in advanced-stage Ewing sarcoma: implications for immune recognition. *J Pathol* 2009; **218**(2): 222-231. e-pub ahead of print 2009/03/11; doi: 10.1002/path.2537
 57. Staeger MS, Gorelov V, Bulankin A, Fischer U, Dumon K, Hohndorf L *et al.* Stable transgenic expression of IL-2 and HSV1-tk by single and fusion tumor cell lines bearing EWS/FLI-1 chimeric genes. *Pediatr Hematol Oncol* 2003; **20**(2): 119-140. e-pub ahead of print 2003/01/30; doi: 10.1080/0880010390158612
 58. Geraghty DE, Koller BH, Orr HT. A human major histocompatibility complex class I gene that encodes a protein with a shortened cytoplasmic segment. *Proc Natl Acad Sci U S A* 1987; **84**(24): 9145-9149. e-pub ahead of print 1987/12/01; doi: 10.1073/pnas.84.24.9145
 59. Koller BH, Geraghty DE, Shimizu Y, DeMars R, Orr HT. HLA-E. A novel HLA class I gene expressed in resting T lymphocytes. *J Immunol* 1988; **141**(3): 897-904. e-pub ahead of print 1988/08/01;
 60. Geraghty DE, Wei XH, Orr HT, Koller BH. Human leukocyte antigen F (HLA-F). An expressed HLA gene composed of a class I coding sequence linked to a novel transcribed repetitive element. *J Exp Med* 1990; **171**(1): 1-18. e-pub ahead of print 1990/01/01; doi: 10.1084/jem.171.1.1
 61. Kochan G, Escors D, Breckpot K, Guerrero-Setas D. Role of non-classical MHC class I molecules in cancer immunosuppression. *Oncoimmunology* 2013; **2**(11): e26491. e-pub ahead of print 2014/02/01; doi: 10.4161/onci.26491
 62. Persson G, Melsted WN, Nilsson LL, Hviid TVF. HLA class Ib in pregnancy and pregnancy-related disorders. *Immunogenetics* 2017; **69**(8-9): 581-595. e-pub ahead of print 2017/07/13; doi: 10.1007/s00251-017-0988-4
 63. LeMaoult J, Le Discorde M, Rouas-Freiss N, Moreau P, Menier C, McCluskey J *et al.* Biology and functions of human leukocyte antigen-G in health and sickness. *Tissue Antigens* 2003; **62**(4): 273-284. e-pub ahead of print 2003/09/17; doi: 10.1034/j.1399-0039.2003.00143.x
 64. Yan WH, Lin A, Chen BG, Chen SY. Induction of both membrane-bound and soluble HLA-G expression in active human cytomegalovirus infection. *J Infect Dis* 2009; **200**(5): 820-826. e-pub ahead of print 2009/07/22; doi: 10.1086/604733
 65. Verbruggen LA, Rebmann V, Demanet C, De Cock S, Grosse-Wilde H. Soluble HLA-G in rheumatoid arthritis. *Hum Immunol* 2006; **67**(8): 561-567. e-pub ahead of print 2006/08/19; doi: 10.1016/j.humimm.2006.03.023
 66. Zarkhin V, Talisetti A, Li L, Wozniak LJ, McDiarmid SV, Cox K *et al.* Expression of soluble HLA-G identifies favorable outcomes in liver transplant recipients. *Transplantation* 2010; **90**(9): 1000-1005. e-pub ahead of print 2010/09/04; doi: 10.1097/TP.0b013e3181f546af

67. Rapaport AS, Schriewer J, Gilfillan S, Hembrador E, Crump R, Plougastel BF *et al.* The Inhibitory Receptor NKG2A Sustains Virus-Specific CD8(+) T Cells in Response to a Lethal Poxvirus Infection. *Immunity* 2015; **43**(6): 1112-1124. e-pub ahead of print 2015/12/19; doi: 10.1016/j.immuni.2015.11.005
68. Riteau B, Menier C, Khalil-Daher I, Martinozzi S, Pla M, Dausset J *et al.* HLA-G1 co-expression boosts the HLA class I-mediated NK lysis inhibition. *Int Immunol* 2001; **13**(2): 193-201. e-pub ahead of print 2001/02/07; doi: 10.1093/intimm/13.2.193
69. Le Drean E, Vely F, Olcese L, Cambiaggi A, Guida S, Krystal G *et al.* Inhibition of antigen-induced T cell response and antibody-induced NK cell cytotoxicity by NKG2A: association of NKG2A with SHP-1 and SHP-2 protein-tyrosine phosphatases. *Eur J Immunol* 1998; **28**(1): 264-276. e-pub ahead of print 1998/03/04; doi: 10.1002/(SICI)1521-4141(199801)28:01<264::AID-IMMU264>3.0.CO;2-O
70. Castelli EC, Veiga-Castelli LC, Yaghi L, Moreau P, Donadi EA. Transcriptional and posttranscriptional regulations of the HLA-G gene. *J Immunol Res* 2014; **2014**: 734068. e-pub ahead of print 2014/04/18; doi: 10.1155/2014/734068
71. Altvater B, Kailayangiri S, Pérez Lanuza LF, Urban K, Greune L, Flügge M *et al.* HLA-G and HLA-E Immune Checkpoints Are Widely Expressed in Ewing Sarcoma but Have Limited Functional Impact on the Effector Functions of Antigen-Specific CAR T Cells. *Cancers* 2021; **13**(12): 2857.
72. Rizzo R, Lanzoni G, Stignani M, Campioni D, Alviano F, Ricci F *et al.* A simple method for identifying bone marrow mesenchymal stromal cells with a high immunosuppressive potential. *Cytotherapy* 2011; **13**(5): 523-527. e-pub ahead of print 2010/12/22; doi: 10.3109/14653249.2010.542460
73. Selmani Z, Naji A, Zidi I, Favier B, Gaiffe E, Obert L *et al.* Human leukocyte antigen-G5 secretion by human mesenchymal stem cells is required to suppress T lymphocyte and natural killer function and to induce CD4+CD25highFOXP3+ regulatory T cells. *Stem Cells* 2008; **26**(1): 212-222. e-pub ahead of print 2007/10/13; doi: 10.1634/stemcells.2007-0554
74. Riggi N, Cironi L, Provero P, Suva ML, Kaloulis K, Garcia-Echeverria C *et al.* Development of Ewing's sarcoma from primary bone marrow-derived mesenchymal progenitor cells. *Cancer Res* 2005; **65**(24): 11459-11468. e-pub ahead of print 2005/12/17; doi: 10.1158/0008-5472.CAN-05-1696
75. Tirode F, Laud-Duval K, Prieur A, Delorme B, Charbord P, Delattre O. Mesenchymal stem cell features of Ewing tumors. *Cancer Cell* 2007; **11**(5): 421-429. e-pub ahead of print 2007/05/08; doi: 10.1016/j.ccr.2007.02.027
76. Spurny C, Kailayangiri S, Altvater B, Jamitzky S, Hartmann W, Wardelmann E *et al.* T cell infiltration into Ewing sarcomas is associated with local expression of immune-inhibitory HLA-G. *Oncotarget* 2018; **9**(5): 6536-6549. e-pub ahead of print 2018/02/22; doi: 10.18632/oncotarget.23815
77. Fujiwara T, Fukushi J, Yamamoto S, Matsumoto Y, Setsu N, Oda Y *et al.* Macrophage infiltration predicts a poor prognosis for human ewing sarcoma. *Am J Pathol* 2011; **179**(3): 1157-1170. e-pub ahead of print 2011/07/21; doi: 10.1016/j.ajpath.2011.05.034
78. Handl M, Hermanova M, Hotarkova S, Jarkovsky J, Mudry P, Shatokhina T *et al.* Clinicopathological correlation of tumor-associated macrophages in Ewing sarcoma. *Biomed Pap Med Fac Univ Palacky Olomouc Czech Repub* 2018; **162**(1): 54-60. e-pub ahead of print 2017/11/25; doi: 10.5507/bp.2017.049
79. Denton NL, Chen CY, Hutzen B, Currier MA, Scott T, Nartker B *et al.* Myelolytic Treatments Enhance Oncolytic Herpes Virotherapy in Models of Ewing Sarcoma by Modulating the Immune Microenvironment. *Mol Ther Oncolytics* 2018; **11**: 62-74. e-pub ahead of print 2018/12/07; doi: 10.1016/j.omto.2018.10.001
80. Bronte V, Brandau S, Chen SH, Colombo MP, Frey AB, Greten TF *et al.* Recommendations for myeloid-derived suppressor cell nomenclature and characterization standards. *Nat Commun* 2016; **7**: 12150. e-pub ahead of print 2016/07/07; doi: 10.1038/ncomms12150
81. Veglia F, Sanseviero E, Gabrilovich DI. Myeloid-derived suppressor cells in the era of increasing myeloid cell diversity. *Nat Rev Immunol* 2021. e-pub ahead of print 2021/02/03; doi: 10.1038/s41577-020-00490-y
82. Serafini P, Borrello I, Bronte V. Myeloid suppressor cells in cancer: recruitment, phenotype, properties, and mechanisms of immune suppression. *Semin Cancer Biol* 2006; **16**(1): 53-65. e-pub ahead of print 2005/09/20; doi: 10.1016/j.semcancer.2005.07.005
83. Gabrilovich DI, Ostrand-Rosenberg S, Bronte V. Coordinated regulation of myeloid cells by tumours. *Nat Rev Immunol* 2012; **12**(4): 253-268. e-pub ahead of print 2012/03/23; doi: 10.1038/nri3175

84. Zhang H, Maric I, DiPrima MJ, Khan J, Orentas RJ, Kaplan RN *et al.* Fibrocytes represent a novel MDSC subset circulating in patients with metastatic cancer. *Blood* 2013; **122**(7): 1105-1113. doi: 10.1182/blood-2012-08-449413
85. Altvater B, Kailayangiri S, Theimann N, Ahlmann M, Farwick N, Chen C *et al.* Common Ewing sarcoma-associated antigens fail to induce natural T cell responses in both patients and healthy individuals. *Cancer Immunol Immunother* 2014; **63**(10): 1047-1060. e-pub ahead of print 2014/06/29; doi: 10.1007/s00262-014-1574-3
86. Evdokimova V, Ruzanov P, Gassmann H, Zaidi SH, Peltekova V, Heisler LE *et al.* Exosomes transmit retroelement RNAs to drive inflammation and immunosuppression in Ewing Sarcoma. *bioRxiv* 2019: 806851. doi: 10.1101/806851
87. Atrekhany KN, Drutskaya MS, Nedospasov SA, Grivennikov SI, Kuprash DV. Chemokines, cytokines and exosomes help tumors to shape inflammatory microenvironment. *Pharmacol Ther* 2016; **168**: 98-112. e-pub ahead of print 2016/09/11; doi: 10.1016/j.pharmthera.2016.09.011
88. Gassmann H, Schneider K, Evdokimova V, Ruzanov P, Schober SJ, Xue B *et al.* Ewing Sarcoma-Derived Extracellular Vesicles Impair Dendritic Cell Maturation and Function. *Cells* 2021; **10**(8). e-pub ahead of print 2021/08/28; doi: 10.3390/cells10082081
89. Lissat A, Joerschke M, Shinde DA, Braunschweig T, Meier A, Makowska A *et al.* IL6 secreted by Ewing sarcoma tumor microenvironment confers anti-apoptotic and cell-disseminating paracrine responses in Ewing sarcoma cells. *BMC Cancer* 2015; **15**: 552. e-pub ahead of print 2015/07/29; doi: 10.1186/s12885-015-1564-7
90. Hanahan D, Weinberg RA. Hallmarks of cancer: the next generation. *Cell* 2011; **144**(5): 646-674. e-pub ahead of print 2011/03/08; doi: 10.1016/j.cell.2011.02.013
91. Kauer M, Ban J, Kofler R, Walker B, Davis S, Meltzer P *et al.* A molecular function map of Ewing's sarcoma. *PLoS One* 2009; **4**(4): e5415. e-pub ahead of print 2009/05/01; doi: 10.1371/journal.pone.0005415
92. Felix A, Berlanga P, Toulmonde M, Landman-Parker J, Dumont S, Vassal G *et al.* Systematic review of phase-I/II trials enrolling refractory and recurrent Ewing sarcoma: Actual knowledge and future directions to optimize the research. *Cancer Med* 2021; **10**(5): 1589-1604. e-pub ahead of print 2021/01/17; doi: 10.1002/cam4.3712
93. Morales E, Olson M, Iglesias F, Dahiya S, Luetkens T, Atanackovic D. Role of immunotherapy in Ewing sarcoma. *J Immunother Cancer* 2020; **8**(2). e-pub ahead of print 2020/12/10; doi: 10.1136/jitc-2020-000653
94. Horowitz MM, Gale RP, Sondel PM, Goldman JM, Kersey J, Kolb HJ *et al.* Graft-versus-leukemia reactions after bone marrow transplantation. *Blood* 1990; **75**(3): 555-562. e-pub ahead of print 1990/02/01;
95. Kolb HJ. Graft-versus-leukemia effects of transplantation and donor lymphocytes. *Blood* 2008; **112**(12): 4371-4383. e-pub ahead of print 2008/11/26; doi: 10.1182/blood-2008-03-077974
96. Koscielniak E, Gross-Wieltsch U, Treuner J, Winkler P, Klingebiel T, Lang P *et al.* Graft-versus-Ewing sarcoma effect and long-term remission induced by haploidentical stem-cell transplantation in a patient with relapse of metastatic disease. *J Clin Oncol* 2005; **23**(1): 242-244. e-pub ahead of print 2004/12/31; doi: 10.1200/JCO.2005.05.940
97. Thiel U, Schober SJ, Ranft A, Gassmann H, Jabar S, Gall K *et al.* No difference in survival after HLA mismatched versus HLA matched allogeneic stem cell transplantation in Ewing sarcoma patients with advanced disease. *Bone Marrow Transplant* 2021. e-pub ahead of print 2021/01/31; doi: 10.1038/s41409-020-01200-x
98. Schober SJ, von Luettichau I, Wawer A, Steinhäuser M, Salat C, Schwinger W *et al.* Donor lymphocyte infusions in adolescents and young adults for control of advanced pediatric sarcoma. *Oncotarget* 2018; **9**(32): 22741-22748. e-pub ahead of print 2018/06/02; doi: 10.18632/oncotarget.25228
99. Kuwana Y, Asakura Y, Utsunomiya N, Nakanishi M, Arata Y, Itoh S *et al.* Expression of chimeric receptor composed of immunoglobulin-derived V regions and T-cell receptor-derived C regions. *Biochem Biophys Res Commun* 1987; **149**(3): 960-968. e-pub ahead of print 1987/12/31; doi: 10.1016/0006-291x(87)90502-x
100. Gross G, Gorochov G, Waks T, Eshhar Z. Generation of effector T cells expressing chimeric T cell receptor with antibody type-specificity. *Transplant Proc* 1989; **21**(1 Pt 1): 127-130. e-pub ahead of print 1989/02/01;

101. Sadelain M, Riviere I, Brentjens R. Targeting tumours with genetically enhanced T lymphocytes. *Nat Rev Cancer* 2003; **3**(1): 35-45. e-pub ahead of print 2003/01/02; doi: 10.1038/nrc971
102. Chmielewski M, Abken H. TRUCKS, the fourth-generation CAR T cells: Current developments and clinical translation. *ADVANCES IN CELL AND GENE THERAPY* 2020; **3**(3): e84. doi: <https://doi.org/10.1002/acg2.84>
103. Koneru M, Purdon TJ, Spriggs D, Koneru S, Brentjens RJ. IL-12 secreting tumor-targeted chimeric antigen receptor T cells eradicate ovarian tumors in vivo. *Oncoimmunology* 2015; **4**(3): e994446. e-pub ahead of print 2015/05/08; doi: 10.4161/2162402X.2014.994446
104. Jin L, Tao H, Karachi A, Long Y, Hou AY, Na M *et al.* CXCR1- or CXCR2-modified CAR T cells co-opt IL-8 for maximal antitumor efficacy in solid tumors. *Nat Commun* 2019; **10**(1): 4016. e-pub ahead of print 2019/09/07; doi: 10.1038/s41467-019-11869-4
105. Caruana I, Savoldo B, Hoyos V, Weber G, Liu H, Kim ES *et al.* Heparanase promotes tumor infiltration and antitumor activity of CAR-redirection T lymphocytes. *Nat Med* 2015; **21**(5): 524-529. e-pub ahead of print 2015/04/08; doi: 10.1038/nm.3833
106. Papadouli I, Mueller-Berghaus J, Beuneu C, Ali S, Hofner B, Petavy F *et al.* EMA Review of Axicabtagene Ciloleucel (Yescarta) for the Treatment of Diffuse Large B-Cell Lymphoma. *Oncologist* 2020; **25**(10): 894-902. e-pub ahead of print 2020/04/28; doi: 10.1634/theoncologist.2019-0646
107. Albinger N, Hartmann J, Ullrich E. Current status and perspective of CAR-T and CAR-NK cell therapy trials in Germany. *Gene Therapy* 2021. doi: 10.1038/s41434-021-00246-w
108. Liu G, Rui W, Zhao X, Lin X. Enhancing CAR-T cell efficacy in solid tumors by targeting the tumor microenvironment. *Cell Mol Immunol* 2021; **18**(5): 1085-1095. e-pub ahead of print 2021/04/01; doi: 10.1038/s41423-021-00655-2
109. Kailayangiri S, Altvater B, Meltzer J, Pscherer S, Luecke A, Dierkes C *et al.* The ganglioside antigen G(D2) is surface-expressed in Ewing sarcoma and allows for MHC-independent immune targeting. *Br J Cancer* 2012; **106**(6): 1123-1133. e-pub ahead of print 2012/03/01; doi: 10.1038/bjc.2012.57
110. Majzner RG, Theruvath JL, Nellan A, Heitzeneder S, Cui Y, Mount CW *et al.* CAR T Cells Targeting B7-H3, a Pan-Cancer Antigen, Demonstrate Potent Preclinical Activity Against Pediatric Solid Tumors and Brain Tumors. *Clin Cancer Res* 2019; **25**(8): 2560-2574. e-pub ahead of print 2019/01/19; doi: 10.1158/1078-0432.CCR-18-0432
111. Hegde M, Joseph SK, Pashankar F, DeRenzo C, Sanber K, Navai S *et al.* Tumor response and endogenous immune reactivity after administration of HER2 CAR T cells in a child with metastatic rhabdomyosarcoma. *Nat Commun* 2020; **11**(1): 3549. e-pub ahead of print 2020/07/17; doi: 10.1038/s41467-020-17175-8
112. Majzner RG, Rietberg SP, Sotillo E, Dong R, Vachharajani VT, Labanieh L *et al.* Tuning the Antigen Density Requirement for CAR T-cell Activity. *Cancer Discov* 2020; **10**(5): 702-723. e-pub ahead of print 2020/03/21; doi: 10.1158/2159-8290.CD-19-0945
113. Walker AJ, Majzner RG, Zhang L, Wanhainen K, Long AH, Nguyen SM *et al.* Tumor Antigen and Receptor Densities Regulate Efficacy of a Chimeric Antigen Receptor Targeting Anaplastic Lymphoma Kinase. *Mol Ther* 2017; **25**(9): 2189-2201. e-pub ahead of print 2017/07/06; doi: 10.1016/j.ymthe.2017.06.008
114. Harris DT, Hager MV, Smith SN, Cai Q, Stone JD, Kruger P *et al.* Comparison of T Cell Activities Mediated by Human TCRs and CARs That Use the Same Recognition Domains. *J Immunol* 2018; **200**(3): 1088-1100. e-pub ahead of print 2017/12/31; doi: 10.4049/jimmunol.1700236
115. Sykulev Y, Joo M, Vturina I, Tsomides TJ, Eisen HN. Evidence that a single peptide-MHC complex on a target cell can elicit a cytolytic T cell response. *Immunity* 1996; **4**(6): 565-571. e-pub ahead of print 1996/06/01; doi: 10.1016/s1074-7613(00)80483-5
116. Scanlan MJ, Gure AO, Jungbluth AA, Old LJ, Chen YT. Cancer/testis antigens: an expanding family of targets for cancer immunotherapy. *Immunol Rev* 2002; **188**: 22-32. e-pub ahead of print 2002/11/26; doi: 10.1034/j.1600-065x.2002.18803.x
117. Robbins PF, Morgan RA, Feldman SA, Yang JC, Sherry RM, Dudley ME *et al.* Tumor regression in patients with metastatic synovial cell sarcoma and melanoma using genetically engineered lymphocytes reactive with NY-ESO-1. *J Clin Oncol* 2011; **29**(7): 917-924. e-pub ahead of print 2011/02/02; doi: 10.1200/JCO.2010.32.2537

118. Ramachandran I, Lowther DE, Dryer-Minnerly R, Wang R, Fayngerts S, Nunez D *et al.* Systemic and local immunity following adoptive transfer of NY-ESO-1 SPEAR T cells in synovial sarcoma. *J Immunother Cancer* 2019; **7**(1): 276. e-pub ahead of print 2019/10/28; doi: 10.1186/s40425-019-0762-2
119. Evans CH, Liu F, Porter RM, O'Sullivan RP, Merghoub T, Lunsford EP *et al.* EWS-FLI1-targeted cytotoxic T-cell killing of multiple tumor types belonging to the Ewing sarcoma family of tumors. *Clin Cancer Res* 2012; **18**(19): 5341-5351. e-pub ahead of print 2012/08/11; doi: 10.1158/1078-0432.CCR-12-1985
120. Meyer-Wentrup F, Richter G, Burdach S. Identification of an immunogenic EWS-FLI1-derived HLA-DR-restricted T helper cell epitope. *Pediatr Hematol Oncol* 2005; **22**(4): 297-308. e-pub ahead of print 2005/07/16; doi: 10.1080/08880010590935194
121. Grunewald TG, Diebold I, Esposito I, Plehm S, Hauer K, Thiel U *et al.* STEAP1 is associated with the invasive and oxidative stress phenotype of Ewing tumors. *Mol Cancer Res* 2012; **10**(1): 52-65. e-pub ahead of print 2011/11/15; doi: 10.1158/1541-7786.MCR-11-0524
122. von Heyking K, Calzada-Wack J, Gollner S, Neff F, Schmidt O, Hensel T *et al.* The endochondral bone protein CHM1 sustains an undifferentiated, invasive phenotype, promoting lung metastasis in Ewing sarcoma. *Mol Oncol* 2017; **11**(9): 1288-1301. e-pub ahead of print 2017/03/21; doi: 10.1002/1878-0261.12057
123. Gallegos ZR, Taus P, Gibbs ZA, McGlynn K, Gomez NC, Davis I *et al.* EWSR1-FLI1 Activation of the Cancer/Testis Antigen FATE1 Promotes Ewing Sarcoma Survival. *Mol Cell Biol* 2019; **39**(14). e-pub ahead of print 2019/05/01; doi: 10.1128/MCB.00138-19
124. Liu XF, Helman LJ, Yeung C, Bera TK, Lee B, Pastan I. XAGE-1, a new gene that is frequently expressed in Ewing's sarcoma. *Cancer Res* 2000; **60**(17): 4752-4755. e-pub ahead of print 2000/09/15;
125. Brinkmann U, Vasmatzis G, Lee B, Pastan I. Novel genes in the PAGE and GAGE family of tumor antigens found by homology walking in the dbEST database. *Cancer Res* 1999; **59**(7): 1445-1448. e-pub ahead of print 1999/04/10;
126. Thiel U, Pirson S, Muller-Spahn C, Conrad H, Busch DH, Bernhard H *et al.* Specific recognition and inhibition of Ewing tumour growth by antigen-specific allo-restricted cytotoxic T cells. *Br J Cancer* 2011; **104**(6): 948-956. e-pub ahead of print 2011/03/17; doi: 10.1038/bjc.2011.54
127. Schirmer D, Grunewald TG, Klar R, Schmidt O, Wohleber D, Rubio RA *et al.* Transgenic antigen-specific, HLA-A*02:01-allo-restricted cytotoxic T cells recognize tumor-associated target antigen STEAP1 with high specificity. *Oncoimmunology* 2016; **5**(6): e1175795. e-pub ahead of print 2016/07/30; doi: 10.1080/2162402X.2016.1175795
128. Kirschner A, Thiede M, Grunewald TG, Alba Rubio R, Richter GH, Kirchner T *et al.* Pappalysin-1 T cell receptor transgenic allo-restricted T cells kill Ewing sarcoma in vitro and in vivo. *Oncoimmunology* 2017; **6**(2): e1273301. e-pub ahead of print 2017/03/28; doi: 10.1080/2162402X.2016.1273301
129. Blaeschke F, Thiel U, Kirschner A, Thiede M, Rubio RA, Schirmer D *et al.* Human HLA-A*02:01/CHM1+ allo-restricted T cell receptor transgenic CD8+ T cells specifically inhibit Ewing sarcoma growth in vitro and in vivo. *Oncotarget* 2016; **7**(28): 43267-43280. e-pub ahead of print 2016/06/10; doi: 10.18632/oncotarget.9218
130. Thiel U, Schober SJ, Einspieler I, Kirschner A, Thiede M, Schirmer D *et al.* Ewing sarcoma partial regression without GvHD by chondromodulin-I/HLA-A*02:01-specific allorestricted T cell receptor transgenic T cells. *Oncoimmunology* 2017; **6**(5): e1312239. e-pub ahead of print 2017/06/24; doi: 10.1080/2162402X.2017.1312239
131. Peng W, Huang X, Yang D. EWS/FLI-1 peptide-pulsed dendritic cells induces the antitumor immunity in a murine Ewing's sarcoma cell model. *Int Immunopharmacol* 2014; **21**(2): 336-341. e-pub ahead of print 2014/05/28; doi: 10.1016/j.intimp.2014.05.013
132. Dagher R, Long LM, Read EJ, Leitman SF, Carter CS, Tsokos M *et al.* Pilot trial of tumor-specific peptide vaccination and continuous infusion interleukin-2 in patients with recurrent Ewing sarcoma and alveolar rhabdomyosarcoma: an inter-institute NIH study. *Med Pediatr Oncol* 2002; **38**(3): 158-164. e-pub ahead of print 2002/02/12; doi: 10.1002/mpo.1303
133. Suminoe A, Matsuzaki A, Hattori H, Koga Y, Hara T. Immunotherapy with autologous dendritic cells and tumor antigens for children with refractory malignant solid tumors. *Pediatr Transplant* 2009; **13**(6): 746-753. e-pub ahead of print 2008/12/11; doi: 10.1111/j.1399-3046.2008.01066.x

134. Merchant MS, Bernstein D, Amoako M, Baird K, Fleisher TA, Morre M *et al.* Adjuvant Immunotherapy to Improve Outcome in High-Risk Pediatric Sarcomas. *Clin Cancer Res* 2016; **22**(13): 3182-3191. e-pub ahead of print 2016/01/30; doi: 10.1158/1078-0432.CCR-15-2550
135. Nemunaitis J. Multifunctional vaccines in cancer: the 'triad' approach. *Expert Rev Vaccines* 2011; **10**(6): 713-715. e-pub ahead of print 2011/06/23; doi: 10.1586/erv.11.78
136. Ghisoli M, Barve M, Schneider R, Mennel R, Lenarsky C, Wallraven G *et al.* Pilot Trial of FANG Immunotherapy in Ewing's Sarcoma. *Mol Ther* 2015; **23**(6): 1103-1109. e-pub ahead of print 2015/04/29; doi: 10.1038/mt.2015.43
137. Ghisoli M, Barve M, Mennel R, Lenarsky C, Horvath S, Wallraven G *et al.* Three-year Follow up of GMCSF/bi-shRNA(furin) DNA-transfected Autologous Tumor Immunotherapy (Vigil) in Metastatic Advanced Ewing's Sarcoma. *Mol Ther* 2016; **24**(8): 1478-1483. e-pub ahead of print 2016/04/26; doi: 10.1038/mt.2016.86
138. Rubin SM, Sage J, Skotheim JM. Integrating Old and New Paradigms of G1/S Control. *Mol Cell* 2020; **80**(2): 183-192. e-pub ahead of print 2020/09/19; doi: 10.1016/j.molcel.2020.08.020
139. Finn RS, Aleshin A, Slamon DJ. Targeting the cyclin-dependent kinases (CDK) 4/6 in estrogen receptor-positive breast cancers. *Breast Cancer Res* 2016; **18**(1): 17. e-pub ahead of print 2016/02/10; doi: 10.1186/s13058-015-0661-5
140. Pan Q, Sathe A, Black PC, Goebell PJ, Kamat AM, Schmitz-Draeger B *et al.* CDK4/6 Inhibitors in Cancer Therapy: A Novel Treatment Strategy for Bladder Cancer. *Bladder Cancer* 2017; **3**(2): 79-88. e-pub ahead of print 2017/05/19; doi: 10.3233/BLC-170105
141. Narasimha AM, Kaulich M, Shapiro GS, Choi YJ, Sicinski P, Dowdy SF. Cyclin D activates the Rb tumor suppressor by mono-phosphorylation. *Elife* 2014; **3**. e-pub ahead of print 2014/05/31; doi: 10.7554/eLife.02872
142. Kennedy AL, Vallurupalli M, Chen L, Crompton B, Cowley G, Vazquez F *et al.* Functional, chemical genomic, and super-enhancer screening identify sensitivity to cyclin D1/CDK4 pathway inhibition in Ewing sarcoma. *Oncotarget* 2015; **6**(30): 30178-30193. e-pub ahead of print 2015/09/05; doi: 10.18632/oncotarget.4903
143. Suryadinata R, Sadowski M, Sarcevic B. Control of cell cycle progression by phosphorylation of cyclin-dependent kinase (CDK) substrates. *Biosci Rep* 2010; **30**(4): 243-255. e-pub ahead of print 2010/03/27; doi: 10.1042/BSR20090171
144. Lundberg AS, Weinberg RA. Functional inactivation of the retinoblastoma protein requires sequential modification by at least two distinct cyclin-cdk complexes. *Mol Cell Biol* 1998; **18**(2): 753-761. e-pub ahead of print 1998/02/03; doi: 10.1128/MCB.18.2.753
145. Rivadeneira DB, Mayhew CN, Thangavel C, Sotillo E, Reed CA, Grana X *et al.* Proliferative suppression by CDK4/6 inhibition: complex function of the retinoblastoma pathway in liver tissue and hepatoma cells. *Gastroenterology* 2010; **138**(5): 1920-1930. e-pub ahead of print 2010/01/27; doi: 10.1053/j.gastro.2010.01.007
146. Weinberg RA. *The biology of CANCER. Chapter 8: pRb and Control of the Cell Cycle Clock*, Garland Science, Taylor & Francis Group, LCC: 270 Madison Avenue, New York, NY 10016, USA, 2007.
147. Du Q, Guo X, Wang M, Li Y, Sun X, Li Q. The application and prospect of CDK4/6 inhibitors in malignant solid tumors. *J Hematol Oncol* 2020; **13**(1): 41. e-pub ahead of print 2020/05/03; doi: 10.1186/s13045-020-00880-8
148. Li T, Xiong Y, Wang Q, Chen F, Zeng Y, Yu X *et al.* Ribociclib (LEE011) suppresses cell proliferation and induces apoptosis of MDA-MB-231 by inhibiting CDK4/6-cyclin D-Rb-E2F pathway. *Artif Cells Nanomed Biotechnol* 2019; **47**(1): 4001-4011. e-pub ahead of print 2019/10/08; doi: 10.1080/21691401.2019.1670670
149. Sathe A, Koshy N, Schmid SC, Thalgott M, Schwarzenbock SM, Krause BJ *et al.* CDK4/6 Inhibition Controls Proliferation of Bladder Cancer and Transcription of RB1. *J Urol* 2016; **195**(3): 771-779. e-pub ahead of print 2015/09/01; doi: 10.1016/j.juro.2015.08.082
150. Lynce F, Shajahan-Haq AN, Swain SM. CDK4/6 inhibitors in breast cancer therapy: Current practice and future opportunities. *Pharmacol Ther* 2018; **191**: 65-73. e-pub ahead of print 2018/06/23; doi: 10.1016/j.pharmthera.2018.06.008

151. Dowless M, Lowery CD, Shackelford T, Renschler M, Stephens J, Flack R *et al.* Abemaciclib Is Active in Preclinical Models of Ewing Sarcoma via Multipronged Regulation of Cell Cycle, DNA Methylation, and Interferon Pathway Signaling. *Clin Cancer Res* 2018; **24**(23): 6028-6039. e-pub ahead of print 2018/08/23; doi: 10.1158/1078-0432.CCR-18-1256
152. Guenther LM, Dharia NV, Ross L, Conway A, Robichaud AL, Catlett JL, 2nd *et al.* A Combination CDK4/6 and IGF1R Inhibitor Strategy for Ewing Sarcoma. *Clin Cancer Res* 2019; **25**(4): 1343-1357. e-pub ahead of print 2018/11/07; doi: 10.1158/1078-0432.CCR-18-0372
153. Van Mater D, Gururangan S, Becher O, Campagne O, Leary S, Phillips JJ *et al.* A phase I trial of the CDK 4/6 inhibitor palbociclib in pediatric patients with progressive brain tumors: A Pediatric Brain Tumor Consortium study (PBTC-042). *Pediatr Blood Cancer* 2021; **68**(4): e28879. e-pub ahead of print 2021/01/07; doi: 10.1002/pbc.28879
154. Cash T, Aguilera D, Macy ME, Hoffman L, Dorris K, McCracken C *et al.* Abstract C002: Phase 1 study of abemaciclib in children with recurrent and refractory solid tumors including malignant brain tumors. *Molecular Cancer Therapeutics* 2019; **18**(12 Supplement): C002-C002. doi: 10.1158/1535-7163.Targ-19-c002
155. Geoerger B, Bourdeaut F, DuBois SG, Fischer M, Geller JI, Gottardo NG *et al.* A Phase I Study of the CDK4/6 Inhibitor Ribociclib (LEE011) in Pediatric Patients with Malignant Rhabdoid Tumors, Neuroblastoma, and Other Solid Tumors. *Clin Cancer Res* 2017; **23**(10): 2433-2441. e-pub ahead of print 2017/04/23; doi: 10.1158/1078-0432.CCR-16-2898
156. Dean JL, Thangavel C, McClendon AK, Reed CA, Knudsen ES. Therapeutic CDK4/6 inhibition in breast cancer: key mechanisms of response and failure. *Oncogene* 2010; **29**(28): 4018-4032. e-pub ahead of print 2010/05/18; doi: 10.1038/onc.2010.154
157. Taylor-Harding B, Aspuria PJ, Agadjanian H, Cheon DJ, Mizuno T, Greenberg D *et al.* Cyclin E1 and RTK/RAS signaling drive CDK inhibitor resistance via activation of E2F and ETS. *Oncotarget* 2015; **6**(2): 696-714. e-pub ahead of print 2015/01/06; doi: 10.18632/oncotarget.2673
158. Chaikovsky AC, Sage J. Beyond the Cell Cycle: Enhancing the Immune Surveillance of Tumors Via CDK4/6 Inhibition. *Mol Cancer Res* 2018; **16**(10): 1454-1457. e-pub ahead of print 2018/06/24; doi: 10.1158/1541-7786.MCR-18-0201
159. Finn RS, Dering J, Conklin D, Kalous O, Cohen DJ, Desai AJ *et al.* PD 0332991, a selective cyclin D kinase 4/6 inhibitor, preferentially inhibits proliferation of luminal estrogen receptor-positive human breast cancer cell lines in vitro. *Breast Cancer Res* 2009; **11**(5): R77. e-pub ahead of print 2009/10/31; doi: 10.1186/bcr2419
160. Lu Y, Ussery GD, Muncaster MM, Gallie BL, Blanck G. Evidence for retinoblastoma protein (RB) dependent and independent IFN-gamma responses: RB coordinately rescues IFN-gamma induction of MHC class II gene transcription in noninducible breast carcinoma cells. *Oncogene* 1994; **9**(4): 1015-1019. e-pub ahead of print 1994/04/01;
161. Zhu X, Pattenden S, Bremner R. pRB is required for interferon-gamma-induction of the MHC class II alpha gene. *Oncogene* 1999; **18**(35): 4940-4947. e-pub ahead of print 1999/09/22; doi: 10.1038/sj.onc.1202876
162. Goel S, DeCristo MJ, Watt AC, BrinJones H, Sceneay J, Li BB *et al.* CDK4/6 inhibition triggers anti-tumour immunity. *Nature* 2017; **548**(7668): 471-475. e-pub ahead of print 2017/08/17; doi: 10.1038/nature23465
163. Deng J, Wang ES, Jenkins RW, Li S, Dries R, Yates K *et al.* CDK4/6 Inhibition Augments Antitumor Immunity by Enhancing T-cell Activation. *Cancer Discov* 2018; **8**(2): 216-233. e-pub ahead of print 2017/11/05; doi: 10.1158/2159-8290.CD-17-0915
164. Dienz O, Eaton SM, Krahl TJ, Diehl S, Charland C, Dodge J *et al.* Accumulation of NFAT mediates IL-2 expression in memory, but not naïve, CD4⁺ T cells. *Proceedings of the National Academy of Sciences* 2007; **104**(17): 7175-7180. doi: 10.1073/pnas.0610442104
165. Teo ZL, Versaci S, Dushyanthen S, Caramia F, Savas P, Mintoff CP *et al.* Combined CDK4/6 and PI3Kalpha Inhibition Is Synergistic and Immunogenic in Triple-Negative Breast Cancer. *Cancer Res* 2017; **77**(22): 6340-6352. e-pub ahead of print 2017/09/28; doi: 10.1158/0008-5472.CAN-17-2210
166. Schaer DA, Beckmann RP, Dempsey JA, Huber L, Forest A, Amaladas N *et al.* The CDK4/6 Inhibitor Abemaciclib Induces a T Cell Inflamed Tumor Microenvironment and Enhances the Efficacy of PD-L1 Checkpoint Blockade. *Cell Rep* 2018; **22**(11): 2978-2994. e-pub ahead of print 2018/03/15; doi: 10.1016/j.celrep.2018.02.053

167. Lai AY, Sorrentino JA, Dragnev KH, Weiss JM, Owonikoko TK, Rytlewski JA *et al.* CDK4/6 inhibition enhances antitumor efficacy of chemotherapy and immune checkpoint inhibitor combinations in preclinical models and enhances T-cell activation in patients with SCLC receiving chemotherapy. *J Immunother Cancer* 2020; **8**(2). e-pub ahead of print 2020/10/03; doi: 10.1136/jitc-2020-000847
168. Uzhachenko RV, Bharti V, Ouyang Z, Blevins A, Mont S, Saleh N *et al.* Metabolic modulation by CDK4/6 inhibitor promotes chemokine-mediated recruitment of T cells into mammary tumors. *Cell Rep* 2021; **35**(1): 108944. e-pub ahead of print 2021/04/08; doi: 10.1016/j.celrep.2021.108944
169. Russell SJ, Peng KW. Viruses as anticancer drugs. *Trends Pharmacol Sci* 2007; **28**(7): 326-333. e-pub ahead of print 2007/06/19; doi: 10.1016/j.tips.2007.05.005
170. Dock G. The influence of complicating diseases upon leukaemia. *Am J Med Sci* 1904; **127**: 563-592.
171. Bierman HR, Crile DM, Dod KS, Kelly KH, Petrakis NL, White LP *et al.* Remissions in leukemia of childhood following acute infectious disease: staphylococcus and streptococcus, varicella, and feline panleukopenia. *Cancer* 1953; **6**(3): 591-605. e-pub ahead of print 1953/05/01; doi: 10.1002/1097-0142(195305)6:3<591::aid-cnrc2820060317>3.0.co;2-m
172. Huebner RJ, Bell JA, Rowe WP, Ward TG, Suskind RG, Hartley JW *et al.* Studies of adenoidal-pharyngeal-conjunctival vaccines in volunteers. *J Am Med Assoc* 1955; **159**(10): 986-989. e-pub ahead of print 1955/11/05; doi: 10.1001/jama.1955.02960270006002
173. Farrera-Sal M, Fillat C, Alemany R. Effect of Transgene Location, Transcriptional Control Elements and Transgene Features in Armed Oncolytic Adenoviruses. *Cancers (Basel)* 2020; **12**(4). e-pub ahead of print 2020/04/29; doi: 10.3390/cancers12041034
174. Southam CM. Present status of oncolytic virus studies. *Trans N Y Acad Sci* 1960; **22**: 657-673. e-pub ahead of print 1960/06/01; doi: 10.1111/j.2164-0947.1960.tb00739.x
175. Russell SJ, Peng KW, Bell JC. Oncolytic virotherapy. *Nat Biotechnol* 2012; **30**(7): 658-670. e-pub ahead of print 2012/07/12; doi: 10.1038/nbt.2287
176. Luhl NC, Zirngibl F, Dorneburg C, Wei J, Dahlhaus M, Barth TF *et al.* Attenuated measles virus controls pediatric acute B-lineage lymphoblastic leukemia in NOD/SCID mice. *Haematologica* 2014; **99**(6): 1050-1061. e-pub ahead of print 2014/04/05; doi: 10.3324/haematol.2013.087205
177. Alemany R, Balague C, Curiel DT. Replicative adenoviruses for cancer therapy. *Nat Biotechnol* 2000; **18**(7): 723-727. e-pub ahead of print 2000/07/11; doi: 10.1038/77283
178. Nakamura T, Russell SJ. Oncolytic measles viruses for cancer therapy. *Expert Opin Biol Ther* 2004; **4**(10): 1685-1692. e-pub ahead of print 2004/10/06; doi: 10.1517/14712598.4.10.1685
179. Conry RM, Westbrook B, McKee S, Norwood TG. Talimogene laherparepvec: First in class oncolytic virotherapy. *Hum Vaccin Immunother* 2018; **14**(4): 839-846. e-pub ahead of print 2018/02/09; doi: 10.1080/21645515.2017.1412896
180. Latchman DS. Herpes simplex virus-based vectors for the treatment of cancer and neurodegenerative disease. *Curr Opin Mol Ther* 2005; **7**(5): 415-418. e-pub ahead of print 2005/10/27;
181. Kelly E, Russell SJ. History of oncolytic viruses: genesis to genetic engineering. *Mol Ther* 2007; **15**(4): 651-659. e-pub ahead of print 2007/02/15; doi: 10.1038/sj.mt.6300108
182. Fueyo J, Gomez-Manzano C, Alemany R, Lee PS, McDonnell TJ, Mitlianga P *et al.* A mutant oncolytic adenovirus targeting the Rb pathway produces anti-glioma effect in vivo. *Oncogene* 2000; **19**(1): 2-12. e-pub ahead of print 2000/01/25; doi: 10.1038/sj.onc.1203251
183. Heise C, Hermiston T, Johnson L, Brooks G, Sampson-Johannes A, Williams A *et al.* An adenovirus E1A mutant that demonstrates potent and selective systemic anti-tumoral efficacy. *Nat Med* 2000; **6**(10): 1134-1139. e-pub ahead of print 2000/10/04; doi: 10.1038/80474
184. Molecular Design of Oncolytic Adenoviruses. 2016.
185. Van Agthoven JF, Xiong JP, Alonso JL, Rui X, Adair BD, Goodman SL *et al.* Structural basis for pure antagonism of integrin alphaVbeta3 by a high-affinity form of fibronectin. *Nat Struct Mol Biol* 2014; **21**(4): 383-388. e-pub ahead of print 2014/03/25; doi: 10.1038/nsmb.2797
186. Lang FF, Conrad C, Gomez-Manzano C, Yung WKA, Sawaya R, Weinberg JS *et al.* Phase I Study of DNX-2401 (Delta-24-RGD) Oncolytic Adenovirus: Replication and Immunotherapeutic Effects in Recurrent

- Malignant Glioma. *J Clin Oncol* 2018; **36**(14): 1419-1427. e-pub ahead of print 2018/02/13; doi: 10.1200/JCO.2017.75.8219
187. Khuri FR, Nemunaitis J, Ganly I, Arseneau J, Tannock IF, Romel L *et al.* a controlled trial of intratumoral ONYX-015, a selectively-replicating adenovirus, in combination with cisplatin and 5-fluorouracil in patients with recurrent head and neck cancer. *Nat Med* 2000; **6**(8): 879-885. e-pub ahead of print 2000/08/10; doi: 10.1038/78638
188. O'Shea CC, Johnson L, Bagus B, Choi S, Nicholas C, Shen A *et al.* Late viral RNA export, rather than p53 inactivation, determines ONYX-015 tumor selectivity. *Cancer Cell* 2004; **6**(6): 611-623. e-pub ahead of print 2004/12/21; doi: 10.1016/j.ccr.2004.11.012
189. Rodriguez R, Schuur ER, Lim HY, Henderson GA, Simons JW, Henderson DR. Prostate attenuated replication competent adenovirus (ARCA) CN706: a selective cytotoxic for prostate-specific antigen-positive prostate cancer cells. *Cancer Res* 1997; **57**(13): 2559-2563. e-pub ahead of print 1997/07/01;
190. Zhang L, Akbulut H, Tang Y, Peng X, Pizzorno G, Sapi E *et al.* Adenoviral vectors with E1A regulated by tumor-specific promoters are selectively cytolytic for breast cancer and melanoma. *Mol Ther* 2002; **6**(3): 386-393. e-pub ahead of print 2002/09/17; doi: 10.1006/mthe.2002.0680
191. Hemminki O, Diaconu I, Cerullo V, Pesonen SK, Kanerva A, Joensuu T *et al.* Ad3-hTERT-E1A, a fully serotype 3 oncolytic adenovirus, in patients with chemotherapy refractory cancer. *Mol Ther* 2012; **20**(9): 1821-1830. e-pub ahead of print 2012/08/09; doi: 10.1038/mt.2012.115
192. Wirth T, Kuhnel F, Kubicka S. Telomerase-dependent gene therapy. *Curr Mol Med* 2005; **5**(2): 243-251. e-pub ahead of print 2005/06/25; doi: 10.2174/1566524053586536
193. Martinez-Velez N, Garcia-Moure M, Marigil M, Gonzalez-Huarriz M, Puigdelloses M, Gallego Perez-Larraya J *et al.* The oncolytic virus Delta-24-RGD elicits an antitumor effect in pediatric glioma and DIPG mouse models. *Nat Commun* 2019; **10**(1): 2235. e-pub ahead of print 2019/05/30; doi: 10.1038/s41467-019-10043-0
194. Garcia-Moure M, Gonzalez-Huarriz M, Labiano S, Guruceaga E, Bandres E, Zalacain M *et al.* Delta-24-RGD, an Oncolytic Adenovirus, Increases Survival and Promotes Proinflammatory Immune Landscape Remodeling in Models of AT/RT and CNS-PNET. *Clin Cancer Res* 2021; **27**(6): 1807-1820. e-pub ahead of print 2020/12/31; doi: 10.1158/1078-0432.CCR-20-3313
195. Garcia-Castro J, Alemany R, Cascallo M, Martinez-Quintanilla J, Arriero Mdel M, Lassaletta A *et al.* Treatment of metastatic neuroblastoma with systemic oncolytic virotherapy delivered by autologous mesenchymal stem cells: an exploratory study. *Cancer Gene Ther* 2010; **17**(7): 476-483. e-pub ahead of print 2010/02/20; doi: 10.1038/cgt.2010.4
196. Ruano D, Lopez-Martin JA, Moreno L, Lassaletta A, Bautista F, Andion M *et al.* First-in-Human, First-in-Child Trial of Autologous MSCs Carrying the Oncolytic Virus Icovir-5 in Patients with Advanced Tumors. *Mol Ther* 2020; **28**(4): 1033-1042. e-pub ahead of print 2020/02/14; doi: 10.1016/j.ymthe.2020.01.019
197. Fujiwara-Okada Y, Matsumoto Y, Fukushi J, Setsu N, Matsuura S, Kamura S *et al.* Y-box binding protein-1 regulates cell proliferation and is associated with clinical outcomes of osteosarcoma. *Br J Cancer* 2013; **108**(4): 836-847. e-pub ahead of print 2013/03/07; doi: 10.1038/bjc.2012.579
198. Sauthoff H, Heitner S, Rom WN, Hay JG. Deletion of the adenoviral E1b-19kD gene enhances tumor cell killing of a replicating adenoviral vector. *Hum Gene Ther* 2000; **11**(3): 379-388. e-pub ahead of print 2000/03/04; doi: 10.1089/10430340050015851
199. Lu Q, Yu DH, Fang C, Liu F, Ye X, Zhao Y *et al.* Influence of E3 region on conditionally replicative adenovirus mediated cytotoxicity in hepatocellular carcinoma cells. *Cancer Biol Ther* 2009; **8**(12): 1125-1132. e-pub ahead of print 2009/05/19; doi: 10.4161/cbt.8.12.8445
200. Hansen TH, Bouvier M. MHC class I antigen presentation: learning from viral evasion strategies. *Nat Rev Immunol* 2009; **9**(7): 503-513. e-pub ahead of print 2009/06/06; doi: 10.1038/nri2575
201. Rognoni E, Widmaier M, Haczek C, Mantwill K, Holzmuller R, Gansbacher B *et al.* Adenovirus-based virotherapy enabled by cellular YB-1 expression in vitro and in vivo. *Cancer Gene Ther* 2009; **16**(10): 753-763. e-pub ahead of print 2009/04/14; doi: 10.1038/cgt.2009.20
202. Fueyo J, Alemany R, Gomez-Manzano C, Fuller GN, Khan A, Conrad CA *et al.* Preclinical characterization of the antiglioma activity of a tropism-enhanced adenovirus targeted to the retinoblastoma pathway. *J Natl Cancer Inst* 2003; **95**(9): 652-660. e-pub ahead of print 2003/05/08; doi: 10.1093/jnci/95.9.652

203. Zhu J, Huang X, Yang Y. Innate immune response to adenoviral vectors is mediated by both Toll-like receptor-dependent and -independent pathways. *J Virol* 2007; **81**(7): 3170-3180. e-pub ahead of print 2007/01/19; doi: 10.1128/JVI.02192-06
204. Ahi YS, Bangari DS, Mittal SK. Adenoviral vector immunity: its implications and circumvention strategies. *Curr Gene Ther* 2011; **11**(4): 307-320. e-pub ahead of print 2011/04/02; doi: 10.2174/156652311796150372
205. Oliveira ERA, Bouvier M. Immune evasion by adenoviruses: a window into host-virus adaptation. *FEBS Lett* 2019; **593**(24): 3496-3503. e-pub ahead of print 2019/11/19; doi: 10.1002/1873-3468.13682
206. Workenhe ST, Mossman KL. Oncolytic virotherapy and immunogenic cancer cell death: sharpening the sword for improved cancer treatment strategies. *Mol Ther* 2014; **22**(2): 251-256. e-pub ahead of print 2013/09/21; doi: 10.1038/mt.2013.220
207. Tesniere A, Panaretakis T, Kepp O, Apetoh L, Ghiringhelli F, Zitvogel L *et al.* Molecular characteristics of immunogenic cancer cell death. *Cell Death Differ* 2008; **15**(1): 3-12. e-pub ahead of print 2007/11/17; doi: 10.1038/sj.cdd.4402269
208. Kroemer G, Galluzzi L, Kepp O, Zitvogel L. Immunogenic cell death in cancer therapy. *Annu Rev Immunol* 2013; **31**: 51-72. e-pub ahead of print 2012/11/20; doi: 10.1146/annurev-immunol-032712-100008
209. Obeid M, Tesniere A, Ghiringhelli F, Fimia GM, Apetoh L, Perfettini JL *et al.* Calreticulin exposure dictates the immunogenicity of cancer cell death. *Nat Med* 2007; **13**(1): 54-61. e-pub ahead of print 2006/12/26; doi: 10.1038/nm1523
210. Michaud M, Martins I, Sukkurwala AQ, Adjemian S, Ma Y, Pellegatti P *et al.* Autophagy-dependent anticancer immune responses induced by chemotherapeutic agents in mice. *Science* 2011; **334**(6062): 1573-1577. e-pub ahead of print 2011/12/17; doi: 10.1126/science.1208347
211. Casares N, Pequignot MO, Tesniere A, Ghiringhelli F, Roux S, Chaput N *et al.* Caspase-dependent immunogenicity of doxorubicin-induced tumor cell death. *J Exp Med* 2005; **202**(12): 1691-1701. e-pub ahead of print 2005/12/21; doi: 10.1084/jem.20050915
212. van Vloten JP, Workenhe ST, Wootton SK, Mossman KL, Bridle BW. Critical Interactions between Immunogenic Cancer Cell Death, Oncolytic Viruses, and the Immune System Define the Rational Design of Combination Immunotherapies. *J Immunol* 2018; **200**(2): 450-458. e-pub ahead of print 2018/01/10; doi: 10.4049/jimmunol.1701021
213. Lichtenegger E, Koll F, Haas H, Mantwill K, Janssen KP, Laschinger M *et al.* The Oncolytic Adenovirus XVir-N-31 as a Novel Therapy in Muscle-Invasive Bladder Cancer. *Hum Gene Ther* 2019; **30**(1): 44-56. e-pub ahead of print 2018/06/20; doi: 10.1089/hum.2018.026
214. Cerullo V, Seiler MP, Mane V, Brunetti-Pierri N, Clarke C, Bertin TK *et al.* Toll-like receptor 9 triggers an innate immune response to helper-dependent adenoviral vectors. *Mol Ther* 2007; **15**(2): 378-385. e-pub ahead of print 2007/01/20; doi: 10.1038/sj.mt.6300031
215. Suzuki M, Cerullo V, Bertin TK, Cela R, Clarke C, Guenther M *et al.* MyD88-dependent silencing of transgene expression during the innate and adaptive immune response to helper-dependent adenovirus. *Hum Gene Ther* 2010; **21**(3): 325-336. e-pub ahead of print 2009/10/15; doi: 10.1089/hum.2009.155
216. Lam E, Stein S, Falck-Pedersen E. Adenovirus detection by the cGAS/STING/TBK1 DNA sensing cascade. *J Virol* 2014; **88**(2): 974-981. e-pub ahead of print 2013/11/08; doi: 10.1128/JVI.02702-13
217. Atasheva S, Yao J, Shayakhmetov DM. Innate immunity to adenovirus: lessons from mice. *FEBS Lett* 2019; **593**(24): 3461-3483. e-pub ahead of print 2019/11/27; doi: 10.1002/1873-3468.13696
218. Kantari C, Pederzoli-Ribeil M, Witko-Sarsat V. The role of neutrophils and monocytes in innate immunity. *Contrib Microbiol* 2008; **15**: 118-146. e-pub ahead of print 2008/05/31; doi: 10.1159/000136335
219. Tang J, Olive M, Champagne K, Flomenberg N, Eisenlohr L, Hsu S *et al.* Adenovirus hexon T-cell epitope is recognized by most adults and is restricted by HLA DP4, the most common class II allele. *Gene Ther* 2004; **11**(18): 1408-1415. e-pub ahead of print 2004/07/23; doi: 10.1038/sj.gt.3302316
220. Tang J, Olive M, Pulmanusahakul R, Schnell M, Flomenberg N, Eisenlohr L *et al.* Human CD8+ cytotoxic T cell responses to adenovirus capsid proteins. *Virology* 2006; **350**(2): 312-322. e-pub ahead of print 2006/02/28; doi: 10.1016/j.virol.2006.01.024

221. Keib A, Mei YF, Cicin-Sain L, Busch DH, Dennehy KM. Measuring Antiviral Capacity of T Cell Responses to Adenovirus. *J Immunol* 2019; **202**(2): 618-624. e-pub ahead of print 2018/12/12; doi: 10.4049/jimmunol.1801003
222. Mole RH. Whole body irradiation; radiobiology or medicine? *Br J Radiol* 1953; **26**(305): 234-241. e-pub ahead of print 1953/05/01; doi: 10.1259/0007-1285-26-305-234
223. Craig DJ, Nanavaty NS, Devanaboyina M, Stanbery L, Hamouda D, Edelman G *et al.* The abscopal effect of radiation therapy. *Future Oncol* 2021; **17**(13): 1683-1694. e-pub ahead of print 2021/03/18; doi: 10.2217/fo-2020-0994
224. Havunen R, Santos JM, Sorsa S, Rantapero T, Lumen D, Siurala M *et al.* Abscopal Effect in Non-injected Tumors Achieved with Cytokine-Armed Oncolytic Adenovirus. *Mol Ther Oncolytics* 2018; **11**: 109-121. e-pub ahead of print 2018/12/21; doi: 10.1016/j.omto.2018.10.005
225. Kuryk L, Moller AW, Jaderberg M. Abscopal effect when combining oncolytic adenovirus and checkpoint inhibitor in a humanized NOG mouse model of melanoma. *J Med Virol* 2019; **91**(9): 1702-1706. e-pub ahead of print 2019/05/14; doi: 10.1002/jmv.25501
226. Ribas A, Dummer R, Puzanov I, VanderWalde A, Andtbacka RHI, Michielin O *et al.* Oncolytic Virotherapy Promotes Intratumoral T Cell Infiltration and Improves Anti-PD-1 Immunotherapy. *Cell* 2017; **170**(6): 1109-1119 e1110. e-pub ahead of print 2017/09/09; doi: 10.1016/j.cell.2017.08.027
227. Sun L, Funchain P, Song JM, Rayman P, Tannenbaum C, Ko J *et al.* Talimogene Laherparepvec combined with anti-PD-1 based immunotherapy for unresectable stage III-IV melanoma: a case series. *J Immunother Cancer* 2018; **6**(1): 36. e-pub ahead of print 2018/05/17; doi: 10.1186/s40425-018-0337-7
228. Kakiuchi Y, Kuroda S, Kanaya N, Kumon K, Tsumura T, Hashimoto M *et al.* Local oncolytic adenovirotherapy produces an abscopal effect via tumor-derived extracellular vesicles. *Mol Ther* 2021. e-pub ahead of print 2021/05/24; doi: 10.1016/j.ymthe.2021.05.015
229. Wheeler S, Santos A. DNATRIX Announces Positive Data from Phase 2 CAPTIVE (KEYNOTE-192) Study with DNX-2401 in Patients with Recurrent Glioblastoma Highlighted in an Oral Late-Breaking Presentation During Society for Neuro-oncology (SNO) Annual Meeting. In. online, 2020.
230. Hwang JK, Hong J, Yun CO. Oncolytic Viruses and Immune Checkpoint Inhibitors: Preclinical Developments to Clinical Trials. *Int J Mol Sci* 2020; **21**(22). e-pub ahead of print 2020/11/20; doi: 10.3390/ijms21228627
231. Maude SL, Hucks GE, Seif AE, Talekar MK, Teachey DT, Baniewicz D *et al.* The effect of pembrolizumab in combination with CD19-targeted chimeric antigen receptor (CAR) T cells in relapsed acute lymphoblastic leukemia (ALL). *Journal of Clinical Oncology* 2017; **35**(15_suppl): 103-103. doi: 10.1200/JCO.2017.35.15_suppl.103
232. Chong EA, Alanio C, Svoboda J, Nasta SD, Landsburg DJ, Lacey SF *et al.* Pembrolizumab for B-cell lymphomas relapsing after or refractory to CD19-directed CAR T-cell therapy. *Blood* 2021. e-pub ahead of print 2021/09/09; doi: 10.1182/blood.2021012634
233. Kailayangiri S, Altwater B, Lesch S, Balbach S, Gottlich C, Kuhnemundt J *et al.* EZH2 Inhibition in Ewing Sarcoma Upregulates GD2 Expression for Targeting with Gene-Modified T Cells. *Mol Ther* 2019; **27**(5): 933-946. e-pub ahead of print 2019/03/19; doi: 10.1016/j.ymthe.2019.02.014
234. Charan M, Dravid P, Cam M, Audino A, Gross AC, Arnold MA *et al.* GD2-directed CAR-T cells in combination with HGF-targeted neutralizing antibody (AMG102) prevent primary tumor growth and metastasis in Ewing sarcoma. *Int J Cancer* 2020; **146**(11): 3184-3195. e-pub ahead of print 2019/10/18; doi: 10.1002/ijc.32743
235. Hogquist KA, Jameson SC, Heath WR, Howard JL, Bevan MJ, Carbone FR. T cell receptor antagonist peptides induce positive selection. *Cell* 1994; **76**(1): 17-27. e-pub ahead of print 1994/01/14; doi: 10.1016/0092-8674(94)90169-4
236. Pan J, Yang JF, Deng BP, Zhao XJ, Zhang X, Lin YH *et al.* High efficacy and safety of low-dose CD19-directed CAR-T cell therapy in 51 refractory or relapsed B acute lymphoblastic leukemia patients. *Leukemia* 2017; **31**(12): 2587-2593. e-pub ahead of print 2017/05/12; doi: 10.1038/leu.2017.145
237. Li J, Li W, Huang K, Zhang Y, Kupfer G, Zhao Q. Chimeric antigen receptor T cell (CAR-T) immunotherapy for solid tumors: lessons learned and strategies for moving forward. *J Hematol Oncol* 2018; **11**(1): 22. e-pub ahead of print 2018/02/13; doi: 10.1186/s13045-018-0568-6

238. DeRenzo C, Gottschalk S. Genetic Modification Strategies to Enhance CAR T Cell Persistence for Patients With Solid Tumors. *Front Immunol* 2019; **10**: 218. e-pub ahead of print 2019/03/05; doi: 10.3389/fimmu.2019.00218
239. Labarta-Bajo L, Nilsen SP, Humphrey G, Schwartz T, Sanders K, Swafford A *et al.* Type I IFNs and CD8 T cells increase intestinal barrier permeability after chronic viral infection. *J Exp Med* 2020; **217**(12). e-pub ahead of print 2020/09/04; doi: 10.1084/jem.20192276
240. Haile ST, Conner J, Mackall C. Abstract 2304: Attenuated oncolytic virus HSV1716 increases *in vivo* expansion of GD2- targeting CAR T cells in murine solid tumor models. *Cancer Research* 2016; **76**(14 Supplement): 2304-2304. doi: 10.1158/1538-7445.Am2016-2304
241. Achard C, Surendran A, Wedge ME, Ungerechts G, Bell J, Ilkow CS. Lighting a Fire in the Tumor Microenvironment Using Oncolytic Immunotherapy. *EBioMedicine* 2018; **31**: 17-24. e-pub ahead of print 2018/05/05; doi: 10.1016/j.ebiom.2018.04.020
242. Tahtinen S, Gronberg-Vaha-Koskela S, Lumen D, Merisalo-Soikkeli M, Siurala M, Airaksinen AJ *et al.* Adenovirus Improves the Efficacy of Adoptive T-cell Therapy by Recruiting Immune Cells to and Promoting Their Activity at the Tumor. *Cancer Immunol Res* 2015; **3**(8): 915-925. e-pub ahead of print 2015/05/16; doi: 10.1158/2326-6066.CIR-14-0220-T
243. Rezaei R, Esmaeili Gouvarchin Ghaleh H, Farzanehpour M, Dorostkar R, Ranjbar R, Bolandian M *et al.* Combination therapy with CAR T cells and oncolytic viruses: a new era in cancer immunotherapy. *Cancer Gene Ther* 2021. e-pub ahead of print 2021/06/24; doi: 10.1038/s41417-021-00359-9
244. Watanabe N, McKenna MK, Rosewell Shaw A, Suzuki M. Clinical CAR-T Cell and Oncolytic Virotherapy for Cancer Treatment. *Mol Ther* 2021; **29**(2): 505-520. e-pub ahead of print 2020/11/02; doi: 10.1016/j.ymthe.2020.10.023
245. Esaki S, Nigim F, Moon E, Luk S, Kiyokawa J, Curry W, Jr. *et al.* Blockade of transforming growth factor-beta signaling enhances oncolytic herpes simplex virus efficacy in patient-derived recurrent glioblastoma models. *Int J Cancer* 2017; **141**(11): 2348-2358. e-pub ahead of print 2017/08/13; doi: 10.1002/ijc.30929
246. Currier MA, Eshun FK, Sholl A, Chernoguz A, Crawford K, Divanovic S *et al.* VEGF blockade enables oncolytic cancer virotherapy in part by modulating intratumoral myeloid cells. *Mol Ther* 2013; **21**(5): 1014-1023. e-pub ahead of print 2013/03/14; doi: 10.1038/mt.2013.39
247. Lv B, Li J, Li M, Zhuo Y, Ren K, Li E *et al.* Enhancement of adenovirus infection and adenoviral vector-mediated gene delivery by bromodomain inhibitor JQ1. *Sci Rep* 2018; **8**(1): 11554. e-pub ahead of print 2018/08/03; doi: 10.1038/s41598-018-28421-x
248. Kim DR, Park MY, Lim HJ, Park JS, Cho YJ, Lee SW *et al.* Combination therapy of conditionally replicating adenovirus and histone deacetylase inhibitors. *Int J Mol Med* 2012; **29**(2): 218-224. e-pub ahead of print 2011/11/15; doi: 10.3892/ijmm.2011.831
249. Lypova N, Lanceta L, Gibson A, Vega S, Garza-Morales R, McMasters KM *et al.* Targeting Palbociclib-Resistant Estrogen Receptor-Positive Breast Cancer Cells via Oncolytic Virotherapy. *Cancers (Basel)* 2019; **11**(5). e-pub ahead of print 2019/05/19; doi: 10.3390/cancers11050684
250. May WA, Grigoryan RS, Keshelava N, Cabral DJ, Christensen LL, Jenabi J *et al.* Characterization and drug resistance patterns of Ewing's sarcoma family tumor cell lines. *PLoS One* 2013; **8**(12): e80060. e-pub ahead of print 2013/12/07; doi: 10.1371/journal.pone.0080060
251. Castro BA, Flanigan P, Jahangiri A, Hoffman D, Chen W, Kuang R *et al.* Macrophage migration inhibitory factor downregulation: a novel mechanism of resistance to anti-angiogenic therapy. *Oncogene* 2017; **36**(26): 3749-3759. e-pub ahead of print 2017/02/22; doi: 10.1038/onc.2017.1
252. Misson P, van den Brule S, Barbarin V, Lison D, Huaux F. Markers of macrophage differentiation in experimental silicosis. *J Leukoc Biol* 2004; **76**(5): 926-932. e-pub ahead of print 2004/08/05; doi: 10.1189/jlb.0104019
253. Leiro J, Alvarez E, Arranz JA, Laguna R, Uriarte E, Orallo F. Effects of cis-resveratrol on inflammatory murine macrophages: antioxidant activity and down-regulation of inflammatory genes. *J Leukoc Biol* 2004; **75**(6): 1156-1165. e-pub ahead of print 2004/02/26; doi: 10.1189/jlb.1103561
254. Schober SJ, Thiede M, Gassmann H, Prexler C, Xue B, Schirmer D *et al.* MHC Class I-Restricted TCR-Transgenic CD4(+) T Cells Against STEAP1 Mediate Local Tumor Control of Ewing Sarcoma In Vivo. *Cells* 2020; **9**(7). e-pub ahead of print 2020/07/03; doi: 10.3390/cells9071581

255. Busch DH, Pilip IM, Vijh S, Pamer EG. Coordinate regulation of complex T cell populations responding to bacterial infection. *Immunity* 1998; **8**(3): 353-362. e-pub ahead of print 1998/04/07; doi: 10.1016/s1074-7613(00)80540-3
256. Pfaffl MW. A new mathematical model for relative quantification in real-time RT-PCR. *Nucleic Acids Res* 2001; **29**(9): e45. e-pub ahead of print 2001/05/09; doi: 10.1093/nar/29.9.e45
257. Richter GH, Plehm S, Fasan A, Rossler S, Unland R, Bennani-Baiti IM *et al.* EZH2 is a mediator of EWS/FLI1 driven tumor growth and metastasis blocking endothelial and neuro-ectodermal differentiation. *Proc Natl Acad Sci U S A* 2009; **106**(13): 5324-5329. e-pub ahead of print 2009/03/18; doi: 10.1073/pnas.0810759106
258. Zheng S, Wang W, Aldahdooh J, Malyutina A, Shadbahr T, Pessia A *et al.* SynergyFinder Plus: towards a better interpretation and annotation of drug combination screening datasets. *bioRxiv* 2021: 2021.2006.2001.446564. doi: 10.1101/2021.06.01.446564
259. Muller-Hermelink N, Braumuller H, Pichler B, Wieder T, Mailhammer R, Schaak K *et al.* TNFR1 signaling and IFN-gamma signaling determine whether T cells induce tumor dormancy or promote multistage carcinogenesis. *Cancer Cell* 2008; **13**(6): 507-518. e-pub ahead of print 2008/06/10; doi: 10.1016/j.ccr.2008.04.001
260. Wightman SC, Uppal A, Pitroda SP, Ganai S, Burnette B, Stack M *et al.* Oncogenic CXCL10 signalling drives metastasis development and poor clinical outcome. *Br J Cancer* 2015; **113**(2): 327-335. e-pub ahead of print 2015/06/05; doi: 10.1038/bjc.2015.193
261. Chen B, Khodadoust MS, Liu CL, Newman AM, Alizadeh AA. Profiling Tumor Infiltrating Immune Cells with CIBERSORT. *Methods Mol Biol* 2018; **1711**: 243-259. e-pub ahead of print 2018/01/19; doi: 10.1007/978-1-4939-7493-1_12
262. Schober SJ, Thiede M, Schirmer D, Wohlleber D, Richter G, Busch DH *et al.* Abstract LB-106: Allorepertoire-derived HLA class I/peptide-specific T cell receptor transgenic CD4⁺ T cells mediate antitumor responses in Ewing sarcoma mimicking allo-rejection. *Cancer Research* 2018; **78**(13 Supplement): LB-106-LB-106. doi: 10.1158/1538-7445.Am2018-lb-106
263. Dudek M, Pfister D, Donakonda S, Filpe P, Schneider A, Laschinger M *et al.* Auto-aggressive CXCR6(+) CD8 T cells cause liver immune pathology in NASH. *Nature* 2021; **592**(7854): 444-449. e-pub ahead of print 2021/03/26; doi: 10.1038/s41586-021-03233-8
264. Somersalo K, Anikeeva N, Sims TN, Thomas VK, Strong RK, Spies T *et al.* Cytotoxic T lymphocytes form an antigen-independent ring junction. *The Journal of Clinical Investigation* 2004; **113**(1): 49-57. doi: 10.1172/JCI19337
265. Ianevski A, Giri AK, Gautam P, Kononov A, Potdar S, Saarela J *et al.* Prediction of drug combination effects with a minimal set of experiments. *Nature Machine Intelligence* 2019; **1**(12): 568-577. doi: 10.1038/s42256-019-0122-4
266. R Core Team. R: A language and environment for statistical computing. In: *R Foundation for Statistical Computing, Vienna, Austria*. URL <https://www.R-project.org/>, 2021.
267. Chao MP, Jaiswal S, Weissman-Tsukamoto R, Alizadeh AA, Gentles AJ, Volkmer J *et al.* Calreticulin is the dominant pro-phagocytic signal on multiple human cancers and is counterbalanced by CD47. *Sci Transl Med* 2010; **2**(63): 63ra94. e-pub ahead of print 2010/12/24; doi: 10.1126/scitranslmed.3001375
268. Tseng D, Volkmer JP, Willingham SB, Contreras-Trujillo H, Fathman JW, Fernhoff NB *et al.* Anti-CD47 antibody-mediated phagocytosis of cancer by macrophages primes an effective antitumor T-cell response. *Proc Natl Acad Sci U S A* 2013; **110**(27): 11103-11108. e-pub ahead of print 2013/05/22; doi: 10.1073/pnas.1305569110
269. Groom JR, Luster AD. CXCR3 in T cell function. *Exp Cell Res* 2011; **317**(5): 620-631. e-pub ahead of print 2011/03/08; doi: 10.1016/j.yexcr.2010.12.017
270. Koch JA. Combining Oncolytic Virotherapy with Target Therapy in Bladder Cancer. Dissertation. Technical University of Munich. In. TUM online, 2021.
271. Koch J, Schober, S.J., Hindupur, S, Klein, F., Mantwill, K., Ehrenfeld, M., Schillinger, U., Hohnecker, T., Pan, Q., Steiger, K., Aichler, M., Gschend, J., Holm, P.S., Narowth, R. . Targeting the RB/E2F repressive complex by CDK4/6 inhibitors amplifies the oncolytic potency of XVir-N-31. *Nature Communications (in revision)*. KJ, SJS, HS contributed equally. PSH and RN share senior authorship 2021.

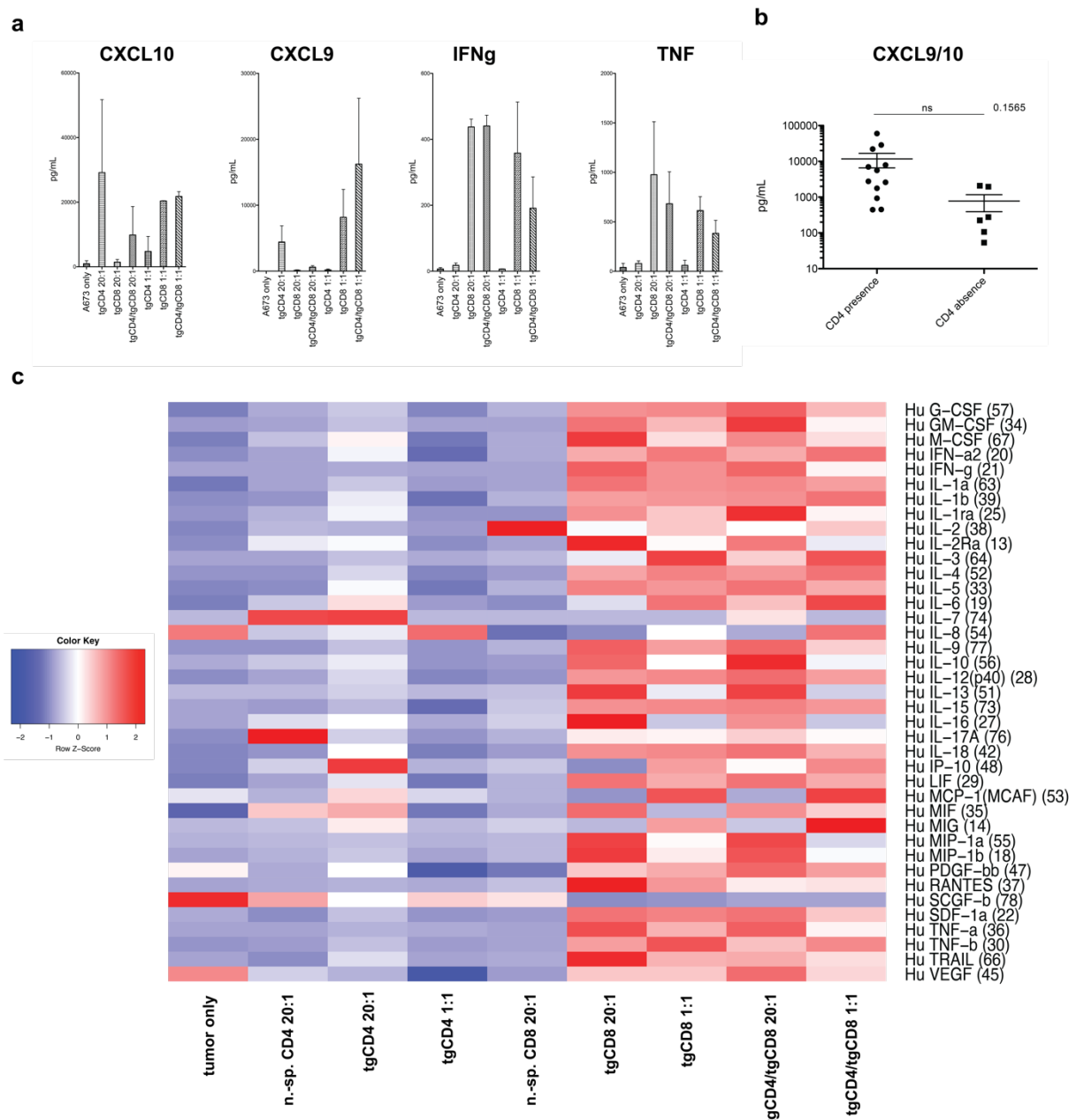
272. Flint J, Shenk T. Adenovirus E1A protein paradigm viral transactivator. *Annu Rev Genet* 1989; **23**: 141-161. e-pub ahead of print 1989/01/01; doi: 10.1146/annurev.ge.23.120189.001041
273. Fry DW, Harvey PJ, Keller PR, Elliott WL, Meade M, Trachet E *et al.* Specific inhibition of cyclin-dependent kinase 4/6 by PD 0332991 and associated antitumor activity in human tumor xenografts. *Mol Cancer Ther* 2004; **3**(11): 1427-1438. e-pub ahead of print 2004/11/16;
274. Berge EO, Knappskog S, Geisler S, Staalesen V, Pacal M, Borresen-Dale AL *et al.* Identification and characterization of retinoblastoma gene mutations disturbing apoptosis in human breast cancers. *Mol Cancer* 2010; **9**: 173. e-pub ahead of print 2010/07/03; doi: 10.1186/1476-4598-9-173
275. Enot DP, Vacchelli E, Jacquelot N, Zitvogel L, Kroemer G. TumGrowth: An open-access web tool for the statistical analysis of tumor growth curves. *Oncoimmunology* 2018; **7**(9): e1462431. e-pub ahead of print 2018/09/20; doi: 10.1080/2162402X.2018.1462431
276. Puigdelloses M, Garcia-Moure M, Labiano S, Laspidea V, Gonzalez-Huarriz M, Zalacain M *et al.* CD137 and PD-L1 targeting with immunovirotherapy induces a potent and durable antitumor immune response in glioblastoma models. *J Immunother Cancer* 2021; **9**(7). e-pub ahead of print 2021/07/21; doi: 10.1136/jitc-2021-002644
277. Krabbe T, Marek J, Groll T, Steiger K, Schmid RM, Krackhardt AM *et al.* Adoptive T Cell Therapy Is Complemented by Oncolytic Virotherapy with Fusogenic VSV-NDV in Combination Treatment of Murine Melanoma. *Cancers (Basel)* 2021; **13**(5). e-pub ahead of print 2021/04/04; doi: 10.3390/cancers13051044
278. Hendrickx R, Stichling N, Koelen J, Kuryk L, Lipiec A, Greber UF. Innate immunity to adenovirus. *Hum Gene Ther* 2014; **25**(4): 265-284. e-pub ahead of print 2014/02/12; doi: 10.1089/hum.2014.001
279. Glatman Zaretsky A, Engiles JB, Hunter CA. Infection-induced changes in hematopoiesis. *J Immunol* 2014; **192**(1): 27-33. e-pub ahead of print 2013/12/24; doi: 10.4049/jimmunol.1302061
280. Jakubzick CV, Randolph GJ, Henson PM. Monocyte differentiation and antigen-presenting functions. *Nat Rev Immunol* 2017; **17**(6): 349-362. e-pub ahead of print 2017/04/25; doi: 10.1038/nri.2017.28
281. Bosshart H, Heinzelmann M. THP-1 cells as a model for human monocytes. *Ann Transl Med* 2016; **4**(21): 438. e-pub ahead of print 2016/12/13; doi: 10.21037/atm.2016.08.53
282. Deng Y, Govers C, Ter Beest E, van Dijk AJ, Hettinga K, Wichers HJ. A THP-1 Cell Line-Based Exploration of Immune Responses Toward Heat-Treated BLG. *Front Nutr* 2020; **7**: 612397. e-pub ahead of print 2021/02/02; doi: 10.3389/fnut.2020.612397
283. Clouet E, Bechara R, Raffalli C, Damiens MH, Groux H, Pallardy M *et al.* The THP-1 cell toolbox: a new concept integrating the key events of skin sensitization. *Arch Toxicol* 2019; **93**(4): 941-951. e-pub ahead of print 2019/02/27; doi: 10.1007/s00204-019-02416-7
284. Wu TH, Li YY, Wu TL, Chang JW, Chou WC, Hsieh LL *et al.* Culture supernatants of different colon cancer cell lines induce specific phenotype switching and functional alteration of THP-1 cells. *Cell Immunol* 2014; **290**(1): 107-115. e-pub ahead of print 2014/06/25; doi: 10.1016/j.cellimm.2014.05.015
285. Krabbe TA. Oncolytic Virotherapy with the Fusogenic VSV-NDV Platform Complementing Adoptive T Cell Therapy. In: Technical University of Munich KuPflMI, (ed). TUM online, 2020.
286. Watanabe K, Luo Y, Da T, Guedan S, Ruella M, Scholler J *et al.* Pancreatic cancer therapy with combined mesothelin-redirected chimeric antigen receptor T cells and cytokine-armed oncolytic adenoviruses. *JCI Insight* 2018; **3**(7). e-pub ahead of print 2018/04/06; doi: 10.1172/jci.insight.99573
287. Park JA, Cheung NV. GD2 or HER2 targeting T cell engaging bispecific antibodies to treat osteosarcoma. *J Hematol Oncol* 2020; **13**(1): 172. e-pub ahead of print 2020/12/12; doi: 10.1186/s13045-020-01012-y
288. Andrade D, Redecha PB, Vukelic M, Qing X, Perino G, Salmon JE *et al.* Engraftment of peripheral blood mononuclear cells from systemic lupus erythematosus and antiphospholipid syndrome patient donors into BALB-RAG-2^{-/-} IL-2R γ ^{-/-} mice: a promising model for studying human disease. *Arthritis Rheum* 2011; **63**(9): 2764-2773. e-pub ahead of print 2011/05/12; doi: 10.1002/art.30424
289. Shinkai Y, Rathbun G, Lam KP, Oltz EM, Stewart V, Mendelsohn M *et al.* RAG-2-deficient mice lack mature lymphocytes owing to inability to initiate V(D)J rearrangement. *Cell* 1992; **68**(5): 855-867. e-pub ahead of print 1992/03/06; doi: 10.1016/0092-8674(92)90029-c

290. Minas TZ, Surdez D, Javaheri T, Tanaka M, Howarth M, Kang HJ *et al.* Combined experience of six independent laboratories attempting to create an Ewing sarcoma mouse model. *Oncotarget* 2017; **8**(21): 34141-34163. e-pub ahead of print 2016/05/19; doi: 10.18632/oncotarget.9388
291. Ito M, Kobayashi K, Nakahata T. NOD/Shi-scid IL2rgamma(null) (NOG) mice more appropriate for humanized mouse models. *Curr Top Microbiol Immunol* 2008; **324**: 53-76. e-pub ahead of print 2008/05/17; doi: 10.1007/978-3-540-75647-7_3
292. Traggiai E, Chicha L, Mazzucchelli L, Bronz L, Piffaretti JC, Lanzavecchia A *et al.* Development of a human adaptive immune system in cord blood cell-transplanted mice. *Science* 2004; **304**(5667): 104-107. e-pub ahead of print 2004/04/06; doi: 10.1126/science.1093933
293. Biswas A, Bruder D, Wolf SA, Jeron A, Mack M, Heimesaat MM *et al.* Ly6C(high) monocytes control cerebral toxoplasmosis. *J Immunol* 2015; **194**(7): 3223-3235. e-pub ahead of print 2015/02/25; doi: 10.4049/jimmunol.1402037
294. Terry RL, Getts DR, Deffrasnes C, van Vreden C, Campbell IL, King NJ. Inflammatory monocytes and the pathogenesis of viral encephalitis. *J Neuroinflammation* 2012; **9**: 270. e-pub ahead of print 2012/12/19; doi: 10.1186/1742-2094-9-270
295. Clements DR, Sterea AM, Kim Y, Helson E, Dean CA, Nunokawa A *et al.* Newly recruited CD11b+, GR-1+, Ly6C(high) myeloid cells augment tumor-associated immunosuppression immediately following the therapeutic administration of oncolytic reovirus. *J Immunol* 2015; **194**(9): 4397-4412. e-pub ahead of print 2015/04/01; doi: 10.4049/jimmunol.1402132
296. Dumont C, Jacquier A, Verine J, Noel F, Goujon A, Wu CL *et al.* CD8(+)PD-1(-)ILT2(+) T Cells Are an Intratumoral Cytotoxic Population Selectively Inhibited by the Immune-Checkpoint HLA-G. *Cancer Immunol Res* 2019; **7**(10): 1619-1632. e-pub ahead of print 2019/08/28; doi: 10.1158/2326-6066.CIR-18-0764
297. Franco-Luzon L, Garcia-Mulero S, Sanz-Pamplona R, Melen G, Ruano D, Lassaletta A *et al.* Genetic and Immune Changes Associated with Disease Progression under the Pressure of Oncolytic Therapy in A Neuroblastoma Outlier Patient. *Cancers (Basel)* 2020; **12**(5). e-pub ahead of print 2020/05/02; doi: 10.3390/cancers12051104
298. Dhatchinamoorthy K, Colbert JD, Rock KL. Cancer Immune Evasion Through Loss of MHC Class I Antigen Presentation. *Front Immunol* 2021; **12**: 636568. e-pub ahead of print 2021/03/27; doi: 10.3389/fimmu.2021.636568
299. Majzner RG, Mackall CL. Tumor Antigen Escape from CAR T-cell Therapy. *Cancer Discov* 2018; **8**(10): 1219-1226. e-pub ahead of print 2018/08/24; doi: 10.1158/2159-8290.CD-18-0442
300. Junttila MR, de Sauvage FJ. Influence of tumour micro-environment heterogeneity on therapeutic response. *Nature* 2013; **501**(7467): 346-354. e-pub ahead of print 2013/09/21; doi: 10.1038/nature12626
301. Walsh SR, Simovic B, Chen L, Bastin D, Nguyen A, Stephenson K *et al.* Endogenous T cells prevent tumor immune escape following adoptive T cell therapy. *J Clin Invest* 2019; **129**(12): 5400-5410. e-pub ahead of print 2019/11/05; doi: 10.1172/JCI126199
302. Gulley JL, Madan RA, Pachynski R, Mulders P, Sheikh NA, Trager J *et al.* Role of Antigen Spread and Distinctive Characteristics of Immunotherapy in Cancer Treatment. *J Natl Cancer Inst* 2017; **109**(4). e-pub ahead of print 2017/04/05; doi: 10.1093/jnci/djw261
303. Woller N, Gurlevik E, Fleischmann-Mundt B, Schumacher A, Knocke S, Kloos AM *et al.* Viral Infection of Tumors Overcomes Resistance to PD-1-immunotherapy by Broadening Neoantigenome-directed T-cell Responses. *Mol Ther* 2015; **23**(10): 1630-1640. e-pub ahead of print 2015/06/27; doi: 10.1038/mt.2015.115
304. Wang G, Kang X, Chen KS, Jehng T, Jones L, Chen J *et al.* An engineered oncolytic virus expressing PD-L1 inhibitors activates tumor neoantigen-specific T cell responses. *Nat Commun* 2020; **11**(1): 1395. e-pub ahead of print 2020/03/15; doi: 10.1038/s41467-020-15229-5
305. Das K, Belnoue E, Rossi M, Hofer T, Danklmaier S, Nolden T *et al.* A modular self-adjuvanting cancer vaccine combined with an oncolytic vaccine induces potent antitumor immunity. *Nat Commun* 2021; **12**(1): 5195. e-pub ahead of print 2021/09/02; doi: 10.1038/s41467-021-25506-6
306. Klar R, Schober S, Rami M, Mall S, Merl J, Hauck SM *et al.* Therapeutic targeting of naturally presented myeloperoxidase-derived HLA peptide ligands on myeloid leukemia cells by TCR-transgenic T cells. *Leukemia* 2014; **28**(12): 2355-2366. e-pub ahead of print 2014/04/17; doi: 10.1038/leu.2014.131

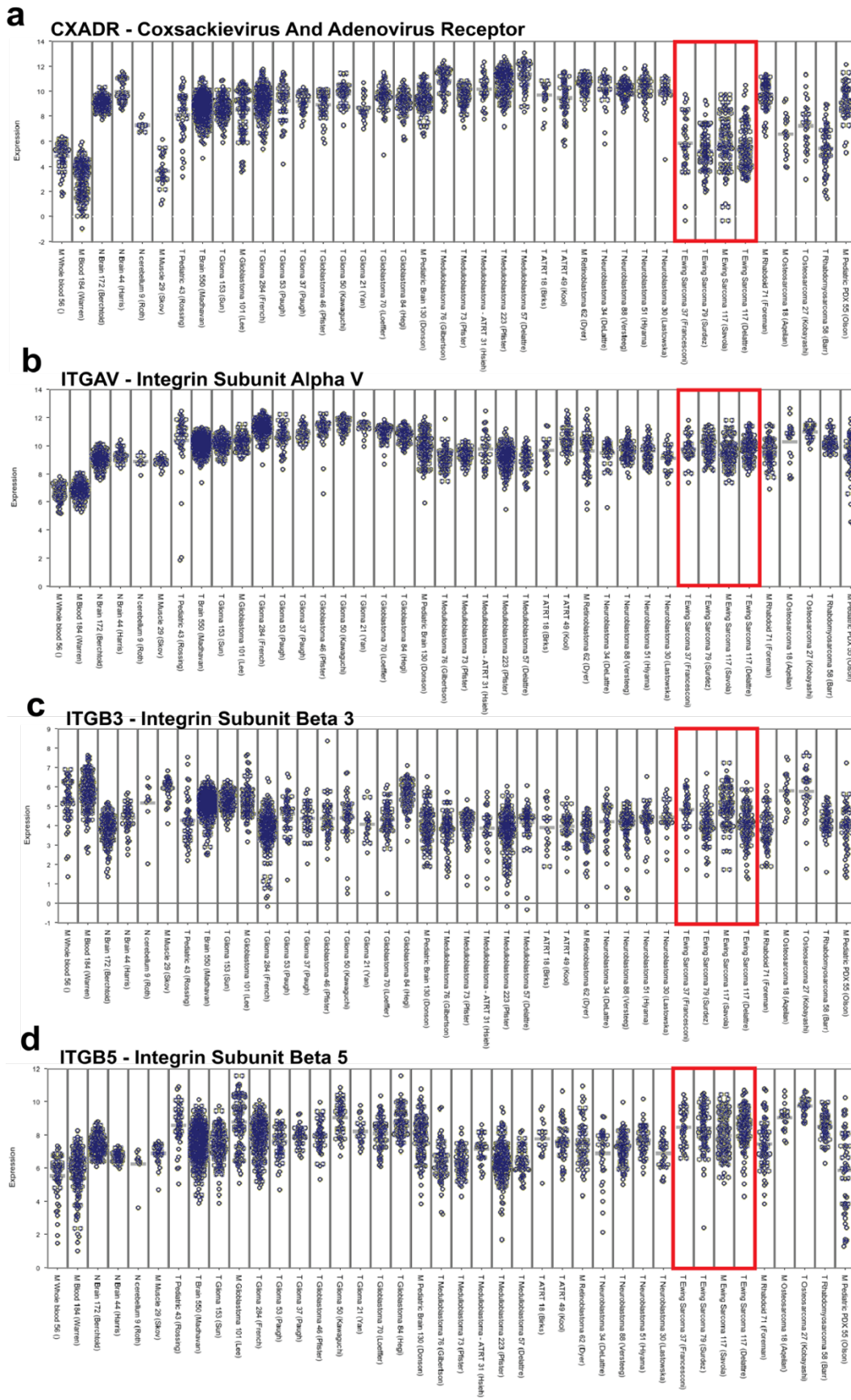
307. Bassani-Sternberg M, Braunlein E, Klar R, Engleitner T, Sinitcyn P, Audehm S *et al.* Direct identification of clinically relevant neoepitopes presented on native human melanoma tissue by mass spectrometry. *Nat Commun* 2016; **7**: 13404. e-pub ahead of print 2016/11/22; doi: 10.1038/ncomms13404
308. Rajaraman S, Canjuga D, Ghosh M, Codrea MC, Sieger R, Wedekink F *et al.* Measles Virus-Based Treatments Trigger a Pro-inflammatory Cascade and a Distinctive Immunopeptidome in Glioblastoma. *Mol Ther Oncolytics* 2019; **12**: 147-161. e-pub ahead of print 2019/02/19; doi: 10.1016/j.omto.2018.12.010
309. Zhang L, Hedjran F, Larson C, Perez GL, Reid T. A novel immunocompetent murine model for replicating oncolytic adenoviral therapy. *Cancer Gene Ther* 2015; **22**(1): 17-22. e-pub ahead of print 2014/12/20; doi: 10.1038/cgt.2014.64
310. Jogler C, Hoffmann D, Theegarten D, Grunwald T, Uberla K, Wildner O. Replication properties of human adenovirus in vivo and in cultures of primary cells from different animal species. *J Virol* 2006; **80**(7): 3549-3558. e-pub ahead of print 2006/03/16; doi: 10.1128/JVI.80.7.3549-3558.2006
311. Lichtenstein DL, Spencer JF, Doronin K, Patra D, Meyer JM, Shashkova EV *et al.* An acute toxicology study with INGN 007, an oncolytic adenovirus vector, in mice and permissive Syrian hamsters; comparisons with wild-type Ad5 and a replication-defective adenovirus vector. *Cancer Gene Ther* 2009; **16**(8): 644-654. e-pub ahead of print 2009/02/07; doi: 10.1038/cgt.2009.5
312. Li X, Wang P, Li H, Du X, Liu M, Huang Q *et al.* The Efficacy of Oncolytic Adenovirus Is Mediated by T-cell Responses against Virus and Tumor in Syrian Hamster Model. *Clin Cancer Res* 2017; **23**(1): 239-249. e-pub ahead of print 2016/07/21; doi: 10.1158/1078-0432.CCR-16-0477
313. Smith K, Ying B, Ball AO, Beard CW, Spindler KR. Interaction of mouse adenovirus type 1 early region 1A protein with cellular proteins pRb and p107. *Virology* 1996; **224**(1): 184-197. e-pub ahead of print 1996/10/01; doi: 10.1006/viro.1996.0520
314. Robinson M, Li B, Ge Y, Ko D, Yendluri S, Harding T *et al.* Novel immunocompetent murine tumor model for evaluation of conditionally replication-competent (oncolytic) murine adenoviral vectors. *J Virol* 2009; **83**(8): 3450-3462. e-pub ahead of print 2009/02/06; doi: 10.1128/JVI.02561-08
315. Morales-Molina A, Rodriguez-Milla MA, Gimenez-Sanchez A, Perise-Barrios AJ, Garcia-Castro J. Cellular Virotherapy Increases Tumor-Infiltrating Lymphocytes (TIL) and Decreases their PD-1(+) Subsets in Mouse Immunocompetent Models. *Cancers (Basel)* 2020; **12**(7). e-pub ahead of print 2020/07/28; doi: 10.3390/cancers12071920
316. Morales-Molina A, Gambera S, Cejalvo T, Moreno R, Rodriguez-Milla MA, Perise-Barrios AJ *et al.* Antitumor virotherapy using syngeneic or allogeneic mesenchymal stem cell carriers induces systemic immune response and intratumoral leukocyte infiltration in mice. *Cancer Immunol Immunother* 2018; **67**(10): 1589-1602. e-pub ahead of print 2018/08/02; doi: 10.1007/s00262-018-2220-2
317. McKenna MK, Rosewell-Shaw A, Suzuki M. Modeling the Efficacy of Oncolytic Adenoviruses In Vitro and In Vivo: Current and Future Perspectives. *Cancers (Basel)* 2020; **12**(3). e-pub ahead of print 2020/03/12; doi: 10.3390/cancers12030619
318. Alemany R, Suzuki K, Curiel DT. Blood clearance rates of adenovirus type 5 in mice. *J Gen Virol* 2000; **81**(Pt 11): 2605-2609. e-pub ahead of print 2000/10/20; doi: 10.1099/0022-1317-81-11-2605
319. Di Paolo NC, Shayakhmetov DM. Adenovirus de-targeting from the liver. *Curr Opin Mol Ther* 2009; **11**(5): 523-531. e-pub ahead of print 2009/10/07;
320. Niemann J, Woller N, Brooks J, Fleischmann-Mundt B, Martin NT, Kloos A *et al.* Molecular retargeting of antibodies converts immune defense against oncolytic viruses into cancer immunotherapy. *Nat Commun* 2019; **10**(1): 3236. e-pub ahead of print 2019/07/22; doi: 10.1038/s41467-019-11137-5
321. Croyle MA, Chirmule N, Zhang Y, Wilson JM. PEGylation of E1-deleted adenovirus vectors allows significant gene expression on readministration to liver. *Hum Gene Ther* 2002; **13**(15): 1887-1900. e-pub ahead of print 2002/10/25; doi: 10.1089/104303402760372972
322. Schmid M, Ernst P, Honegger A, Suomalainen M, Zimmermann M, Braun L *et al.* Adenoviral vector with shield and adapter increases tumor specificity and escapes liver and immune control. *Nat Commun* 2018; **9**(1): 450. e-pub ahead of print 2018/02/02; doi: 10.1038/s41467-017-02707-6
323. Workenhe ST, Simmons G, Pol JG, Lichty BD, Halford WP, Mossman KL. Immunogenic HSV-mediated oncolysis shapes the antitumor immune response and contributes to therapeutic efficacy. *Mol Ther* 2014; **22**(1): 123-131. e-pub ahead of print 2013/12/18; doi: 10.1038/mt.2013.238

8 Appendix

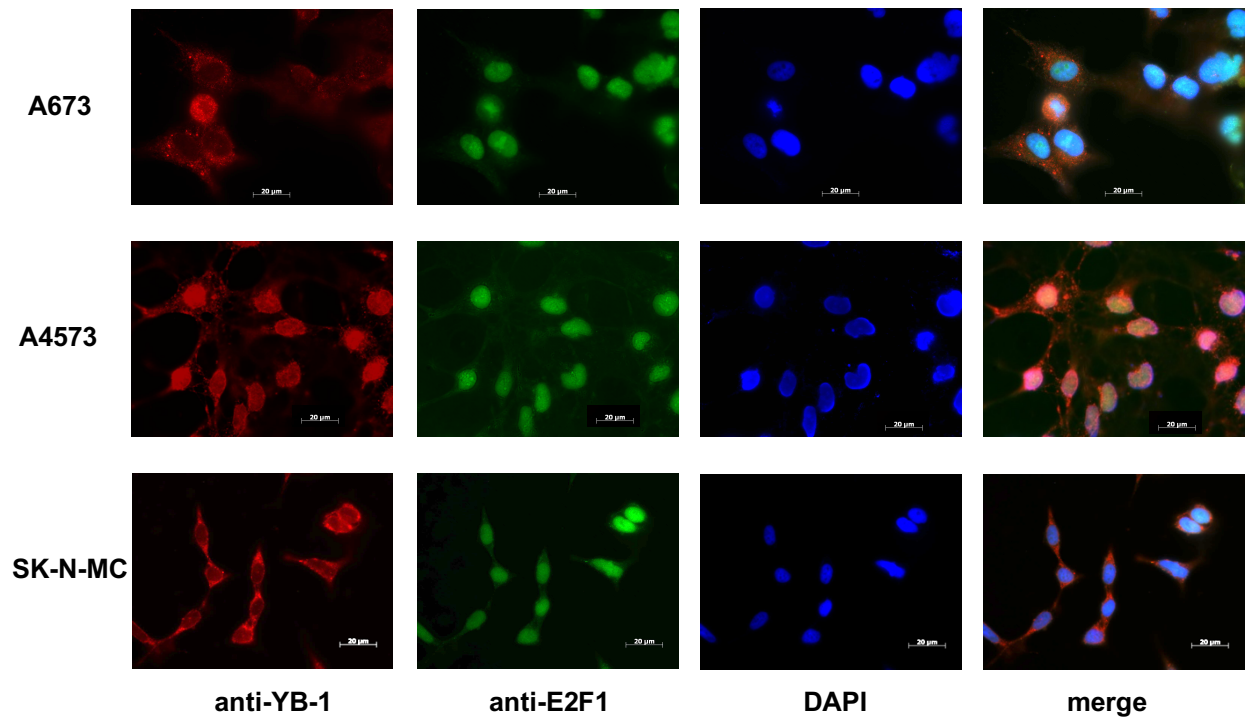
8.1 Supplemental Figures



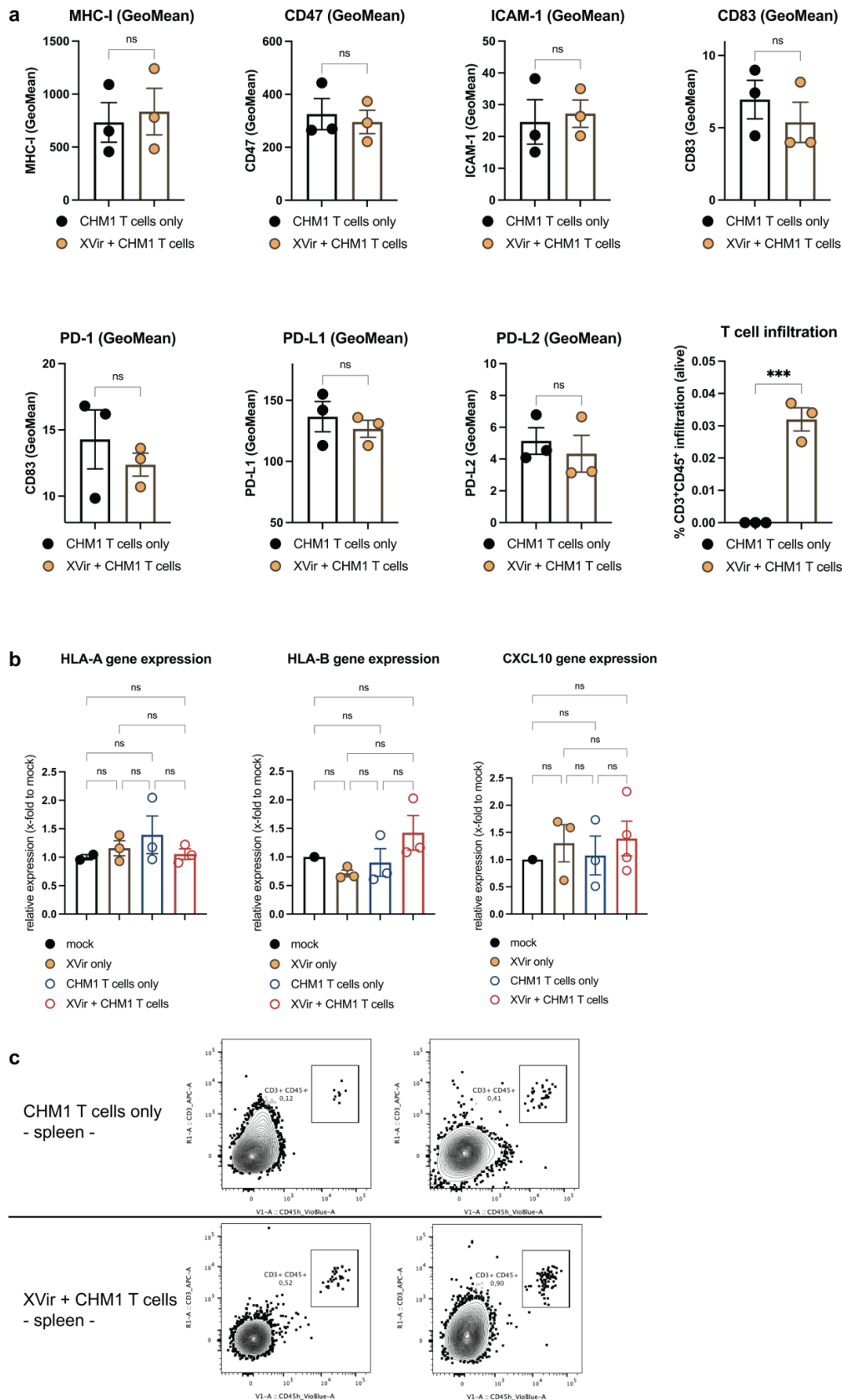
Extended Data Figure 1²⁵⁴: Chemo-/Cytokine release patterns from coculture experiments of A673 tumor cells and T cells. (a) CXCL 9/10, IFN γ and TNF α release patterns of tumor only (4 replicates), non-specific (n.-sp.) CD4⁺, CD8⁺ and *STEAP1₁₃₀/HLA-A*02:01-specific TCR transgenic CD4⁺ (tgCD4)*, CD8⁺ (*tgCD8*) T cells as well as tgCD4/tgCD8 T cells at effector-to-target ratios 20:1 and 1:1. Results represent mean and standard deviation of 3 independent experiments (for E:T=20:1) and 2 independent experiments (for 1:1) from 2 different donors. (b) Comparison of CXCL9/10 levels within tgCD4⁺ T cell-containing settings (CD4 presence) versus tgCD8⁺ T cell-containing settings at E:T=20:1. (c) Heatmap of 39 selected chemo-/cytokines from above mentioned coculture experiments. The heatmap was generated from means of chemo-/cytokines (same replicates were applied as explained under a) using the *heatmap2* script in R.



Extended Data Figure 2: Expression levels of possible XVir-N-31 surface receptors in publicly available data sets. Analyses were conducted online with R2¹, extracted and depicted as log2 gene expression here. EWS datasets are marked with a red quadrant.

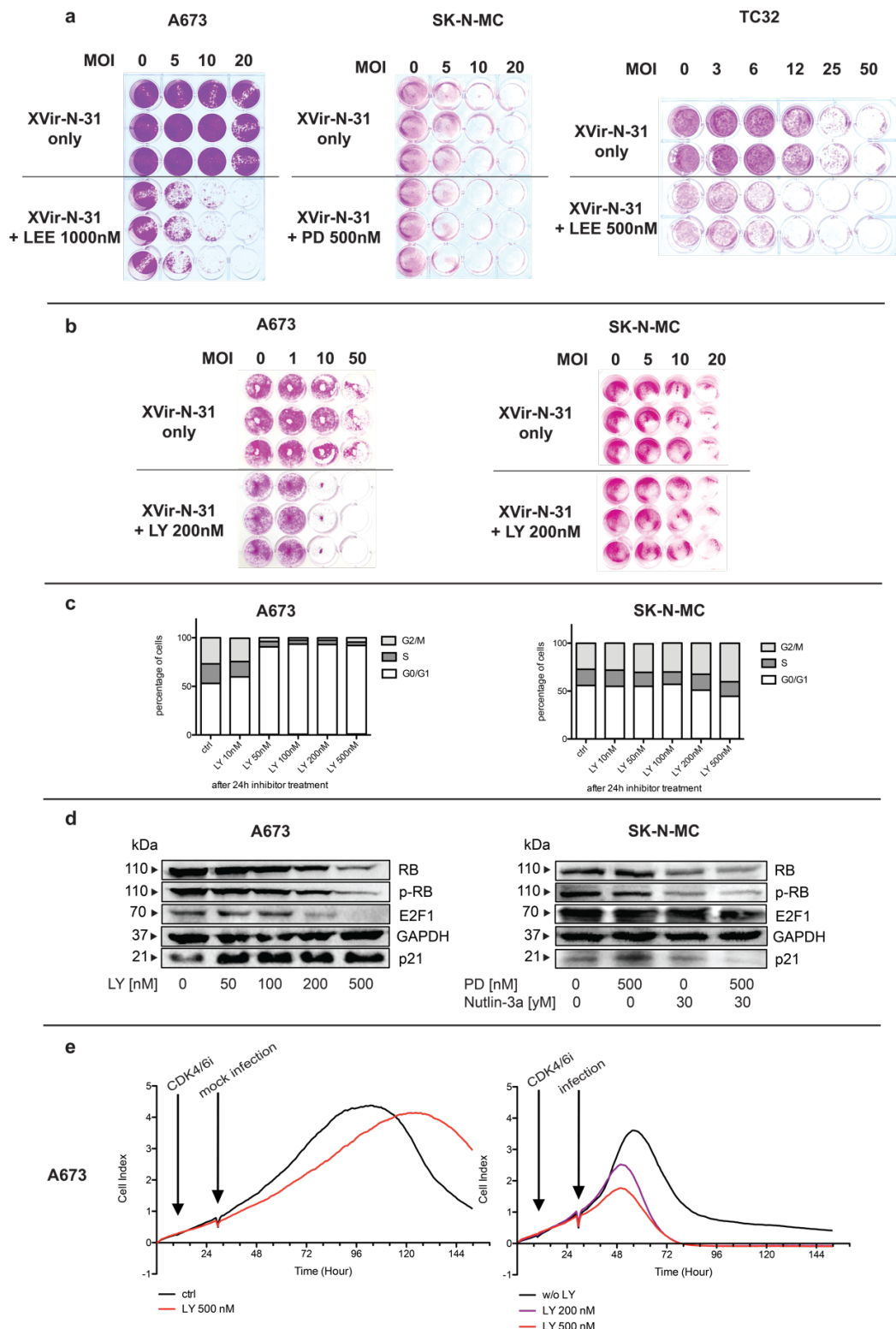


Extended Data Figure 3: Immunofluorescence staining of YB-1, E2F1 and DAPI in EwS cell lines A673, A4573 and SK-N-MC. 2.5×10^4 cells were plated on ibidi μ -slide VI 0.4 and fixed 24-36 hours afterwards and stained with anti-YB-1 antibody (red), anti-E2F1-antibody (green) and DAPI. Imaging was done with Axiovert 100 microscope using fluorescent light with 100x magnification.

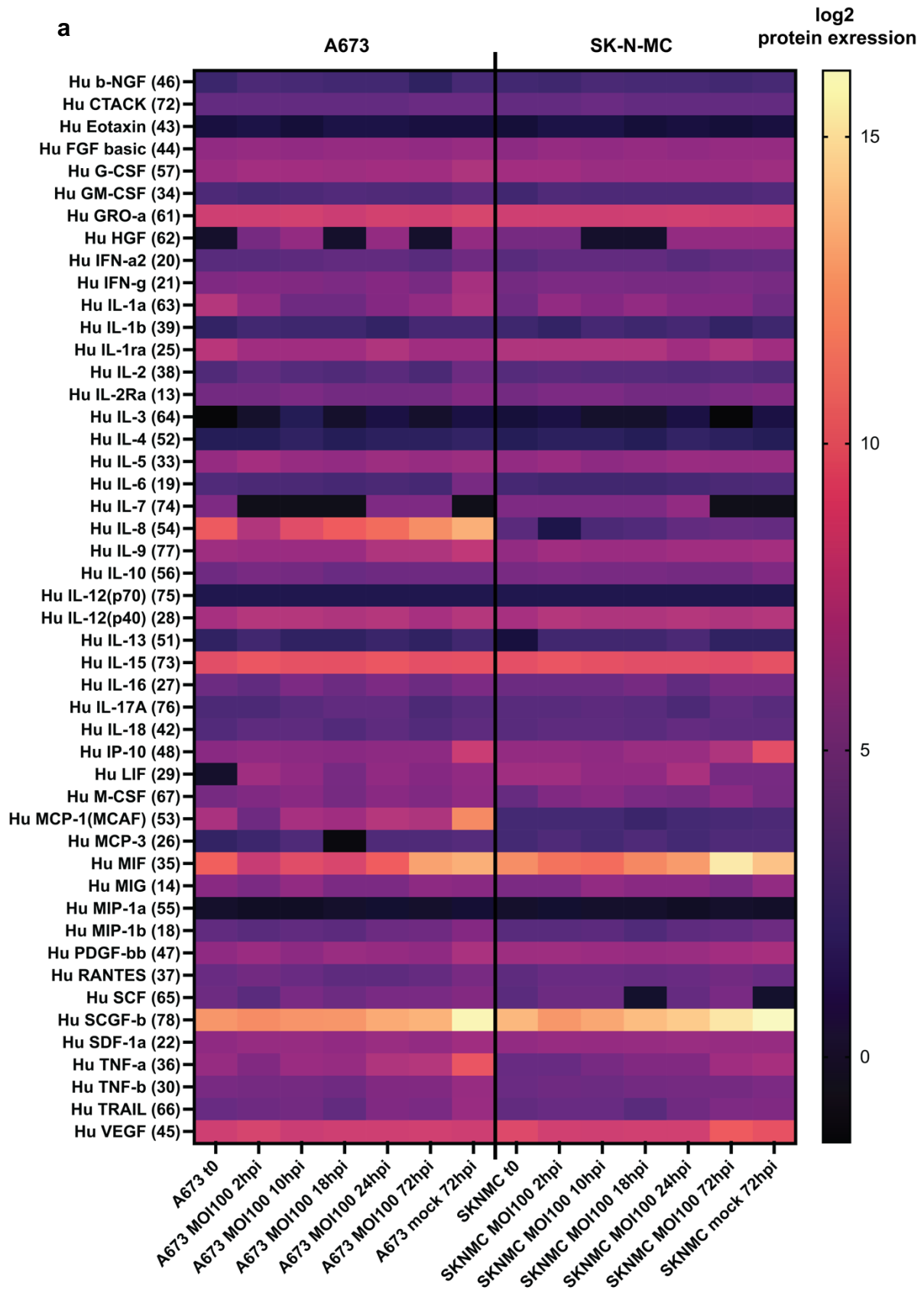


Extended Data Figure 4: CHM1 T cells and XVir-N-31 induces T cell infiltration and increases *in vivo* persistence of. (a) Flow cytometry assessment of surface markers on explanted tumors (single cell suspension after enzymatic and mechanical digestion (respective antibodies and dilutions are provided in [Table 13](#)) and T cell infiltration in tumors, after dead cell exclusion with Viability dye, gated on mouse/human CD45 double negative cells for tumor surface markers and on human

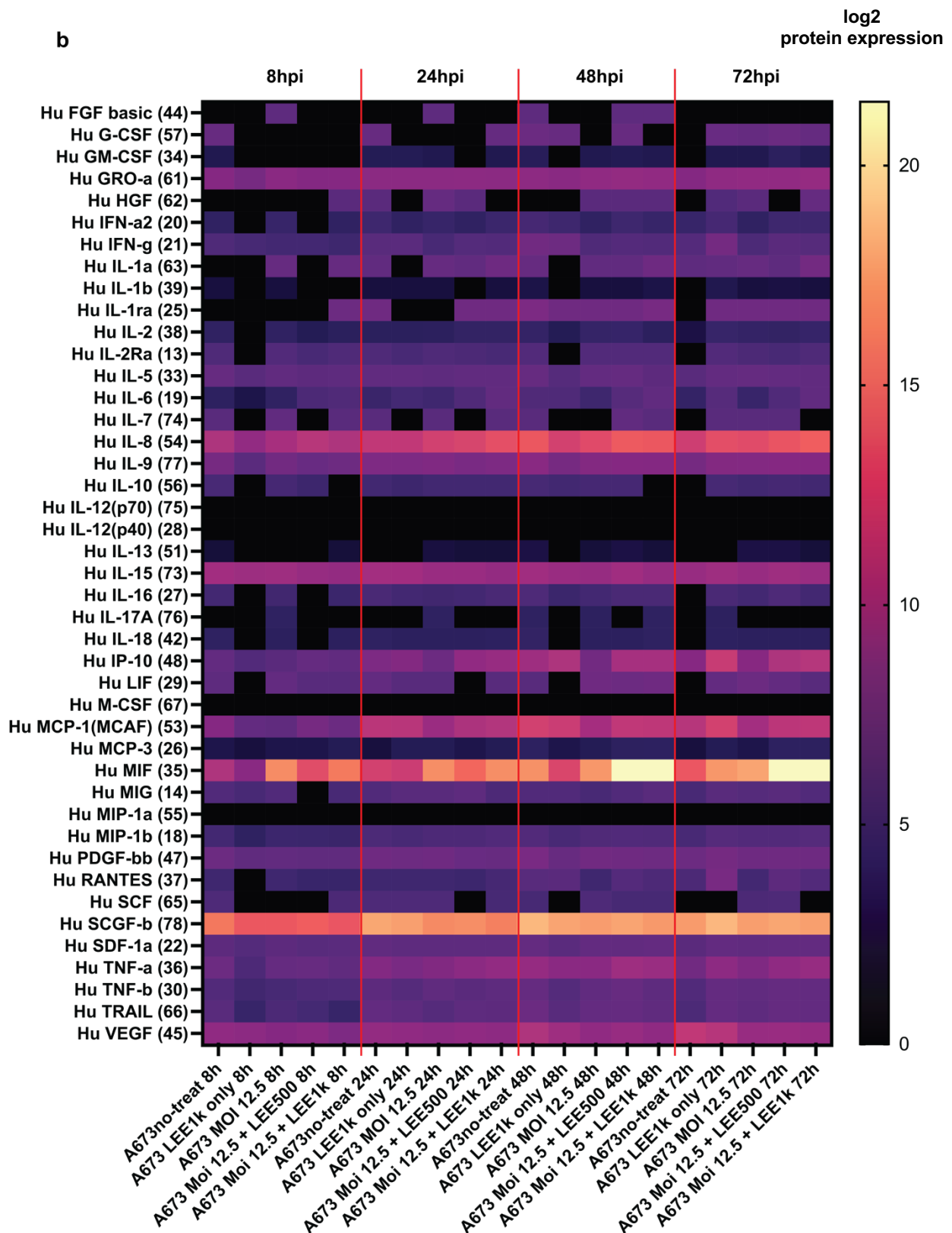
CD45/CD3 double positive cells for evaluation of TILs. **(b)** Assessment of HLA-A, -B, and CXCL10 gene expression by sqRT-PCR (GAPHD or β actin was used for normalization, mean expression of mock animals served as control). Each dot represents one animal or the mean of mock animals in b. **(c)** Engrafted human CD45/CD3 double positive T cells in spleens of 2 representative animals per group, after Statistical analyses were performed in Prism 9 using unpaired two-tailed student' t-test (in a) Tukey's multiple comparison in combination with ordinary one-way ANOVA. Significance levels are indicated as asterisks: * $p < 0.05$, ** $p < 0.01$, $p^{***} < 0.005$, $p^{****} < 0.0001$, ns = not significant. Error bars indicate the SEM.



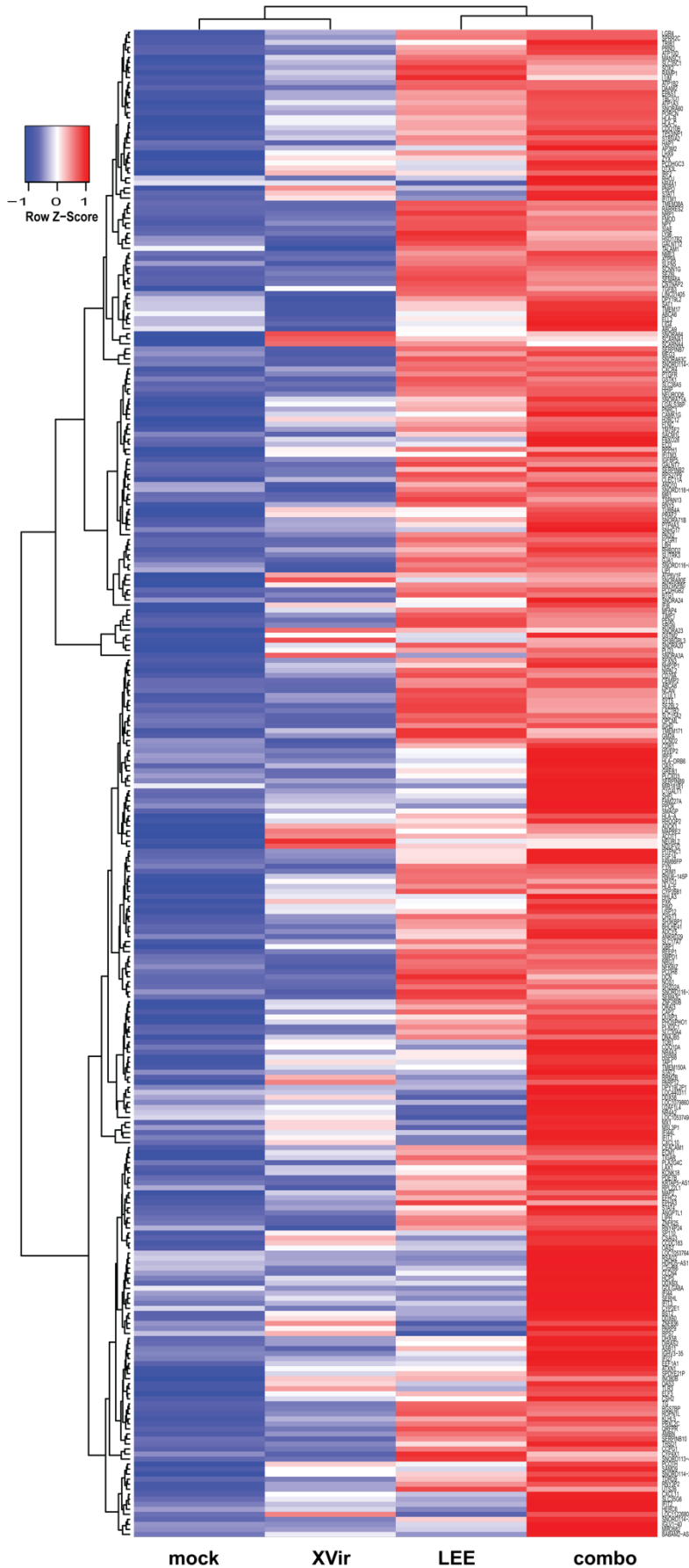
Extended Data Figure 5: Combination of XVir-N-31 and CDK4/6i increases tumor cell lysis which is accompanied by G1 cell cycle state and reduction of RB. (a+b) Cell survival analysis of EwS cell lines A673, SK-N-MC, and TC32 treated with XVir-N-31 only versus combination with CDK4/6i (LEE, LY, PD at indicated concentrations). **(c)** CDK4/6i-sensitive A673 shows a dose-dependent increase in cells in G1/G0 cell cycle phase whereas in CDK4/6i-resistant SK-N-MC G1/G0 cell cycle state cannot be induced, which is accompanied by **(d)** downregulation of (p-)RB/E2F1 protein levels. The MDM2-inhibitor nutlin-3a in CDK4/6i-resistant SK-N-MC induces a reduction of (p-)RB/E2F1 protein levels. **(e)** xCELLigence assay of A673 contact-dependent cell growth with CDK4/6i and consecutive XVir-infection (added at timepoint indicated by arrows) shows earlier and dose-dependent detachment (indicative of tumor cell lysis) by the combination Tx.



Extended Data Figure 6a: Chemo-/Cytokines - Infection dynamics in A673 and SK-N-MC. Log₂ levels of secreted factors in the supernatant of XVir-N-31-infected cells at indicated time points (t 0-2-10-18-24-72hpi) with MOI100 analyzed by Multiplex Immunoassay.

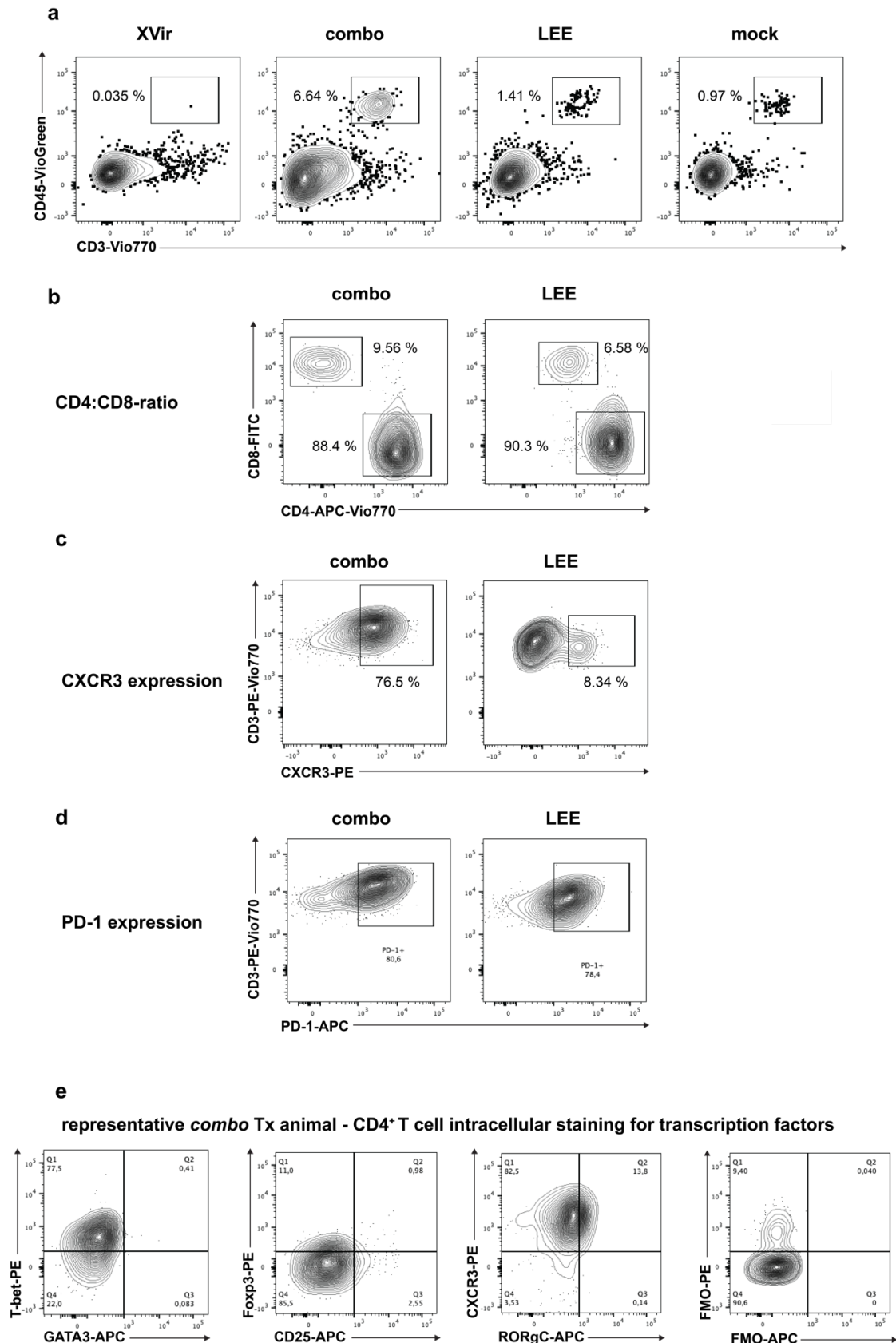


Extended Data Figure 6b: Chemo/Cytokines - Infection dynamics in A673 with CDK4/6 inhibitor LEE011. Log₂ levels of secreted factors in the supernatant of XVir-N-31-infected cells at indicated time points (t 0-2-10-18-24-72hpi) with MOI12.5 analyzed by Multiplex Immunoassay. CDK4/6i treatment was started 24h prior infection with LEE011 1000nM (1k), 500nM (500) or mock.

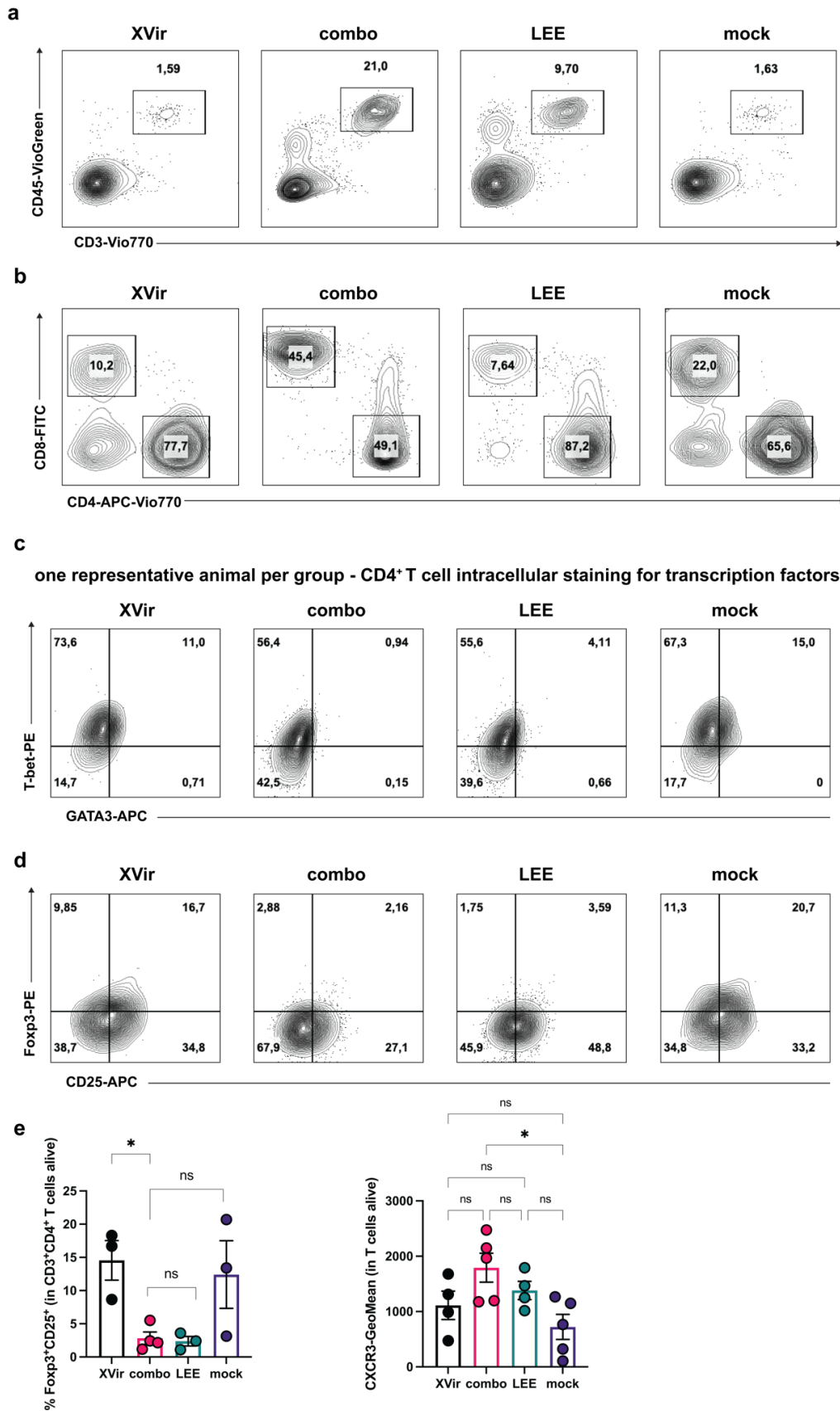


Extended Data Figure 7: Heatmap of 300 most upregulated genes in *combo* (log₂, fold change compared to *mock*). Blue = low expression, red = high expression.

Transcriptome analysis from one representative animal per group, 3 days after 1 XVir-N-31-injection (or PBS-injection) and 5 days after start of daily LEE011 (or mock) treatment. Expression data was generated by *Affymetrix Human Gene 1.0 ST arrays* after annotation with *R package pd.hugene10st.hs.entrezg* and normalization. Heatmaps were generated with the *R package heatmaps.2*.

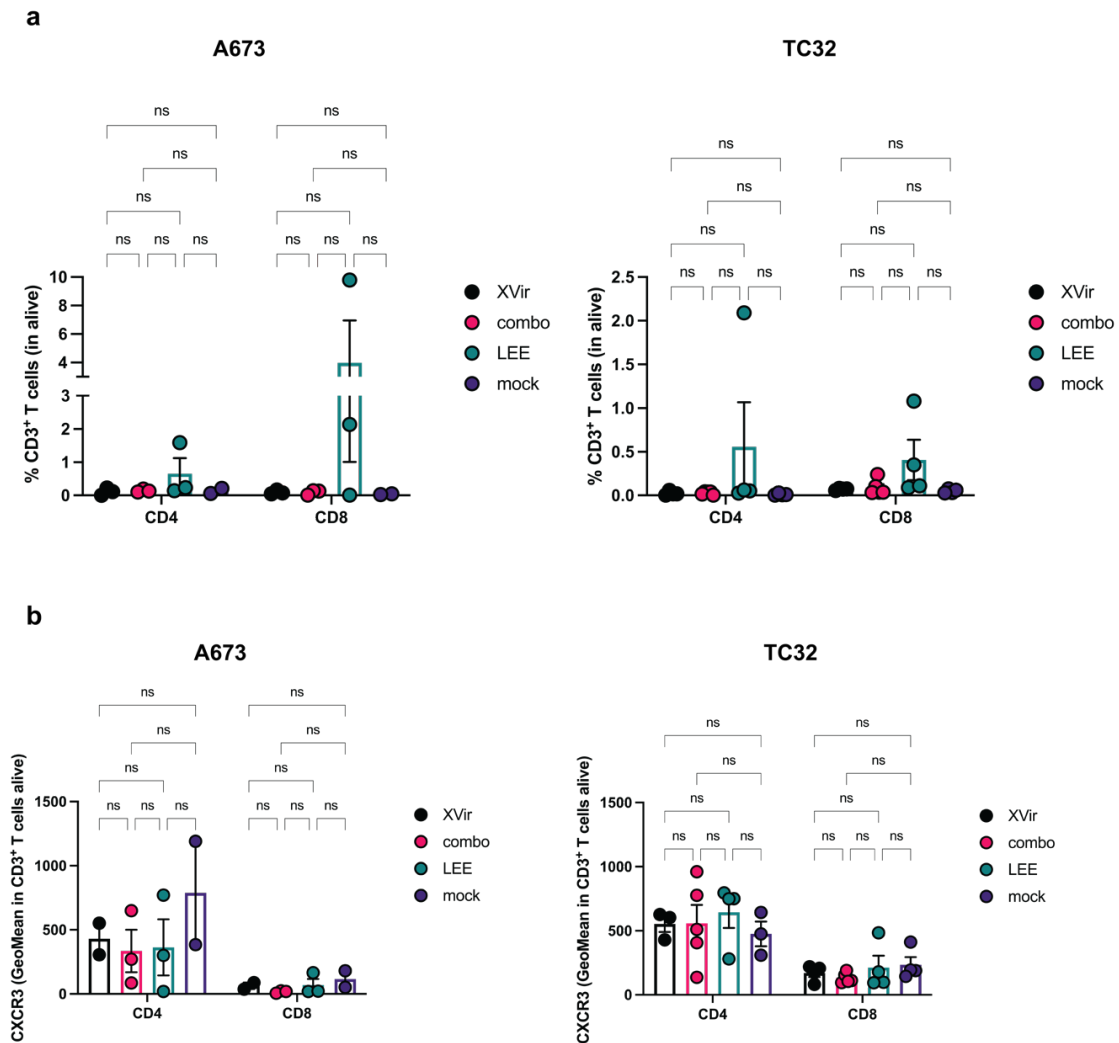


Extended Data Figure 8: Characterization of tumor-infiltrating T cells at the end of experiment (A673 xenografts, LEE011 + XVir-N-31) Flow cytometry analysis of (a) TILs (human CD45/CD3 double positive in alive cell gate) from one representative animal per group, (b) exemplary analysis of CD4:CD8 ratios of TILs from (a), (c) CXCR3 expression on TILs shown in (a), (d) and PD-1 expression. (e) Intracellular staining of transcription factors was performed. Herein presented is the CD4-positive alive gate to identify T_{H1} (T-bet positive), T_{H2} (GATA3 positive), T_{Reg} (CD25/Foxp3 double positive) T_{H17} (RORgC positive) cells together with respective FMO control (right).

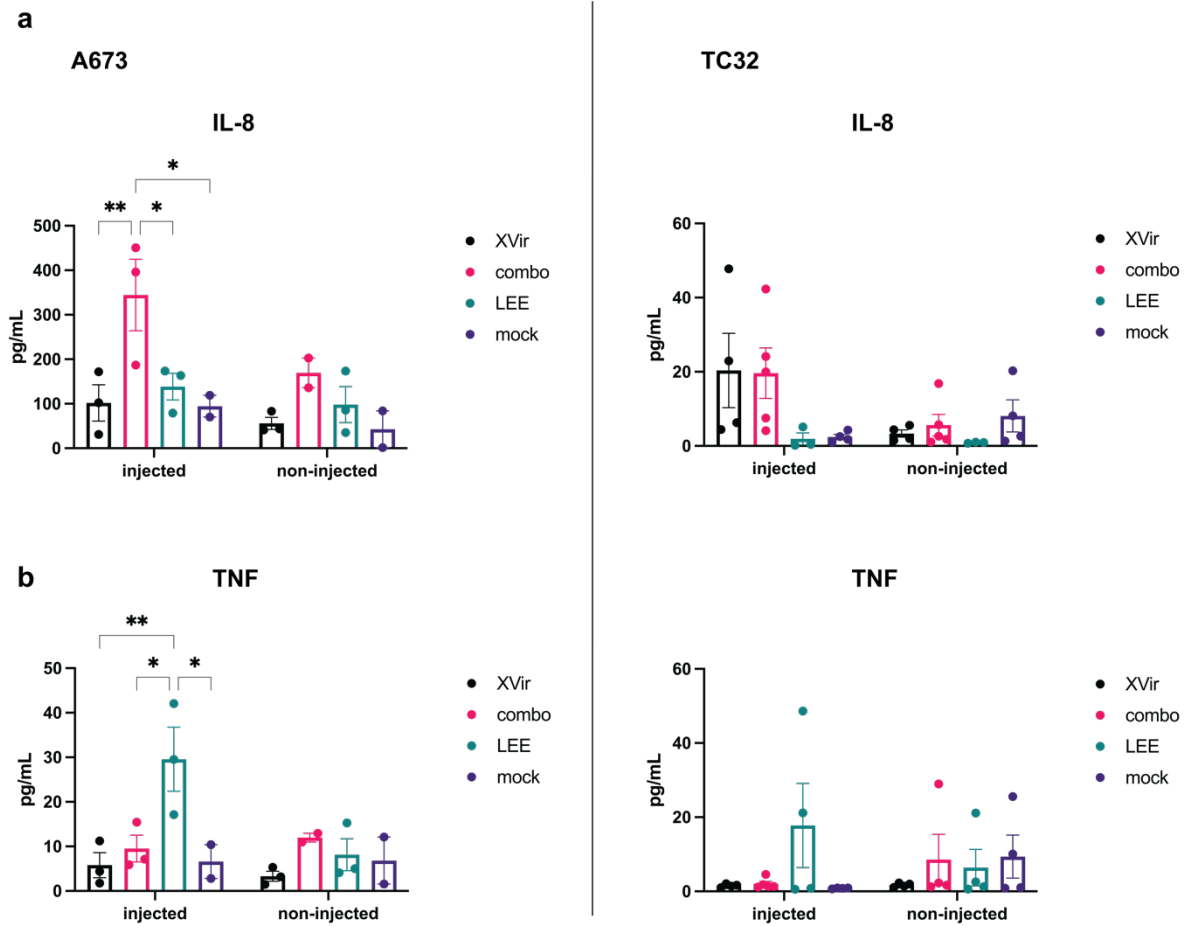


Extended Data Figure 9: Human T cell engraftment in spleens of A673-xenografted animals at end of experiment. Flow cytometry analysis of (a) human T cells (human CD45/CD3 double positive in alive cell gate) from one representative animal per group, (b) exemplary analysis of CD4:CD8 ratios of engrafted T cells, (c) intracellular staining of transcription factors for one representative animal per group to identify T_{H1} (T-bet positive), T_{H2} (GATA3 positive), and (d) T_{Reg} (CD25/Foxp3 double positive)

compared to FMO controls. (e) Column bars of relative percentages of (left) T_{Reg} cells and (right) CXCR3 expression in T cell gate. Each dot represents one spleen (or animal). Statistical analysis of T_{Reg} relative frequencies was performed using a paired t-test to recognize tendencies. Ordinary one-way ANOVA and Tukey's multiple comparison was applied for CXCR3 expression levels. Significance levels are indicated as asterisks: * $p < 0.05$, ns = not significant. Error bars indicate the SEM.



Extended Data Figure 10: Human T cell engraftment in spleens at 4 days after 2nd XVir-injection
 Flow cytometry analysis of (a) relative numbers of CD4 and CD8 positive T cells in human CD45/CD3 double positive cells in alive cell gate and (b) respective expression of CXCR3 in spleens from A673 and TC32 xenografted animals. Each dot represents one spleen (or animal). from one representative animal per group. Two-way ANOVA and Tukey's multiple comparison was applied, ns = not significant. Error bars indicate the SEM.



Extended Data Figure 11: IL-8 and TNF in the TME – 4 days after 2nd XVir-injection. (a) IL-8 and (b) TNF concentration in the tumor microenvironment of explanted xenografts was evaluated after mechanical dissection of tumors in 4mL PBS for A673 and TC32. Statistical analysis was performed by Tukey's multiple comparison combined with two-way ANOVA. Significance levels are indicated as asterisks: * $p < 0.05$, ** $p < 0.01$, not shown when not significant. Error bars indicate the SEM.

8.2 List of figures

Figure 1: Transcriptome-based analysis reveals positive correlation of CXCL10 expression with increased CD8 ⁺ T cell and M1 macrophage transcripts and genes involved in antigen presentation	page 42
Figure 2: EwS-redirected TCR transgenic CD4 ⁺ T cells exhibit antitumor activity <i>in vitro</i> and mediate local control of s.c.-xenografted A673 cell line	page 44
Figure 3: Analysis of receptor expression for oncolytic adenovirus XVir-N-31	page 46
Figure 4: Established EwS cell lines are susceptible to adenovirus-RGD infection inducing XVir-N-31-mediated oncolysis and <i>de novo</i> formation of infectious viral particles	page 48
Figure 5: CHM1 ³¹⁹ /HLA-A*02:01-restricted TCR-transgenic CD8 ⁺ T cells and XVir-N-31 synergistically lyse tumor cells <i>in vitro</i>	page 50
Figure 6: Combination of CHM1 ³¹⁹ /HLA-A*02:01-restricted TCR-transgenic CD8 ⁺ T cells (CHM1 T cells) and XVir-N-31 increase therapy response and survival	page 52
Figure 7: XVir-N-31 increases phagocytic and antigen-presenting capacities resulting in superior antigen-specific CD8 ⁺ T cell proliferation	page 54
Figure 8: Combination of XVir-N-31 and CDK4/6 inhibition increase oncolysis and viral replication <i>in vitro</i> and increases therapy response and survival <i>in vivo</i>	page 57
Figure 9: siRNA-mediated knock-down of RB protein increases viral <i>fiber DNA</i> in CDK4/6i-resistant cell line SK-N-MC	page 58
Figure 10: <i>Combo</i> Tx increases CXCL10 release in XVir-N-31-infected A673 condition medium	page 60
Figure 11: CDK4/6-inhibitor with LEE011 induces CXCL10 protein levels in <i>LEE</i> and <i>Combo</i> Tx <i>in vitro</i>	page 61
Figure 12: Combination of XVir-N-31 and CDK4/6 inhibitor LEE011 increases viral replication and immunogenicity of xenografted EwS tumors <i>in vivo</i>	page 62
Figure 13: Combination of XVir-N-31 and CDK4/6 inhibitor LEE011 increases survival and local tumor control	page 65
Figure 14: Combination of XVir-N-31 and CDK4/6 inhibitor LEE011 induces T cell infiltration and increases T cell engraftment	page 67
Figure 15: Combination of XVir-N-31 and CDK4/6 inhibitor LEE011 induces an abscopal effect	page 68
Figure 16: Combination of XVir-N-31 and CDK4/6 inhibitor LEE011 induces CXCL10 in the tumor microenvironment	page 69
Figure 17: Combination of XVir-N-31 and CDK4/6 inhibitor LEE011 induces mouse monocyte infiltration in injected tumors	page 71
Figure 18: Combination of XVir-N-31 and CDK4/6 inhibitor LEE011 induces maturation of THP-1 and monocytic immature dendritic cells <i>in vitro</i>	page 73
Figure 19: Combination of XVir-N-31 and CDK4/6 inhibitor LEE011 increase antigen-specific T cell proliferation and activation	page 75
Figure 20: Combination of XVir-N-31, LEE011, and CHM1 CD8 ⁺ T cells further increases synergistic killing of tumor cells <i>in vitro</i>	page 77
Extended Data Figure 1: Chemo-/Cytokine release patterns from coculture experiments of A673 tumor cells and T cells	page 109
Extended Data Figure 2: Expression levels of possible XVir-N-31 surface receptors in publicly available data sets	page 109
Extended Data Figure 3: Immunofluorescence staining of YB-1, E2F1 and DAPI in EwS cell lines A673, A4573 and SK-N-MC	page 110
Extended Data Figure 4: CHM1 T cells and XVir-N-31 induces T cell infiltration and increases <i>in vivo</i> persistence of CHM1 T cells	page 111

Extended Data Figure 5: Combination of XVir-N-31 and CDK4/6i increases tumor cell lysis which is accompanied by G1 cell cycle state and reduction of RB	page 113
Extended Data Figure 6a: Chemo-/Cytokines - Infection dynamics in A673 and SK-N-MC	page 114
Extended Data Figure 6b: Chemo-/Cytokines - Infection dynamics in A673 with CDK4/6 inhibitor LEE011	page 115
Extended Data Figure 7: Heatmap of 300 most upregulated genes in <i>combo</i>	page 116
Extended Data Figure 8: Characterization of tumor-infiltrating T cells at the end of experiment (A673 xenografts, LEE011 + XVir-N-31)	page 117
Extended Data Figure 9: Human T cell engraftment in spleens of A673-xenografted animals at end of experiment	page 118
Extended Data Figure 10: Human T cell engraftment in spleens at 4 days after 2 nd XVir-injection	page 119
Extended Data Figure 11: IL-8 and TNF in the TME – 4 days after 2 nd XVir-injection	page 120

8.3 List of tables

Table 1: List of manufacturers	page 21
Table 2: List of chemicals and reagents	page 22
Table 3: List of consumables	page 24
Table 4: Equipment	page 25
Table 5: Software	page 27
Table 6: Kits	page 27
Table 7: Buffers and gels for western blot analysis	page 27
Table 8: Buffers and solutions for cell cycle analysis	page 28
Table 9: Media	page 28
Table 10: Universal and specific buffers/solutions	page 28
Table 11: Cell lines used for experiments	page 29
Table 12: Cell lines used for experimental support	page 29
Table 13: Antibodies for flow cytometry – anti-human	page 29
Table 14: Antibodies for flow cytometry/purification – anti-mouse	page 30
Table 15: Antibodies for flow cytometry – intracellular staining (human and mouse)	page 30
Table 16: Further dyes and solutions used for flow cytometry (non-conjugated)	page 31
Table 17: Antibodies for WB, HTT, IF and flow cytometry	page 31
Table 18: Primer Sequences	page 32
Table 19: sqPCR protocol	page 37
Table 20: Analysis of significantly overexpressed pathway-associated genes in <i>combo</i> Tx compared to <i>mock</i>	page 63

8.4 List of abbreviations

%	Percent sign
°C	Degree Celcius
ACT	Ddoptive (T) cell transfer
Ad	Adenovirus
allo	Allogenic
AMP	Adenosine monophosphate
ANOVA	Analysis of variance
APC	Antigen-presenting cell
APC	Allophycocyanin
ARG1	Arginase 1
ATCC	American Type Culture Collection
ATP	Adenosine triphosphate
AYA	Adolescents and young adults
BET	Bromodomain and extra-terminal
BM	Bone marrow
BMBF	Federal Ministry of Education and Research
CALR	Calreticulin
CAR	Chimeric antigen receptor
CAR	Coxsackie and adenovirus receptor
CCL	C-C Motif Chemokine Ligand
CCLE	Cancer Cell Line Encyclopdia
CCR	Childhood Cancer Repository
CD	Cluster of differentiation
CD248	Endosialin
CDK	Cyclin-Dependent Kinase
CDKN2A	CDK4 Inhibitor P16-INK4
ChIP	Chromatin immunoprecipitation
CHM1	Chondromodulin-1
CIITA	Endogenous class II transactivator
cm	Centimeter
CM	Condition medium
CO ₂	Carbon dioxide
CR	Conserved region
CXCL	C-X-C Motif Chemokine Ligand
CXCR	C-X-C Motif Chemokine Receptor
DAB	3,3'-diaminobenzidine in chromogen
DAMP	Danger-associated molecular patterns
DAPI	4',6-diamidino-2-phenylindole
DC	Dendritic cell
DLI	Donor lymphocyte infusion
DMEM	Dulbecco's Modified Eagle's Medium
DMSO	Dimethylsulfoxide
DNA	Eoxyribonucleic acid
DNMT	DNA Methyltransferase
Dr.	Doctor
ds	Double-stranded
DSMZ	German Collection of Microorganism and Cell Culture
DTT	Dithiothreitol
E:T	effector-to-target
E2F	E2F Transcription Factors
ECM	extracellular matrix
EDTA	Ethylenediaminetetraacetic acid
EMA	European Medicine Agency
ERG	ETS Transcription Factor ERG
ERV	Endogenous retroviral element
EtOH	Ethanol
ETS	Erythroblast Transformation Specific
ETV1	ETS Variant Transcription Factor 1
ETV4	ETS Variant Transcription Factor 4

EV	Extracellular vesicle
EwS	Ewing sarcoma
EWSR1	EWS RNA Binding Protein 1
EZH2	Enhancer of Zeste Homolog 2
FATE1	Fetal And Adult Testis-Expressed Transcript Protein 1
FCS	Fetal calf serum
FDA	Food and Drug Administration
FEV	FEV Transcription Factor, ETS Family Member
FITC	Fluorescein isothiocyanate
FLI1	Friend Leukemia Virus Integration 1
FlowCy	Flow cytometry
G	Gauge
g	Gramm
GATA3	GATA Binding Protein 3
G _{D2}	Ganglioside D2
GM-CSF	Granulocyte-Macrophage Colony-Stimulating Factor
GMP	Guanosine monophosphate
GvT	Graft-versus-tumor
Gy	Gray
h	Hours
HCl	Hydrochloric acid
HDAC	Histone acetylation
HEPES	Zwitterionic sulfonic acid buffering agent
HER2	Human Epithelia Growth Factor Receptor 2
HIF1	Hypoxia-inducible factor 1
HLA	Human leukocyte antigen
HMGB1	High-mobility group box 1
hpi	Hours post infection
HRP	Horseradish peroxidase
HSCT	Hematopoietic stem cell transplantation
HSV	Herpes simplex virus
HTT	Hexon titer test
i.p.	Intraperitoneal
i.t.	Intratumoral
i.v.	Intravenous
ICAM-1	Intercellular Adhesion Molecule 1
ICB	Immune checkpoint blockade
ICD	Immunogenic cell death
IDO	Indoleamine oxidase
IF	Immunofluorescence
IFN	Interferon
IFU	Infectious units
IGF1	Insulin-Like Growth Factor
IL	Interleukin
IP-10	Interferon gamma-induced protein 10
KD	Knock-down
L	Liter
LAF-1	Lymphocyte Function Associated Antigen-1
LAP	Latency-associated peptide
LEE011, LEE	Ribociclib
LINE	Long interspersed elements
LIPI	Lipase I
LY2835219, LY	Abemaciclib
M	Molar
MCP-1,	Monocyte Chemoattractant Protein-1
MDSC	Myeloid-derived suppressor cell
med.	Medicine
MeOH	Methanol
MHC	Major histocompatibility antigen
MIF	Macrophage Migration Inhibitory Factor
min	Minutes
mL	Milliliter

mM	Milimol
mm	Milimeter
μm	Mikro
MMP9	Matrix metallopeptidase 9
MOI	Multiplicity of infection
MSC	Mesenchymal stem cell
MTD	Maximum tolerated dose
n	Number
n.-sp.	Non-specific
Na	Sodium
NaCl	Sodium chloride
NaN ₃	Sodium azide
NaOH	Sodium hydroxide
NaVO ₃	Sodium metavanadate
NEAA	Non-Essential Amino Acid
NFAT4	T cell Transcription Factor NFAT4
NK	Natural killer
nm	Nanometer
nM	Nanomol
NOS2	Nitric Oxide Synthase 2
NY-ESO-1	New York Esophageal Squamous Cell Carcinoma 1
OAd	Oncolytic adenoviruse
oHSV	Oncolytic HSV
OS	Overall survival
OV	Oncolytic virus
OVA	Ovalbumin
p	Pico
p21	Cyclin-Dependent Kinase Inhibitor 1
PAMP	Pathogen-associated molecular patterns
PAPPA	Pregnancy-Associated Plasma Protein A
PBMC	Peripheral blood mononuclear cells
PBS	Phosphate Buffered Saline
PCR	Polymerase chain rection
PD-0332991, PD	Palbociclib
PD-1	Programmed cell death protein 1
PD-L1	Programmed cell death-ligand 1
PDGF-b	Platelet-derived Growth Factor-beta
PE	Phycoerythrin
PerCP	Peridinin chlorophyll protein
PFS	Progression free survival
PGE ₂	Prostaglandin E ₂
PhD	Doctor of philosophy
PI	Propidium iodide
Prof.	Professor
Rag2	Recombination activating gene 2 protein
RB	Retinoblastoma
rcf	Relative centrifugal force
rer. nat.	Rerum naturalium
RGD	Arginine, Glycine, and Aspartate
RNA	Ribonucleic acid
rpm	Rounds per minute
RR	Response rate
RT	Reverse transcription
s.c.	Subcutaneous
SCGF-b	Stem Cell Growth Factor-beta
SDS	Sodium dodecyl sulfate
seq	Sequencing
sh	Short hairpin
si	Small inhibitory
smi	Small molecule inhibitors
sq	Semi-quantitative
SRB	Sulforhodamine B sodium salt

STAG2	Cohesion Subunit SA2
STAT	Signal Transducer And Activator Of Transcription
STEAP1	Six transmembrane epithelia antigen of the prostate 1
T-VEC	Talimogene laherparepvec
TAM	Tumor-associated macrophage
TCA	Trichloroacetic acid
TCR	T cell receptors
tg	Transgenic
TGF-beta	Transforming Growth Factor Beta
TIL	Tumor-infiltrating lymphocyte
TLR	Toll-like Receptor
TME	Tumor microenvironment
TMED	Tetramethylethylenediamine
TP53	Tumor Suppressor P53
TRAIL-R2	Death Receptor 5
TRIS	Tris(hydroxymethyl)aminomethane
USA	United States of America
VEGF	Vascular Endothelial Growth Factor
VIDE	Vincristine, ifosfamide, doxorubicin and etoposide
VSV	Vesicular stomatitis virus
WB	Western blot
x	fold
XAGE-1	X Antigen Family Member 1A
XVir	XVir-N-31, OAd
YB-1	Y-box binding protein 1
μ L	Mikroliter

8.5 Declaration of shared data in two dissertations

Data from following chapters presented in this PhD thesis were generated together with Caroline Schöning and will also be published in her MD thesis (*Dr. med.*):

- 4.4.4 Combination of XVir-N-31 and CDK4/6 inhibitor LEE011 increases viral replication and exerts immunological antitumor effects *in vivo*
- 4.4.5 Combination of XVir-N-31 and CDK4/6 inhibitor LEE011 increases survival *in vivo*
- 4.4.6 Combination of XVir-N-31 and CDK4/6 inhibitor LEE011 induces T cell infiltration
- 4.4.7 Combination of XVir-N-31 and CDK4/6 inhibitor LEE011 induces an abscopal effect
- 4.4.8 Combination of XVir-N-31 and CDK4/6 inhibitor LEE011 induces mouse monocyte infiltration in injected tumors

Concerning exploitation of respective data, a publication is planned, with Dr. med. Sebastian J. Schober as first author and Carline Schöning as second author.

Hereby both parties confirm that aforementioned data was generated in collaboration, and authorship order and contributions are mutually agreed.

Location and date

Location and date

Caroline Schöning (signature)

Sebastian J. Schober (signature)

8.6 Acknowledgement

I would like to thank my supervisor Prof. Dr. med. Stefan Burdach for his support, his genuine interest in new fields of research, for connecting me to the field of oncolytic virotherapy and his encouragement to become an independent researcher. He and PD Dr. med. Uwe Thiel provided the frame for this work.

Furthermore, I'm deeply grateful to Prof. Dr. rer. nat. Per Sonne Holm, my first mentor, for the introduction to virotherapy and its fascinating potential to fight cancer, which was always transported by him with great enthusiasm, deep knowledge, and perfect support concerning experimental conduct throughout my PhD study. He and the whole team at the Department of Experimental Urology, together with PD Dr. rer. nat. Roman Nawroth, provided generous insight into their expertise of cell cycle inhibition and virotherapy, which allowed me to transfer relevant methods to the Department of Pediatrics. Without this fruitful, friendly, and highly professional work environment, this PhD study would have not been possible. In this regard, also a special thanks to Prof. Dr. rer. nat. Per Sonne Holm and Klaus Mantwill for providing adenoviral constructs and the relatively high amount of XVir-N-31 needed for *in vivo* studies.

I'm also deeply indebted to my second mentor, PD Dr. med. Uwe Thiel, who accompanied me since my research work started at the Department of Pediatrics. His honest, sincere, and supporting nature, coupled with deep immunological understanding and experimental expertise, ensured a joyful and productive environment. He helped me not to lose focus and provided motivation whenever needed, whilst always having an open ear for private and professional challenges.

Next, I would like to thank my colleague Dr. med. Hendrik Gaßmann for his help. With him I experienced drawbacks and success in research, established new methods, had eye-opening insights, and could always exchange about both private and professional issues, no matter what time of the day.

Furthermore, I'm indebted to the current and former technicians in our lab, especially Melanie Thiede, Corazon Cordass, and Jennifer Eck. They helped me tremendously to establish new techniques, provided cells, and performed experiments.

I'm grateful for the Dr. med. candidates which I supervised/still supervise for their research projects namely: Charlotte Middendorf, Julia Lutsch, Pia Knoch, Caroline Schöning, and Josefine von Ofen. Especially without the help of Caroline Schöning, the laborious and time-consuming *in vivo* presented here could have not been possible. Also due to the kind and fun personalities of all my colleagues in the lab, I was always happy to be able to work there.

Thank you to all other people I collaborated with inside and outside of TUM. It was always straight forward and uncomplicated.

Lastly, I would like to thank my family. Thank you to my brother-in-law Dr. rer. nat. Michael Dudek for revising this thesis and the fruitful and inspiring discussions and experimental insights. Furthermore, I would like to thank my sisters for their help and understanding, my father, mother, and grandparents for the continuous support and help in any aspects of life. The biggest thank you is dedicated to my wife Patcharee for her love, her support, patience, and her understanding in the past years.

8.7 Publications related to this PhD work

Original articles (peer-reviewed)

Schober, S.J., Thiede, M., Gassmann, H., Prexler, C., Xue, B., Schirmer, D., Wohlleber, D., Stein, S., Grünewald, T., Busch, D. H., Richter, G., Burdach, S., & Thiel, U. (2020). MHC Class I-Restricted TCR-Transgenic CD4⁺ T Cells Against STEAP1 Mediate Local Tumor Control of Ewing Sarcoma In Vivo. *Cells*, 9(7), 1581. <https://doi.org/10.3390/cells9071581>

Thiel, U.*, **Schober, S.J.***, Ranft, A., Gassmann, H., Jabar, S., Gall, K., von Luettichau, I., Wawer, A., Koscielniak, E., Diaz, M.A., Ussowicz, M., Kazantsev, I., Afanasyev, B., Merker, M., Klingebiel, A., Prete, A., Gruhn, B., Bader, P., Jürgens, H., Dirksen, U., Handgretinger, R., Burdach, S., Lang, P. (2021). No difference in survival after HLA mismatched versus HLA matched allogeneic stem cell transplantation in Ewing sarcoma patients with advanced disease. *Bone Marrow Transplantation* (2021). <https://doi.org/10.1038/s41409-020-01200-x>. *these authors contributed equally. Burdach, S. and Lang, P. share senior-authorship.

Gassmann, H.*, Schneider, K.*, Evdokimova, V., Ruzanov, P., **Schober, S.J.**, Xue, B., von Heyking, K., Thiede, M., Richter, G.H.S., Pfaffl, M.W., Noessner, E., Stein, L. D., Sorensen, P.H., Burdach, S.E.G., Thiel, U. (2021). Ewing Sarcoma-Derived Extracellular Vesicles Impair Dendritic Cell Maturation and Function. *Cells* (accepted 2021/08/10). *these authors contributed equally. Thiel, U. and Burdach, S.E.G. share senior-authorship.

Koch, J.*, **Schober, S.J.***, Hindupur, S.*, Klein, F., Mantwill, K., Ehrenfeld, M., Schillinger, U., Hohnecker, T., Pan, Q., Steiger, K., Aichler, M., Gschend, J., Holm, P.S., Nawroth, R. (2021) Targeting the RB/E2F repressive complex by CDK4/6 inhibitors amplifies the oncolytic potency of XVir-N-31. *Nature Communications* (in revision, 2021). *these authors contributed equally. Holm, P.S. and Nawroth, R. share senior-authorship.

Review articles (peer-reviewed)

Grünewald, T. G., Alonso, M., Avnet, S., Banito, A., Burdach, S., Cidre-Aranaz, F., Di Pompo, G., Distel, M., Dorado-Garcia, H., Garcia-Castro, J., González-González, L., Grigoriadis, A. E., Kasan, M., Koelsche, C., Krumbholz, M., Lecanda, F., Lemma, S., Longo, D. L., Madrigal-Esquivel, C., Morales-Molina, Á., Musa, J., Ohmura, S., Ory, B., Pereira-Silva, M., Perut, F., Rodrigues, R., Seeling, C., Al Shaaili, N., Shaabani, S., Shrivastava, K., Sinha, S., Tomazou, E.M., Trautmann, M., Vela, M., Versleijen-Jonkers, Y. M., Visgauss, J., Zalacain, M., **Schober, S.J.**, Lissat, A., English, W.R., Baldini, N., Heymann, D. (2020). Sarcoma treatment in the era of molecular medicine. *EMBO molecular medicine*, 12(11), e11131. <https://doi.org/10.15252/emmm.201911131>

Contributions to congresses/preprints

Evdokimova, V., Ruzanov, P., Gassmann, H., Zaidi, S.H., Peltekova, V., Heisler, L.E., McPherson, J.D., Orlic-Milacic, M., Specht, K., Steiger, K., **Schober, S.J.**, Thiel, U., McKee, T.D., Zaidi, M., Spring, C.M., Lapouble, E., Delattre, O., Burdach, S., Stein, L.D., Sorensen, P.H. (2019) Exosomes transmit retroelement RNAs to drive inflammation and immunosuppression in Ewing Sarcoma. *bioRxiv*, 806851, <https://doi.org/10.1101/806851>

Schober, S.J., Thiel, U., Thiede, M., Ehrenfeld, M., Nawroth, R., Richter, G.H.S, Burdach, S.E.G., Holm, P.S. (2020) Abstract A48: YB-1-based oncolytic virotherapy in combination with CDK4/6-inhibitors against Ewing sarcoma. *Cancer Res.*, 80, A48. <https://doi.org/10.1158/1538-7445.PEDCA19-A48>

Middendorf, C., Thiel, U., Kordass, C., Nawroth, R., Burdach, S.E.G., **Schober, S.J.***, Holm, P.S.* (2020) Abstract 5000: YB-1 based oncolytic virotherapy in combination with small molecule inhibitors for treatment of refractory osteosarcoma. *Cancer Res.*, 80, 5000. <https://doi.org/10.1158/1538-7445.AM2020-5000> * shared senior authorship (corrected).